

NBSIR 75-760

# Proceedings of Piezoelectric and Pyroelectric Symposium-Workshop

---

Martin G. Broadhurst, Coordinator

Institute for Materials Research  
National Bureau of Standards  
Washington, D. C. 20234

September 1975

Final

Prepared for  
Office of Naval Research  
Arlington, Va. 22044

U. S. Army Research Office  
Durham, North Carolina 27706



NBSIR 75-760

**PROCEEDINGS OF PIEZOELECTRIC AND  
PYROELECTRIC SYMPOSIUM-WORKSHOP**

---

Martin G. Broadhurst, Coordinator

Institute for Materials Research  
National Bureau of Standards  
Washington, D. C. 20234

September 1975

Final

Prepared for  
Office of Naval Research  
Arlington, Va. 22044

U. S. Army Research Office  
Durham, North Carolina 27706



---

**U.S. DEPARTMENT OF COMMERCE, Rogers C.B. Morton, *Secretary***  
**James A. Baker, III, *Under Secretary***  
**Dr. Betsy Ancker-Johnson, *Assistant Secretary for Science and Technology***  
**NATIONAL BUREAU OF STANDARDS, Ernest Ambler, *Acting Director***



# PIEZOELECTRIC AND PYROELECTRIC SYMPOSIUM - WORKSHOP

April 15 and 16, 1975

*Sponsored by:*

Office of Naval Research  
Army Research Office  
National Bureau of Standards

Lecture Room A  
Administration Building  
National Bureau of Standards  
Gaithersburg, Maryland

## PROGRAM

April 15, 1975

- 8:45 a.m. Welcome to NBS:  
Dr. Ronald K. Eby  
*Chief, Polymers Division  
National Bureau of Standards*
- 8:50 Introductory Remarks:  
Dr. Kenneth Wynne,  
*Workshop Co-Chairman  
Chemistry Program Office  
Office of Naval Research*
- 8:55 Guidelines for the Symposium-  
Workshop:  
Dr. Martin G. Broadhurst,  
*Workshop Co-Chairman,  
Chief, Bulk Properties Section  
Polymers Division  
National Bureau of Standards*
- 9:00 Technical Presentations
- 10:30 Coffee Break
- 10:45 Technical Presentations
- 1:00 p.m. Lunch
- 2:00 Technical Presentations
- 3:00 Coffee Break
- 3:15 Technical Presentations
- 5:00 End of Session

April 16, 1975

- 9:00 a.m. Technical Presentations
- 10:30 Coffee Break
- 10:45 "Specialty" Workshops
- 12:30 p.m. Lunch
- 1:30 Combined Workshops
- 3:00 Anticipated Conclusion of  
Conference

## ORDER OF TECHNICAL PRESENTATIONS

1. E. Fukada,  
The Institute of Physical & Chemical Research, Japan  
*"Piezoelectricity in Polarized Polyvinylidene Fluoride"*
2. J. Lando,  
Case Western Reserve University, Cleveland, Ohio  
*"Crystal Structures of Polyvinylidene Fluoride and Its Copolymers"*
3. R. Glen Kepler,  
Sandia Laboratories, Albuquerque, New Mexico  
*"Texture and Pyroelectricity in Polyvinylidene Fluoride"*
4. J. Ricca,  
Army Materials & Mechanics Research Ctr., Watertown, Mass.  
*"Dependence of the Piezoelectric Activity of Polyvinylidene Fluoride by High Speed Uniaxial Stretching and Subsequent Poling"*
5. G. Pfister,  
Xerox Corporation, Rochester, New York  
*"Thermally Stimulated Currents and Morphology in Polyvinylidene Fluoride"*
6. G. T. Davis,  
National Bureau of Standards, Washington, D. C.  
*"Piezoelectricity and Pyroelectricity in a Poly(vinylidene fluoride-tetrafluoroethylene) Copolymer"*
7. J. Bergman,  
Bell Telephone Laboratories, Murray Hill, New Jersey  
*"Polyvinylidene Fluoride as an Active Device Element"*
8. M. Litt,  
Case Western Reserve University, Cleveland, Ohio  
*"Ferroelectric Model Compounds and Polymers (?)"*
9. S. Carr,  
Northwestern University, Evanston, Illinois  
*"Origins of Persistent Electrical Polarizations of Polymer Solids"*
10. R. Phelan,  
National Bureau of Standards, Boulder Colorado  
*"Pyroelectric Polymers Applied to Optical Radiation Measurements"*
11. H. Kawai,  
Yokohama Municipal University, Yokohama, Japan
12. M. Labes and R. Salomon,  
Temple University, Philadelphia, Pa.  
*"Pyroelectricity in PVF<sub>2</sub>"*
13. J. Powers,  
Naval Underwater Systems Center, New London, Conn.  
*"Preliminary Investigations of Piezoelectric Polymers for Sonar Applications"*
14. S. Edelman,  
National Bureau of Standards Washington, D. C.  
*"Piezoelectric Polymer Measuring Instruments"*

TABLE OF CONTENTS

	<u>Page</u>
Attendees List . . . . .	1
Letter of Invitation . . . . .	5
Introduction . . . . .	6
"Piezoelectricity in Polarized Polyvinylidene Fluoride" by E. Fukada and Mitsumasa Oshiki . . . . .	8
"Piezoelectric Polymer Research in Japan" by E. Fukada . . . . .	34
"The Melting Temperature-Composition Curves of Poly(vinylidene fluoride)-Poly (vinyl fluoride) Mixtures and Vinylidene Fluoride-Vinyl Fluoride Copolymers" by J. B. Lando . . . . .	35
"Texture and Pyroelectricity in Polyvinylidene Fluoride" by R. G. Kepler . . . . .	46
"Dependence of the Piezoelectric Activity of Polyvinylidene Fluoride Upon High Speed Uniaxial Stretching and Subsequent Poling" by R. J. Shuford, A. F. Wilde, J. J. Ricca and G. R. Thomas . . . . .	59
"Thermally Stimulated Currents and Morphology in PVF <sub>2</sub> " by M. Abkowitz, P. J. Luca, G. Pfister and W. M. Prest, Jr. . . . .	96
"Piezoelectricity and Pyroelectricity in a Poly(vinylidene fluoride-tetra- fluoroethylene) Copolymer" by G. T. Davis . . . . .	120
"Polyvinylidene Fluoride as an Active Device Element" by J. G. Bergman . . . . .	138
"Scanning for Ferroelectricity in Polycrystalline Materials" by M. Litt, Che-hsiung Hsu, P. Basu and S. M. Aharoni . . . . .	165
"Origins of Persistent Electrical Polarization in Polymer Solids" by S. H. Carr . . . . .	189
"Pyroelectric Polymers Applied to Optical Radiation Measurements" by R. J. Phelan, Jr. . . . .	196
"Pyroelectricity in PVF <sub>2</sub> " by R. E. Salomon and M. M. Labes . . . . .	199
"Preliminary Investigations of Piezoelectric Polymers" by J. M. Powers . . . . .	209
"Piezoelectric Polymer Measuring Instruments" by S. Edelman . . . . .	210



ATTENDEES LIST

Piezoelectric and Pyroelectric Symposium-Workshop

April 15-16, 1975

Louis A. Abbagnaro  
CBS Laboratories  
227 High Ridge Road  
Stamford, Conn. 06905

William S. Barnhart  
Pennwalt Corporation  
900 First Avenue  
King of Prussia, Pa. 19406

John Bergman  
Bell Telephone Laboratories  
Holmdel, N. J. 07733

George L. Boyer  
Office of Naval Research  
800 N. Quincy Street  
Arlington, Va. 22217

Phillip Bloomfield  
National Bureau of Standards  
Polymers Division  
Washington, D. C. 20234

Martin Broadhurst  
National Bureau of Standards  
Polymers Division  
Washington, D. C. 20234

Robert B. Bunker  
AFML  
6500 Christy N-E  
Albuquerque, New Mexico 87109

Anthony J. Bur  
National Bureau of Standards  
Polymers Division  
Washington, D. C. 20234

Stephen H. Carr  
Northwestern University  
2145 Sheridan Road  
Evanston, Illinois 60201

Mario J. Cellarosi  
National Bureau of Standards  
Matls. Bldg. Rm. B322  
Washington, D. C. 20234

Tony Clemente  
Bolt, Beranek, Newman  
Cambridge, Mass. 02134

G. Thomas Davis  
National Bureau of Standards  
Polymers Division  
Washington, D. C. 20234

A. Dereggi  
National Bureau of Standards  
Polymers Division  
Washington, D. C. 20234

J. F. Ditter  
Chemical Systems  
1852 McGaw Avenue  
Irvine, Calif. 92705

Ronald K. Eby  
National Bureau of Standards  
Polymers Division  
Washington, D. C. 20234

S. Edelman  
National Bureau of Standards  
Polymers Division  
Washington, D. C. 20234

Barry Farmer  
National Bureau of Standards  
Polymers Division  
Washington, D. C. 20234

John Ferraris  
National Bureau of Standards  
Polymers Division  
Washington, D. C. 20234

Richard Ferren  
Pennwalt Corporation  
900 First Avenue  
King of Prussia, Pa. 19406

Robert B. Fox  
Naval Research Laboratory  
Washington, D. C. 20375

Freeman W. Fraim  
Thermo Electron Corporation  
101 First Avenue  
Waltham, Mass. 02154

Eiichi Fukada  
The Institute of Physical  
and Chemical Research  
Wako, Saitama, JAPAN

L. Garn  
Night Vision Laboratory  
Ft. Belvoir, Va. 22060

Daniel E. Gilbert  
Research Triangle Institute  
P.O. Box 12194  
Research Triangle Park, N. C. 27709

John K. Gillham  
Princeton University  
Dept. of Chemical Engineering  
Princeton, N. J. 08540

Thomas A. Giordano  
CBS Laboratories  
227 High Ridge Road  
Stamford, Conn. 06905

V. S. Goel  
Nuclear Regulatory Commission  
Bethesda, Maryland

A. M. Glass  
Bell Telephone Laboratories  
Mountain Avenue  
Murray Hill, N. J. 07974

James R. Griffith  
U.S. Naval Research Laboratory  
Washington, D. C. 20375

Jay Charles Hicks  
Naval Undersea Center  
San Diego, Calif. 92132

R. Glen Kepler  
Sandia Laboratories  
Organic Materials R&D Dept. 5810  
Albuquerque, New Mexico 87115

F. Khoury  
National Bureau of Standards  
Polymers Division  
Washington, D. C. 20234

M. M. Labes  
Temple University  
13th & Norris Streets  
Philadelphia, Pa. 19122

Jerome B. Lando  
Case Western Reserve University  
Dept. of Macromolecular Science  
University Circle  
Cleveland, Ohio 44106

Morton Litt  
Case Western Reserve University  
Dept. of Macromolecular Science  
University Circle  
Cleveland, Ohio 44106

Dick Madden  
Bolt, Beranek, Newman  
Cambridge, Mass. 02134

Rudolph J. Marcus  
Office of Naval Research Branch Office  
1030 East Green Street  
Pasadena, Calif. 91106

G. Kirby Miller  
GTE - Sylvania  
Box 188  
Mountain View, Calif. 94042

Jean A. Montemarano  
Naval Ship R & D Center  
Annapolis, Maryland 21402

Fredrick Mopsik  
National Bureau of Standards  
Polymers Division  
Washington, D. C. 20234

Preston V. Murphy  
Thermo Electron, S.A.  
Infanta Carlota 32  
Barcelona, SPAIN

Raymond Naar  
Tufts University  
Pearson Laboratory  
Medford, Mass. 02155

George Neece  
Office of Naval Research  
800 N. Quincy Street  
Arlington, Va. 22044

John H. Parker  
903 Meadow Lane  
Vienna, Va. 22180

Leighton H. Peebles, Jr.  
Office of Naval Research  
495 Summer Street  
Boston, Mass. 02210

Robert J. Phelan, Jr.  
National Bureau of Standards  
Electromagnetics Division  
325 Broadway  
Boulder, Colorado 80302

Gustav R. Pfister  
Xerox Corporation  
Research Center  
Webster, New York 14580

Ted O. Poehler  
Johns Hopkins University  
Applied Physics Laboratory  
Baltimore, Maryland 21218

James M. Powers  
Naval Underwater Systems Center  
New London Lab  
New London, Conn. 06320

William M. Prest  
Xerox Corporation  
800 Phillips Road  
Webster, New York 14582

Peter F. Radice  
Pennwalt Corporation  
438 Springhouse Road  
King of Prussia, Pa. 19406

Joseph P. Reardon  
Naval Research Laboratory  
Code 6170  
Washington, D. C. 20375

Kennard Reynard  
Horizons Inc.  
23800 Mercantice Road  
Cleveland, Ohio 44060

John Ricca  
Army Materials & Mechanics Research Ctr.  
Watertown, Mass. 02172

D. C. Robinson  
National Bureau of Standards  
EM 219  
Washington, D. C. 20234

Steven Roth  
National Bureau of Standards  
Polymers Division  
Washington, D. C. 20234

Charles F. Rowell  
Office of Naval Research  
Chicago Branch Office  
536 S. Clark Street  
Chicago, Illinois 60605

Barrie S. H. Royce  
Princeton University  
Materials Laboratory  
D 416 Duffield Hall (E.Q.)  
Princeton, N. J. 08540

Robert E. Salomon  
Temple University  
Chemistry Dept.  
13th & Norris Streets  
Philadelphia, Pa. 19122

E. Sharp  
Night Vision Laboratory  
Ft. Belvoir, Va. 22060

Richard J. Shuford  
Army Materials & Mechanics Research Ctr.  
Arsenal Street  
Watertown, Mass. 02172

Joseph Simmons  
Catholic University  
Washington, D. C. 20017

Davis R. Squire  
U.S. Army Research Office  
Box CM, Duke Station  
Durham, N. C. 27706

Charles Smyth  
Princeton University  
Princeton, N. J. 08540

E. M. Stanley  
Naval Ship R & D Center  
Annapolis, Maryland 21401

Alan Taylor  
3M Company  
St. Paul Minn.

C. C. Walker  
Naval Sea Systems Command  
Dept. of the Navy  
Washington, D. C. 20362

Hugh Wright  
Bolt, Beranek, Newman  
Cambridge, Mass. 02134

Kenneth J. Wynne  
Office of Naval Research  
Chemistry Program  
800 N. Quincy Street  
Arlington, Va. 22044



**UNITED STATES DEPARTMENT OF COMMERCE**  
**National Bureau of Standards**  
Washington, D.C. 20234

LETTER OF INVITATION

We are in the process of organizing a symposium-workshop to be held at the National Bureau of Standards on April 15-16, 1975. The meeting is jointly sponsored by the Office of Naval Research, the Army Research Office and NBS.

The purpose of the meeting is to bring together scientists and program managers from DOD, university laboratories and industrial laboratories involved in research on and manufacture of piezoelectric and pyroelectric polymer materials and devices. We intend to exchange current information on research and development activities in order to stimulate new efforts in this field and promote the development and application of polymers for transducer applications.

We look forward to your reply to this invitation and hope you will be able to accept. Included is a list of persons who have been invited and we welcome the names of other key people whom you believe should also be included. General information about food, housing, transportation and meeting rooms will be sent to you at a later date along with a meeting schedule.

Sincerely yours,

MARTIN G. BROADHURST  
Chief, Bulk Properties Section  
Polymers Division

Enclosure



## Introduction

This report contains manuscripts of talks that were presented at a Symposium-Workshop on Piezoelectric Polymers which was held at the National Bureau of Standards, Gaithersburg, Maryland on April 15 and 16, 1975. The meeting was initiated by Dr. Kenneth Wynne, Chemistry Program Office of the Office of Naval Research\* and the program was arranged by Dr. Martin Broadhurst, Polymers Division, NBS. The meeting was cosponsored and supported by ONR, Arlington, Virginia, the Army Research Office, Durham, North Carolina, and NBS.

The purpose of this Symposium-Workshop was to bring together scientists and program managers from federal (primarily DoD), industrial, university, and other laboratories who are involved in the research on and manufacture of piezoelectric and pyroelectric polymer materials and devices, in order to exchange information about and stimulate further work on the new and rapidly developing measurement technology involving polymer transducers. This meeting is particularly important at this time because highly active polymer films are not yet available to device manufacturers in the U.S. or to potential users such as DoD. Potential manufacturers are reluctant to produce polymer films for this purpose because of uncertainty of their market value. Both manufacturers and users are reluctant to invest heavily in polymer transducers because of a lack of such important information as the nature of the underlying mechanism, transducer reliability and life-time, ways of optimizing polymer sensitivity and fabrication procedures.

---

\*This symposium is part of the ONR annual program review, the first session of which was held at ONR in Arlington, Virginia on April 14. Only those papers of most general interest in the area of piezoelectricity are included in this Proceeding and other papers dealing with potentially useful new polymers will be compiled and distributed separately.

Offsetting these uncertainties is the growing awareness that simplicity of fabrication, economy, flexibility, toughness and high sensitivity make polymers attractive candidates for novel devices. In fact, piezoelectric polymer headphones from Japan and pyroelectric polymer radiation sensors in the U.S. are already in commercial production and potential new applications ranging from patient pulse-monitoring transducers to ship hull coatings to make large aperture sonar antennas were discussed at the meeting.

Following a series of talks which are represented by the manuscripts on the following pages, a timely workshop discussion confirmed that many measurement and development problems are yet to be overcome.

In order to speed up distribution of these Proceedings, the following papers were reproduced as received from the authors with only minor modifications. Since these papers did not meet the uniformity requirements for reproduction as an official NBS publication, this report is to be considered as an informal account of the Symposium and will be distributed to Symposium attendees and other interested parties and to DoD as previously agreed.

Some of the work has been published previously elsewhere and some of the papers are being submitted by the authors for publication elsewhere.

References to information in this report should be made to:

Nat. Bur. Stand. (U.S.), Interagency Report,  
NBSIR 75-760, page number, (September 1975).

Copies in paper or microfiche form may be obtained from the National Technical Information Service, (NTIS), Springfield, Va. 22151.

Commercial materials are identified in this paper to adequately specify the experimental procedure. Such identification does not imply recommendation or endorsement by the National Bureau of Standards.

Eiichi Fukada and Mitsumasa Oshiki\*

The Institute of Physical and Chemical Research

Wako, Saitama 351, Japan

### Abstract

The mathematical expressions for the complex piezoelectric stress-constant,  $e_{31} = e_{31}' - ie_{31}''$ , the complex electrostrictive constant,  $\kappa_{31} = \kappa_{31}' - i\kappa_{31}''$ , and the complex dielectric constant,  $\epsilon_3 = \epsilon_3' - i\epsilon_3''$ , are derived by non-equilibrium thermodynamics. The basic assumption is that the orientation of dipoles produces the residual polarization. The determination of these quantities has been made for polyvinylidene fluoride films over a temperature range from  $-100^\circ\text{C}$  to  $100^\circ\text{C}$  at a frequency of 20 Hz. The residual polarization after heat treatment is found to be constant independent of temperature.

### Introduction

The origin of the piezoelectricity in the stretched and polarized films of polyvinylidene fluoride has been discussed by many investigators.<sup>1-11</sup> A plausible explanation is that the polarization originates in the stress-induced reorientation of dipoles which have been preferentially alligned in the direction normal to the film surface due to stretching and subsequent poling procedures. Another mechanism proposed is that the polarization is induced by

---

\*Department of Physics, Gakushuin University, Mejiro, Tokyo

the inhomogeneous strain coupled with the distribution of space charge inside the film.

In this paper first we shall derive theoretical expressions for the piezoelectric constant and electrostrictive constant in the electrified polymer and then present some experimental data on the temperature variation of some physical properties related to piezoelectricity for polyvinylidene fluoride electret films.

### Theory

It has been demonstrated that the piezoelectric and electrostrictive constants of polymers are complex quantities and are represented as  $e = e' - ie''$  and  $\kappa = \kappa' - i\kappa''$ . The piezoelectric stress-constant,  $e$ , can be determined either by measuring the polarization,  $P$ , under a given strain  $S$ , under short-circuited conditions,  $\left(\frac{\partial P}{\partial S}\right)_E$ , or by measuring the stress,  $T$ , under a given electric field,  $E$ , at the clamped condition,  $-\left(\frac{\partial T}{\partial E}\right)_S$ . In the equilibrium state, the equality of these two derivatives has been proved from the thermodynamic principles.<sup>12</sup>

The electrostrictive constant is determined either by measuring the stress proportional to the square of the electric field,  $-\frac{1}{2}\left(\frac{\partial^2 T}{\partial E^2}\right)_S$ , or by measuring the strain dependence of the dielectric constant,  $\left(\frac{\partial \epsilon}{\partial S}\right)_E$ . The equality of the equilibrium values of the electrostrictive constant derived from these two different observations has also been proved by the thermodynamic principles.<sup>13</sup>

Now, the piezoelectric constant for polymers is defined as a complex quantity, i.e.,  $e = e' - ie''$ . The equality of this complex quantity measured by the direct and converse piezoelectric effects, is not self-evident. The equality of the complex electrostrictive constants determined by the two different methods, is not proved, either.

In order to derive the theoretical expressions for  $e$  and  $\kappa$  as complex quantities, we have to use non-equilibrium thermodynamics.<sup>14</sup> First we shall introduce the Helmholtz free energy,  $F$ , as follows

$$F = \frac{1}{2} G^P (S - \nu P^2)^2 + \frac{1}{2} \alpha (P - P_0 \xi)^2 + \frac{1}{2} \beta (P - P_0 \zeta)^2 + \frac{1}{2} \lambda \xi^2. \quad (1)$$

The first term shows the elastic energy taking into account the electrostrictive strain,  $\nu P^2$ , which is proportional to the square of polarization  $p$ .  $G^P$  is the elastic constant at  $P=0$ . The second and third terms show the dielectric energy involving two internal variables  $\xi$  and  $\zeta$ .  $\xi$  represents an ordering parameter which changes slowly with time during the poling process under a static electric field.  $P_0 \xi$  is approximately the residual polarization,  $P_r$ , after poling.  $P_0$  is the polarization per unit of  $\xi$  or  $\zeta$ . Since static polarization in an electret decays with time very gradually, the state with  $P_r$  is not thermodynamically stable. Thus we introduce the fourth term which represents the increase of free energy due to  $\xi$ . The third term in  $F$  is the dielectric energy, which involves another ordering parameter,  $\zeta$ , which varies in time scale of a rate comparable

with the period of the alternating excitation, under which the dielectric, piezoelectric and electrostrictive measurements are made. When an external excitation is not present,  $\zeta$  is given by  $P_r/P_0$ . In eq. 1,  $\alpha$  and  $\beta$  are coefficients related to the dielectric constant.

If we expand the first term of eq. 1 and neglect the  $P^4$  term, then we have

$$F = \frac{1}{2}G^P S^2 + \frac{1}{2}\alpha (P-P_0\xi)^2 + \frac{1}{2}\beta (P-P_0\zeta)^2 - \gamma SP^2 + \frac{1}{2}\lambda\xi^2 \quad (2)$$

where  $\gamma = G^P \nu$ .

From eq. 2 we derive the stress,  $T$ , and the field,  $E$ , as

$$T = \left( \frac{\partial F}{\partial S} \right)_{P, \xi, \zeta} = G^P S - \gamma P^2 \quad (3)$$

$$E = \left( \frac{\partial F}{\partial P} \right)_{S, \xi, \zeta} = \alpha (P-P_0\xi) + \beta (P-P_0\zeta) - 2\gamma SP \quad (4)$$

The affinity,  $A_\zeta$ , conjugate to  $\zeta$  is given by

$$A_\zeta = - \left( \frac{\partial F}{\partial \zeta} \right)_{S, P, \xi} = \beta P_0 (P-P_0\zeta). \quad (5)$$

Solving for  $P$  from eq. 4, putting  $E=0$  and  $T=0$ , and using the approximation  $2\gamma S/(\alpha+\beta) \ll 1$ , we find that the residual polarization,  $P_r$ , and the residual strain,  $S_r$ , are

$$P_r = P_0 \xi_0 = P_0 \zeta_0, \quad (6)$$

$$S_r = \gamma P_r^2 / G^P. \quad (7)$$

Now we shall consider the case when an external excitation is applied to a sample which is specified by  $P_r$ ,  $S_r$ ,  $\xi_0$ , and  $\zeta_0$ . Since  $\xi$  changes only during the poling process,  $\zeta$  will be considered a variable during the measurement. The polarization,  $P$ , and the stress,  $T$ , are expanded as functions of  $E$ ,  $S$ , and  $\zeta$  at  $P_r$ ,  $S_r$ ,  $\xi_0$  and  $\zeta_0$ . The results are

$$\Delta P = \frac{E}{\alpha+\beta} + \frac{2\gamma P_r}{\alpha+\beta} \Delta S + \frac{\beta P_0}{\alpha+\beta} \Delta \zeta + \frac{2\gamma}{(\alpha+\beta)^2} E \Delta S + \frac{2\gamma \beta P_0}{(\alpha+\beta)^2} \Delta \zeta \Delta S \quad (8)$$

$$\begin{aligned}
T = & \left( G^P - \frac{4\gamma^2 P_r^2}{\alpha+\beta} \right) \Delta S - \frac{2\gamma P_r}{\alpha+\beta} E - \frac{2\gamma\beta P_o P_r}{\alpha+\beta} \Delta\zeta \\
& - \frac{4\gamma^3 P_r^2}{(\alpha+\beta)^2} \Delta S^2 - \frac{\gamma}{(\alpha+\beta)^2} E^2 - \frac{\gamma\beta^2 P_o^2}{(\alpha+\beta)^2} \Delta\zeta^2 \\
& - \frac{8\gamma^2 P_r}{(\alpha+\beta)^2} E\Delta S - \frac{8\gamma^2\beta P_o P_r}{(\alpha+\beta)^2} \Delta S\Delta\zeta - \frac{2\gamma\beta P_o}{(\alpha+\beta)^2} E\Delta\zeta \quad (9)
\end{aligned}$$

In eqs 8 and 9, the expression for  $\Delta\zeta$  is unknown.

The affinity,  $A_\zeta$ , is zero when  $\zeta = \zeta_o$ . The temporal change of  $\zeta$  is given by the following equation, introducing a kinetic coefficient  $\mu$ ,

$$\dot{\Delta\zeta} = \mu A_\zeta \quad (10)$$

Substituting eq 5 into eq. 10 we have

$$\begin{aligned}
\dot{\Delta\zeta} = & \beta\mu P_o \left\{ \frac{E}{\alpha+\beta} + \frac{2\gamma P_r}{\alpha+\beta} \Delta S + \frac{\beta P_o}{\alpha+\beta} \Delta\zeta \right. \\
& \left. + \frac{2\gamma}{(\alpha+\beta)^2} E\Delta S + \frac{2\gamma\beta P_o}{(\alpha+\beta)^2} \Delta\zeta\Delta S - P_o\Delta\zeta \right\} \quad (11)
\end{aligned}$$

For the sinusoidal excitations, we put

$$\begin{aligned}
E &= E_A (e^{i\omega_E t} + e^{-i\omega_E t}) \\
\Delta S &= S_A (e^{i\omega_S t} + e^{-i\omega_S t}) \quad (12)
\end{aligned}$$

Combining eqs. 10, 11 and 12, we have

$$\begin{aligned}
\Delta\zeta = & \frac{E_A e^{i\omega_E t}}{\alpha P_o (1+i\omega_E \tau)} + \frac{2\gamma P_r S_A e^{i\omega_S t}}{\alpha P_o (1+i\omega_S \tau)} \\
& + \frac{2\gamma S_A E_A e^{i(\omega_E + \omega_S)t}}{\alpha P_o (\alpha+\beta) \{1+i(\omega_E + \omega_S)\tau\}} \left( 1 + \frac{\beta}{\alpha} \frac{1}{1+i\omega_E \tau} \right) \\
& + \frac{2\gamma S_A E_A e^{i(\omega_E - \omega_S)t}}{\alpha P_o (\alpha+\beta) \{1+i(\omega_E - \omega_S)\tau\}} \left( 1 + \frac{\beta}{\alpha} \frac{1}{1+i\omega_E \tau} \right) \\
& + \Delta\bar{\zeta} \quad (13)
\end{aligned}$$

where  $\Delta\bar{\zeta}$  represents the complex conjugate of the previous four terms. We have introduced a relaxation time,  $\tau$ , which is defined by

$$\tau = \frac{\alpha + \beta}{\alpha\beta\mu P_0^2} \quad (14)$$

Introducing eq. 12 and 13 into eq. 8,

$$\begin{aligned} \Delta P = & \frac{1}{\alpha + \beta} \left( 1 + \frac{\beta}{\alpha} \frac{1}{1 + i\omega_E \tau} \right) E_A e^{i\omega_E t} \\ & + \frac{2\gamma P_r}{\alpha + \beta} \left( 1 + \frac{\beta}{\alpha} \frac{1}{1 + i\omega_E \tau} \right) S_A e^{i\omega_S t} \\ & + \frac{2\gamma}{(\alpha + \beta)^2} \left( 1 + \frac{\beta}{\alpha} \frac{1}{1 + i\omega_E \tau} \right) \left\{ 1 + \frac{\beta}{\alpha} \frac{1}{1 + i(\omega_E + \omega_S) \tau} \right\} E_A S_A e^{i(\omega_E + \omega_S) t} \\ & + \frac{2\gamma}{(\alpha + \beta)^2} \left( 1 + \frac{\beta}{\alpha} \frac{1}{1 + i\omega_E \tau} \right) \left\{ 1 + \frac{\beta}{\alpha} \frac{1}{1 + i(\omega_E - \omega_S) \tau} \right\} E_A S_A e^{i(\omega_E - \omega_S) t} \\ & + \Delta\bar{P} \end{aligned} \quad (15)$$

Using  $P_A^{\omega_E}$  to denote the amplitude of  $\Delta P$  with the angular frequency  $\omega_E$ , the complex susceptibility is given by

$$\eta^* = \frac{P_A^{\omega_E}}{E_A} = \frac{1}{\alpha + \beta} \left( 1 + \frac{\beta}{\alpha} \frac{1}{1 + i\omega_E \tau} \right) \quad (16)$$

and the complex dielectric constant is given by

$$\epsilon^* = 1 + \frac{4\pi}{\alpha + \beta} \left( 1 + \frac{\beta}{\alpha} \frac{1}{1 + i\omega_E \tau} \right). \quad (17)$$

Using  $P_A^{\omega_S}$  to denote the amplitude of  $\Delta P$  with angular frequency  $\omega_S$ , the complex piezoelectric stress-constant is given by

$$e^* = \frac{P_A^{\omega_S}}{S_A} = \frac{2\gamma P_r}{\alpha + \beta} \left( 1 + \frac{\beta}{\alpha} \frac{1}{1 + i\omega_S \tau} \right) \quad (18)$$

Using  $P_A^+$ ,  $P_A^-$  to denote the amplitudes of  $\Delta P$  with angular frequencies  $(\omega_E + \omega_S)$  and  $(\omega_E - \omega_S)$ , the complex electrostrictive constant is given by

$$\begin{aligned}
(\kappa^\pm)^* &= 4\pi P_A^\pm / E_A S_A \\
&= \frac{8\pi\gamma}{(\alpha+\beta)^2} \left\{ 1 + \frac{\beta}{\alpha} \frac{1}{1+i\omega_E\tau} \right\} \left\{ 1 + \frac{\beta}{\alpha} \frac{1}{1+i(\omega_E \pm \omega_S)\tau} \right\} \quad (19)
\end{aligned}$$

With static strain ( $\dot{\omega}_S=0$ ), the electrostrictive constant is expressed as

$$\kappa^* = \frac{8\pi\gamma}{(\alpha+\beta)^2} \left( 1 + \frac{\beta}{\alpha} \frac{1}{1+i\omega_E\tau} \right)^2 \quad (20)$$

Next, from eq. 9, we obtain

$$\begin{aligned}
T &= G^P - \left\{ \frac{4\gamma^2 P_r^2}{\alpha+\beta} \left( 1 + \frac{\beta}{\alpha} \frac{1}{1+i\omega_S\tau} \right) \right\} S_A e^{i\omega_S t} \\
&\quad - \frac{2\gamma P_r}{\alpha+\beta} \left( 1 + \frac{\beta}{\alpha} \frac{1}{1+i\omega_E\tau} \right) E_A e^{i\omega_E t} \\
&\quad - \frac{\gamma}{(\alpha+\beta)^2} \left( 1 + \frac{\beta}{\alpha} \frac{1}{1+i\omega_E\tau} \right) E_A^2 e^{2i\omega_E t} \\
&\quad + \tilde{T} \quad (21)
\end{aligned}$$

where  $\tilde{T}$  denotes the complex conjugates and higher terms.

Using  $T_A^{\omega_S}$  to denote the amplitude of stress with the angular frequency  $\omega_S$ , the complex elastic constant is given by

$$(G^E)^* = \frac{T_A^{\omega_S}}{S_A} = G^P - \frac{4\gamma^2 P_r^2}{\alpha+\beta} \left( 1 + \frac{\beta}{\alpha} \frac{1}{1+i\omega_S\tau} \right) \quad (22)$$

Using  $T_A^{\omega_E}$  to denote the amplitude of stress with the angular frequency  $\omega_E$ , the complex piezoelectric stress-constant is given by

$$e^* = - \frac{T_A^{\omega_E}}{E_A} = \frac{2\gamma P_r}{\alpha+\beta} \left( 1 + \frac{\beta}{\alpha} \frac{1}{1+i\omega_E\tau} \right) \quad (23)$$

Using  $T_A^{2\omega_E}$  to denote the amplitude of stress with the angular frequency  $2\omega_E$ , the complex electrostrictive constant is

$$\kappa^* = - \frac{8\pi T_A^{2\omega_E}}{E_A^2} = \frac{8\pi\gamma}{(\alpha+\beta)^2} \left(1 + \frac{\beta}{\alpha} \frac{1}{1+i\omega_E\tau}\right)^2 \quad (24)$$

Eq. 18 and eq. 23 show that the values of  $e^*$  derived from both the direct piezoelectric effect and the converse piezoelectric effect are equal complex quantities if the exciting frequencies are the same. Eq. 20 and eq. 24 show that  $\kappa^*$  derived from the strain-dependence of the dielectric constant is equal as a complex quantity to that derived from the component of stress proportional to square of the electric field.

The following relations, which are known to hold for equilibrium quantities, also apply to complex quantities.

$$(GE)^* = G^P - \frac{(e^*)^2}{\eta^*} \quad (25)$$

$$P_r = \frac{e^*(\epsilon^*-1)}{\kappa^*} \quad (26)$$

The latter equation is used to calculate  $P_r$  from experimental results.

### Experiment

We used polyvinylidene fluoride films subjected to the three different treatments shown in Table 1. The original film was supplied by the Kureha Chemical Co.. The (n-n) samples were prepared by annealing non-poled commercial film at 135°C for 12 hours. The (s-n) samples were prepared by stretching the (n-n) samples to 5 times their original length and annealing them at 130°C for 12 hours. The (s-p) samples were prepared by poling the (s-n) film at 85°C for 2 hours with a static electric field of 500 kV/cm. Infrared absorptions observed at 510  $\text{cm}^{-1}$  and 530  $\text{cm}^{-1}$  shows

that the (n-n) samples contain both I and II crystalline forms, but that the (s-n) and (s-p) samples contain almost entirely I crystalline form. The dimensions of the test sample are about 15x10x0.05 mm. The length is the direction of elongation. Silver was evaporated as electrodes on the central area, 8x5 mm, on both surfaces of the sample.

A schematic diagram of experimental apparatus is shown in Fig. 1. Both ends of the sample are clamped inside a thermostat so that the uniaxial tension is applied in the direction of length, which accords with the direction of elongation. An a.c. voltage with the angular frequency  $\omega$  is applied between the electrodes of the sample, and the resulting tensile stress of the sample in the length direction is detected by a PZT ceramic element. The output of the PZT detector is led to a charge amplifier and four phase sensitive detectors, whose reference voltages have an angular frequency of  $\omega$  or  $2\omega$  and a phase angle of 0 or  $\pi/2$  with respect to the output voltage of oscillator. The outputs from these phase sensitive detectors give  $e'$ ,  $e''$ ,  $\kappa'$ , and  $\kappa''$ . The real and imaginary components of the dielectric constant,  $\epsilon'$ ,  $\epsilon''$ , were also determined simultaneously with the above quantities.

When the electric field  $E_3$  is applied across the thickness of the film, the tensile stress  $T_1$  produced in the stretched direction is given by

$$T_1 = -e_{31}E_3 - (\kappa_{31} + \sigma\epsilon_3)E_3^2/8\pi$$

where the third term on the right hand side represents the Maxwell stress in the film and  $\sigma$  is the Poisson's ratio.

Thus,  $\epsilon_{31} = \epsilon_{31}' - i\epsilon_{31}''$ ,  $\kappa_{31} = \kappa_{31}' - i\kappa_{31}''$ , and  $\epsilon_3 = \epsilon_3' - i\epsilon_3''$  were determined simultaneously as functions of temperature at a frequency of 20 Hz.

Fig. 2 shows the temperature dependence of  $\epsilon_3'$  and  $\epsilon_3''$  for three kinds of samples. It is seen that the stretching of the sample increases  $\epsilon_3'$  and shifts the dispersion to a higher temperature, and that the poling process decreases  $\epsilon_3'$ . This dispersion is caused by the glass transition in <sup>the</sup> non-crystalline phase of polyvinylidene fluoride.

Fig. 3 shows the temperature dependence of  $\kappa_{31}'$  and  $\kappa_{31}''$  for the three kinds of samples. As with  $\epsilon_3'$ ,

stretching increases  $\kappa_{31}'$  and the poling decreases  $\kappa_{31}'$ . According to eq. 19,  $\kappa$  is the variation with strain of the dielectric constant. The density of the sample is changed by the strain. The variation of the dielectric constant due to the variation of density can be calculated from Clausius-Mossotti's equation.

This correction term was added to the observed value of  $\kappa$  in the subsequent calculations of the residual polarization.

Fig. 4 shows the temperature dependence of  $\epsilon_{31}'$  and  $\epsilon_{31}''$  for the stretched and poled sample during the increase of the temperature. The second run of the measurements gave decreased values for  $\epsilon_{31}'$ , but the third run gave the same results as the second run.

Using these experimental data, the residual polarization  $P_r$  was calculated according to eq. 26. The temperature

dependence of  $P_r$  is given in Fig. 5. For the first run, the decrease of  $P_r$  was observed at the glass transition temperature. However, at the second and third runs,  $P_r$  was almost constant independent of temperature. The decrease of  $P_r$  during the first run may indicate a weak polarization in the non-crystalline phase. The persistent  $P_r$  observed at the second and third run may be caused by a strong polarization associated with the crystalline phase.

We have undertaken the measurements of  $e_{31}$ ,  $\kappa_{31}$  and  $\epsilon_3$  during the poling process. If a d.c. bias field,  $E_D$ , is applied to the film, the relation between the stress  $T_1$  and the field  $E_3$  is given by the following formula.

$$T_1 = -e_{31}(E_D + E_3) - \frac{1}{8\pi} (\kappa_{31} + \sigma\epsilon_3)(E_D + E_3)^2 \quad (27)$$

From eq. 27, we can see that there is a contribution to the apparent piezoelectric constant due to the presence of  $E_D$  in addition to the ordinary piezoelectric constant  $e_{31}$ . This piezoelectric constant observed with a d.c. bias field,  $e_{ob}$ , is given by

$$e_{ob} = - \left( \frac{\partial T_1}{\partial E_3} \right)_S = e_{31} + \frac{E_D}{4\pi} (\kappa_{31} + \sigma\epsilon_3). \quad (28)$$

Fig. 6 shows the time variation of  $e_{ob}'$  and  $e_{ob}''$  during poling at 85°C with a field of 200 kV/cm. The lower figure shows the values of  $e_{31}'$  and  $e_{31}''$  derived from eq. 28. It is seen that the piezoelectric e-constant increases in two steps with relaxation times of approximately 1 minute and 100 minutes.

Fig. 7 shows the temporal change of  $\kappa_{31}$  and  $\epsilon_3$  determined simultaneously with  $e_{ob}$ . It is seen that  $\kappa_{31}$  and

$\epsilon_3$  decreases in two steps with relaxation times of approximately 1 minute and 100 minutes.

Fig. 8 shows the temporal change of  $P_r$  calculated from  $e_{31}$ ,  $\kappa_{31}$ , and  $\epsilon_3$  using eq. 26. It is obvious that  $P_r$  increases in two steps with relaxation times of approximately 1 minute and 100 minutes. We suppose that the first step with a relaxation time of about 1 minute may be due to the formation of polarization in the non-crystalline phase either by dipole orientation or by space charge injection. The following step may be due to the formation of polarization in the crystalline phase or at the crystal boundary surfaces, where the reorientation of dipoles or the trapping of charge is induced.

Fig. 9 illustrates the decay of the piezoelectric d-constant of electretized polyvinylidene fluoride films left at room temperature. After an initial decay with a relaxation time of approximately 5 days, the d-constant remains unchanged for about 10 months. The persisting and constant piezoelectric effect could be caused by the residual polarization associated with the crystalline phase of the polymer.

## Summary

The mathematical expressions for the piezoelectric stress-constant,  $e_{31}$ , the electrostrictive constant,  $\kappa_{31}$ , and the dielectric constant,  $\epsilon_3$ , all as complex quantities, have been derived by means of non-equilibrium thermodynamics on the assumption that the dipole orientation produces a residual polarization. The temperature dependence of these quantities for electretized polyvinylidene fluoride films has been experimentally determined at the same frequency of 20 Hz over a temperature range from  $-100^\circ\text{C}$  to  $100^\circ\text{C}$ . The residual polarization calculated from these experimental data is about  $10^3 \text{esu/cm}^2$  independent of temperature. This polarization probably originates from the aligned dipoles associated with <sup>the</sup> crystalline phase. Measurements during poling process show a gradual increase of the residual polarization.

## References

1. R. Hayakawa and Y. Wada, *Adv. Polym. Sci.* 11, 1, (1973)
2. H. Kawai, *Japan. J. Appl. Phys.* 8, 975, (1969)
3. M. Oshiki and E. Fukada, *J. Mat. Sci.* 10, 1, (1975)
4. M. Tamura, K. Ogasawara, N. Ono, and S. Hagiwara, *J. Appl. Phys.* 45, 3768, (1974)
5. N. Murayama and M. Segawa, *J. Petroleum Soc. Japan* 18, 77, (1975) (in Japanese)
6. M. C. Broadhurst, C. G. Malmburg, F. I. Mopsik and W. P. Harris, *Electrets, Charge Storage and Transport in Dielectrics* (Ed. M. M. Perlman, The Electrochemical Society) p.492, (1973)
7. J. Cohen, S. Edelman and C. F. Vezzetti, *ibid* p.505 (1973)
8. G. Dreyfus and J. Lewiner, *ibid* p.517 (1973)
9. H. Sussner, D. Michas, A. Assfalg, S. Hunklinger and K. Dransfeld, *Physics Letters* 45A, 475, (1973)
10. J. G. Bergman Jr., J. H. McFee, and G. R. Crane, *Appl. Phys. Letters* 18, 203, (1971)
11. G. Pfister and M. A. Abkonitz, *J. Appl. Phys.* 45, 1001, (1974)
12. J. F. Nye, *Physical Properties of Crystals*, Oxford Univ. Press (1957)
13. W. P. Mason, *Piezoelectric Crystals and their Application to Ulltasonics* D. van Nostrand (1950)
14. S. R. DeGroot and P. Mazur, *Non-equilibrium thermodynamics*, North Holland Co. (1962)

Table 1

Sample	Treatment
n-n	as-received film was annealed at 130°C for 12 hrs
s-n	n-n film was stretched by 5 times at 65°C and annealed at 130°C for 12 hrs
s-p	s-n film was polarized at 85°C for 2 hrs with a static electric field 500 kV/cm

## Figure Captions

Fig. 1 The schematic diagram of the apparatus for determining the dielectric constant  $\epsilon = \epsilon' - i\epsilon''$ , the piezoelectric stress-constant,  $e = e' - ie''$ , and the electrostrictive constant,  $\kappa = \kappa' - i\kappa''$ , at a frequency of 20 Hz and over a temperature range from  $-100^\circ\text{C}$  to  $100^\circ\text{C}$ .

Fig. 2 The temperature dependence of the dielectric constant,  $\epsilon_3 = \epsilon_3' - i\epsilon_3''$ , for differently treated films of polyvinylidene fluoride (as to notations, see Table 1)

Fig. 3 The temperature dependence of the electrostrictive constant,  $\kappa_{31} = \kappa_{31}' - i\kappa_{31}''$ , for films of polyvinylidene fluoride.

Fig. 4 The temperature dependence of the piezoelectric stress-constant,  $e_{31} = e_{31}' - ie_{31}''$  for an elongated and polarized film of polyvinylidene fluoride. After the first run of measurement, during which the temperature is increased from  $-100^\circ\text{C}$  to  $100^\circ\text{C}$ , the magnitudes of  $e_{31}'$  and  $e_{31}''$  decreased, but the second and third runs of measurement gave the same results.

Fig. 5 The temperature dependence of the residual polarization,  $P_r = e_{31}(\epsilon_3 - 1)/\kappa_{31}$ , for an electretized film of polyvinylidene fluoride. After the first run of measurement,  $P_r$  decreased but the second and third runs gave the same results, where  $P_r$  was independent of temperature.

Fig. 6 The time dependence during the poling process of about 10 hours of the piezoelectric stress-constant,  $e_{ob} = e_{ob}' - ie_{ob}'' = e_{31} + (\kappa_{31} + \sigma\epsilon_3)E_D/4\pi$ , apparently observed under a d.c. bias field  $E_D$ . The values of  $e_{31} = e_{31}' - ie_{31}''$  were corrected using the values of  $\kappa_{31}$  and  $\epsilon_3$  shown in Fig. 7. The poling field  $E_D$  is 200 KV/cm and the poling temperature is 85°C.

Fig. 7 The time dependence during the poling process of about 10 hours of the electrostrictive constant,  $\kappa_{31} = \kappa_{31}' - i\kappa_{31}''$ , and the dielectric constant,  $\epsilon_3 = \epsilon_3' - i\epsilon_3''$ .

Fig. 8 The time dependence during the poling process of about 10 hours of the residual polarization calculated from  $P_r = e_{31}(\epsilon_3 - 1)/\kappa_{31}$ .

Fig. 9 The aging of the piezoelectric strain-constant,  $d_{31} = d_{31}' - id_{31}''$ , for elongated and polarized films of polyvinylidene fluoride for a period of 300 days.

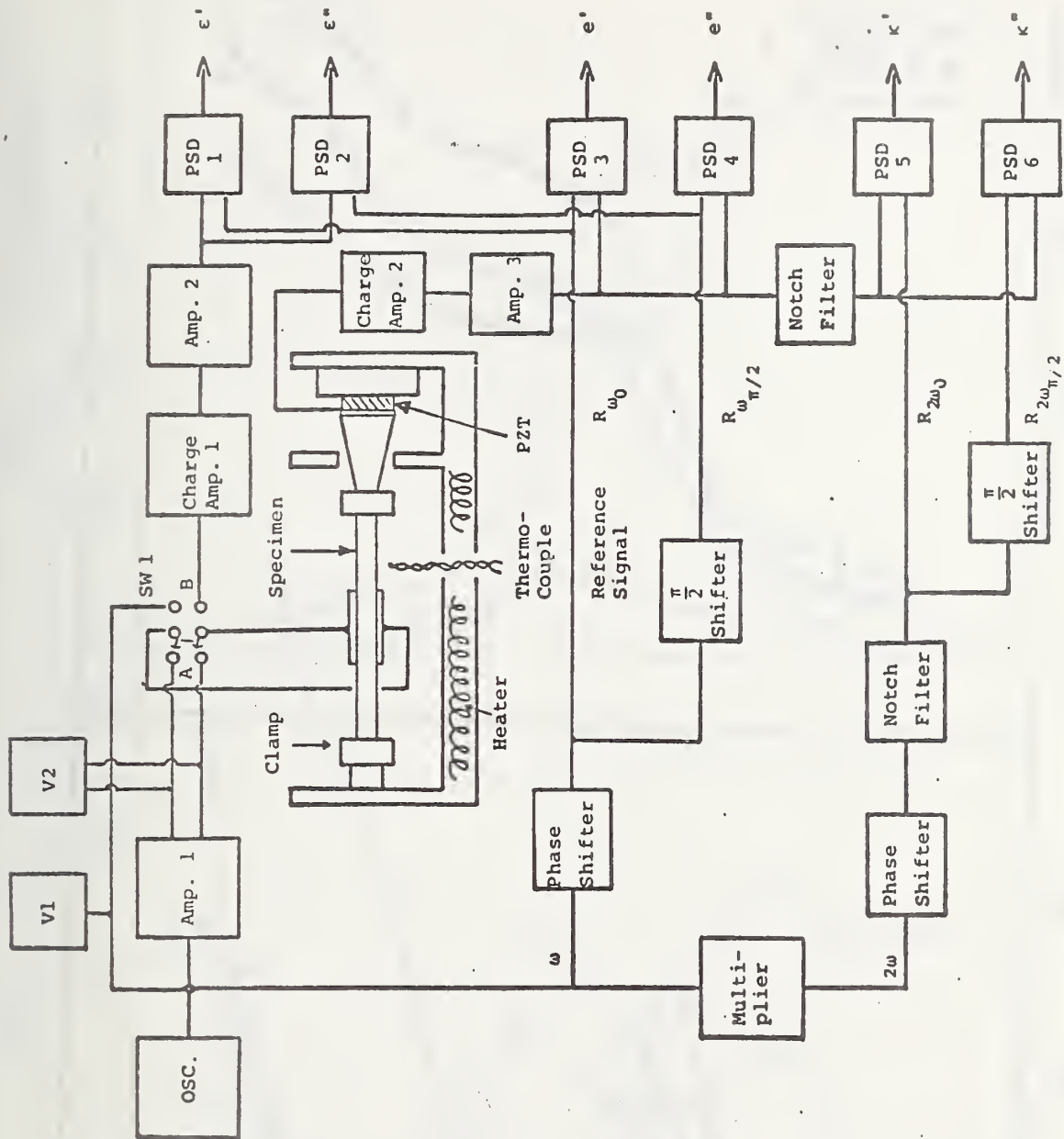
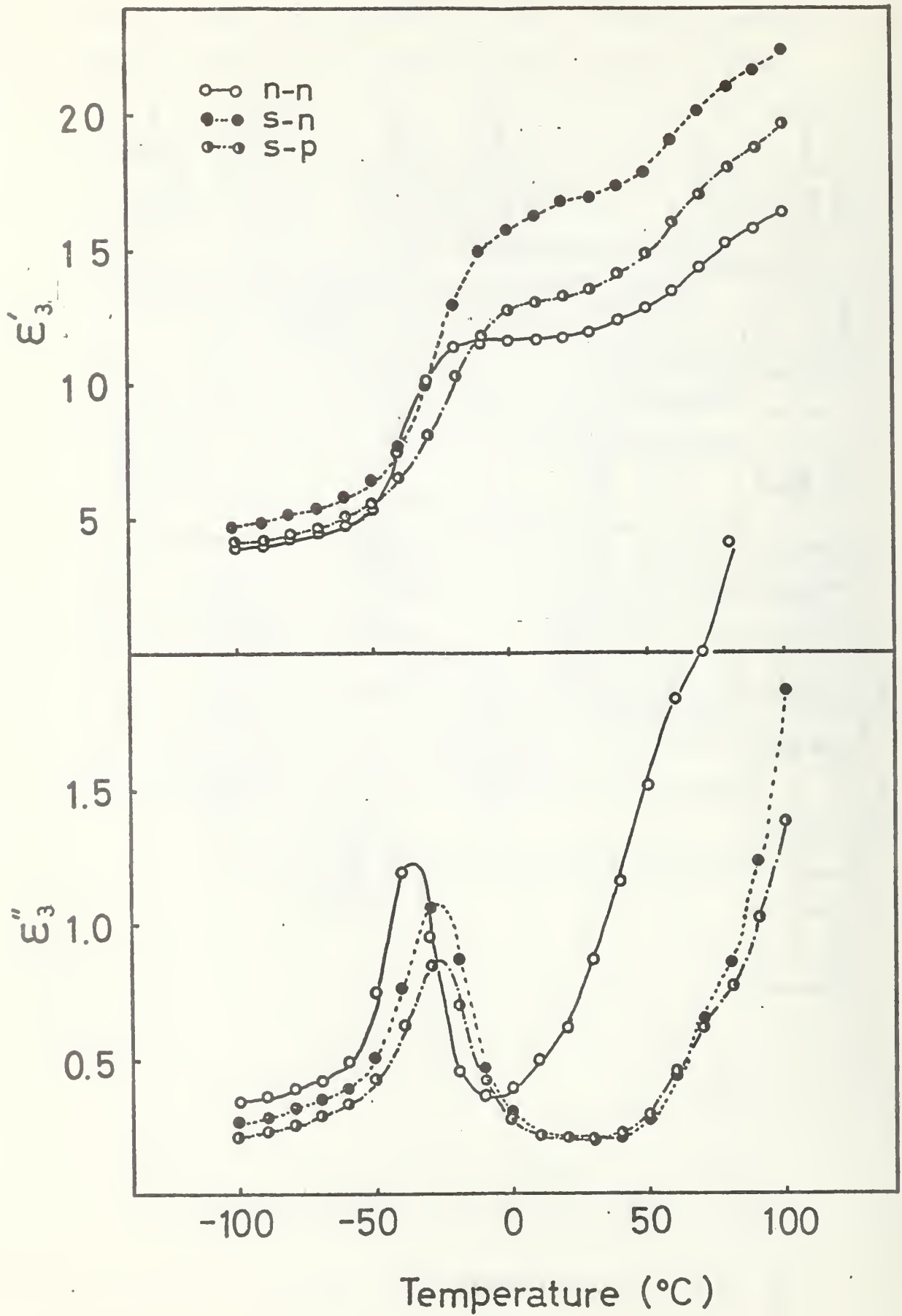


Fig. 1



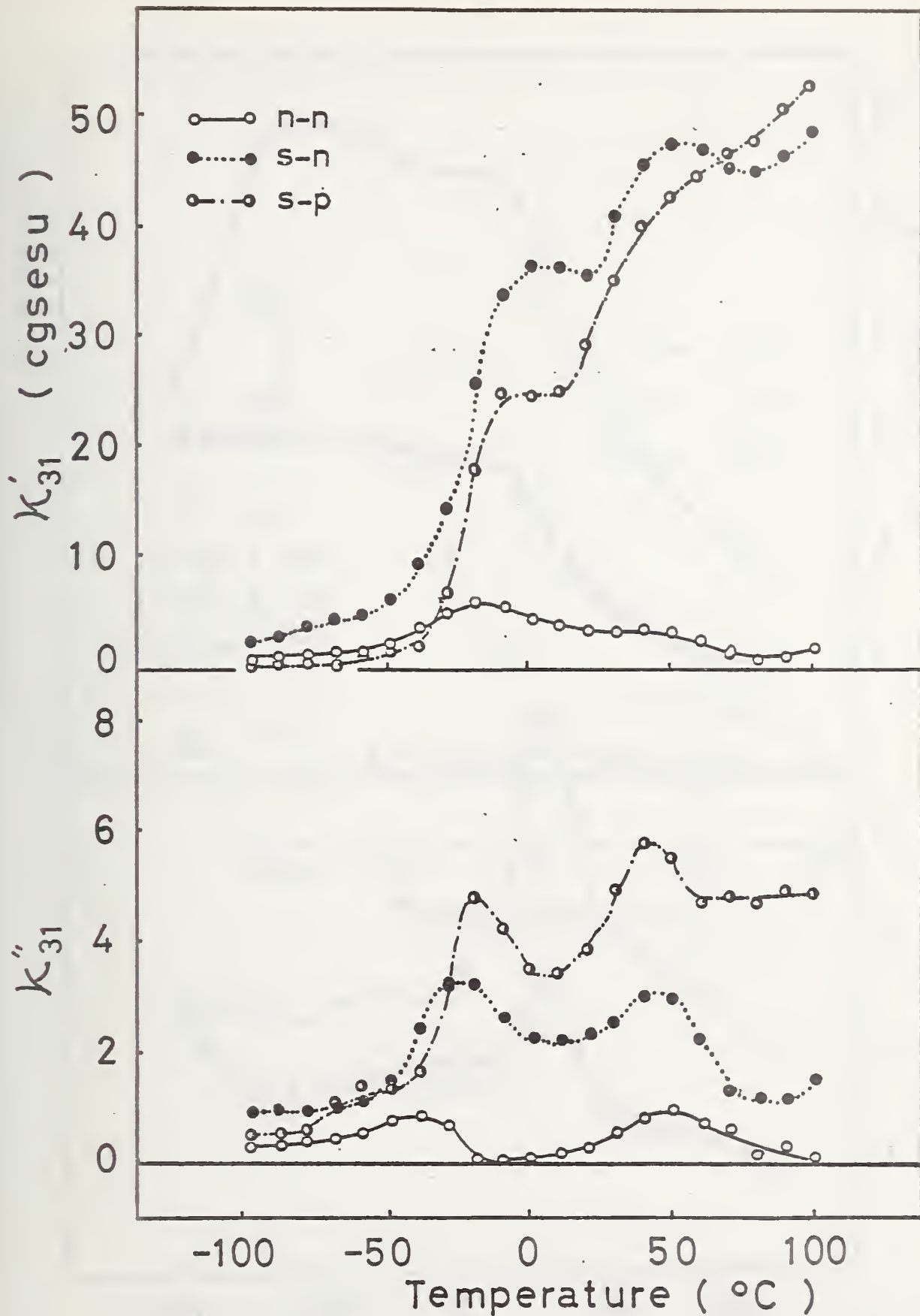
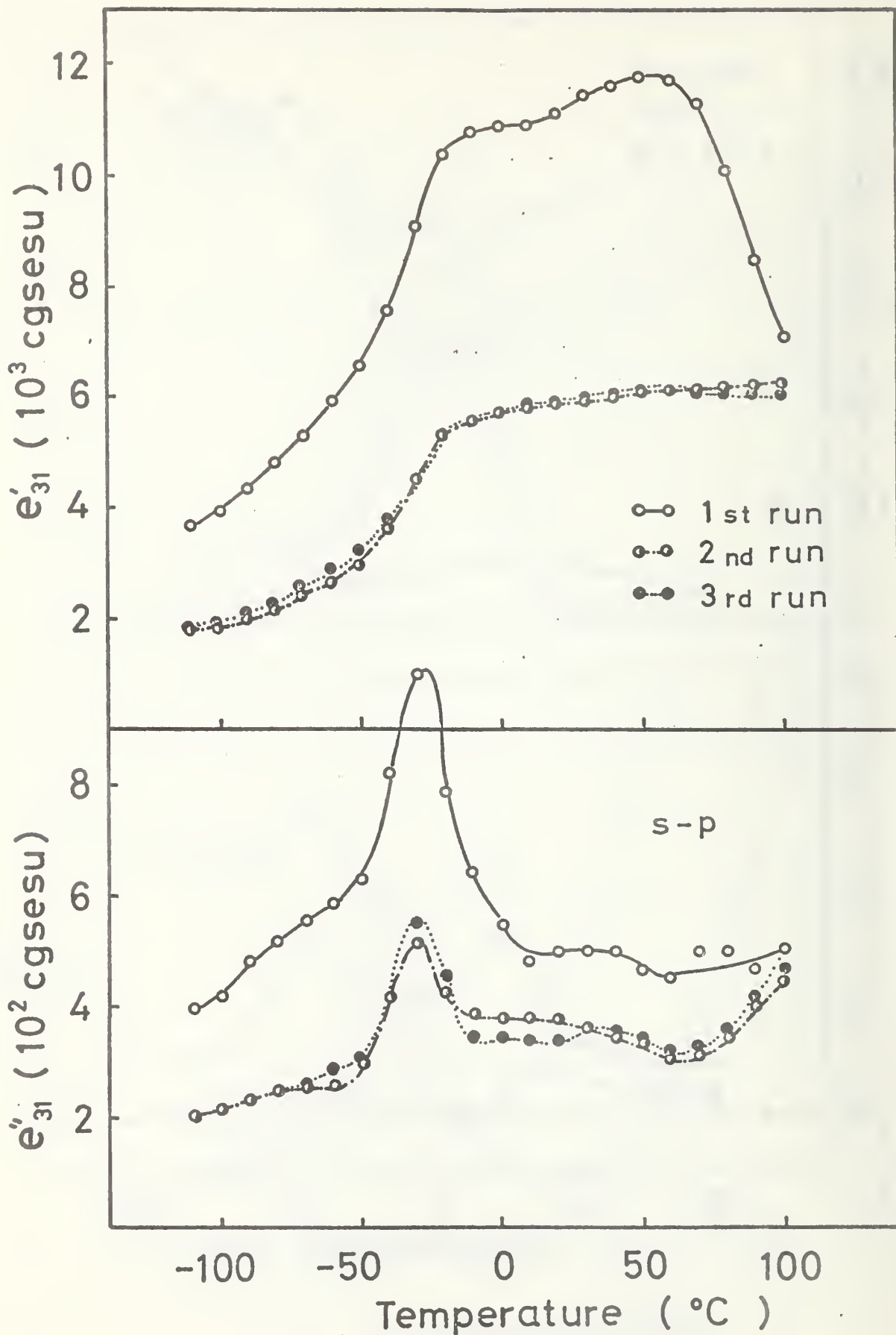


Fig. 3



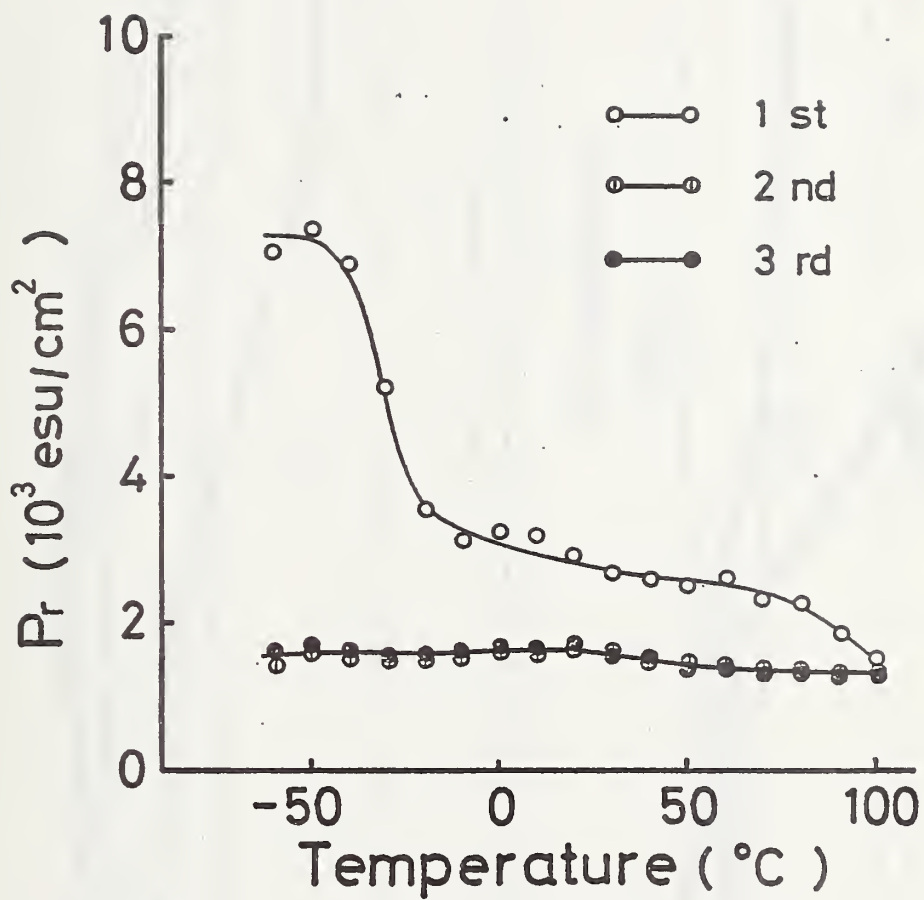


Fig. 5

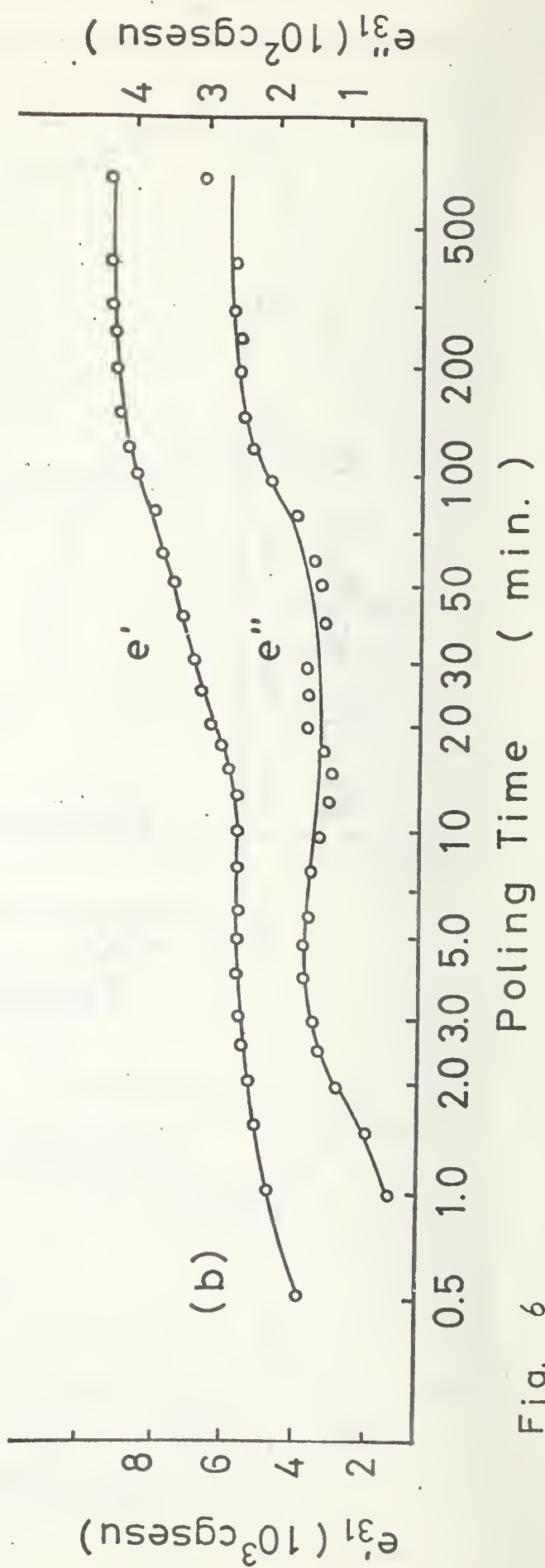
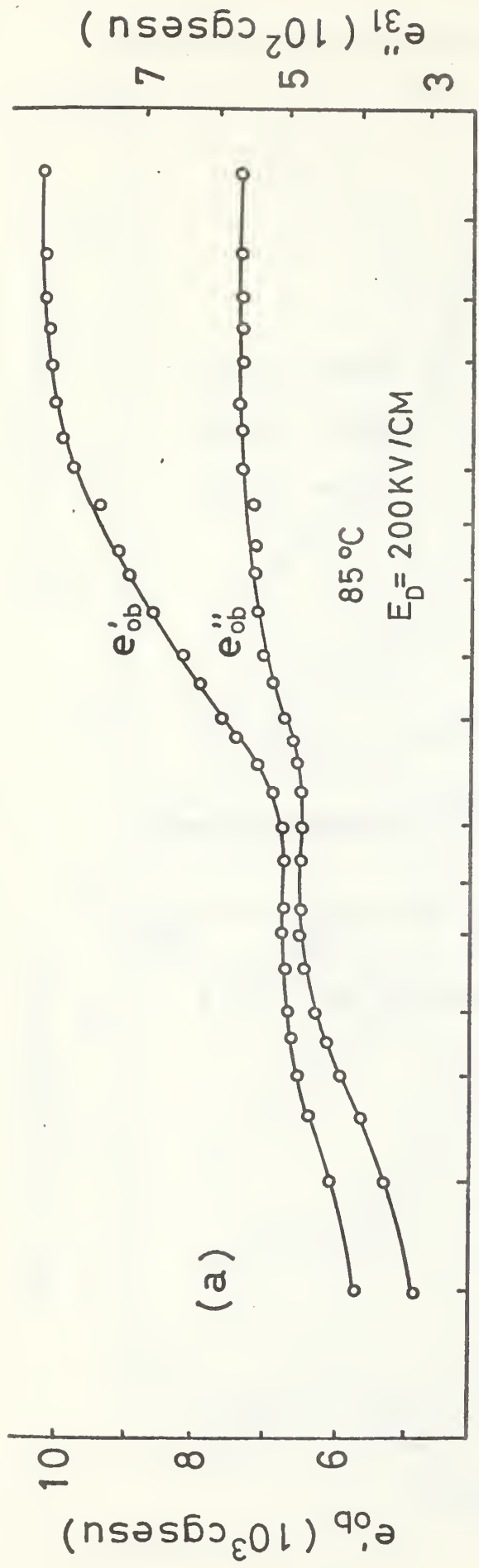


Fig. 6

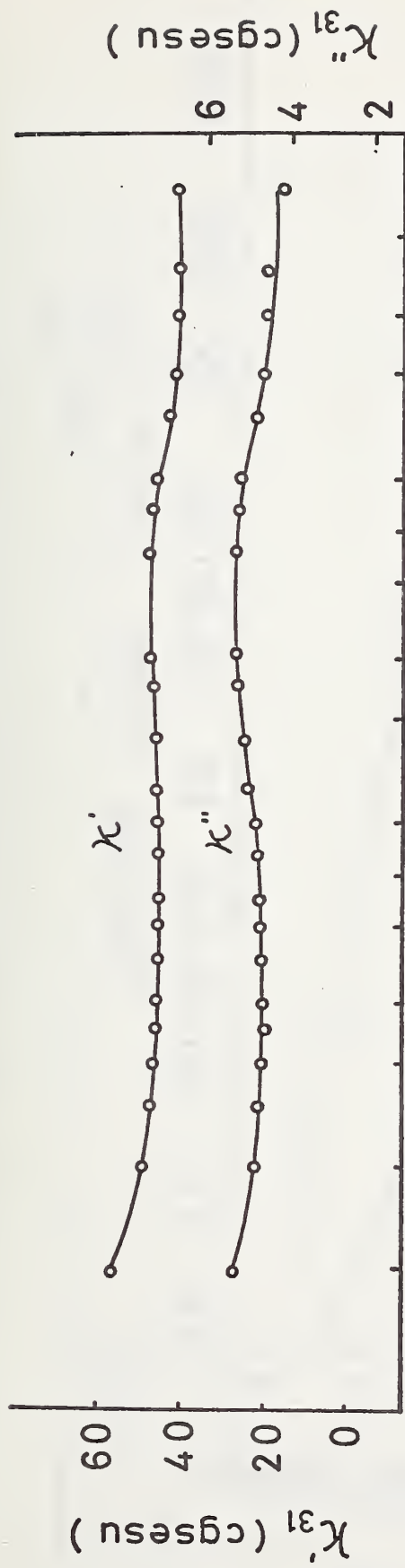


Fig. 31

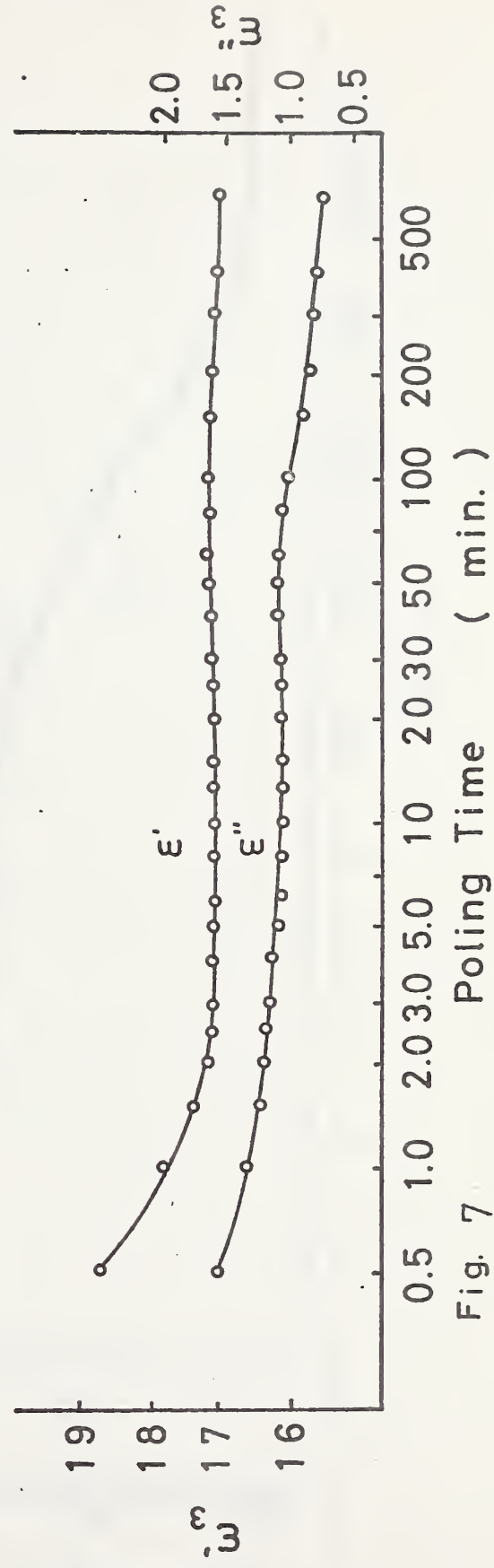


Fig. 7

Poling Time ( min. )

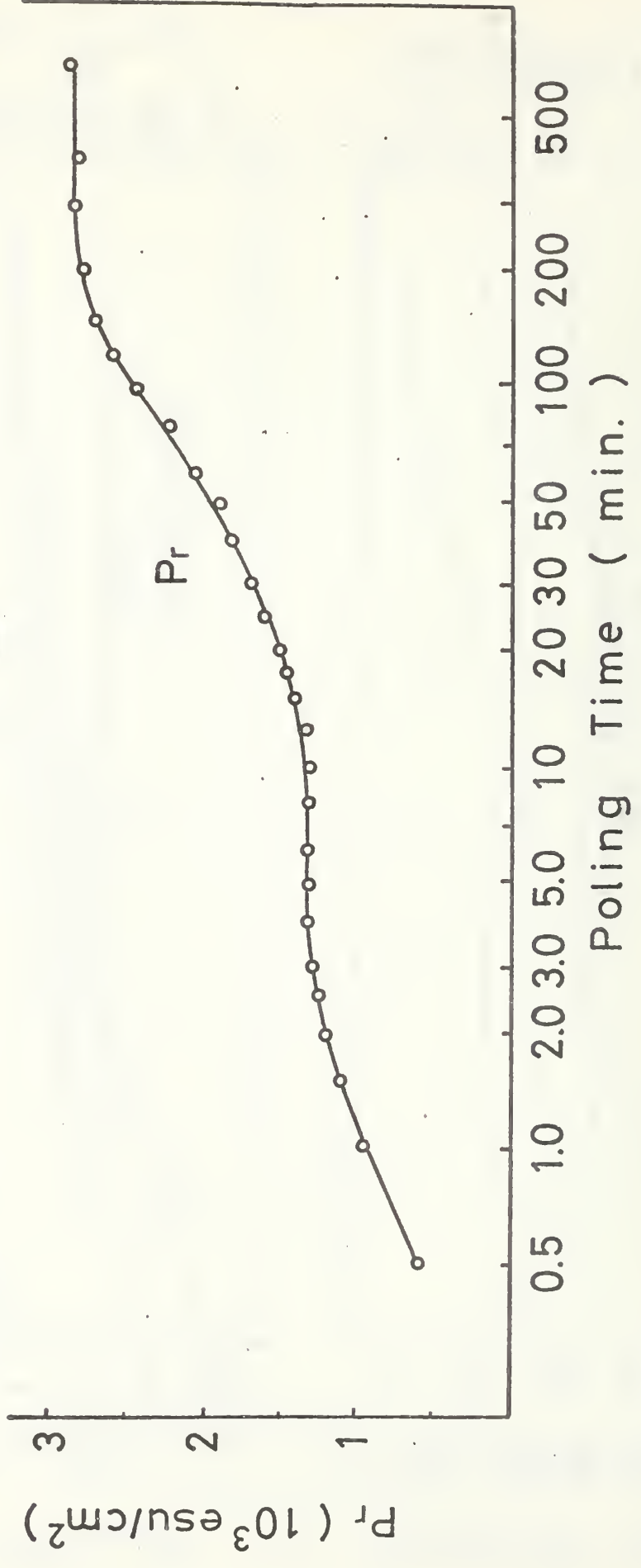


Fig. 8

NO.1 ○  
 S-p NO.2 ●

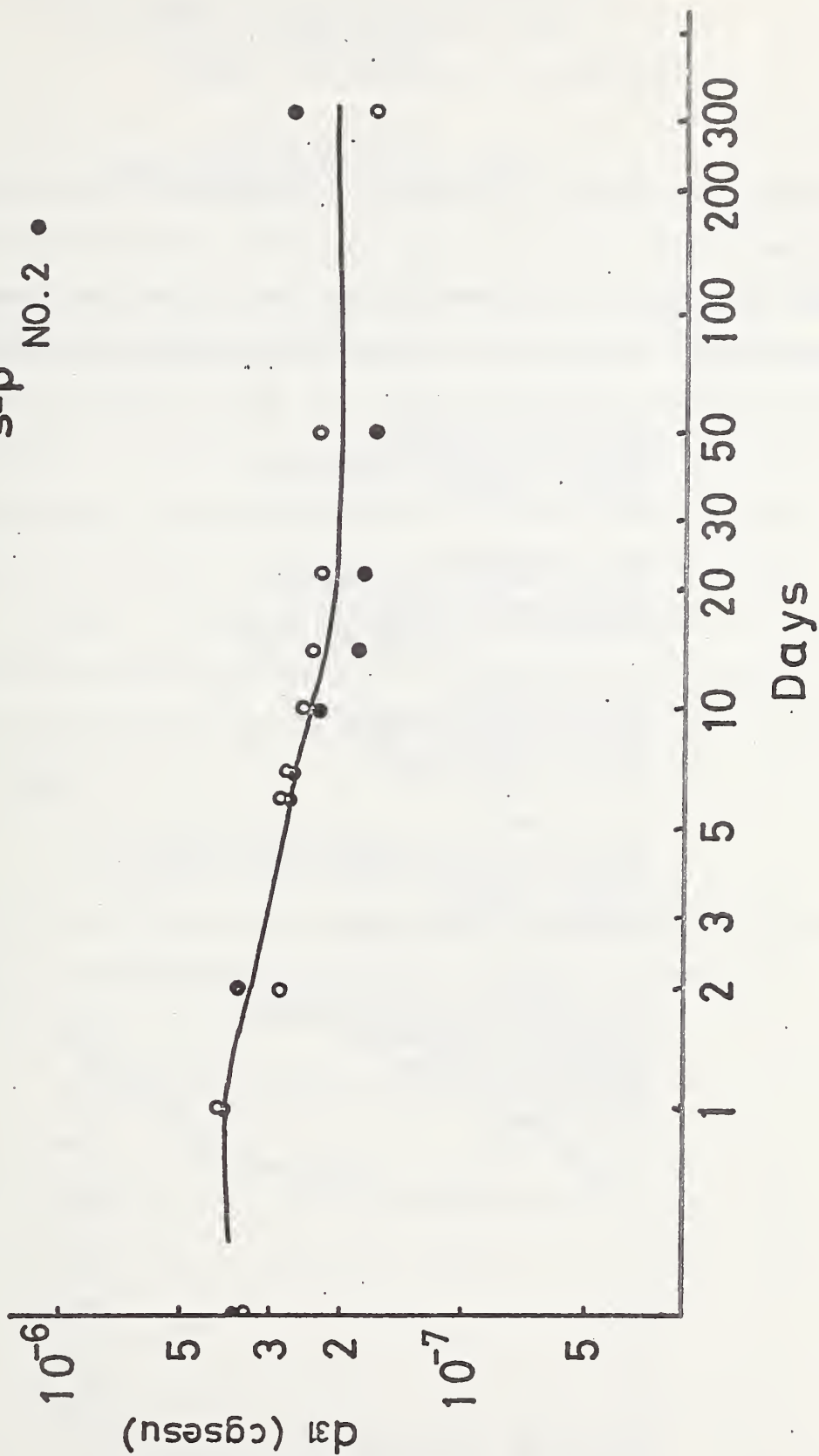


Fig. 9

Piezoelectric Polymer Research in Japan

Unscheduled Presentation by E. Fukada

Following his scheduled presentation Dr. Fukada kindly showed slides and discussed recent results and current theories of several other Japanese scientists who have made substantial contributions to the field of piezoelectric polymers. These scientists who were represented by Dr. Fukada were:

Professor H. Kawai  
Department of Physics  
Yokohama Municipal University  
Yokohama, Japan

Dr. N. Murayama  
Nishiki Research Laboratories  
Kureha Chemical Industry  
Iwaki-shi, Fukushima-ken, Japan

Dr. H. Ohigashi  
Basic Research Laboratories  
Toray Industries, Inc.  
Tebiro, Kamakura 248

Dr. M. Tamura  
Acoustical Engineering Research Laboratory  
Pioneer Electronic Corp.  
4-2610, Hanazono  
Tokorozawa, 359, Japan

Dr. Y. Wada  
Department of Applied Physics  
Faculty of Engineering  
University of Tokyo  
Bunkyo-ku  
Tokyo, Japan

THE MELTING TEMPERATURE-COMPOSITION CURVES OF  
 POLY(VINYLDENE FLUORIDE)-POLY(VINYL FLUORIDE)  
 MIXTURES AND VINYLIDENE FLUORIDE-VINYL  
 FLUORIDE COPOLYMERS .

Jerome B. Lando .  
 Case Western Reserve University  
 Cleveland, Ohio 44106

Recently Natta et. al. (1) have reported that mixtures of the homo-  
 polymers poly(vinylidene fluoride) (PVF<sub>2</sub>) and poly(vinyl fluoride) (PVF)  
 as well as vinylidene fluoride (VF<sub>2</sub>)-vinyl fluoride (VF) copolymers form  
 solid solutions over the entire composition range. However, no explanation  
 of the differences in the melting behavior of the two types of solid  
 solutions as a function of composition was presented. The data were  
 included in Figure 3 of that paper, which is reproduced herein as Figure 1.

These data can be explained using the equation for the freezing point  
 depression of dilute solutions in which the solid separates as a solid  
 solution, namely,

$$\Delta T_f = K_f(1 - k) m$$

where  $\Delta T_f$  is the freezing point depression,  $K_f$  is the molal freezing point  
 lowering,  $m$  is the molality of the solution, and  $k$  is the ratio of

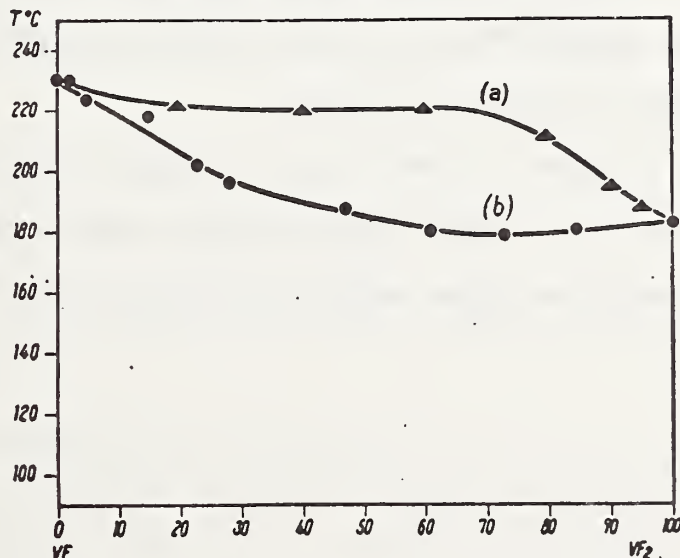


Fig. 1. Melting temperatures of (a) PVF<sub>2</sub>-PVF mixtures  
 and of (b) VF<sub>2</sub>-VF copolymers.

the mole fraction of solute in the solid solution to the mole fraction of solute in the liquid. It can be seen that the value of  $k$  will determine the initial slopes of the curves in Figure 1 from both composition extremes. For  $k$  less than unity there will be a freezing point depression (negative slope) and for  $k$  greater than unity there will be a freezing point elevation (positive slope).

It should be remembered that one of the polymorphic forms of  $PVF_2$  is isomorphous with the crystalline phase of PVF and this form of  $PVF_2$  is stabilized over the entire composition range studied by the presence of either PVF homopolymer or VF comonomer (1).

Considering first the  $VF_2$  side of Figure 1, it can be seen that the initial slope of curve (a), PVF- $PVF_2$  mixture, is positive, indicating that when the solid and liquid phases are in equilibrium the concentration of PVF homopolymer in the solid state is greater than in the liquid. This is not unreasonable since it means that the higher energy  $PVF_2$  chains are melting preferentially. However, curve (b), VF- $VF_2$  copolymer, has an almost zero initial slope, indicating that the compositions of the melt and solid in equilibrium are practically identical. Since the copolymerization of VF with  $VF_2$  is ideal (1), there will be random placement of VF in the  $VF_2$  chains. The chemical bonding between VF and  $VF_2$  will therefore preclude differences in composition between the solid and the melt.

On the VF side of Figure 1 curve (a) has a slightly negative initial slope indicating that there is more  $PVF_2$  in the melt than in the solid at equilibrium. Here again the higher energy of the  $PVF_2$  chains causes them

to melt preferentially. The more negative initial slope of curve (b), VF-VF<sub>2</sub> copolymer indicating more VF<sub>2</sub> in the melt, can be explained by considering the VF<sub>2</sub> units as "defects" in the predominately VF chains. Parts of the crystals containing a higher concentration of VF<sub>2</sub> units will melt preferentially. The initial slope is more negative in curve (b) because the "defects" are chemically incorporated into the polymer chains and do not exist as separate chains.

As would be expected, the differences in the two melting point-composition curves are related to the fact that in the copolymer there are chemical bonds between the two components of the solid solution, whereas such is not the case in the mixtures.

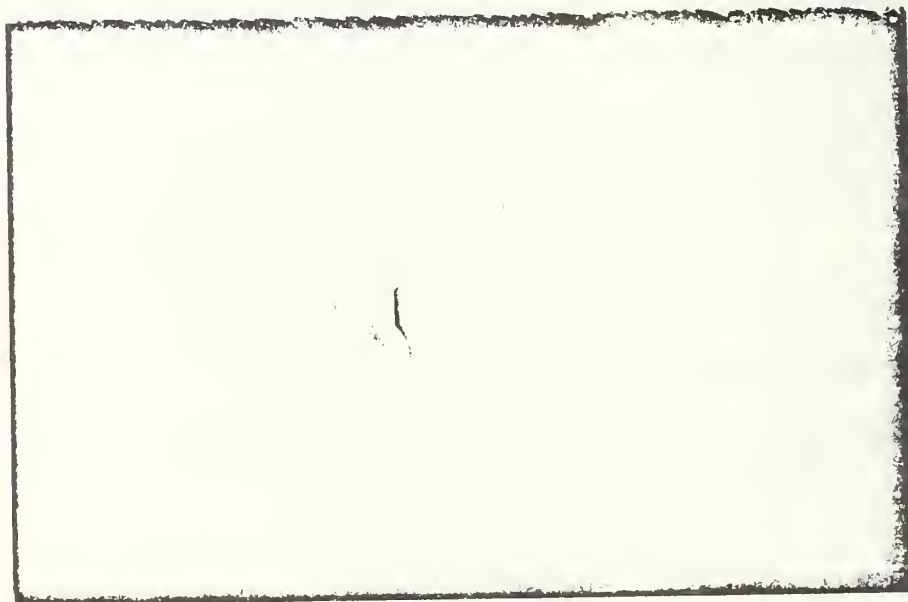
#### References

- (1) C. Natta, C. Allegra, I. W. Bassi, D. Sianesi, G. Caporiccio and E. Torti, J. Polymer Sci. A, 3, 4263 (1965).

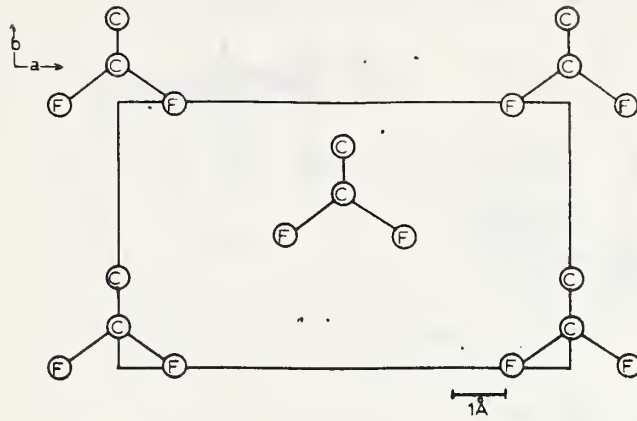
Slides Presented at  
Piezoelectric and Pyroelectric Symposium-Workshop



Slide 1: Fiber Pattern  
Phase I  $PVF_2$

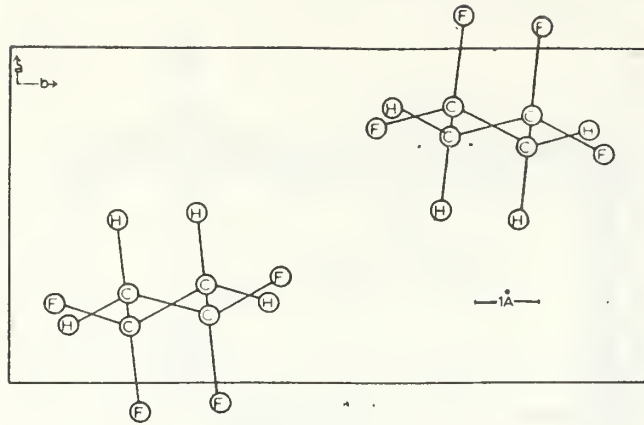


Slide 2: Fiber Pattern  
Phase II  $PVF_2$



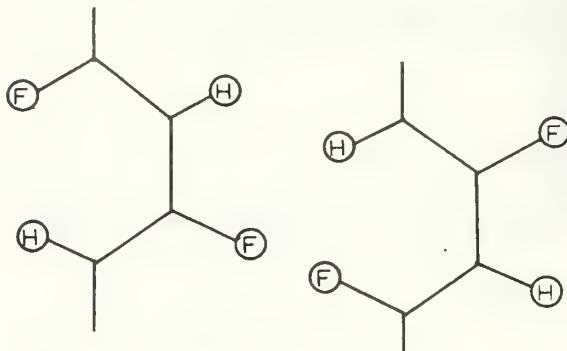
*a-b* projection of the unit cell determined by Lando, Olf, and Peterlin for phase I.

Slide 3

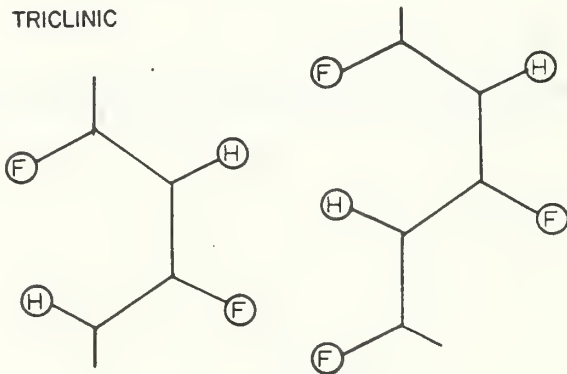


(a)

MONOCLINIC



TRICLINIC



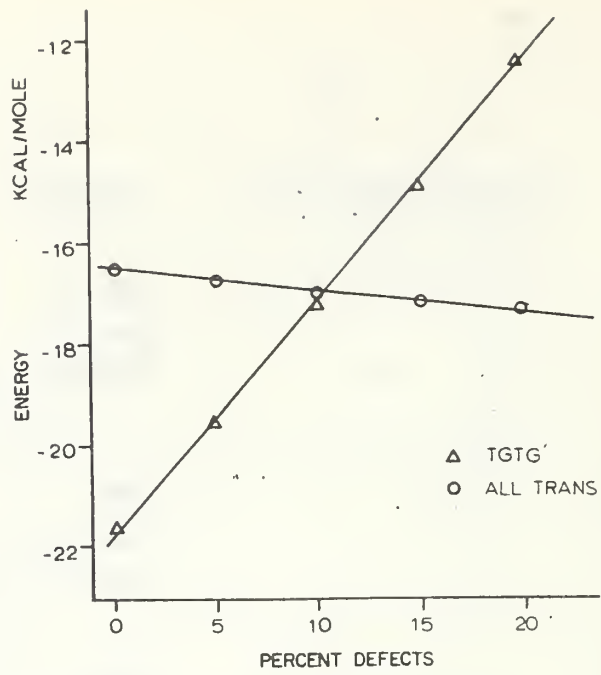
(b)

Slide 4: (a) a-b projection of the unit cell determined by Doll and Lando for phase II.

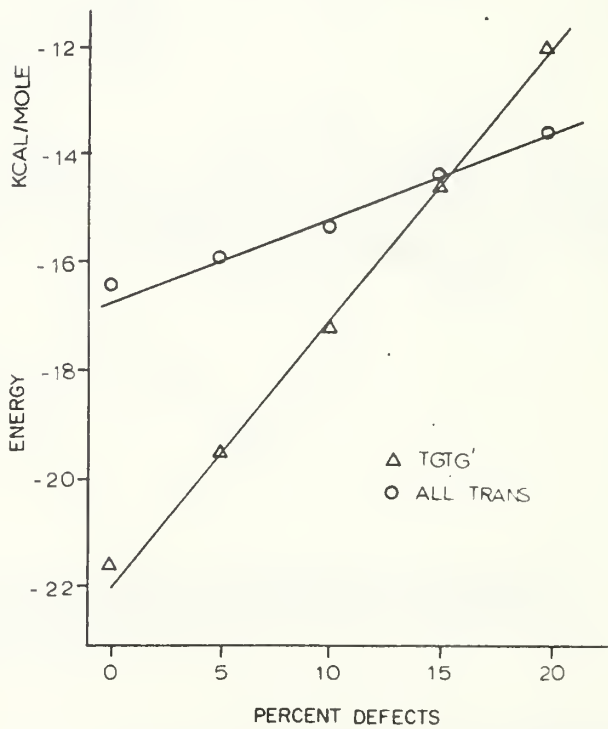
Slide 5: (b) b-c projection of the crystal structures proposed for phase II by Doll and Lando.

<u>Sample</u>	<u>Initial Phase</u>	<u>Treatment</u>	<u>Final Phase</u>
PVF <sub>2</sub>	II	None	II
		Draw 50	I
		Draw 50 - Anneal 180	II
91% VF <sub>2</sub> 9% VF <sub>3</sub>	II	None	II
		Draw 50	I
		Draw 50 - Anneal 190	II
83% VF <sub>2</sub> 17% VF <sub>3</sub>	I	None	I
93% VF <sub>2</sub> 7% VF <sub>4</sub>	I	None	I
		Draw 127	II
		Draw 50 - Anneal 160	I

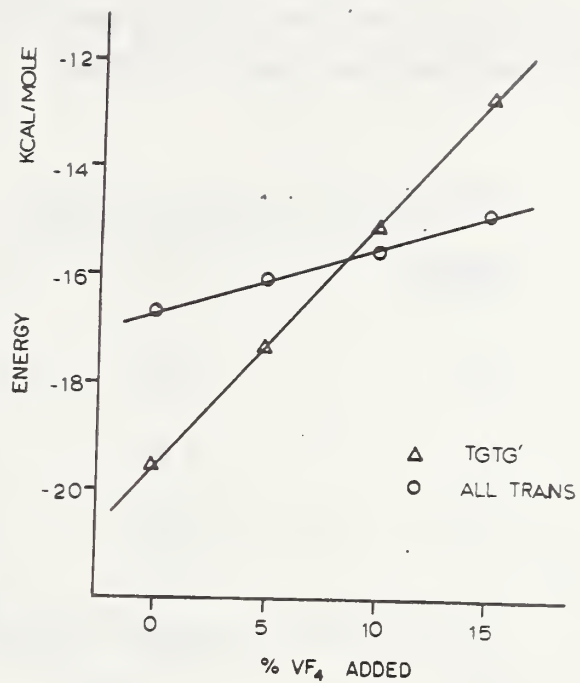
Slide 6 Variation of Crystalline Phase of Poly(Vinylidene Fluoride) and to Copolymers with Treatment.



Slide 7: Potential energy of the all-trans and TGTG' conformations vs HHTT concentration.



Slide 8: Potential energy of the all-trans and TGTG' conformations vs VF<sub>4</sub> concentration.

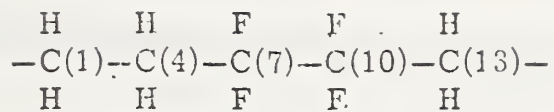


Slide 9: Potential energy of the all-trans and TGTG' conformations vs the concentration of VF<sub>4</sub> added to 5% HHTT defects.

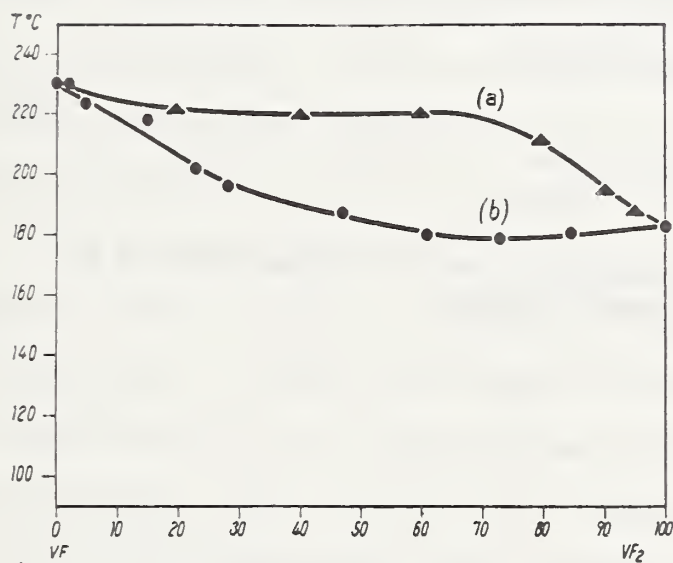
## Slide 10

Summary of the Lattice Constants of PVF<sub>2</sub> and VF<sub>2</sub>  
Copolymers Determined from Power Photographs

<u>Composition</u>	<u>Phase</u>	<u>a</u>	<u>b</u>	<u>c</u>
PVF <sub>2</sub>	II	9.63	5.02	4.62
91-9 VF <sub>2</sub> -VF <sub>3</sub>	II	9.59	4.98	4.66
PVF <sub>2</sub>	I	8.47	4.90	2.56
93-7 VF <sub>2</sub> -TFE	I	8.85	5.00	2.55
83-17 VF <sub>2</sub> -VF <sub>3</sub>	I	8.84	5.03	2.54



Slide 11: Chemical structure of head to head-tail to tail unit.



Slide 12: Melting temperatures of (a) PVF<sub>2</sub>-PVF mixtures and of (b) VF<sub>2</sub>-VF copolymers.

TEXTURE AND PYROELECTRICITY IN POLYVINYLIDENE FLUORIDE\*

R. G. Kepler  
Sandia Laboratories, Albuquerque, New Mexico 87115

X-ray texture studies and mode locked laser experiments are reported which show that the pyroelectricity in polyvinylidene fluoride films results from a quite large temperature dependence of the dipole moment of the unit cell. The mode locked laser experiments also show that the pyroelectricity is predominantly primary pyroelectricity.

---

\*This work supported by the U.S. Energy Research and Development Administration.

In recent years there have been a number of reports of piezoelectricity in polymer films<sup>1</sup> and in 1971 it was reported that films of polyvinylidene fluoride could exhibit a large pyroelectric coefficient.<sup>2</sup> A number of studies have been carried out detailing some of the properties of this pyroelectricity<sup>3</sup> and one attempt has been made to develop a theoretical model.<sup>4</sup> In this paper we report on experiments on polyvinylidene fluoride which show that the poling process, which induces the pyroelectric effect in the films, changes the texture of the films and that the pyroelectricity results from a change in the dipole moment of the unit cell with temperature. It is also shown that the change in the dipole moment with temperature is not a result of the change in the unit cell dimensions with temperature. This is the first report of a macroscopic pyroelectric effect being induced by the application of an electric field at elevated temperatures in which the texture of the material is changed.

Polyvinylidene fluoride ( $\text{PVF}_2$ ) is a crystalline polymer which exists in two stable polymorphs. In Phase I, the crystalline form studied in this work, the molecules are in a planar zig-zag conformation where the unit cell is orthorhombic, space group  $\text{Amm}2$ , with lattice constants  $a = 8.47$ ,  $b = 4.90$ , and  $c$  (chain axis) =  $2.56 \text{ \AA}$ , and two polymer chains per cell.<sup>5</sup> In this crystal structure the dipole moments of the monomer units are all parallel, and since the dipole moment of the monomer unit is  $2.1\text{D}$ , a single crystal of  $\text{PVF}_2$  in which the dipoles were rigidly aligned would have a spontaneous polarization of  $13.2 \text{ \mu C/cm}^2$ . Experimentally it

has been shown that a polarization of as much as  $3.0 \mu\text{C}/\text{cm}^2$  can be achieved in polycrystalline films which have been poled by subjecting them to high electric fields at elevated temperature.<sup>6</sup> It has also been shown that poled films can exhibit pyroelectric coefficients as large as  $3 \times 10^{-9} \text{ C}/\text{cm}^2\text{K}.$ <sup>2</sup>

In order to determine the influence of the poling process on the polymer films we have studied x-ray pole figures of poled and unpoled films and have found that poling changes the texture of the films. In a poled sample the unit cells are preferentially oriented with their dipole moments parallel to the applied field.

Samples of  $\text{PVF}_2$  were prepared for this study by stretching, at  $50^\circ\text{C}$ , 7 mil thick films, available commercially from Pennwalt Corporation, to five times their original length. After stretching, the films were annealed at  $130^\circ\text{C}$  for one half hour. Raman light scattering studies have been carried out on these films<sup>7</sup> and it has been shown that they are essentially all Phase I and that the molecular chain axes are highly aligned in the draw direction. The stretched films were poled by applying 600 kV/cm at  $100^\circ\text{C}$  for 1/2 hour and then cooling the sample to room temperature with the field applied.

Reflection x-ray pole figures<sup>8</sup> were determined for the most intense x-ray diffraction peak for  $\text{Cu K}\alpha$  radiation. This peak has been indexed as the sum of 2(110) and (200) reflections.<sup>5</sup> The figures obtained for unpoled films (lower half of figure) and poled films (upper half of figure) are shown in Fig. 1. The draw direction for each pole figure is vertical.

Each line in the pole figures is an intensity contour of the reflected x rays in a stereographic projection.

The pole figures for the unpoled samples show that the c-axis of the unit cells is highly aligned in the draw direction, in agreement with the Raman experiments,<sup>7</sup> but that the a and b axes are randomly oriented in a plane perpendicular to the draw direction. In the poled films it is clear that the reflected x-ray intensity has become strongly peaked in the direction perpendicular to the surface of the film. Calculations show that the structure factor contribution from the (110) planes is 4.6 times more intense than the contribution from the (200) planes. If the unit cells were perfectly aligned with their dipole moment parallel to the applied field, the poles of the (110) planes would appear in the pole figure at  $0.27R$  on each side of the center, where  $R$  is the radius of the projection. Therefore, with imperfect alignment a strong broad peak will appear from these planes as is observed. It is known that heating the samples to  $120^{\circ}$  depoles the PVF<sub>2</sub> films<sup>6</sup> and pole figures of depoled samples are the same as unpoled films.

These results show that the poling and depoling process in PVF<sub>2</sub> involves some premelting phenomena by which crystallites melt and recrystallize in different orientations with no apparent change in crystal structure. The melting point for PVF<sub>2</sub> is near  $170^{\circ}\text{C}$ . We have examined the Raman spectra of samples which have been heated to  $150^{\circ}\text{C}$  for 1/2 hour and have been unable to detect any evidence for conversion from Phase I to

Phase II at this temperature. Mechanical loss measurements have been carried out on our samples by K. T. Gillen<sup>9</sup> and he finds a very weak and broad loss peak around 50°C for low frequencies. These results appear to imply that some backbone molecular motion becomes possible at 40 or 50°C which permits the melting and recrystallization process.

In order to distinguish between possible mechanisms for the pyroelectric effect, the time dependence of the generation of the pyroelectric charge was measured. Films of polyvinylidene fluoride were dyed by adding the mode locking or Q switching dye bis (4-dimethylaminodithiobenzil) nickel [Eastman 14015] to a solution of polyvinylidene fluoride in dimethylformamide. Films were cast by evaporating this solution on glass. These films were poled by applying 300 kV/cm at 100°C for 1/2 hour and then cooling them to room temperature with the field applied.

The poled films were placed in the sample holder shown in Fig. 2. The capacitance of the sample was typically less than 50 pf and the signal was fed directly into a 50 Ω cable to a Tektronix 454 oscilloscope. Light from a pulsed mode locked neodymium glass rod laser illuminated the sample through the glass and gold mesh electrode. Figure 3 shows a typical train of pulses observed when the sample is irradiated with a train of mode locked pulses. Each voltage pulse results from a mode locked light pulse. The sign of the voltage pulse depends on the orientation of the film as is expected for the pyroelectric effect.

It has not been possible to determine accurately the absolute magnitude of the fast response pyroelectric effect. In general, a train of 10 to 20 mode locked pulses contained a total energy of approximately 1 joule. In order to make the signal as large as possible it was desirable to absorb as much light as possible but for very short mode locked pulses, optical bleaching can occur at high intensities. In all experiments reported here, even though all the available optical energy was not incident on the sample, optical bleaching was an important effect. A typical pyroelectric sample contained  $5 \times 10^{15}$  dye molecules/cm<sup>2</sup>. Therefore, if the lifetime of the excited state of the dye molecule is longer than the mode locked pulse, a pulse containing more than a few times  $10^{15}$  photons could induce optical bleaching. Five  $\times 10^{15}$  photons corresponds to about  $10^{-3}$  joules.

In a typical experiment, if all the energy incident on the sample had been absorbed, the total observed charge should have been  $8 \times 10^{-10}$  C, a value which was about 30 times larger than that observed experimentally. On the other hand, if it is assumed that half of the dye molecules are excited once by each mode locked pulse, the observed charge was calculated to be about  $2 \times 10^{-11}$  C. On this basis, the experimental results are in reasonable agreement with expectations.

The observation that the major contribution to the pyroelectric charge is induced in less than 4 nsec shows that the pyroelectricity of  $\text{PVF}_2$  is predominantly primary pyroelectricity, the pyroelectricity which occurs without a change in lattice dimensions.<sup>10</sup> The speed of sound in  $\text{PVF}_2$  is

on the order of  $2 \times 10^6$  cm/sec and, therefore, it would take from 25 nsec to 50 nsec for a 90  $\mu\text{m}$  sample to relax mechanically after an instantaneous uniformly absorbed heat pulse. Since the observed pyroelectric response exhibited at most a small contribution with a 25 to 30 nsec time constant, the primary pyroelectric coefficient is substantially larger than the secondary pyroelectric coefficient.

In order to look for relatively slow thermal relaxation contributions to the pyroelectricity, the charge induced by a train of mode locked pulses of laser radiation was integrated over times of the order of 10  $\mu\text{sec}$ . Contributions on the order of 10% of the total induced charge were observed with a time constant of the order of 1  $\mu\text{sec}$ . This effect may arise from heat transfer from the electrodes to the sample.

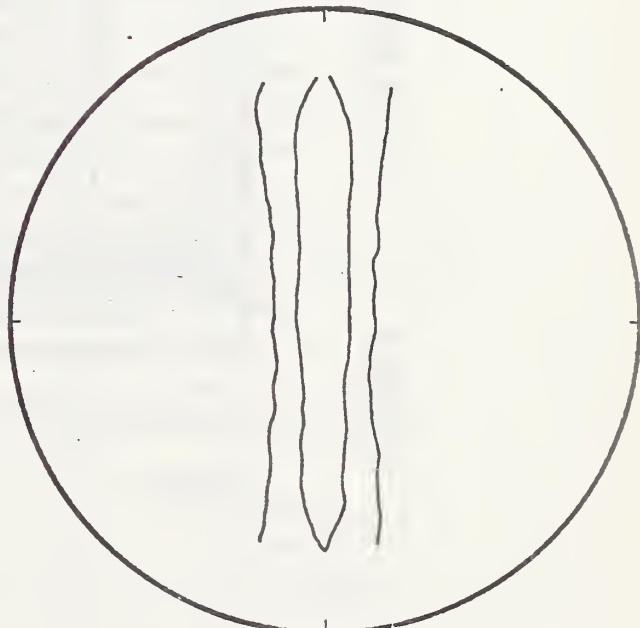
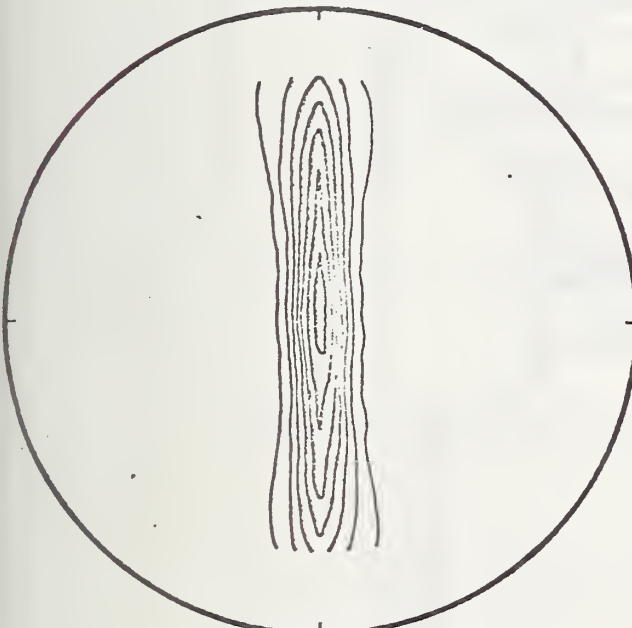
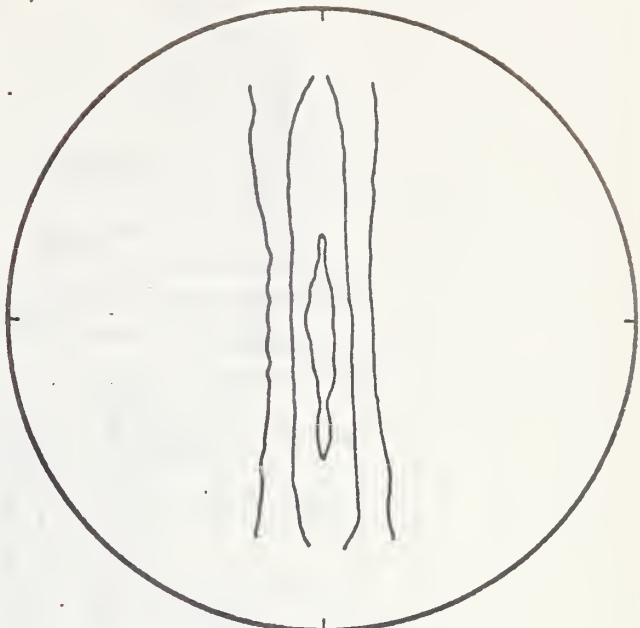
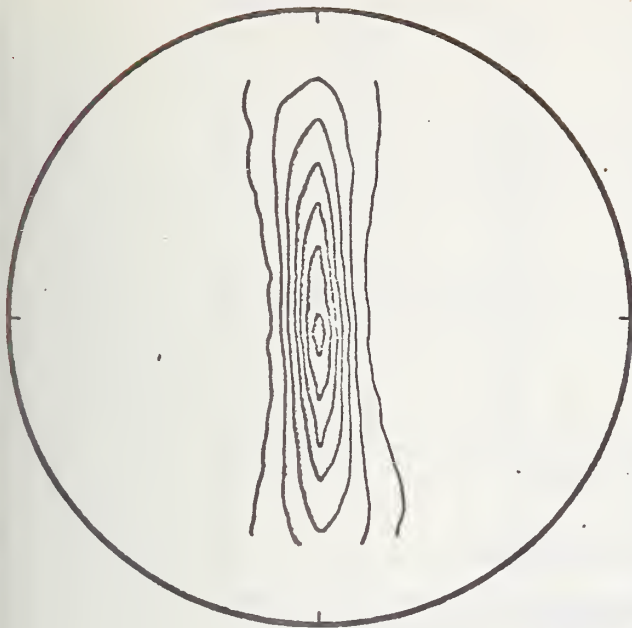
The results presented in this paper show that the pyroelectricity exhibited by  $\text{PVF}_2$  results from a preferential orientation of the unit cells and a strong temperature dependence of the dipole moment of the unit cell. Since the molecule consists of rigid dipoles the temperature dependence of dipole moment of the unit cell apparently arises from thermal motion (libration) of the rigid dipoles.

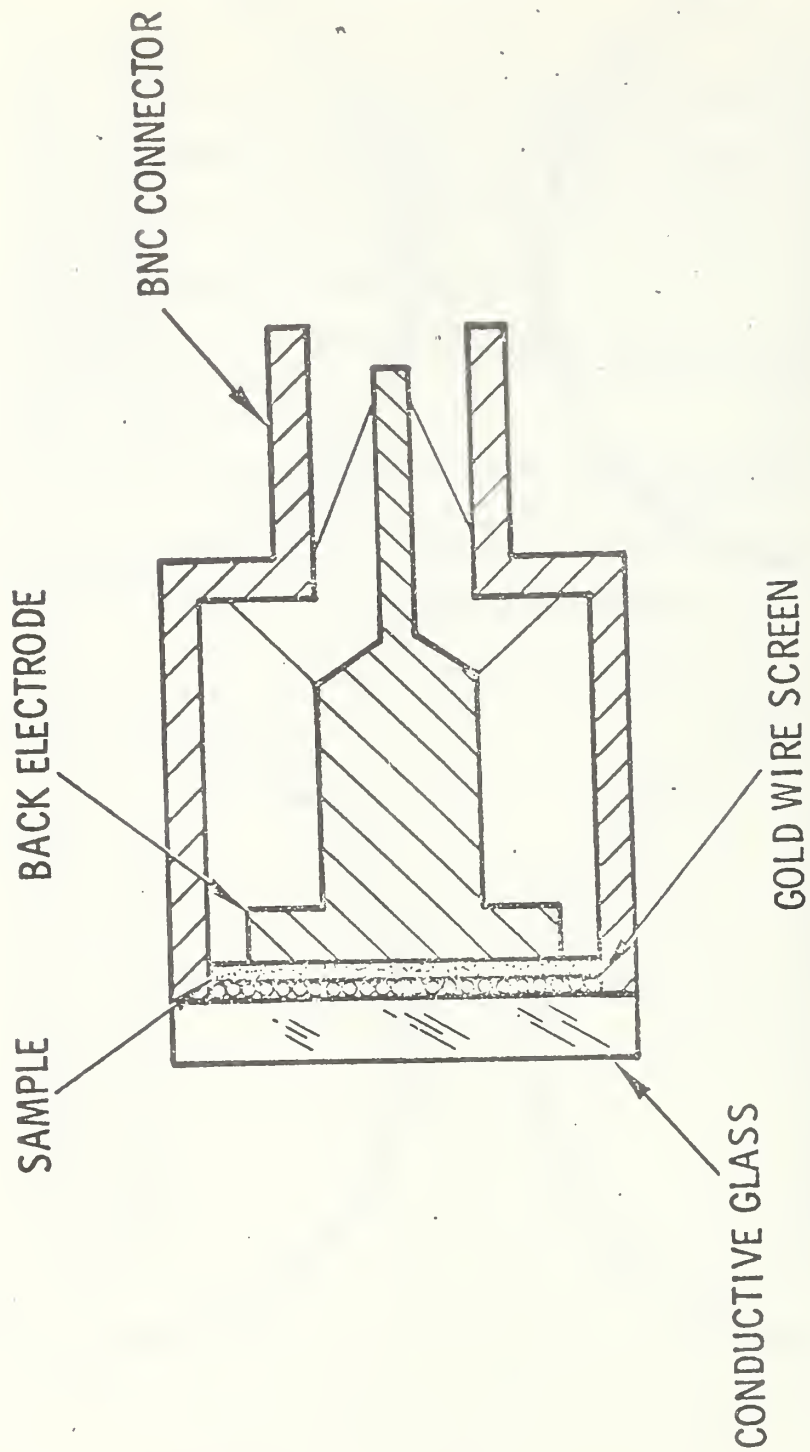
## References

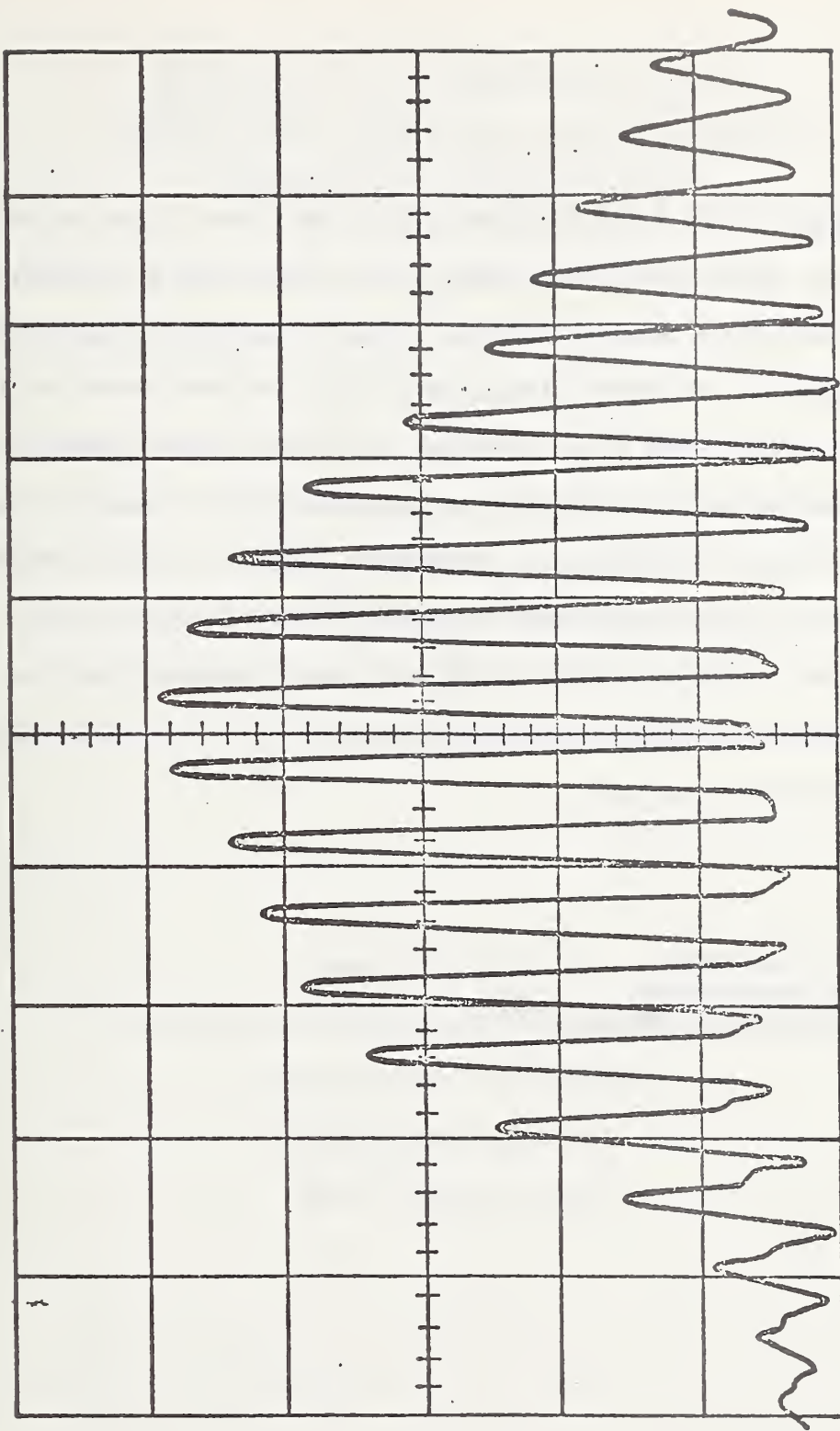
1. R. Hayakawa and Y. Wada, in Advances in Polymer Science, Vol. II, (Springer Verlag, 1973) p. 1.
2. J. G. Bergman, J. H. McFee, and G. R. Crane, Appl. Phys. Lett. 18, 203 (1971).
3. A. M. Glass, J. H. McFee, and J. G. Bergman, Jr., J. Appl. Phys. 42, 5219 (1971); J. H. McFee, J. G. Bergman, Jr., and G. R. Crane, Ferroelectrics 3, 305 (1972); H. Burkard and G. Pfister, J. Appl. Phys. 45, 3360 (1974); P. Buchman, Ferroelectrics 5, 39 (1973).
4. E. W. Aslaksen, J. Chem. Phys. 57, 2358 (1972).
5. J. B. Lando, H. G. Olf, and A. Peterlin, J. Poly. Sci. A-1, 4, 941 (1966).
6. R. G. Kepler, Photo. Sci. Eng., in press.
7. G. Cessac and J. G. Curro, J. Poly. Sci. 12, 695 (1974).
8. J. R. Holland, Handbook of X Rays, (McGraw-Hill, New York, 1967).
9. K. T. Gillen, private communication.
10. J. F. Nye, Physical Properties of Crystals, (Oxford University Press, 1969), p. 189.

## Figure Captions

- Fig. 1 - Pole figures for poled (top) and unpoled (bottom) samples of polyvinylidene fluoride. The lowest intensity contour line in all pole figures corresponds to 200 cps and the contour interval is 100 cps.
- Fig. 2 - The sample holder used for the fast response pyroelectric effect measurements.
- Fig. 3 - A train of current pulses observed from a poled and dyed sample of polyvinylidene when it is irradiated with a train of mode locked pulses from a neodymium laser. The vertical sensitivity is 50 mV/cm across 50  $\Omega$  and the sweep speed is 20 nsec/cm.







Addendum - After I had finished writing the above it was pointed out by L. A. Harrah that the argument about primary versus secondary pyroelectricity requires that the sample's mechanical properties be homogeneous. If crystalline regions of the polymer, which are probably less than  $1000 \text{ \AA}$  in diameter, can relax at the expense of neighboring amorphous regions then the mechanical relaxation time could be less than 0.1 usec. Therefore, before it can be concluded that the pyroelectric effect in polyvinylidene fluoride is predominantly primary pyroelectricity, it has to be shown that the inhomogeneity of the crystalline polymer is not responsible for the observed fast response.

Dr. R. Glen Kepler  
Sandia Laboratories  
Albuquerque, New Mexico 87115

DEPENDENCE OF THE PIEZOELECTRIC ACTIVITY OF  
POLYVINYLIDENE FLUORIDE UPON HIGH SPEED UNIAXIAL  
STRETCHING AND SUBSEQUENT POLING

R. J. SHUFORD, A. F. WILDE,  
J. J. RICCA AND G. R. THOMAS  
ORGANIC MATERIALS LABORATORY  
ARMY MATERIALS & MECHANICS RESEARCH CENTER  
WATERTOWN, MASSACHUSETTS 02172

Paper Presented at  
Piezoelectric and Pyroelectric Symposium-Workshop  
National Bureau of Standards  
Gaithersburg, Maryland  
April 15 and 16, 1975

## INTRODUCTION

Much interest and research in piezoelectricity of synthetic polymers was generated by the initial reports of Kawai<sup>1</sup> and Fukada<sup>2</sup> on the high piezoelectric effect in polyvinylidene fluoride (PVF<sub>2</sub>). This piezoelectric (and pyroelectric) activity occurs as a result of stretching the polymer film, poling in a static electric field at temperatures from 80 to 150°C, and then cooling with the field applied.<sup>3,4,5,6</sup>

On a molecular level, polarization of polymer film in a static electric field is thought to increase the true and/or polarization charges through several mechanisms<sup>5</sup>: 1) alignment of C-F dipoles in the crystalline region<sup>7,8,9,10,11</sup> and 2) injection of homocharges or space charges into the film from the electrodes.<sup>12,13</sup> The actual mechanism of polarization occurring in PVF<sub>2</sub> is probably a combination of the two<sup>5</sup>, the contribution of each depending on the poling conditions.

Polyvinylidene fluoride is a semicrystalline polymer that exists in at least two different crystalline conformations: planar zig zag designated phase I (or  $\beta$ ) and trans-gauche-trans-gauche' designated phase II (or  $\alpha$ ). Polymer films of each molecular conformation can be obtained depending upon the method of film preparation;<sup>5,14,15,16</sup> i.e., casting from a solvent, melt crystallization, annealing temperature, or extrusion. This polymorphism has been determined by infrared spectroscopy<sup>15,17,18,19</sup>, confirmed by laser-Raman studies<sup>20,21,22</sup>, X-ray diffraction and NMR<sup>14,23-27</sup>. The presence of 5 to 6% head-to-head defects in the polymer during polymerization limits the degree of crystallinity that can be obtained and affects the thermodynamic stabilities of the crystalline conformations<sup>14,28,29</sup>.

Changes in the molecular conformation of PVF<sub>2</sub> can occur by mechanical stretching or polarization processes. Orientation of the polymer chains, along with a conversion to crystalline phase I conformation, can be achieved by uniaxial or biaxial stretching at low temperatures<sup>14,15,27</sup>. Increasing the draw temperature increases the phase II content<sup>14</sup>. The piezoelectric activity is enhanced by stretching or rolling the film prior to poling<sup>1-6</sup>. Activation of the oriented films by poling with heat also converts phase II to phase I<sup>19</sup>.

Other workers have investigated the dielectric properties of PVF<sub>2</sub> as a function of frequency, temperature and degree of crystallinity<sup>30-39</sup>. The high temperature  $\alpha$  relaxation peak occurring at 60 to 80°C at 300 Hz is due to molecular motion in the crystalline regions of the polymer. The intensity of this absorption peak increases as the degree of crystallinity or rolling increases. The  $\beta$  relaxation peak which occurs between -40 and -50°C at 300 Hz is due to the micro-Browian motion of the amorphous regions. A lower temperature  $\gamma$  relaxation peak has been assigned to molecular motion in the amorphous regions. Anomalous dielectric behavior of PVF<sub>2</sub> at low frequencies and high temperatures is thought to arise from ionic conduction or ionic impurities present in the polymer<sup>35-39</sup>. Assignment of the molecular modes to the dielectric relaxation has been confirmed by similar observations of relaxation peaks from dynamic mechanical analysis of semi-crystalline polymers.

The purpose of our research in piezoelectric polymers is to evaluate the potential of making piezoelectric polymers transducers for application as on-condition vibration sensors in aircraft. The large piezoelectric effect

reported for PVF<sub>2</sub> suggested that it be a leading candidate for the above application. Therefore our approach has been to use polymer processing and characterization capabilities in our laboratory to impart and to comprehensively study systematic changes in the structure and morphology of PVF<sub>2</sub> and to relate these to subsequent piezoelectric behavior in an attempt to understand, optimize, and utilize the piezoelectric phenomenon. Commercially available extruded PVF<sub>2</sub> film was uniaxially stretched to various draw ratios up to 7/1 at 80°C. The degree of orientation and crystalline chain conformation was determined by infrared spectroscopy, density, birefringence, sonic velocity, and X-ray diffraction. The stretched films were poled in a high D.C. electric field under varying conditions. The static piezoelectric constant of polarized PVF<sub>2</sub> films was determined as a function of draw ratio, degree of orientation, poling temperatures, polarization voltages, and poling time. The effects of stretching and poling on the physical, mechanical, and electrical properties of this film were also determined.

## EXPERIMENTAL

### Film Orientation

Extruded homopolymer PVF<sub>2</sub> film (Kynar, Pennwalt Corp.) was obtained from Westlake Plastics. This film was 5.4 mils thick, had a density of 1.768 g/cc and intrinsic viscosity of 1.37, was slightly oriented (birefringence of 0.0045), and its crystalline portion was in the phase II conformation as determined by infrared spectroscopy.

This PVF<sub>2</sub> film was oriented to varying degrees (draw ratios from 2/1 to 7/1) by uniaxial stretching at high speed in a radiant oven with infrared heaters, according to an AMMRC procedure previously described<sup>40</sup>. The film

temperature during stretching was measured by an infrared sensing temperature indicator (IRCON Model CH34LC) which was focused on the film just outside the exit end of the oven. Typical runs for the PVF<sub>2</sub> film are given in Table I.

TABLE I

Typical Run Conditions for PVF<sub>2</sub> Film Stretching

Draw Ratio	6:1	
Feed Rate	15 ft/min	
Drawing Drum Rate	90 ft/min	
Film Exit Temperature	80°C	
Film Dimensions	Initial	Final
Width	5 inches	2.5 inches
Thickness	5.4 mils	2.6-2.7 mils

### Infrared Spectroscopy

Infrared spectra of the stretched (and poled) films were measured in the far infrared region from 200 to 1000 cm<sup>-1</sup> on the Beckman IR 12 spectrometer. Polarized spectra were recorded in the far infrared region using a silver wire grid polarizer.

### Density and Intrinsic Viscosity

Densities of the polymer films were determined by the gradient density column (carbon tetrachloride-ethylene bromide) at room temperature. Intrinsic viscosity of the as received PVF<sub>2</sub> film was determined in dimethyl formamide at 25°C in an Ubbelohde viscometer.

## Birefringence and Sonic Modulus

Total birefringence of the uniaxially stretched polymer films was obtained by standard interferometric techniques from measurements of the film thickness and retardation. Sonic modulus of the oriented films (parallel to the draw direction) was determined by using a Dynamic Modulus Tester (H.M. Morgan Co.). To improve the accuracy of the results by this method, films ranging in length from 10 to 20 cm. were used, and the calculated sonic moduli were taken as the average of three separate determinations.

## X-Ray Diffraction

Wide angle x-ray diffraction photographs of the PVF<sub>2</sub> films were obtained with Cu K $\alpha$  radiation on a flat plate camera having a sample-to-film distance of 29.86 mm. X-ray photographs were taken in three different directions, corresponding to each of the three mutually perpendicular axes of the film.

## Dynamic Mechanical Analysis

Dynamic mechanical properties were determined with the Rheovibron DDV-IIB Dynamic Viscoelastometer at a constant frequency of 110 Hz. Data were obtained in the form of dynamic modulus and loss tangent as a function of temperature, where the loss tangent ( $\tan \delta$ ) is a measure of viscoelastic energy absorption per cycle in a sample under oscillating strain. Low temperature measurements of the stretched films were difficult to make because of brittleness of the film and slippage in the grips.

## Polarization

PVF<sub>2</sub> films (about 2 inches by 5 inches) were placed between two copper plates (embedded in two electrically insulating blocks made of micarta), clamped together and placed in the center of a controlled temperature oven (Custom Scientific Instruments, Inc.) preheated to a specific temperature, usually 110°C. The poling plates were connected to a high-voltage power supply (Sorensen & Co., Model 9060) having a maximum output of 60 KV D.C. Values of poling voltage were chosen to give poling field strengths generally of 500 or 1000 kV/cm. The temperature of the polymer film during poling which lagged the oven temperature (due to the mass of the insulating blocks) was determined by using a thermocouple embedded in one of the insulating blocks of the poling plates. Typically the poling voltage was not applied until after a 5-minute equilibration in the preheated oven, at which time the poling plate temperature was about 40°C. After 30 minutes poling time in a preheated oven at 100 to 110°C, the maximum film temperature was between 80 to 85°C. The sample was cooled (by opening oven door) with the field applied for at least 15 minutes, at which time the final film temperature was about 65 to 70°C.

## Piezoelectric Activity

The first observations of piezoelectric activity were made by subjecting the stretched poled PVF<sub>2</sub> films to slow cyclic tensile loading in an Instron. Two test modes were employed: sawtooth and sinusoidal. The resulting piezoelectric signals were detected by an oscilloscope. These results served only to demonstrate in a qualitative fashion the piezoelectric behavior of PVF<sub>2</sub>.

Quantitative values of the static piezoelectric constant were obtained by placing known compressive loads upon the stretch poled PVF<sub>2</sub> film with an Instron and measuring the resultant stress-induced output voltage from a coulometer. The coulometer was constructed at AMMRC from a diagram furnished by E. L. Church and H. Jenkinson of the Frankford Arsenal. The coulometer consisted of an operational amplifier (Analog Devices, Inc., Model 310K) with a feedback capacitor connected between the output and input circuits. The coulometer output voltage was read with a Simpson voltmeter, and then converted to values of piezoelectric charge. For loading, the polymer film was placed between two metal plates serving as electrodes, thus avoiding the need for electroding the film prior to measurement. From the incremental values of static compressive load on the polymer film and the corresponding coulometer output voltage, one could calculate the piezoelectric constant ( $d_{33}$ ) by the equation

$$d_{33} = \frac{\text{charge/film area}}{\text{load/film area}}$$

in units of coulombs/newton. The piezoelectric constant was determined at least one day after poling to allow dissipation of residual surface charges on the film.

## RESULTS AND DISCUSSION

It was found that systematic increases on the degree of PVF<sub>2</sub> film stretching produced systematic changes in the properties of the film. These property changes were characterized by a number of methods as described in the Experimental section.

## Infrared Spectroscopy

IR spectroscopy in the far infrared region showed that the crystalline component of the PVF<sub>2</sub> film (as received) was predominantly in the Phase II form<sup>15-23</sup>. See Figure 1. This is evident by the presence of absorption bands at 615, 530, 410, 360, and 290 cm<sup>-1</sup>. As the degree of uniaxial stretching was increased in steps up to 5/1, the IR spectra showed a continuous decrease in the 530 cm<sup>-1</sup> and 410 cm<sup>-1</sup> bands and a concomitant increase with stretching in the 445 cm<sup>-1</sup> band. These results indicate a gradual conversion of Phase II to Phase I due to the stretching process. At further increases in the draw ratio up to 7/1, no further changes were noted in the IR spectra. Both the conventional IR spectra and the polarized IR spectra exhibited no significant dependence upon poling of the PVF<sub>2</sub> films for films which had previously been highly stretched. This agrees with Cessac and Curro<sup>22</sup>, where according to their results and calculations dipole orientations greater than 60 or 80% are not occurring during poling, but where dipole orientations of less than 60% can not be ruled out.

## Density

As the degree of film stretching was increased, the film density also rose, but in an S-shaped fashion as shown in the curve of Figure 2. The increase in density is attributed to the increased content of the higher density phase I form<sup>23-27</sup> and may also result from an increase in the degree of crystallinity.

## Birefringence

The total birefringence measured by these experiments is the sum of the contributions due to the crystalline components, the amorphous components, and the form birefringence. The latter contribution is usually assumed to be small. The increase in birefringence upon stretching, noted in Figure 3,

is attributed primarily to the changes in degree of preferred orientation in the crystalline phase. The leveling off seen at the higher draw ratio suggests a saturation in the degree of crystalline orientation. For highly stretched films no difference in birefringence was observed between poled and unpoled specimens. This agrees with the results of McFee, Berrigman, and Crane<sup>7</sup>.

#### Sonic Modulus

The effect of stretching upon the sonic modulus also appears in Figure 3, where there is seen a continuous increase in modulus with draw ratio. In a semi-crystalline polymer the sonic modulus is the sum of the contributions from the crystalline and amorphous regions. Previous work on oriented semi-crystalline polymers has indicated that the sonic modulus is more sensitive to orientation changes in the amorphous than in the crystalline regions<sup>41</sup>. We might therefore expect from Figure 3 that the orientation in the amorphous region is continuing to increase at the higher draw ratios.

#### X-Ray Diffraction

The X-ray diffraction patterns seen in Figures 4-7 show that at low degrees of stretching the individual crystallites are randomly oriented. As the degree of stretching is increased, the crystallites assume an increasingly preferred orientation as indicated by the gradual breakup of the diffraction rings into spots. Also the changes noticed in the diffraction spacings (Table II) indicate a continuous conversion of Phase II to Phase I with increasing degree of stretching. With the highly stretched PVF<sub>2</sub> films there was no difference produced in the X-ray diffraction patterns by poling. This agrees with the results cited by Cessac and Curro<sup>22</sup>.

## Dynamic Mechanical Analyses

Dynamic mechanical measurements, including loss ( $\tan \delta$ ) and modulus, were determined for the unstretched and stretched PVF<sub>2</sub> films as a function of temperature at a constant frequency of 110 Hz (See Figures 8, 9, 10). A  $\beta$  transition peak occurs between -40 and -20°C in both the unstretched and stretched PVF<sub>2</sub> films. The ratio of the height of the  $\beta$  peak compared to the  $\alpha$  peak (50 to 70°C) decreases in the stretched films. With the stretched films there were no significant differences in dynamic mechanical spectra between upoled and poled specimens.

## Piezoelectric Activity

The first observations of piezoelectric activity were achieved by the slow cyclic tensile loading of the stretched poled PVF<sub>2</sub> films in an Instron test machine. The piezoelectric signals were observed by direct coupling to an oscilloscope. It was found that the piezoelectric voltages measured in this way were proportional to the film loading rates in the sawtooth test (see Figure 11), and were very nearly proportional to the film cyclic test frequency in the sinusoidal test (10 to 30 Hz). At the same time, these piezoelectric voltages were lower than those to be expected from a simple calculation based on a consideration of the PVF<sub>2</sub> film as a parallel-plate capacitor. The observed rate (or frequency) dependence was similar to that reported by Broadhurst et. al.<sup>42,43</sup> who had measured the short-circuit piezoelectric current for polyvinyl chloride films. The rate (or frequency)

dependence of the AMMRC tests was explained by considering the low input impedance of the oscilloscope as a charge leakage path which lowered the instantaneous charge level on the  $PVF_2$  film. A mathematical treatment of the circuit response to the charge generation and charge leakage processes showed that the piezoelectric voltage should be nearly proportional to the time derivative of the loading function at these low test rates. These initial experiments served only as a qualitative demonstration of the piezoelectric activity of  $PVF_2$ .

The quantitative studies of the  $PVF_2$  films involved the determination of the static piezoelectric constant as described in the Experimental section. A typical result from this type of experiment is shown in Figure 12, where the coulometer voltage outputs are plotted against the compressive loads on the film specimens. The curves are highly linear during the loading increments but become slightly non-linear during the unloading increments. These results are quite reproducible after several loading and unloading cycles. The first loading cycle generally produced larger voltages for corresponding loading increments and, upon unloading, returned instead to a voltage greater than zero at zero load. The polarity of the piezoelectric charge was always the same, viz., the face of the  $PVF_2$  film which became positive during the compression loading was the face of the film which was adjacent to the negative poling plate during the poling process.

A few compression tests were performed in which two stretched poled  $PVF_2$  films were stacked one above the other, i.e., mechanically in series. When the films of equal piezoelectric activity were connected electrically in parallel, the piezoelectric activity of the combination was double that

of either film. This agreed with the results of Church<sup>44</sup> who has investigated the piezoelectric activity of multi-layered PVF<sub>2</sub> film assemblies. When we connected our two PVF<sub>2</sub> films electrically in series, we found that the piezoelectric activity of the combination was equal to the average of that of the two individual films. This latter result held for three different cases: the two films were of equal activity, the two films were of unequal activity, and one of the films had zero activity.

With PVF<sub>2</sub> films poled under an effective field of 500 kV/cm, the piezoelectric constant was found to vary with the prior draw ratio in the manner shown by Figure 13. The most rapid increase occurred between draw ratios of 3/1 and 5/1, paralleling the conversion of Phase II crystalline conformation to Phase I as a function of draw ratio as noted by IR spectroscopy. This suggested that the Phase I crystalline material plays a considerable role in the piezoelectric behavior<sup>11,45</sup> in addition to any effect produced by polymer orientation. The apparent leveling off of the piezoelectric constant at the high draw ratios agrees with our results that there is no further conversion of material to the Phase I form and there is no further significant orientation of the crystalline regions at high draw ratios under these experimental conditions. The further increase of sonic modulus at the higher draw ratios indicates that the continuing orientation of the amorphous material may contribute in only a minor way to the piezoelectric constant.

Changes in density were produced by drawing, as previously discussed for Figure 2. The piezoelectric constant, when plotted against density, appears as in Figure 14. This monotonic relationship indicates that the piezoelectric constant may be largely dependent upon the degree of crystallinity and/or the change in crystalline conformation with

stretching. The apparent leveling off of the piezoelectric activity at high draw ratios (see Figure 13) and at high densities (suggested by the cluster of points at high draw ratios on Figure 14) may indicate that the piezoelectric constant is limited by the degree of crystallinity or the phase I content<sup>11,23,28,29</sup>.

A series of experiments was run to determine the effects of the poling variables upon the subsequent piezoelectric activity of the highly stretched PVF<sub>2</sub> films. The effect of the poling voltage upon the piezoelectric constant is shown in Figure 15, where one sees a smoothly rising curve which begins to level off at the higher voltages. This suggests that for these poling times and temperatures we are approaching a limit to the piezoelectric activity that can be attained by this method.

The effect of poling times at final poling temperatures of 80°C and above and fields of 500 kV/cm is seen in Figure 16. The times plotted here refer to the length of time required for the film to be heated through the specified temperature range. There was an additional cooling time of at least 15 minutes to allow the film to reach approximately 70°C. This graph shows that heating times of 5-10 minutes are sufficient to produce the maximum attainable piezoelectric activity under these poling conditions. Other results, not shown here, indicate that longer poling times (60 to 90 minutes) have little effect upon the piezoelectric activity.

The effect of poling temperature upon piezoelectric activity at fixed poling fields (500 kV/cm) and poling times (total, 45 minutes) appears in Figure 17. In these experiments the films were brought

to the specified temperature and annealed for 15 to 30 minutes prior to applying the D.C. voltage. There is a marked effect of temperature, where the piezoelectric constant ranges from 0.5 pcoul/nt at room temperature to values of 6 to 8 pcoul/nt at 60 to 80°C where there is an apparent leveling off of activity. The dashed line in Figure 17 indicates the values to be expected from consideration of results in Figures 15 and 16. Thus annealing of the film prior to poling seems to have a deleterious effect on the piezoelectric activity.

The retention of the piezoelectric activity over a temperature range for highly stretched PVF<sub>2</sub> films poled at 85°C at 1000 KV/cm is plotted in Figure 18. Initial film activity was about 19 pcoul/nt. With no field applied, the films were then reheated between aluminum plates for one hour at the specified temperature and then cooled to room temperature before the piezoelectric activity was again determined. It is seen that the piezoelectric activity was retained under these conditions up to 85-90°C, beyond which there was a continuous decrease with temperature. At 150°C about one-half of the original activity was still retained.

### CONCLUSIONS

From the experiments and results described above, we can draw the following conclusions:

1. Increases in the draw ratio of the PVF<sub>2</sub> film produces continuous conversions from crystalline Phase II to Phase I. At the same time the increase in density may indicate a change in crystalline conformation and/or simultaneous conversion of amorphous polymer regions to a

crystalline form. The leveling off of the birefringence at the high draw ratios suggests that the crystalline phase is undergoing no further orientation, whereas the continuing increase of sonic modulus at high draw ratios indicates that the amorphous regions are still undergoing further orientation.

2. The piezoelectric activity increased with draw ratio, the poling voltage, poling temperature, and poling time.

3. Significant amounts of oriented phase I crystalline material are needed in order to achieve high degrees of piezoelectric activity in  $PVF_2$ .

## LITERATURE CITED

1. Kawai, H. "The Piezoelectricity of Polyvinylidene Fluoride". Japan J. Appl. Phys., V. 8, 1969, p. 975.
2. Fukada, E, and Takashita, S. "Piezoelectric Effect in Polarized Polyvinylidene Fluoride". Japan J. Appl. Phys., V. 8, 1969, p. 960.
3. Nakamura, K., and Wada, Y. "Piezoelectricity, Pyroelectricity, and the Electrostriction Constant of Polyvinylidene Fluoride". J. Polymer Sci.: Part A-2, V. 9, 1971, p. 161.
4. Cohen, J., Edelman, S., and Vezzetti, C. F. "Pyroelectricity and Piezoelectricity in Oriented Films of Polyvinyl Fluoride and Polyvinylidene Fluoride". Electrets Charge Storage and Transport in Dielectrics, Electrochemical Society, 1973.
5. Hayakawa, R., and Wada, Y. "Piezoelectricity and Related Properties of Polymer Films". Advances in Polymer Science, V. 11, 1973, p. 1.
6. Day, G. W., Hamilton, C. A., Peterson, R. L., Phelan, R. J., and Mullen, L. O. "Effects of Poling Conditions on Responsivity and Uniformity of Polarization of PVF<sub>2</sub> Pyroelectric Detectors". Appl. Phys. Letters, v. 24, 1974, p. 456.
7. McFee, J. H., Bergman, J. G., and Crane, G. R. "Pyroelectric and Nonlinear Optical Properties of Poled Polyvinylidene Fluoride Films". Ferroelectrics, v. 3, 1972, p. 305.
8. Glass, A. M., McFee, J. H., and Bergman, J. G. "Pyroelectric Properties of Polyvinylidene Fluoride and Its Use for Infrared Detector". J. Appl. Phys., v. 42, 1971, p. 5219.
9. Aslaksen, E.W. "Theory of the Spontaneous Polarization and the Pyroelectric Coefficient of Linear Chain Polymers". J. Chem. Phys., V. 57, 1972, p. 2358.

10. Buchman, P. "Pyroelectric and Switching Properties of Polyvinylidene Fluoride Film". *Ferroelectrics*, v. 5, 1973, p. 39.
11. Murayama, N. "Piezoelectric and Pyroelectric Effects of Polymer Electrets". *Microsymposium on Electrical Properties of Polymers*, Tokyo, Japan, Jan. 1972.
12. Pfister, G., Abkowitz, M., and Crystal, R. G. "Pyroelectricity in Polyvinylidene Fluoride". *J. Appl. Phys.*, v. 44, 1973, p. 2064.
13. Burkard, H. and Pfister, G. "Reversible Pyroelectricity and Inverse Piezoelectricity in Polyvinylidene Fluoride". *J. Appl. Phys.*, v. 45, 1974, p. 3360.
14. Lando, J.B., Olf, H. G. and Peterlin, A. "Nuclear Magnetic Resonance and X-Ray Determination of the Structure of Polyvinylidene Fluoride". *J. Polymer Sci.: Part A-1*, v. 4, 1966, p. 941.
15. Cortili, G. and Zerbi, G. "Chain Conformations of Polyvinylidene Fluoride as Derived from Its Vibrational Spectrum". *Spectrochimica Acta*, v. 23A, 1967, p. 285.
16. Nakagawa, K. and Ishida, Y. "Annealing Effects in Polyvinylidene Fluoride as Revealed by Specific Volume Measurements, Differential Scanning Calorimetry, and Electron Microscopy". *J. Polymer Sci., Polym. Phys. Ed.*, v. 11, 1973, p. 2153.
17. Wentink, T., Willwerth, L. J., and Phaneuf, J. P. "Properties of Polyvinylidene Fluoride. Part II. Infrared Transmission of Normal and Thermally Decomposed Polymer". *J. Polymer Sci.*, v. 55, 1961, p. 551.
18. Enomoto, S., Kawai, T., and Sugita, M. "Infrared Spectrum of Polyvinylidene Fluoride". *J. Polymer Sci.: Part A-2*, v. 6, 1968, p. 861.

19. Luongo, J. P. "Far-infrared Spectra of Piezoelectric Polyvinylidene Fluoride". J. Polymer Sci.: Part A-2, v. 10, 1972, p. 1119.
20. Boerio, F. J., and Koenig, J. L. "Raman Scattering in Nonplanar Polyvinylidene Fluoride". J. Polymer Sci.: Part A-2, v. 7, 1969, p. 1489.
21. Koenig, J. L. "Raman Scattering of Synthetic Polymers - A Review". Appl. Spectroscopy Rev., v. 4(2), 1971, p. 233.
22. Cessac, G. and Curro, J. G. "Raman Scattering in Uniaxially Oriented Samples of Planar Zigzag Polyvinylidene Fluoride". J. Polymer Sci.: Polymer Physics Ed., v. 12, 1974, p. 695.
23. Doll, W. W. and Lando, J. B. "Polymorphism of Polyvinylidene Fluoride. III. The Crystal Structure of Phase II". J. Macromol. Sci-Phys., v. B4(2), 1970, p. 309.
24. Doll, W. W. and Lando, J. B. "The Polymorphism of Polyvinylidene Fluoride. IV. The Structure of High-Pressure-Crystallized Polyvinylidene Fluoride". J. Macromol. Sci.-Phys., v. B4(4), 1970, p. 889.
25. Doll, W. W. and Lando, J. B. "The Polymorphism of Polyvinylidene Fluoride. V. The Effect of Hydrostatic Pressure on the Melting Behavior of Copolymers of Vinylidene Fluoride". J. Macromol. Sci-Phys., v. B4(4), 1970, p. 897.
26. Toida, Y. and Chujo, R. "High-Resolution NMR Spectra and Conformation of Polyvinylidene Fluoride and their Relation with Crystal Modifications". Polymer J., v. 6, 1974, p. 191.
27. Tadokoro, H., Hasegawa, R., Kobayashi, M., Takahashi, Y., and Chatani, Y. "Molecular Conformation and Packing of Polyvinylidene Fluoride". IUPAC XXIII International Congress, v. II, 1971, p. 865.

28. Doll, W. W. and Lando, J. B. "The Radiation-Initiated Solution Polymerization of Vinylidene Fluoride". *J. Appl. Polymer Sci.*, v. 14, 1970, p. 1767.
29. Farmer, B. L. Hopfinger, A. J., and Lando, J. B. "Polymorphism of Polyvinylidene Fluoride: Potential Energy Calculations of the Effects of Head-to-Head Units on the Chain Conformation and Packing of Polyvinylidene Fluoride". *J. Appl. Phys.*, v. 43, 1972, P. 4293.
30. Wentink, T. "Properties of Polyvinylidene Fluoride. I. Dielectric Measurements". *J. Appl. Phys.*, v. 32, 1961, p. 1063.
31. Peterlin, A. and Elwell, J. H., "Dielectric Constant of Rolled Polyvinylidene Fluoride". *J. Materials Sci.*, v. 2, 1967, p. 1.
32. Sasabe, H. and Saito, S. "Dielectric Relaxations in Polyvinylidene Fluoride". *J. Polymer, Sci.: Part A-2*, v. 7, 1969, p. 1405.
33. Koizumi, N., Yano, S., and Tsunashima, K. "Dielectric Relaxation of Polyvinylidene Fluoride". *Polymer Letters*, v. 7, 1969, p. 59.
34. Bur, A. J. "Dielectric Properties of Fluorine-Containing Polymers". Article in "Fluoropolymers", Ed. by L. A. Wall, Wiley-Interscience, 1972, p. 475.
35. Osaki, S., Uemura, S., and Ishida, Y. "Effects of a Static Electric Field upon Dielectric Properties of Polyvinylidene Fluoride and Polvinyl Fluoride". *J. Polymer Sci.: Part A-2*, v. 9, 1971, p. 585.
36. Uemura, S. "Ionic Contribution to the Complex Dielectric Constant of a Polymer under DC Bias". *J. Polymer Sci.: Polym. Physics Ed.*, v. 10, 1972, p. 2155.
37. Uemura, S. "Low-Frequency Dielectric Behavior of Polyvinylidene Fluoride". *J. Polymer Sci.: Polym. Physics Ed.*, v. 12, 1974, p. 1177.

38. Yano, S. "Dielectric Relaxation and Molecular Motion in Polyvinylidene Fluoride". J. Polymer Sci.: Part A-2, v. 8, 1970, p. 1057.
39. Yano, S. Tadano, K., and Aoki, K. "Alternating-Current Ionic Conduction and Dielectric Relaxation of Polyvinylidene Fluoride at High Temperatures". J. Polymer Sci.: Polymer Physics Ed., v. 12, 1974, p. 1875.
40. Desper, C. R., Lionetta, W. G., and Lewis, R. W., "Radiant Oven Stretching Process for Thin Film Polymeric Armor Material". Army Materials & Mechanics Research Center, Watertown, MA, Technical Report AMMRC TN 74-11, Sept. 1974.
41. Desper, C. R. "Technique for Measuring Orientation in Polymers". CRC Critical Reviews in Macromolecular Science, v. 1, 1973, p. 503.
42. Broadhurst, M. G., Malmberg, C. G., Mopsik, F. I., and Harris, W. P. "Piezo- and Pyroelectricity in Polymer Electrets". Presented at Conference on Electrets, Charge Storage and Transport in Dielectrics, Miami Beach, Fla., Oct. 1972.
43. Broadhurst, M. G., Harris, W. P., Mopsik, F. I., and Malmberg, C. G. "Piezoelectricity, Pyroelectricity and Electrostriction in Polymers". Polymer Preprints, v. 14, 1973, p. 820.
44. Church, E. L. Frankford Arsenal, Private communication, 1975.
45. Tamura, M., Ogasawara, K., Ono, N., and Hagiwara, S. "Piezoelectricity in Uniaxially Stretched Polyvinylidene Fluoride". J. Appl. Phys., v. 45, 1974, p. 3768.

TABLE II

QUALITATIVE COMPARISON OF INTENSITIES OF WIDE ANGLE X-RAY DIFFRACTION OF STRETCHED PVF<sub>2</sub>

DRAW RATIO	INTENSITY* OF PEAKS OCCURRING NEAR THE FOLLOWING									
	d SPACINGS (Å)									
	2.20	2.30	2.47	2.74	3.31	4.29	4.39	4.80	4.95	
ORIGINAL	—	W	VW	VW	M	—	M	—	M	
2/1	VW	↑ VW	—	—	—	—	↓ S	—	—	↓ M
3/1	—	—	—	—	—	+	+	+	+	+
4/1	—	—	—	—	—	S	—	—	—	—
6/1	M	—	VW	—	VW	—	—	—	—	—

+ 4.33 (S)

# 4.89 (M)

\* Arrows Indicate Increasing Intensities

7100-0002

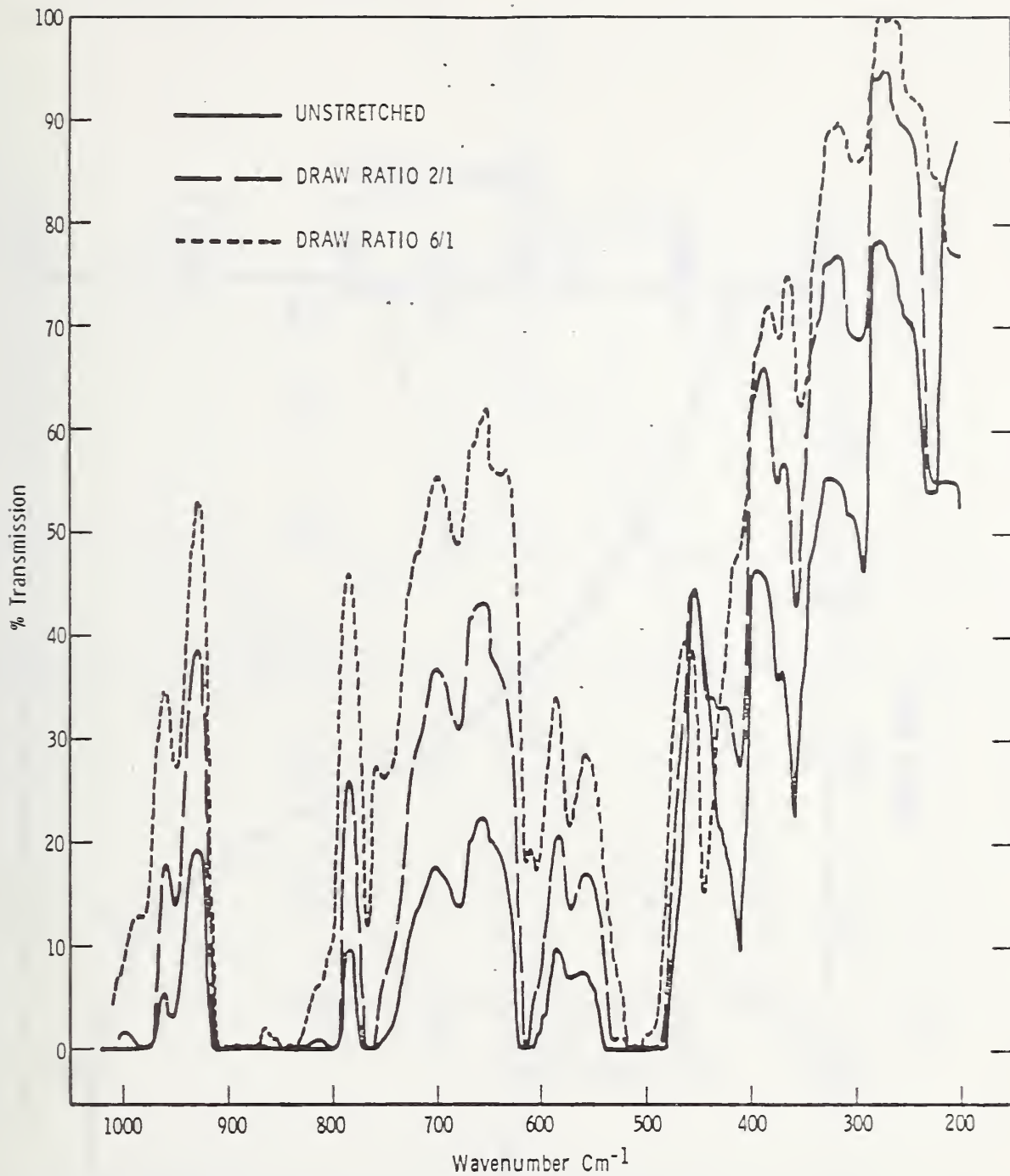


Figure 1

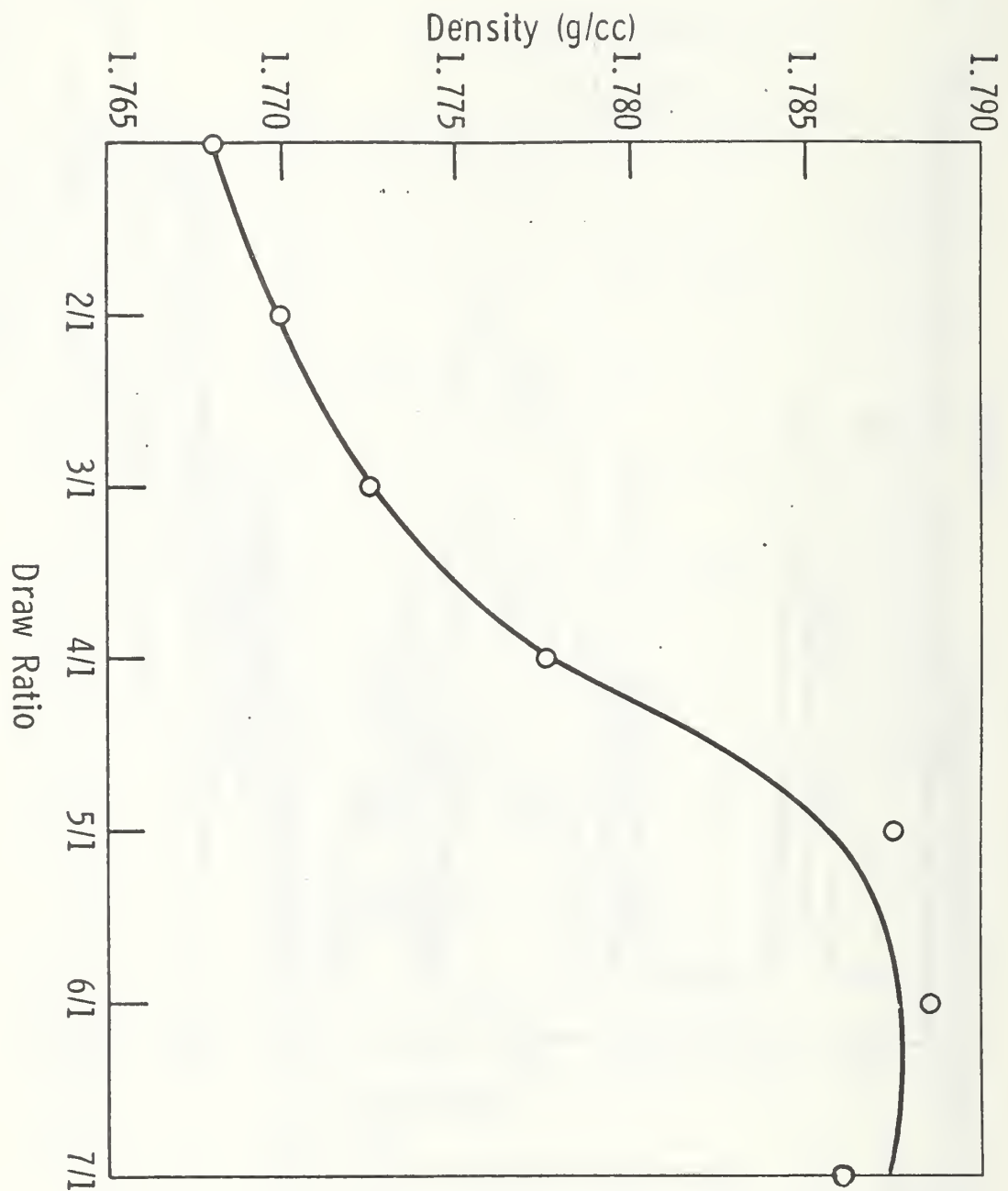


Figure 2

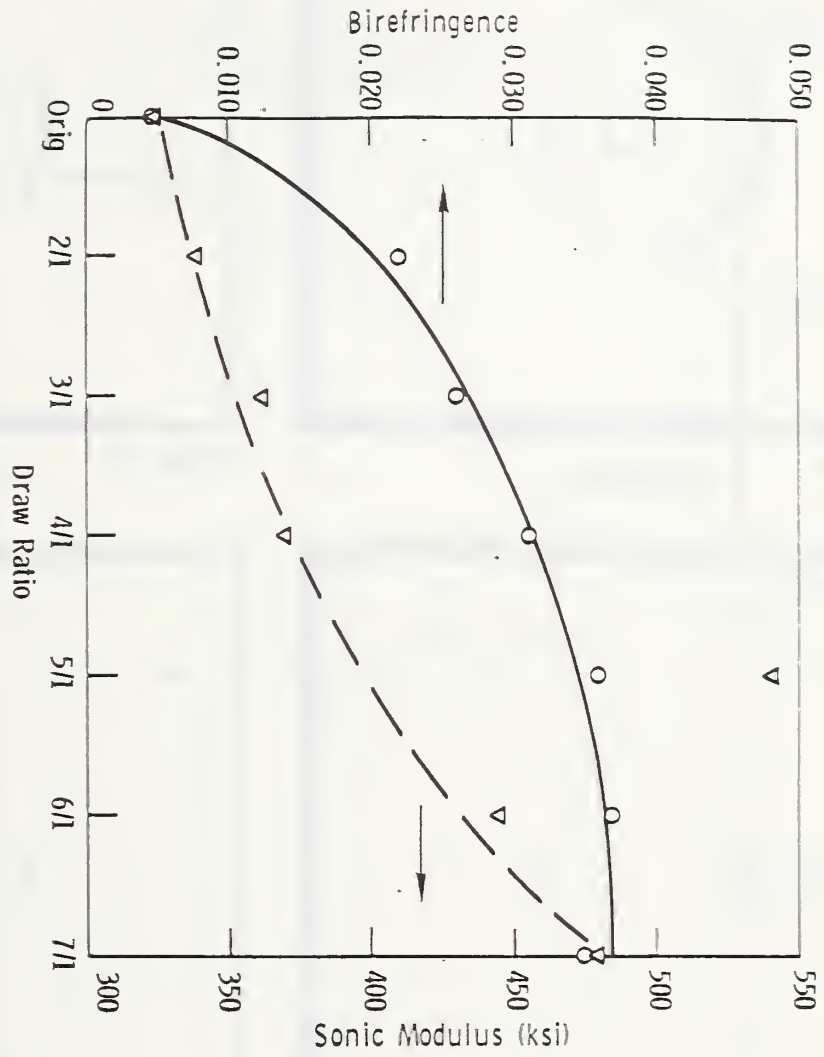


Figure 3

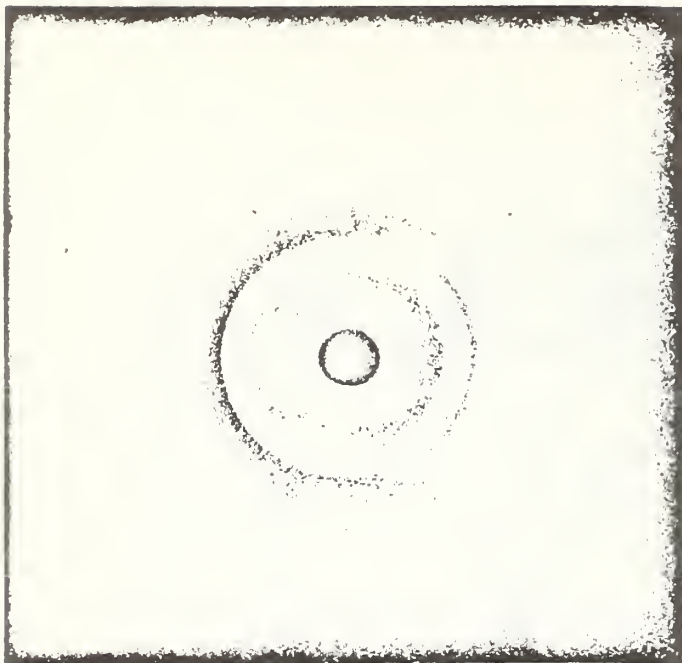


FIG. 4 UNORIENTED



FIG. 5 DRAW RATIO: 2/1

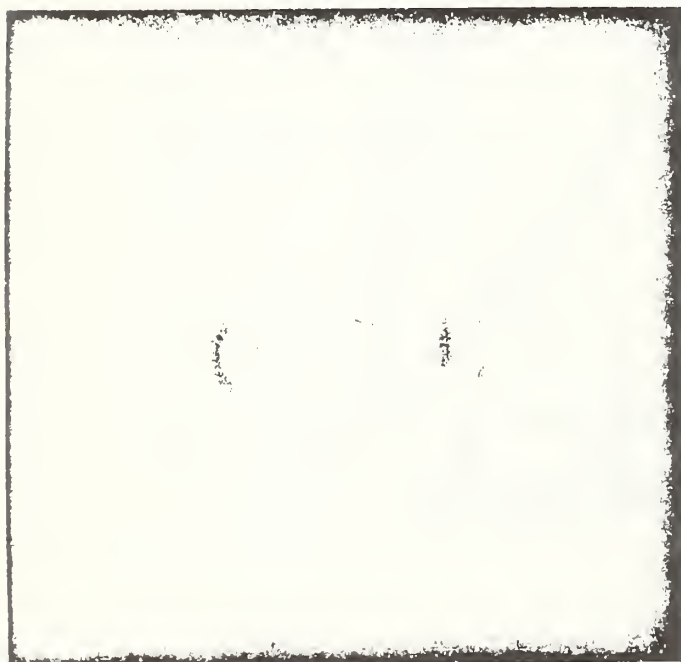


FIG. 6 DRAW RATIO: 4/1



FIG. 7 DRAW RATIO: 6/1

WIDE ANGLE X-RAY DIFFRACTION OF STRETCHED PVF<sub>2</sub> FILM

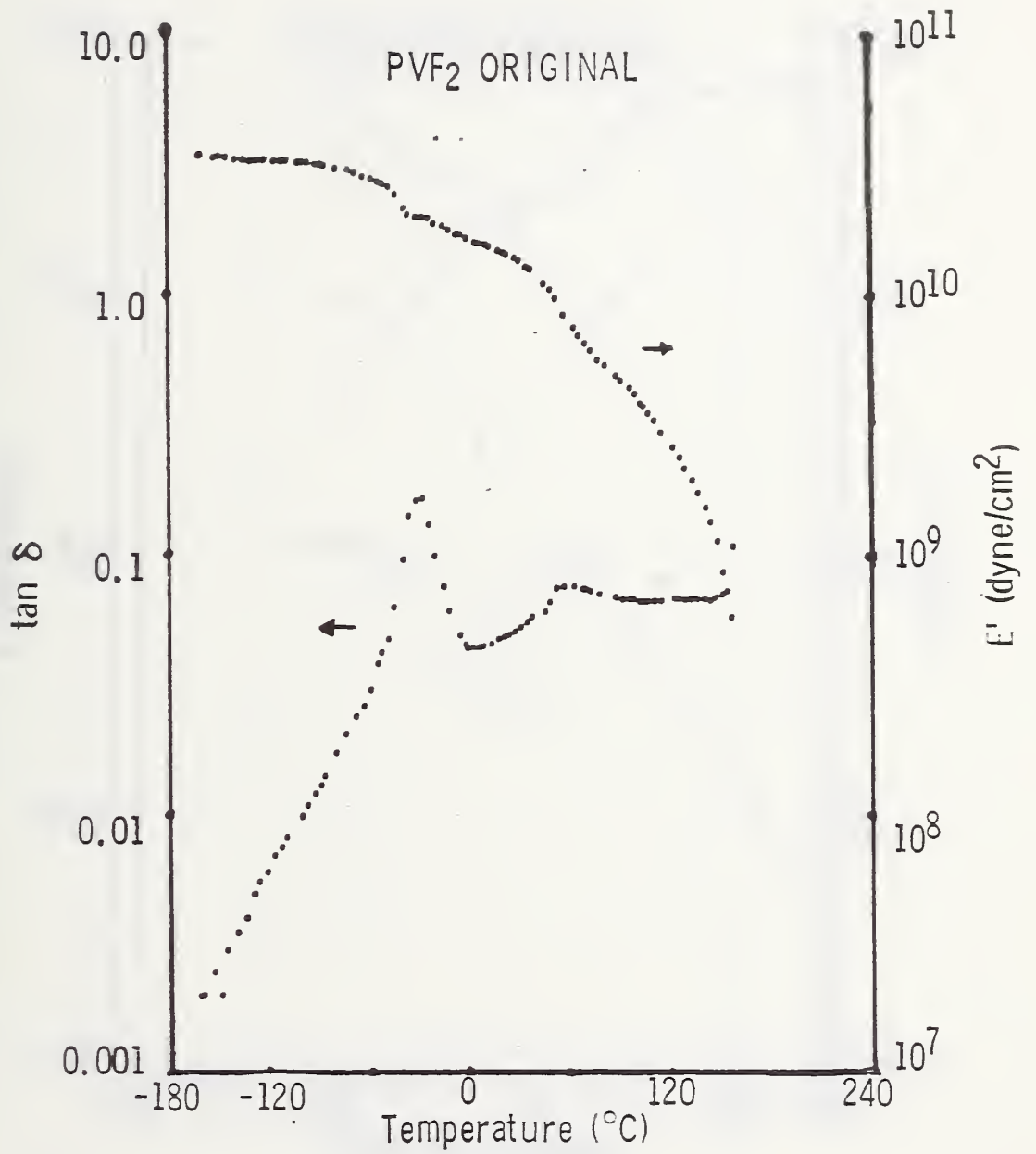


Figure 8

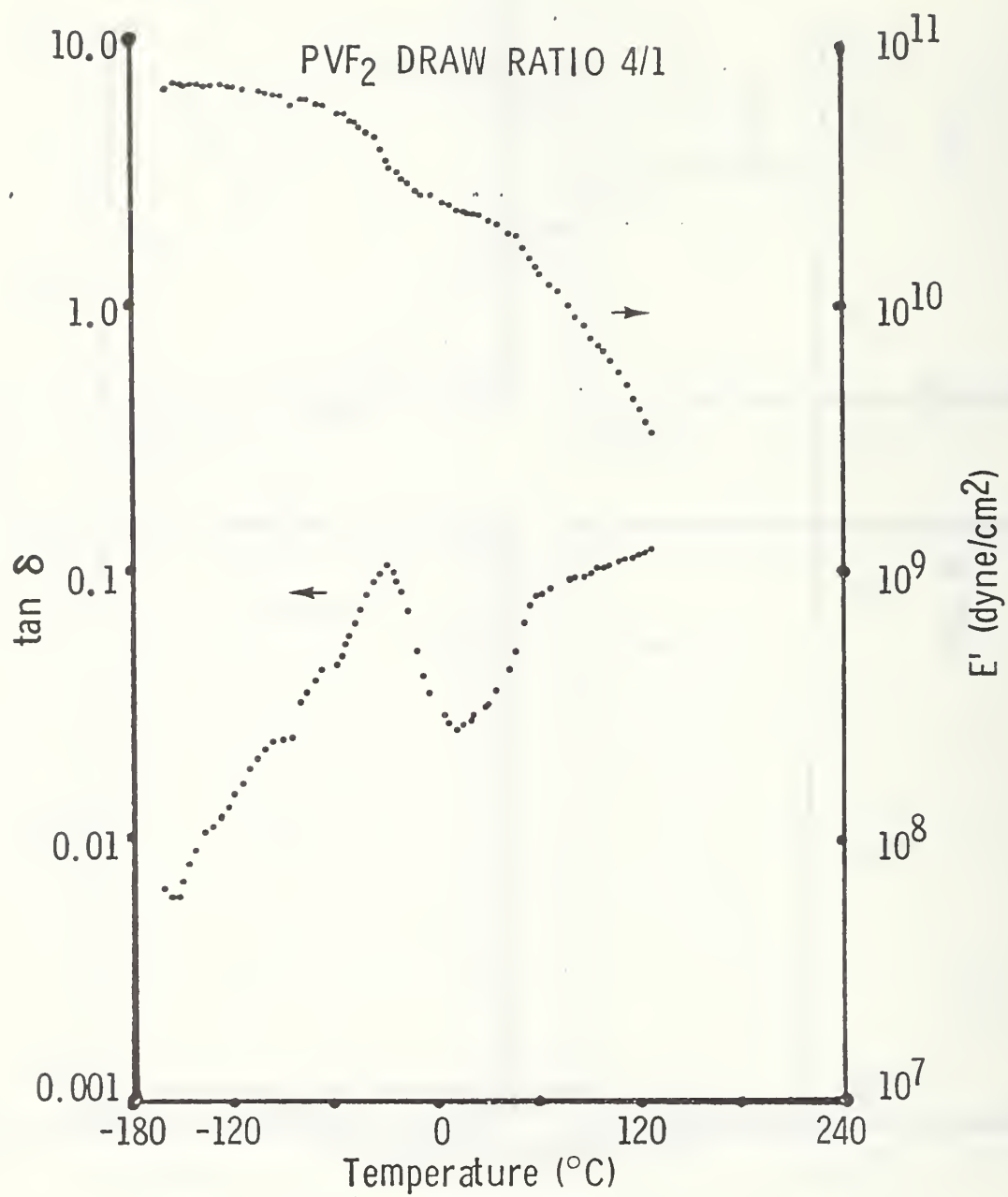


Figure 9

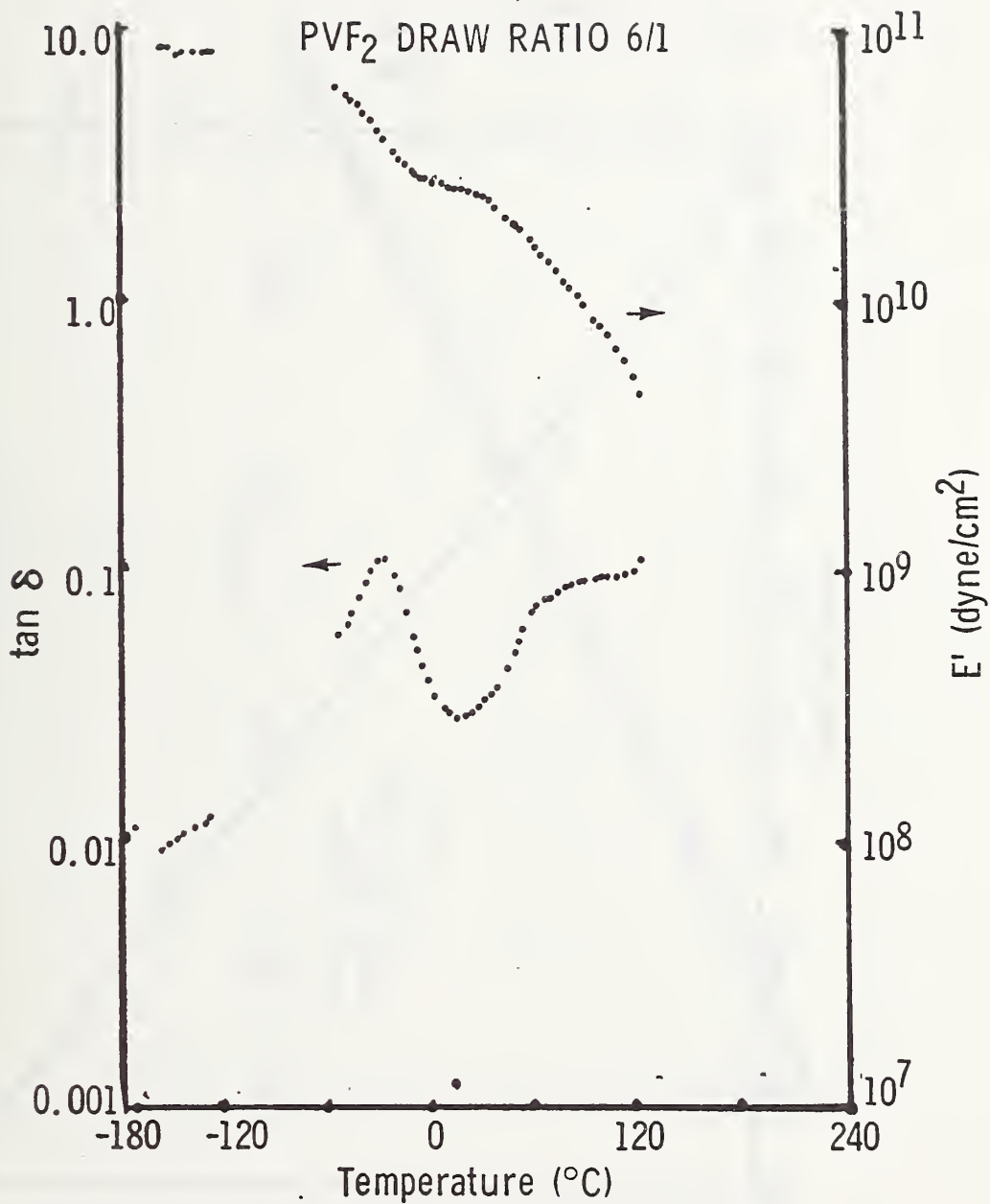


Figure 10

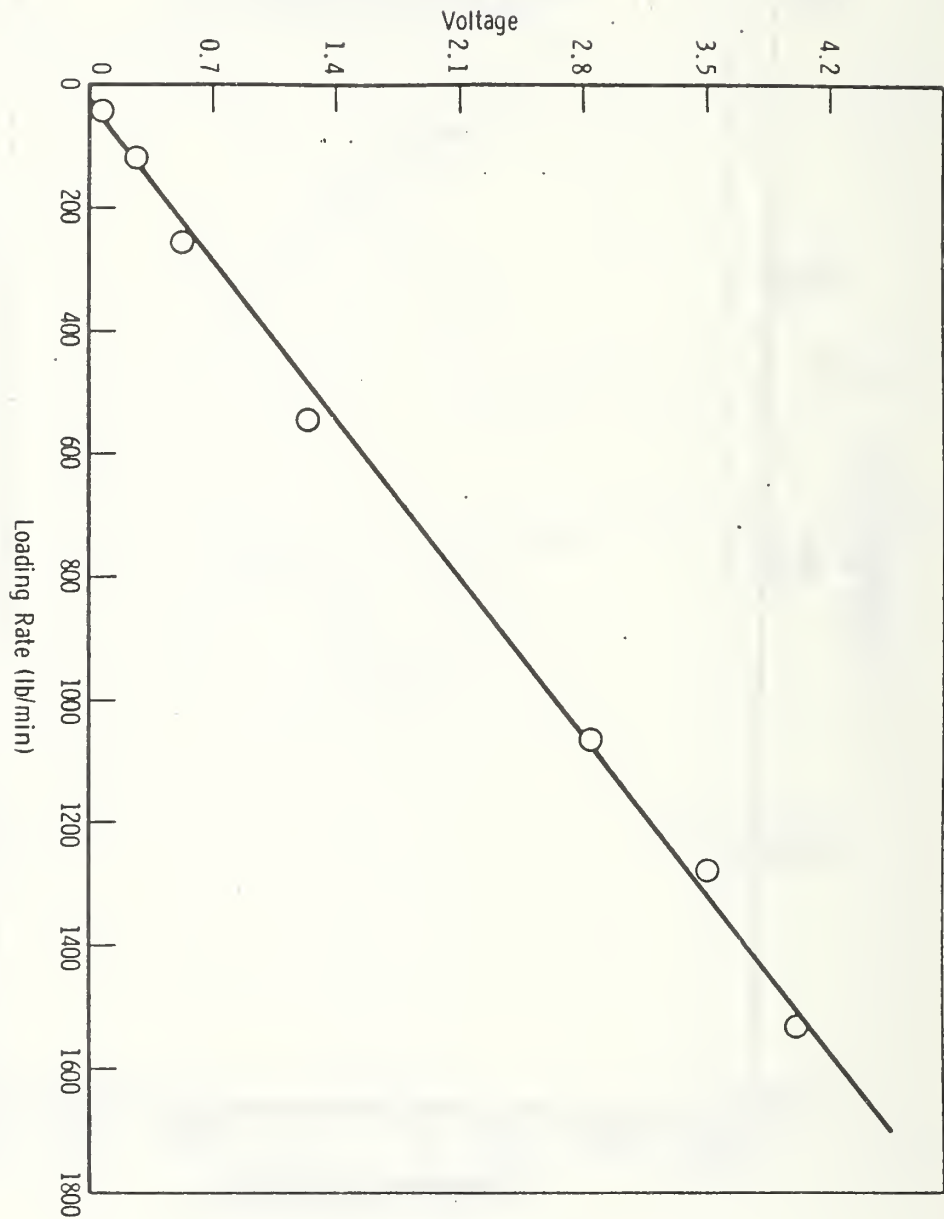


Figure 11

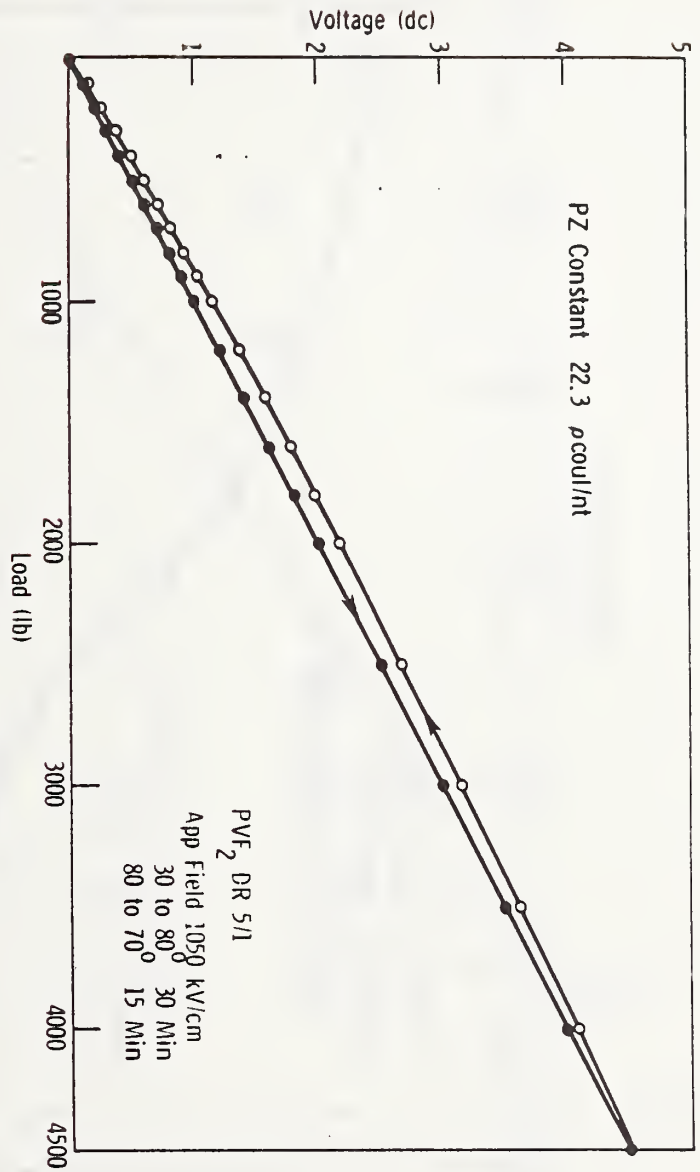


Figure 12

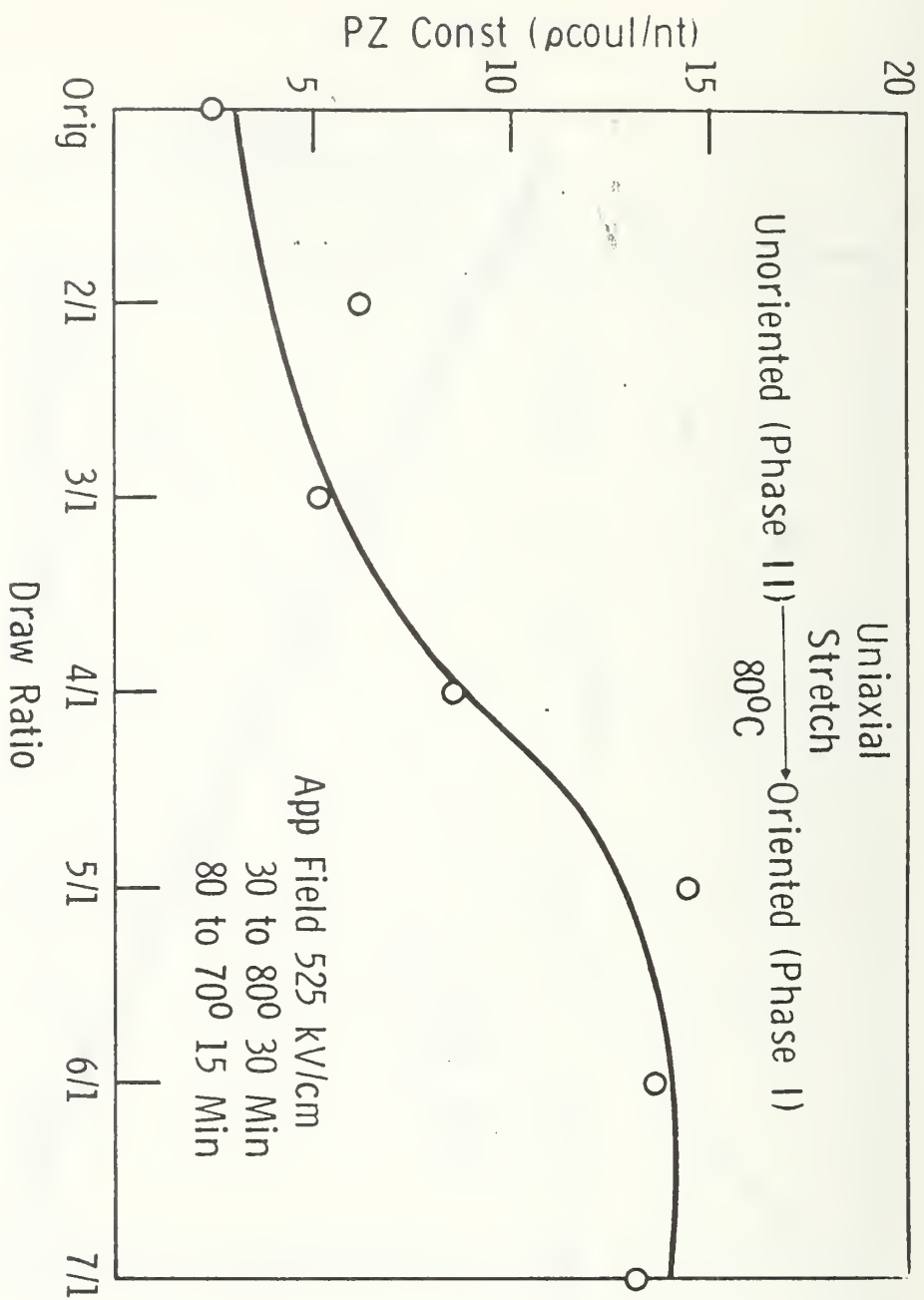


Figure 13

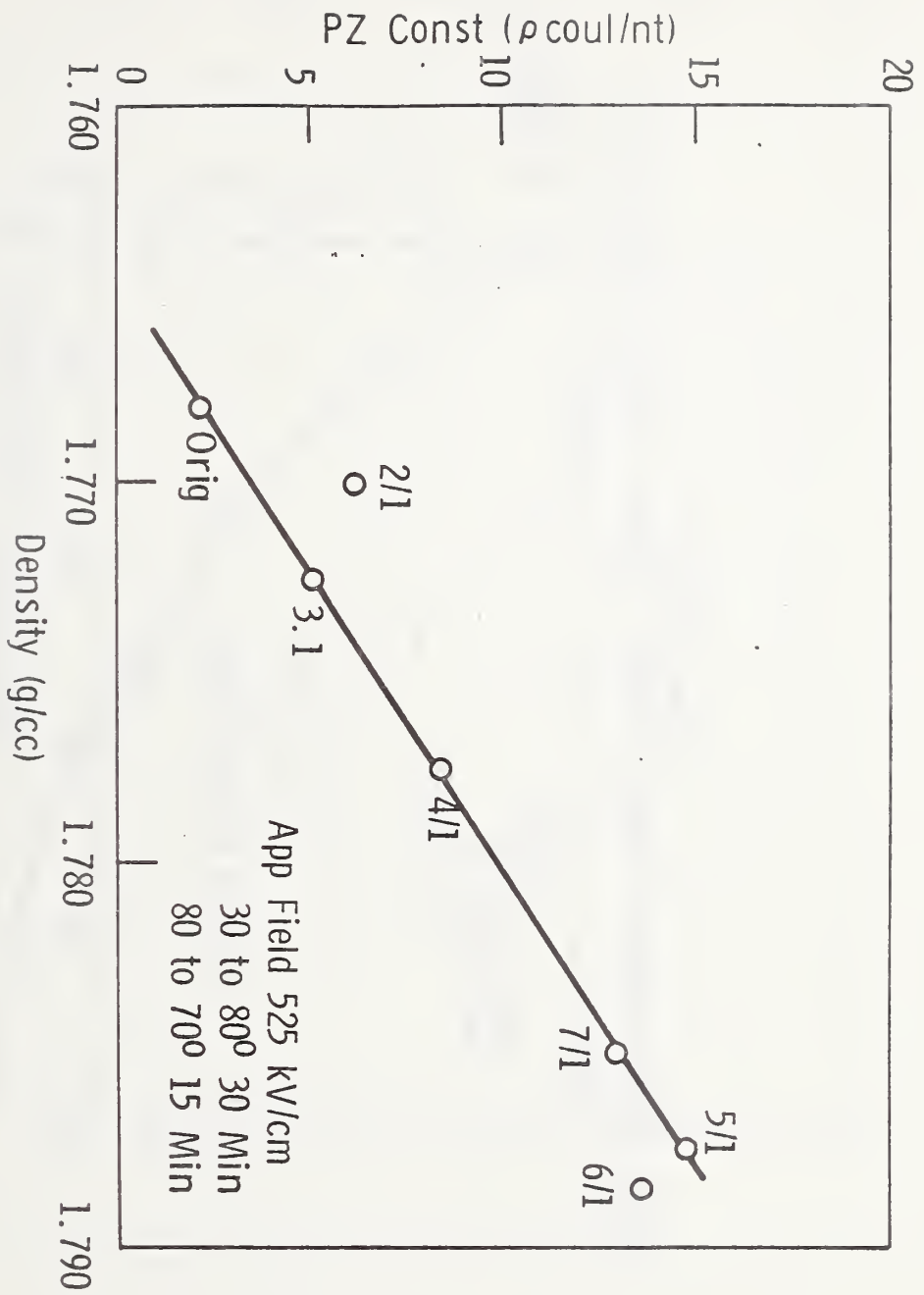


Figure 14

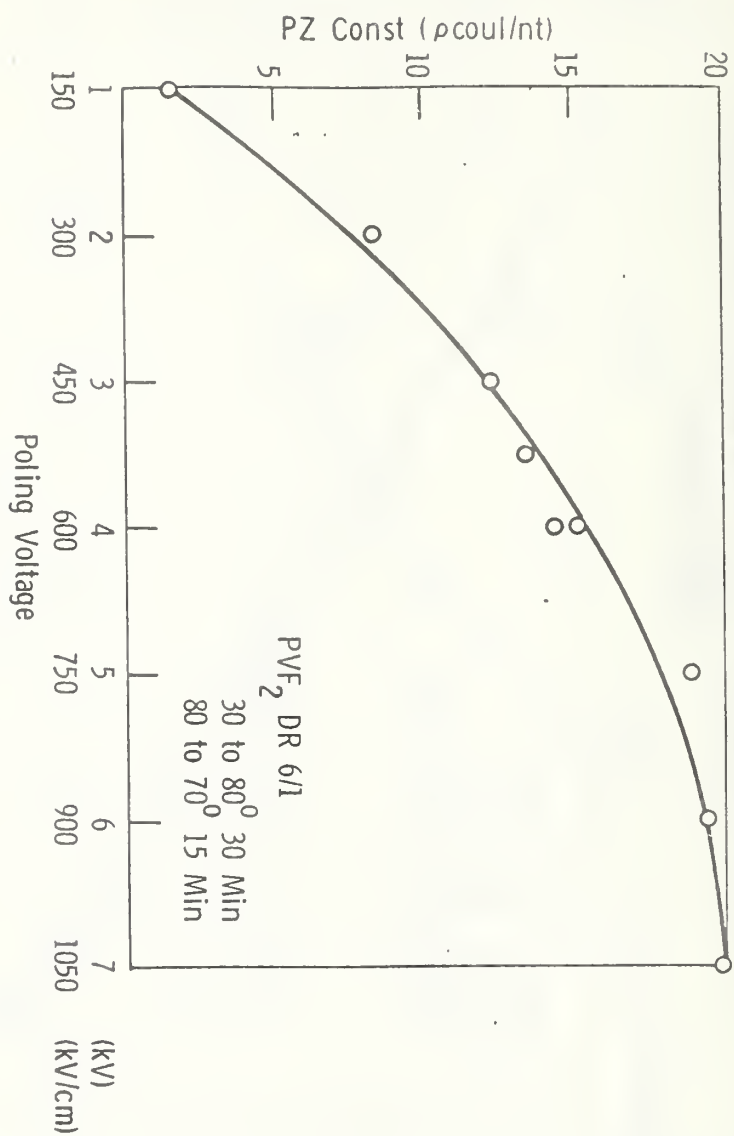


Figure 15

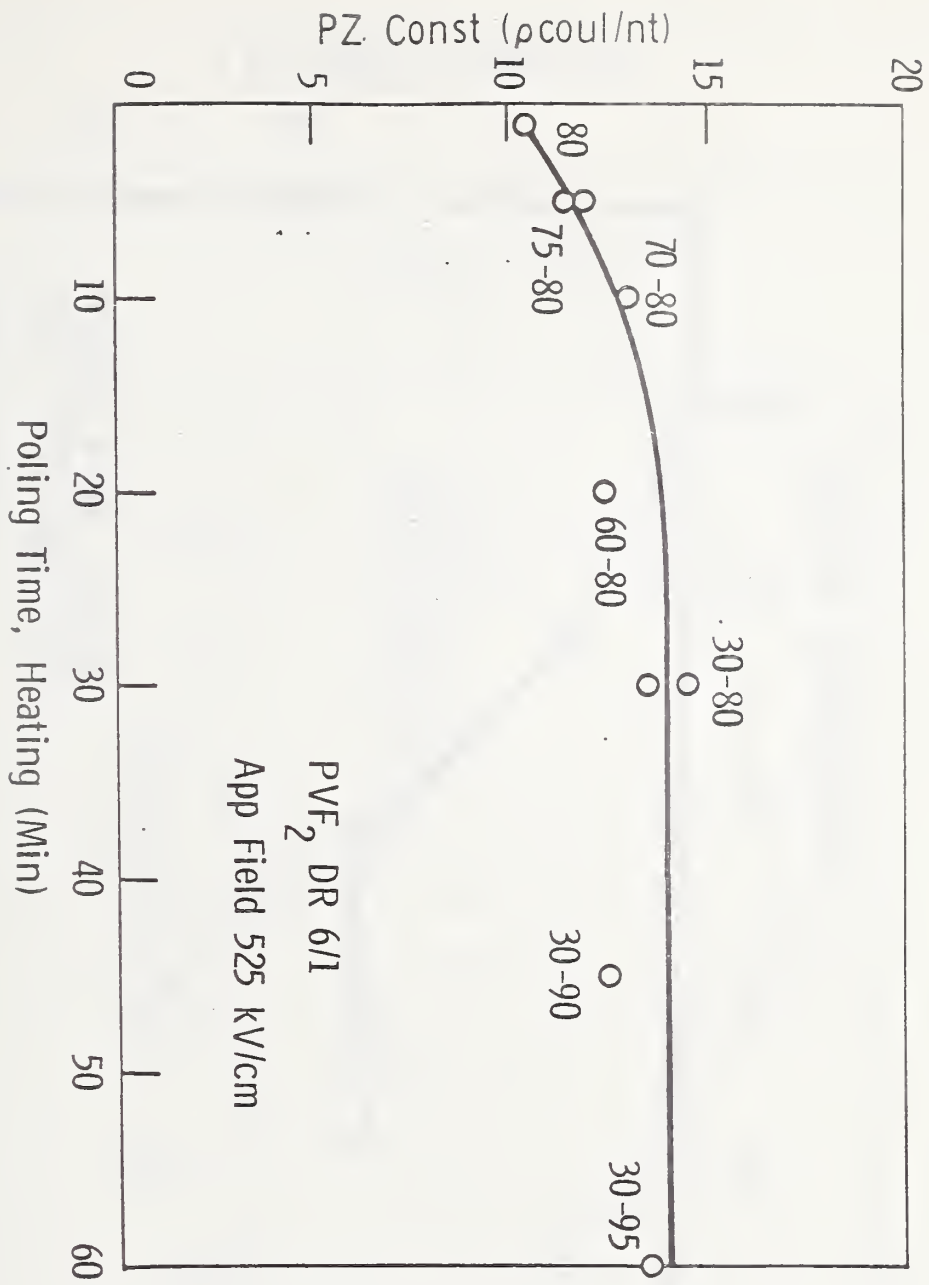


Figure 16

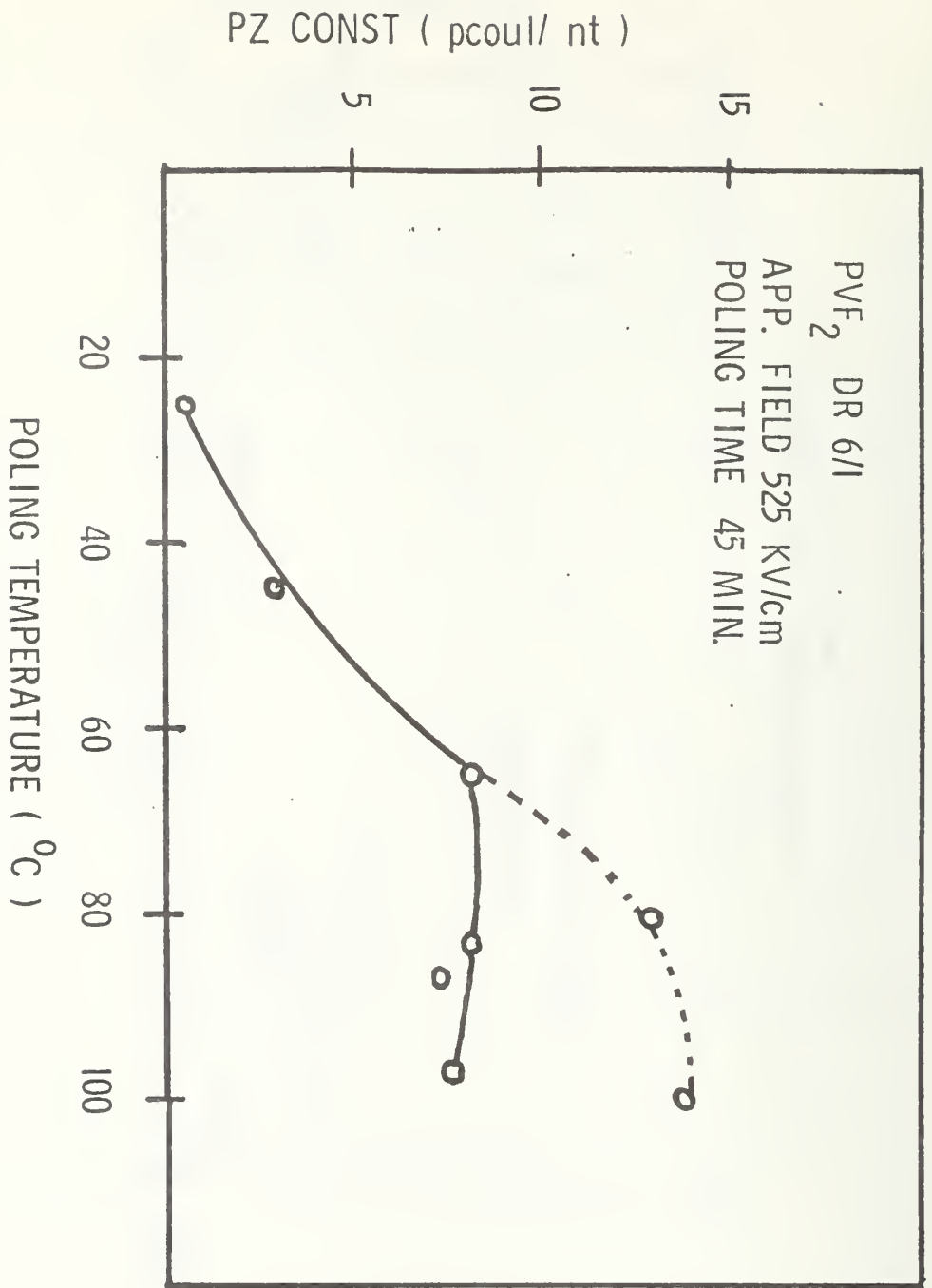


Figure 17

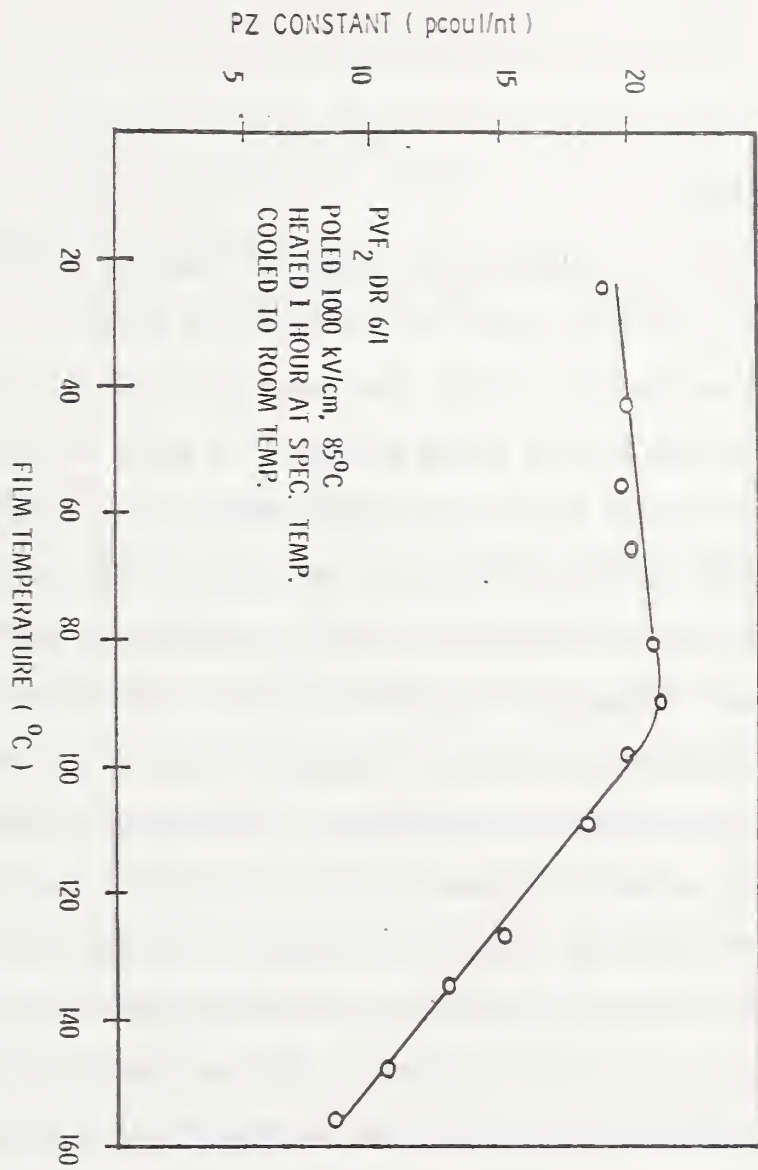


Figure 18

M. Abkowitz, P.J. Luca, G. Pfister and W.M. Prest, Jr.  
Xerox Corporation, Webster, N.Y. 14580

### (1) Introduction

This report will address three topics of interest to the study and understanding of the origin of pyro- and piezoelectric behavior in polarized polymer films, and in particular in PVF<sub>2</sub>. The first part will show that thermally stimulated currents (TSC) are a viable technique to probe the morphological implications of the origin of the poling induced polarization. The  $\alpha_a$ -relaxation in commercial films of PVF<sub>2</sub> will serve as an example. The TSC results will then be related to ac current measurements which, in analogy to the TSC technique, are run at constant frequency on a temperature axis. The relation between the heating rate in the TSC experiment and the frequency in the ac experiment will be demonstrated. By then combining the TSC and ac techniques, we are able to track the  $\alpha_a$ - and  $\alpha_c$ -relaxations in commercial PVF<sub>2</sub> films over 9 decades of frequency. Quite generally, with the method illustrated for the  $\alpha_a$ - and  $\alpha_c$ -relaxations in PVF<sub>2</sub>, structure in the TSC spectrum can be related to structure observed in dielectric and mechanical relaxation studies. This way that structure in the TSC, which is unique to molecular relaxations can be identified, thus overcoming what is often perceived to be a major limitation of an otherwise uniquely powerful technique for studying low frequency molecular motions in polymeric solids.

The second part of the presentation will discuss TSC measurements on samples prepared from Pennwalt and Kureha powder materials. It will be shown that the morphology of these samples, which was controlled by the crystallization tempera-

ture/time history strongly influences the TSC spectrum. In particular, the appearance of a third phase, probably a modified form of the  $\beta$ -crystalline phase, drastically enhances the TSC amplitude.

Finally, the third part presents some field/temperature history effects upon the electrical properties of commercial PVF<sub>2</sub> films. Of particular interest are those effects which were induced at fields and temperatures typically used for poling PVF<sub>2</sub>. Furthermore, evidence for what may be field induced dipole pinning in the amorphous phase of the polymer will be presented. The first and third part of the presentation have been the subject of recent publications, while the results of the second part are in the stage of detailed analysis and some data have to be treated as preliminary.

## (2) The $\alpha_a$ - and $\alpha_c$ -Relaxations

In the TSC experiment, a sample which has previously been polarized by cooling in a dc bias field, is heated at a constant rate under zero bias. The electrodes of the sample are connected to a current meter and the current flowing in the external circuit as the polarized sample is heated, is continuously recorded versus sample temperature. The TSC often exhibits a structure with peaks occurring at temperatures characteristic of molecular relaxations in the polymer. Peaks might arise from reorientation of permanent or induced dipoles or charge release from traps associated with the relaxation process. In addition, of course, trap emptying unrelated to molecular relaxations might also occur.

In PVF<sub>2</sub>, the TSC exhibits a large peak at  $T_g \sim -51^\circ\text{C}$ , which is associated with dipole relaxation, probably of the permanent (CH<sub>2</sub>CF<sub>2</sub>) dipoles ( $\alpha_a$ -relaxation). The evidence for dipole relaxation rather than charge release is illustrated in Fig. 1. For our purpose, only the traces below room temperature are of interest. Trace a shows the TSC following cooling of a 25 $\mu\text{m}$  Kureha PVF<sub>2</sub> film in 3V/ $\mu\text{m}$ . Trace b shows the current measured if an unpoled film, i.e., a film which has been cooled to below  $T_g$  under zero bias, is heated with a 3V/ $\mu\text{m}$  bias field applied. The traces a

and b are equal but of opposite sign. These two experiments already suggest that the TSC peak at  $\sim -50^\circ\text{C}$  is due to a dipole polarization. The observation of a peak in trace b cannot be understood by trapped charge release since the film was cooled under zero bias. In the experiment giving rise to trace b in Fig. 1, the orientation of the dipoles in the polymers amorphous phase initially is random. On heating the sample with the field applied, dipoles respond to the field as they become unfrozen around  $T_g$ . This dipole alignment is observed by a corresponding peak at  $T_g$  in the current flowing in the external circuit. Conversely, in the TSC experiment (trace a) the dipoles initially are aligned and randomize at  $T_g$  when the sample is heated under zero bias field. Additional experiments can be performed to test this interpretation. For instance, heating an unpoled film sandwiched between blocking electrodes under appropriate bias reproduces trace b below  $\sim 0^\circ\text{C}$  (see Fig. 1, trace c). The position  $T_m$  of the TSC peak can be analyzed as a function of the heating rate, applied field and poling temperature. One finds  $\sim 71\text{Kcal/mole}$  as apparent activation energy for the relaxation process at  $T_g$ ,  $\tau(T_g) \sim 500$  sec and  $T_m(\beta \rightarrow 0) = T_g \sim -51^\circ\text{C}$ . A value  $N\bar{\mu}^2 \gtrsim 10^{33} \text{ C}^2/\text{cm}$  is obtained for the average number  $N$  of chain segments with average net dipole moment  $\bar{\mu}$  responding to the dc field at  $T_g$ .

Conventional ac dielectric experiments are performed under isothermal conditions and their relation to the nonisothermal TSC measurement is not straight forward. The connection between TSC and ac experiments, however, is greatly facilitated if the latter is performed at constant frequency as a continuous function of temperature. The problem of connecting the two techniques then reduces to relating the heating rate  $\beta$  in the TSC experiment to the frequency  $\omega$  in the ac experiment. This connection will be explored in the following paragraph.

Operationally, one can relate  $\beta$  and  $\omega$  via the well-known equation that defines the temperature  $T_m$  of the TSC maximum. In the usual framework for an exponentially decaying polarization the condition for the TSC maximum is

$$\frac{dT_m}{dT} = -1/\beta \quad (1)$$

where  $\tau$  is the relaxation time. Inserting for example, an exponential temperature dependence for  $\tau$  Eq. (1) yields

$$\frac{1}{\tau} = \frac{\beta A}{T_m^2} \quad (2)$$

where  $A$  is the activation energy in  $^{\circ}\text{K}$ . It is suggested then that a frequency  $\omega = \frac{1}{\tau}$  can operationally be defined from Eq. (2). For typical values of  $\beta \cong 0.3 - 20^{\circ}\text{C}/\text{min}$  and  $A \sim 20-100 \text{ Kcal}/\text{mole}$ , Eq. (2) would predict  $(\omega/2\pi) \cong 10^{-4} - 10^{-1} \text{ Hz}$ . ac experiments are typically run in the  $10^{-1} - 10^5 \text{ Hz}$  frequency range, hence the connection between TSC and ac experiment should be observable at the highest TSC heating rate  $\beta$  and the lowest ac frequency  $\omega$ . Fig. 2 (lower part) shows the TSC run at  $9^{\circ}\text{C}/\text{min}$ . The upper part of Fig. 2 shows the real part of the ac current run at  $5 \times 10^{-1} \text{ Hz}$ . The similarity of the current peak around  $T_g$  is clearly indicated. As the frequency of the ac experiment is increased, the  $\alpha_a^-$  peak rapidly shifts to higher temperatures and becomes broader. This is shown in Fig. 3, upper part, where the ac peak associated with  $T_g$  is shown for  $5 \times 10^{-1}$  and  $2 \times 10^5 \text{ Hz}$ . The ac current at  $T_g$  is proportional to the frequency of the ac driving field and thus the units in Fig. 3 are relative. The lower part of Fig. 3 shows the linewidth  $\Delta(T_m)$  of the ac peak as a function of the temperature  $T_m$  at which the current peaks. The linewidth  $\Delta(T_m)$  of the ac peak temperature  $T_m$  of the ac and TSC  $\alpha_a^-$  current peaks approach each other as the frequency of the ac experiment approaches the frequency which can operationally be defined from Eq. (2) for the TSC experiment. Eq. (2) can be used to calculate  $1/\tau$  at the temperature  $T_m$  from quantities determined from the TSC experiment. For the glass transition, the WLF relation is more appropriate to describe the temperature dependence of  $\tau$  than a thermally activated process, viz.

$$\tau = \tau_g \exp\left(-\frac{C_1(T-T_g)}{C_2+T-T_g}\right) \quad (3)$$

in which case Eq. (2) reduces to

$$\frac{1}{\tau} = \frac{\beta C_1 C_2}{(C_2 + T_m - T_g)^2} \quad (4)$$

In Eq. (3)  $C_1$  and  $C_2$  are constant which in principle, can be obtained from a least square fit. For our purpose, however, it is sufficient to use the "universal" values  $C_1 = 40$ ,  $C_2 = 51.6^\circ\text{K}$ , which were found for a large number of materials. We calculated  $1/\tau$  from Eq. (4) for various heating rates  $\beta$  and plotted  $\log 1/\tau$  versus  $1/T = 1/T_m$  in Fig. (4) ( $\alpha_a$ -curve, open circles). For the analysis of the ac peak we assumed a phenomenological distribution of relaxation times and so used the Davidson-Cole relation

$$\omega\tau = \tan \phi \quad (5)$$

where  $\phi = \frac{\pi}{2} \frac{1}{\gamma+1}$ .  $\gamma$  is the associated distribution parameter. Although this relation has been derived to analyze the peak of  $\epsilon''$  versus  $\omega$  at constant temperature, it can be used to derive  $1/\tau$  from the peak position of the ac current on the temperature axis if  $\frac{d \ln \gamma}{dT} \ll \frac{d \ln \tau}{dT}$ , a condition which is often satisfied. Using Eq. (5) we calculated  $1/\tau$  from the ac current peak measured at frequency  $\omega$ . The  $\log 1/\tau$  values are plotted in Fig. 4 ( $\alpha_a$ -curve, full circles) as a function of  $1/T = 1/T_m$ . We note that the data derived from TSC and ac experiment join smoothly, demonstrating self consistency of the analysis. Using both techniques, the relaxation behavior of the  $\alpha_a$ -relaxation thus can be mapped out over  $\sim$  nine decades of frequency. The data clearly demonstrate the expected WLF temperature dependence (solid line calculated with the constants  $C_1 = 40$ ,  $C_2 = 51.6^\circ\text{K}$ ).

A similar analysis has been carried out for the  $\alpha_c$ -crystalline relaxation in commercial films of PVF<sub>2</sub>. To study this relaxation the concentration of the  $\alpha$ -phase was enhanced by thermal treatment (see Sec. 3). Fig. 5 shows the temperature shift of the  $\alpha_c$ -relaxation with heating rate (TSC, upper part) and frequency (ac, lower part). The corresponding  $\log 1/\tau$  versus  $1/T = 1/T_m$  plot (Fig. 4,  $\alpha_c$ -curve) shows again, a smooth connection of ac and TSC data and furthermore verifies the expected

thermal activation of the crystalline relaxation process (activation energy  $\sim 21$  Kcal/mole).

### (3) TSC on Samples with Controlled Morphology

To gain further understanding of the origin of the significant pyro- and piezo-electric behavior it is necessary to separate the effects of the different crystallographic phases and morphologies upon the poling induced polarization. In the following, we examine these effects upon the TSC in unoriented samples with controlled crystal phases and microstructure. The films are prepared from powder obtained from Pennwalt Co. (powder number 881, 821 and 401) and from Kureha Chemical Co. (KF-1100). The powder was melted and then quenched to the crystallization temperature  $T_x$ . By varying  $T_x$  and the crystallization time  $t_x$ , various morphologies were produced as verified by temperature dependent IR and DSC. IR absorption spectra are used to distinguish three crystalline phases, the tg-tg' phase  $\alpha$ , the planar zig-zag  $\beta$  and a modification of the  $\beta$  phase called the  $\gamma$ -phase. The  $\alpha$ -phase, identified by IR bands at 530, 615, 764 and  $795\text{cm}^{-1}$  forms from the melt and has the lowest melting temperature. The higher melting  $\beta$ -phase is also crystallized from the melt and is identified by IR bands at 510 and  $840\text{cm}^{-1}$ . The highest melting  $\gamma$ -phase is formed by a crystal-crystal transformation from the  $\alpha$ -phase. The  $\gamma$ -phase is identified by IR bands at 430, 776 and  $810\text{cm}^{-1}$  which appear in addition to the bands characteristic of the  $\beta$ -phase. Fig. 6 shows a Hoffman-Weeks plot of the observed melting temperature  $T_M$  versus crystallization temperature  $T_x$  for samples of 821 powder crystallized from the melt. Also indicated is the halftime of  $\alpha$ -crystallization. It is noted that with increasing  $T_x$  the halftime decreases with progressive rapidity. At higher crystallization temperatures  $\beta$ -crystallization occurs as a competitive process to  $\alpha$ -crystallization. At  $T_x \gtrsim 430^\circ\text{K}$  formation of the  $\gamma$ -phase is observed in addition to the  $\alpha$ - and  $\beta$ -phase. The concentrations of the three phases for this particular 821 powder are given in the Table for different crystallization

temperatures. The relative concentrations, and in particular that of the  $\gamma$ -phase are strongly dependent upon the crystallization time  $t_x$ . The films prepared this way were typically  $50\mu\text{m}$  thick. They were electroded with Au contacts and then cooled in  $\sim 3\text{V}/\mu\text{m}$  to below  $T_g$ . The TSC was then run at  $\sim 7.7^\circ\text{C}/\text{min}$ . Fig. 7 shows TSC traces for samples crystallized from 821 powder at the indicated temperatures  $T_x$ . It is evident that with the appearance  $\gamma$  ( $T_x = 432.5^\circ\text{K}$ ) the TSC increases significantly. For comparison we included a trace recorded on a biaxially oriented commercial film of Kureha PVF<sub>2</sub>, which contains the  $\alpha$ - and  $\beta$ -phases. We also note that with increasing  $T_x$  the amplitude of the  $\alpha_a$ -peak decreases thus indicating an overall increase in crystallinity of the sample. The TSC exhibits a well defined structure, viz. at  $\sim -50^\circ\text{C}$  the  $\alpha_a$ -peak, at  $\sim 25^\circ\text{C}$  the shoulder associated with the  $\alpha_c$ -relaxation and at  $\sim 15^\circ\text{C}$ , shoulders which appear in  $\beta$  and  $\gamma$  containing films. At still higher temperatures ( $75$ - $100^\circ\text{C}$ ) a peak and a shoulder is observed for the  $\alpha$  and  $\beta$  rich samples, respectively. This latter peak would also be indicated for the  $\gamma$  rich films but would be off scale in Fig. 7. Assignments of the peaks which appear in addition to the well documented  $\alpha_a$ - and  $\alpha_c$ -relaxations is very preliminary. It is suggested that the relaxation at  $\sim 15^\circ\text{C}$  is associated with the  $\gamma$ -phase. That it also appears in the  $T_x = 430^\circ\text{K}$  sample is believed to indicate that this sample contains small traces of  $\gamma$ , which are not observed with our IR spectrometer. The higher temperature peak at  $50$ - $75^\circ\text{C}$  is tentatively associated with the  $\beta$ -phase on the basis of the data on the commercial Kureha film. At this point, however, we have not established the uniqueness of the relaxation modes related to the  $\beta$  and  $\gamma$  phases. They might well result from the same underlying mode occurring in differing morphological environments. Fig. 8 shows similar TSC traces on samples prepared from KF-1100 powder. The data in Fig. 7 and 8 thus unambiguously demonstrate that the poling induced polarization is strongly dependent upon sample morphology. The net effect upon the films pyroelectric and piezoelectric response when poled under typical conditions ( $\sim 100^\circ\text{C}$ ,  $\sim 300\text{KV}/\text{cm}$ ) are currently being investigated.

#### (4) Field/Temperature Effects

The temperature range above 100°C is of major technical interest because it is here that poling is known to induce significant reversible pyro- and piezoelectric behavior. In the following, we describe results of ac and TSC measurements performed in conjunction with applied dc bias and sequential in situ thermal cycling. Our principal observations on commercial PVF<sub>2</sub> films are the following:

(i) Momentary application of electric fields at elevated temperatures significantly reduces the current measured at high temperatures. The field induced current suppression by far exceeds the reduction achieved by merely thermalizing in zero electric field at the same temperature. The effect cannot be reversed by reversing field polarity.

(ii) No enhancement of the  $\alpha_c$  absorption attributable to field exposure could be observed.

(iii) Current levels suppressed by electric field exposure could in general, be partially restored by heating under zero bias at temperatures about 20°C below the melting temperature. If the applied field was below the threshold field to induce reversible pyroelectricity, the field effect could be completely reversed in a few thermal cycles but if it exceeded the threshold value, only marginal reversal was attained after hours of persistent high temperature thermalizing.

(iv) Partial pinning of dipoles in the amorphous phase may occur as a consequence of field exposure.

In Fig. 9 some effects are illustrated for a 10Hz ac trace recorded on a 2 mil Pennwalt film. The dashed line a is the first heating-cooling cycle of the as-received film. At the amplifier gain setting chosen to record the traces shown in Fig. 9, the T<sub>g</sub> current peak was shut off and the current stabilized at 108°C to the value indicated as a black dot on the figure without any indication of further drift. A field of 16V/ $\mu$ m, which is well below the threshold field for reversible pyroelectricity was then switched on. The illustrated decrease in current occurred over a span of ~600ms. The sample was now cycled down in temperature under applied field

(horizontal arrow in Figure) to well below  $T_g$ , where the field was switched off. Under zero bias, the sample was now recycled to  $140^\circ\text{C}$  and the broad current loop b shown in the Figure was correspondingly recorded. The reduction in current level at high temperature in the heating half of the cycle is a consequence of previous field exposure. The loop width observed on cooling is a consequence of heating the sample under zero field, a result of high temperature exposure in the thermal cycle used to record the heating part of trace b. With progressive cycling to  $140^\circ\text{C}$  the effect of the field exposure could be substantially erased. Thermally reversing the effect of field exposure became less effective as the field was increased to poling levels, i.e.,  $30\text{-}40\text{V}/\mu\text{m}$ . This is illustrated in the lower part of the figure. The film was exposed to a field of  $37\text{V}/\mu\text{m}$  at  $110^\circ\text{C}$  for 3 hrs. and then cooled under field. Curve c shows the initial current measured under zero dc bias on first heating at an amplifier gain setting identical to that used in the upper figure. Curve d is recorded after heating at  $148^\circ\text{C}$  under zero field for 17 hrs. Only partial restoration to that high temperature current level is indicated. The conductivity after this treatment remains substantially below that measured on both an unpoled unannealed film and a film given comparable thermal history but with no field applied.

Corroborative information from TSC measurements is shown in Fig. 10. An as-received  $25\mu\text{m}$  Kureha film is cooled under zero bias to low temperature, where a  $30\text{V}/\mu\text{m}$  field is switched on. The film is then thermally cycled under field giving rise to loop a. The suppression of current level at high temperature observed in comparing the heating and cooling currents at a given temperature in this range is between two and three orders of magnitude as indicated on the logarithmic ordinate scale. Cooling the film in the presence of the strong dc bias field can freeze-in a polarization and, as a result, the cooling current is suppressed relative to the heating current. An estimate of the frozen-in polarization is obtained from the depolarization current trace b shown in the lower part of Fig. 10. This trace was recorded on heating the film under zero bias following completion of loop a and for the purpose of illustration the negative of the recorded current was plotted. Up

to  $\sim 0^{\circ}\text{C}$  both heating trace a and trace b are identical indicating that below  $0^{\circ}\text{C}$  the difference in heating and cooling currents in loop a is due to a frozen-in polarization. (See Sec. 2) At higher temperatures, however, trace b is orders of magnitudes smaller than heating trace a. This clearly demonstrates that the width of current loop a is not the result of a frozen-in polarization. If the film is now cycled through four complete (a,b) sequences and then run under  $30\text{V}/\mu\text{m}$  field, again starting at low temperature, loop c is obtained. Loop c is similar to loop a below  $0^{\circ}\text{C}$  but the effect of prolonged field exposure and subsequent thermal history is demonstrated when the high temperature loops c and a are compared. The depolarization current following loop c is identical to that following loop a (trace b, lower part, Fig. 10). While the evolution of the initial current trace a into trace c revealed sensitivity to combined thermal and field exposure history, the depolarization current density remained well below the total thermocurrent density measured under bias above  $100^{\circ}\text{C}$ . Furthermore, repeated thermal cycling at  $30\text{V}/\mu\text{m}$  field tended to produce some additional current suppression at high temperatures and some additional loop narrowing relative to trace c. Heating currents, therefore, always remained somewhat larger than cooling currents measured at the same temperature.

Experiments presently underway, suggest lowering of high temperature conductivity by application of an electric field may involve more than one physical mechanism. Whereas poling through blocking contacts permanently reduces ac conductivity, which suggest a field driven perturbation of film microstructure, recent experiments appear to indicate that phenomena reminiscent of thermal switching are also observed. These take the form of transient current instabilities, which appear when a film is cycled from low temperature under high dc bias into the poling temperature range.

Pulsed field experiments indicate that reversible pyroelectric behavior can be induced on a .1-1 sec. time scale for fields and temperatures exceeding specified threshold values. The lowering of ac conductivity by application of a dc

field at poling temperatures (Fig. 9) evidently occurs on the same time scale.

The ac current peak in the temperature range of the glass transition was found to be sensitive to applied dc bias. The effects of applied bias were thermally reversible and not electrostrictive in origin. Typical results are illustrated in Fig. 11 for a  $12\mu\text{m}$  Kureha film measured at 100Hz. Trace a represents the ac current peak observed on a film cooled from  $30^\circ\text{C}$  to  $-180^\circ\text{C}$  under zero dc bias. This annealing procedure always reproduced peak a irrespective of any earlier treatment. When a field of  $40\text{V}/\mu\text{m}$  was applied at  $-180^\circ\text{C}$  and the film then heated at  $4^\circ\text{C}/\text{min}$ . under field to  $+50^\circ\text{C}$  trace b was obtained. If the field was left on at  $+50^\circ\text{C}$  and the film cooled down to  $-180^\circ\text{C}$  trace c resulted. The suppression of the peak amplitude saturated under additional cycling between these terminal temperatures at the same field intensity. The recovery of the current amplitude from that shown on trace c to that shown on trace a after dc bias was removed, was very slow below the glass transition temperature but occurred with increasing rapidity at temperature above  $T_g$ . The effect of applied dc bias field in depressing the ac current peak amplitude was dependent on field intensity. It seems reasonable to tentatively identify this effect with a field induced pinning of dipoles (realignment) in the polymers amorphous phase. This realignment evidently occurs only in the neighborhood of the glass transition temperature and above. In the presence of a dc field, this partial alignment remains stabilized at temperatures well in excess of  $T_g$ .

## FIGURE CAPTIONS

- Figure 1 Trace a: Depolarization current (TSC), i.e., heating in zero field of sample previously cooled under  $3\text{V}/\mu\text{m}$ .  
Trace b: Polarization current, i.e., heating of unpoled sample in  $3\text{V}/\mu\text{m}$ .  
Trace c: Polarization current measured on sample sandwiched between Mylar blocking layers under appropriate bias. Heating rate:  $9^\circ\text{C}/\text{min.}$ , sample:  $25\mu\text{m}$  Kureha  $\text{PVF}_2$ .
- Figure 2 ac current  $J_\omega(T)$  run at  $5 \times 10^{-1}\text{Hz}$  (upper part) and TSC  $J_\beta(T)$  run at  $9^\circ\text{C}/\text{min.}$  to show convergence of TSC and ac lineshape and position of the  $\alpha_a$ -relaxation.
- Figure 3 Upper part: Illustration of temperature shift and broadening of ac current  $\alpha_a$ -peak with increasing frequency.  
Lower part: Temperature linewidth plotted versus temperature  $T_m$  at which ac current peaks. Convergence to the corresponding linewidth of the TSC  $\alpha_a$ -peak is clearly indicated.
- Figure 4 Combined plot of relaxation rate  $\log 1/\tau$  versus temperature  $T_m$  calculated from peak position of ac (full points) and TSC (open points) current peaks for  $\alpha_a$ - and  $\alpha_c$ -relaxations.
- Figure 5 Temperature shift of  $\alpha_c$ -relaxation peak with heating rate (TSC experiment) and frequency (ac experiment). Curves are shifted along ordinate for clarity.  $\alpha_a$ -peak is not shown for the ac current.
- Figure 6 Hoffman-Weeks plot (melting temperature  $T_m$  versus crystallization temperature  $T_x$ ) for samples prepared from 821 Pennwalt powder. Also shown is the halftime of  $\alpha$ -crystallization. The  $\alpha$ ,  $\beta$  and  $\gamma$ -phases were identified by their IR bands at  $530, 615, 764$  and  $795\text{cm}^{-1}$ ;  $510$  and  $840\text{cm}^{-1}$ ; and  $430, 510, 776, 810$  and  $840\text{cm}^{-1}$ , respectively.
- Figure 7 TSC of samples crystallized at different temperature  $T_x$ . Powder 821 Pennwalt. Also shown is the TSC of a commercial  $25\mu\text{m}$  Kureha  $\text{PVF}_2$ . Poling field  $3\text{V}/\mu\text{m}$  heating rate  $7.7^\circ\text{C}/\text{min.}$  The ordinate units are  $J/AgE_p$ , where  $J$ ,  $A$ ,  $\beta$  and  $E_p$  are the current (Amps), electrode area ( $\text{cm}^2$ ), heating rate ( $^\circ\text{K}/\text{sec}$ ) and poling field ( $\text{V}/\text{cm}$ ). The arrows indicate tentative assignment of TSC structure.
- Figure 8 Same as Fig. 7, but samples prepared from KF-1100 (Kureha) powder.
- Figure 9 ac current at  $10\text{Hz}$  measured on  $2\text{mil}$  Pennwalt  $\text{PVF}_2$  subjected to various field/temperature history.  
(a) fresh film  
(b) following application of  $16\text{V}/\mu\text{m}$  at  $108^\circ\text{C}$  and cooling in field.  
(c) following poling ( $110^\circ\text{C}$ , 3 hrs.,  $37\text{V}/\mu\text{m}$ ).  
(d) following 17 hrs. anneal at  $148^\circ\text{C}$ .
- Figure 10 TSC current measured on  $25\mu\text{m}$  Kureha  $\text{PVF}_2$  subjected to various field/temperature history. Starting temperature for each cycle  $-100^\circ\text{C}$ . Heating rate  $8.3^\circ\text{C}/\text{min.}$

FIGURE CAPTIONS (con't)

- (a) fresh film under dc field
- (b) depolarization current following (a).
- (c) under field after four complete not shown (a,b) sequences.
- (d) depolarization current following (c).

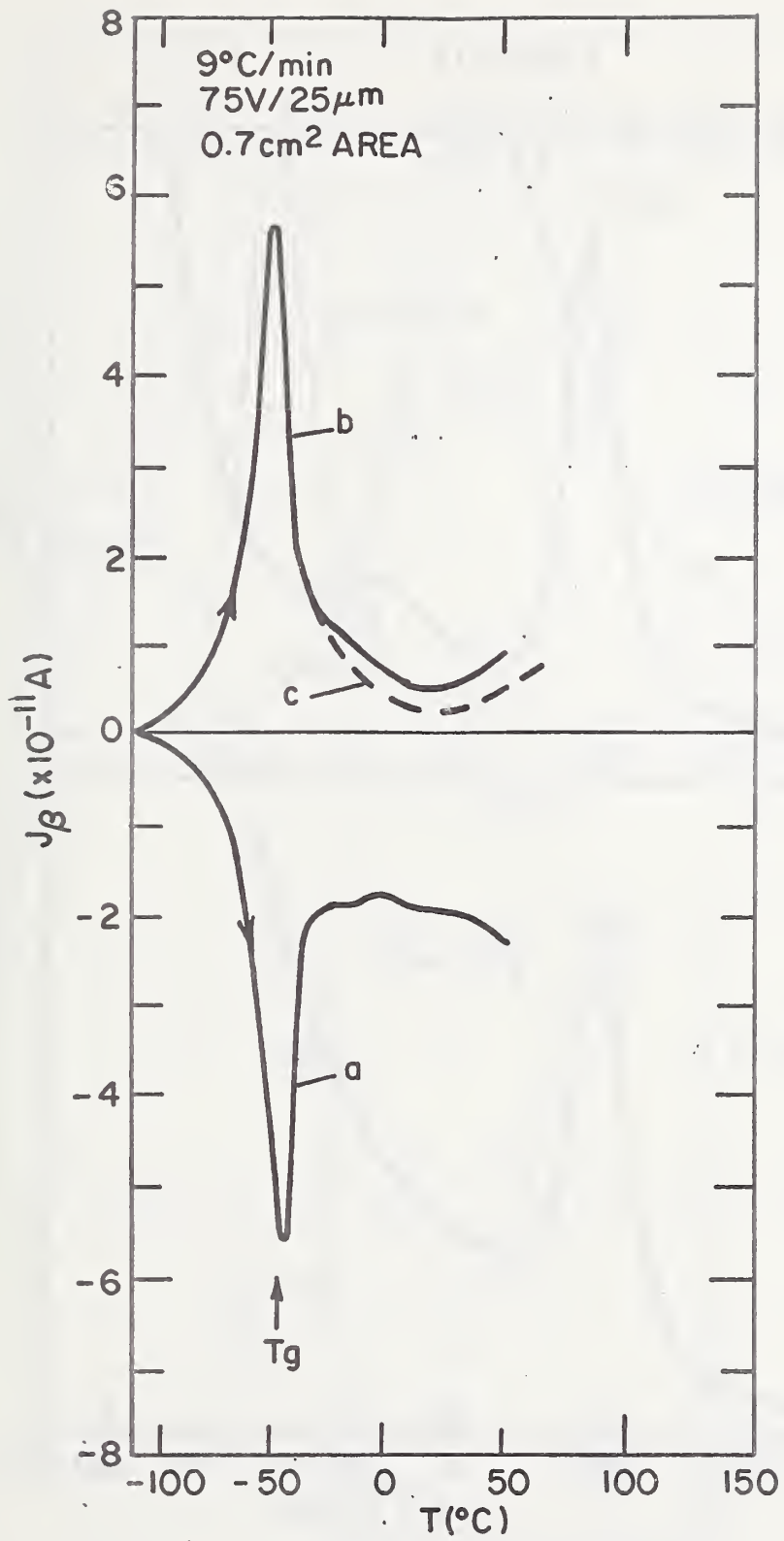
Figure 11 ac current near  $T_g$  recorded at 100Hz for 12 $\mu$ m Kureha sample subjected to various field/temperature history.

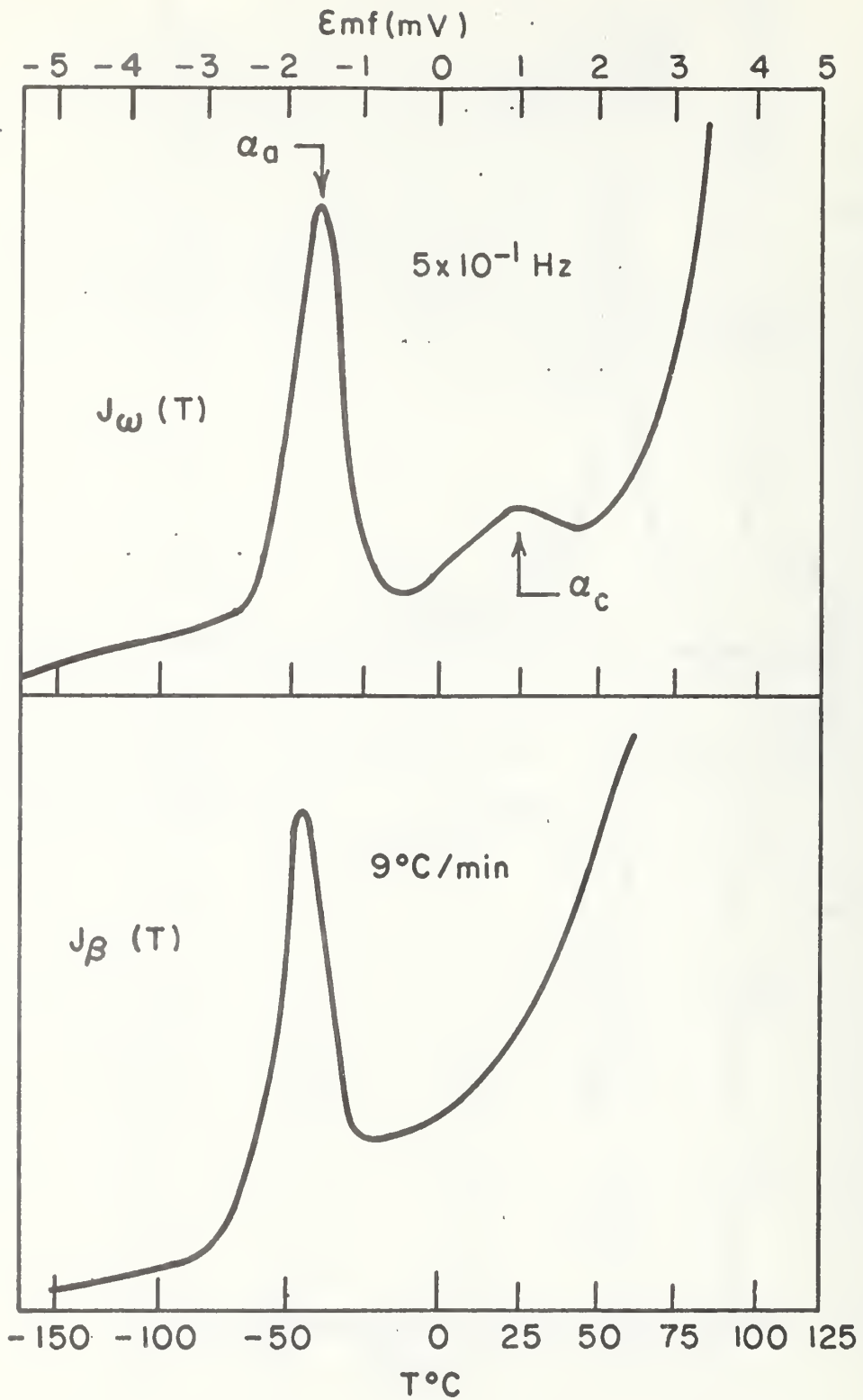
- (a) heating trace fresh sample.
- (b) heating trace for sample (a) with 40V/ $\mu$ m applied.
- (c) cooling trace for sample (b) with 40V/ $\mu$ m applied.

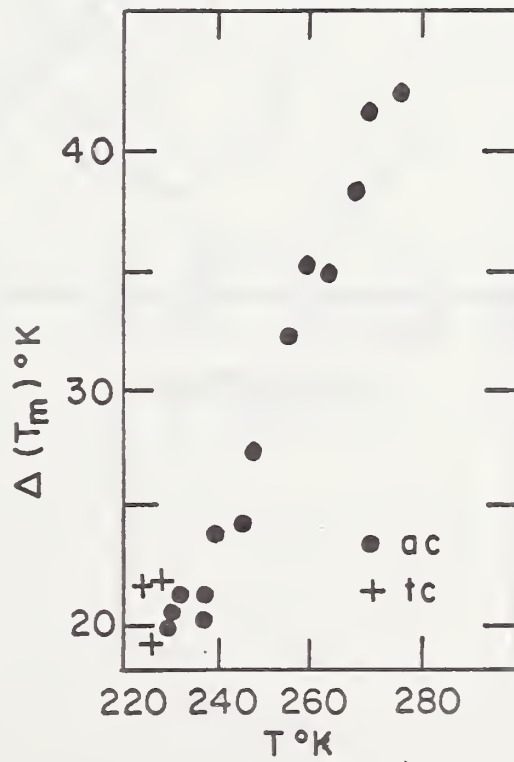
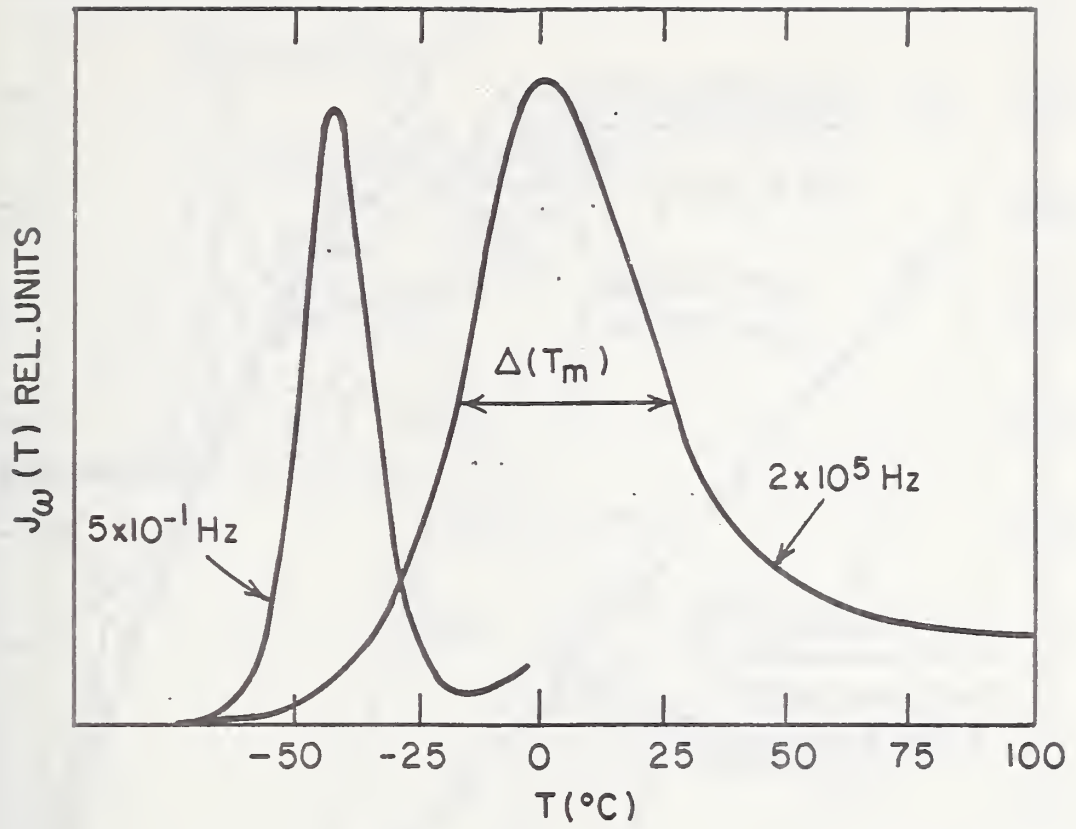
TABLE 1

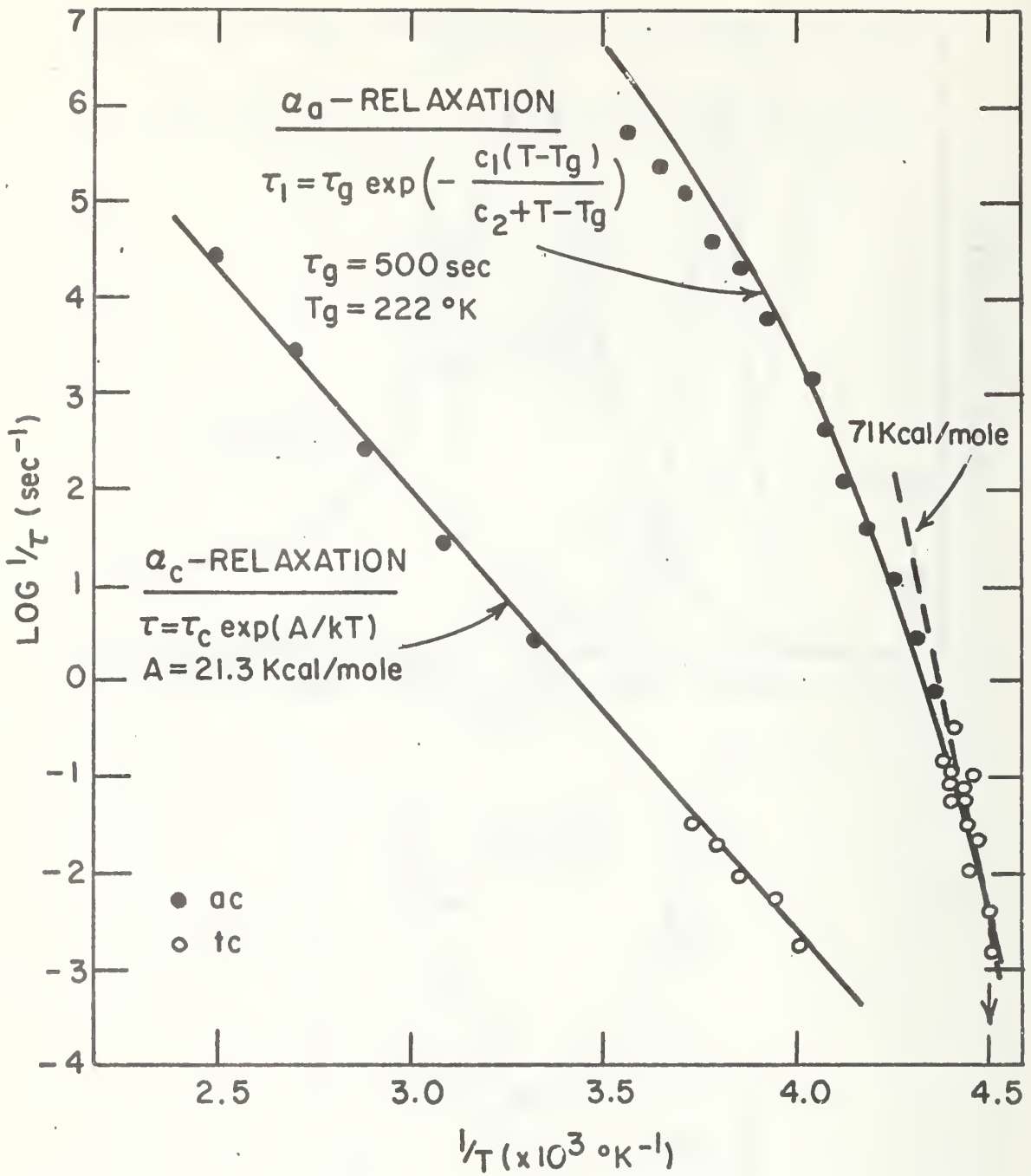
Concentrations (in percent of total weight) of  $\alpha$ -,  $\beta$ - and  $\gamma$ -phases calculated from DSC traces for the 821 samples discussed in the text. A comparable heat of fusion (25 cal/g) was assumed for the three phases. The concentration of the  $\gamma$ -phase is strongly time ( $t_x$ ) dependent.

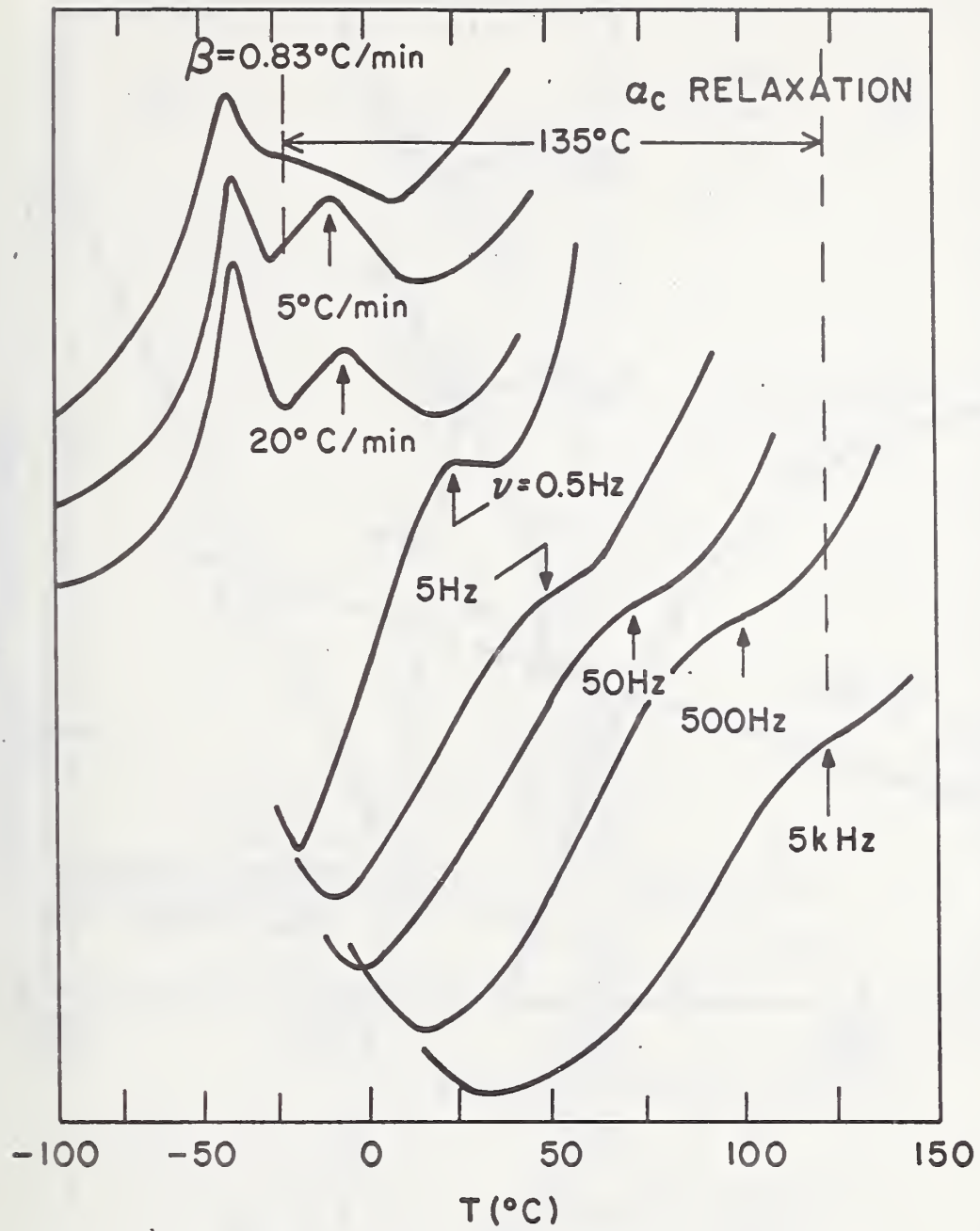
$T_x$ ( $^{\circ}$ K)	$\alpha$	$\beta$	$\gamma$
420	46 $\pm$ 4	$\sim$ 0	$\sim$ 0
430	44 $\pm$ 4	2 $\pm$ 1	$\approx$ 0
432.5	40 $\pm$ 4	4 $\pm$ 1	2 $\pm$ 1
435	37 $\pm$ 4	4 $\pm$ 1	5 $\pm$ 1

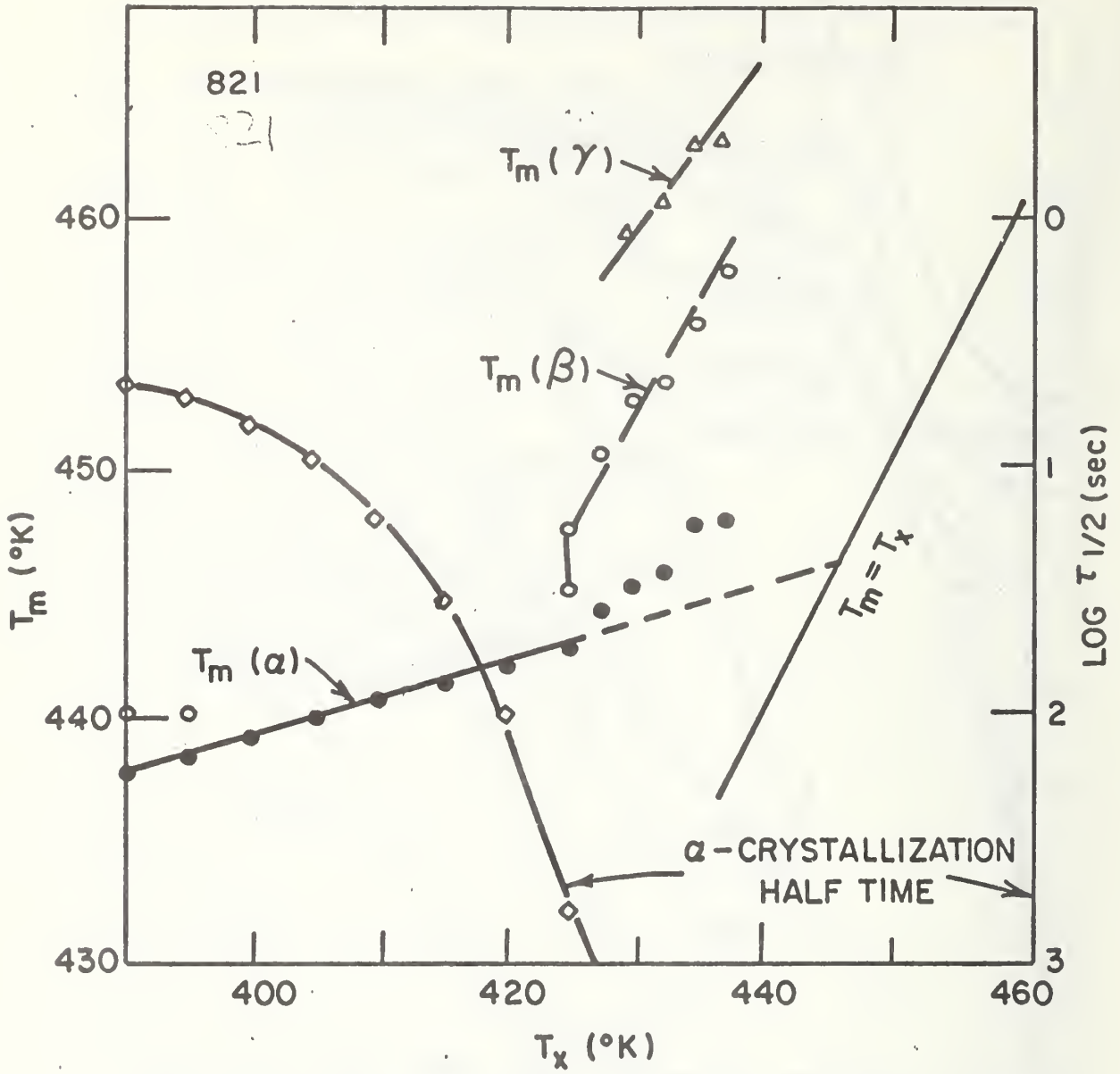


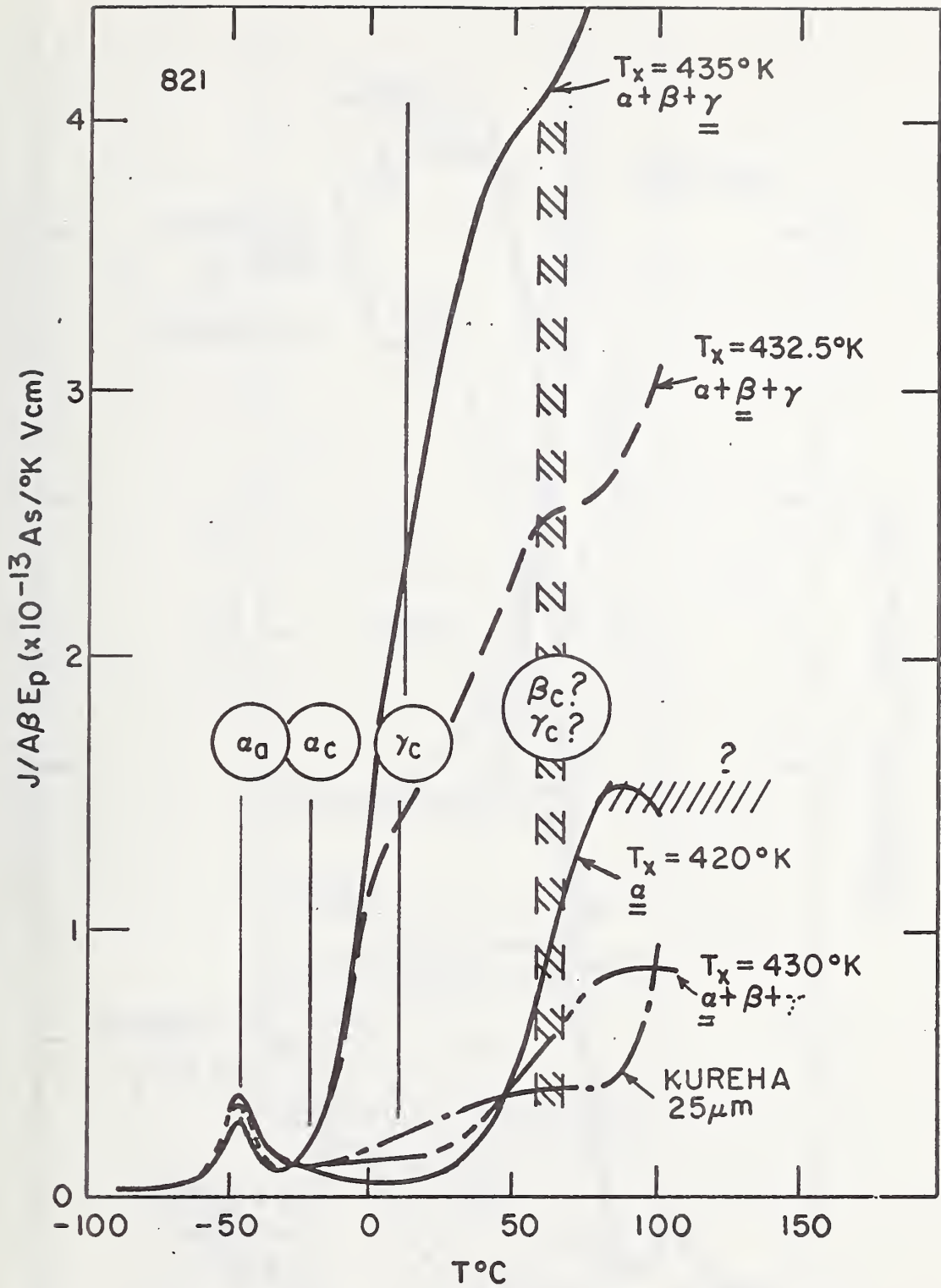


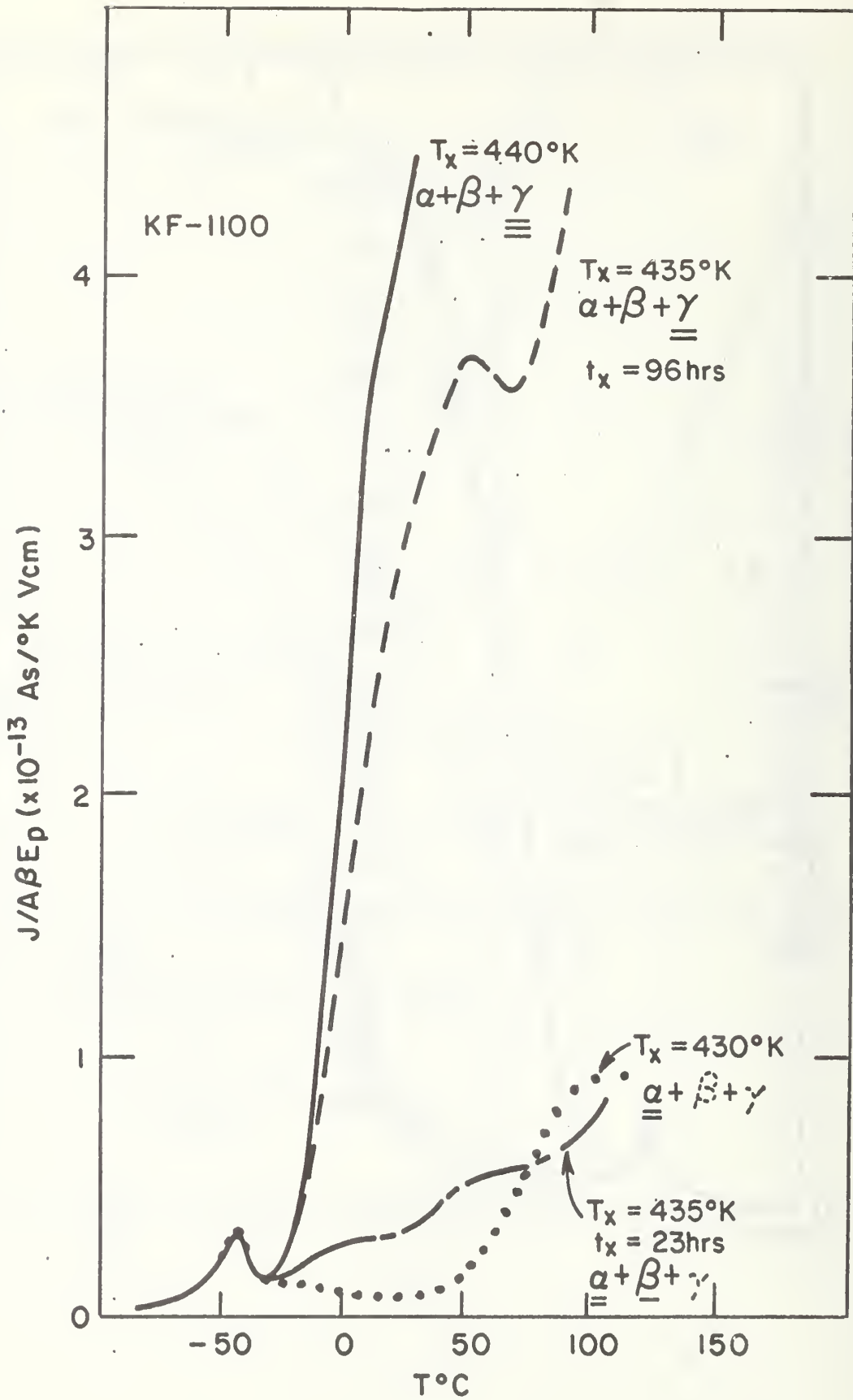


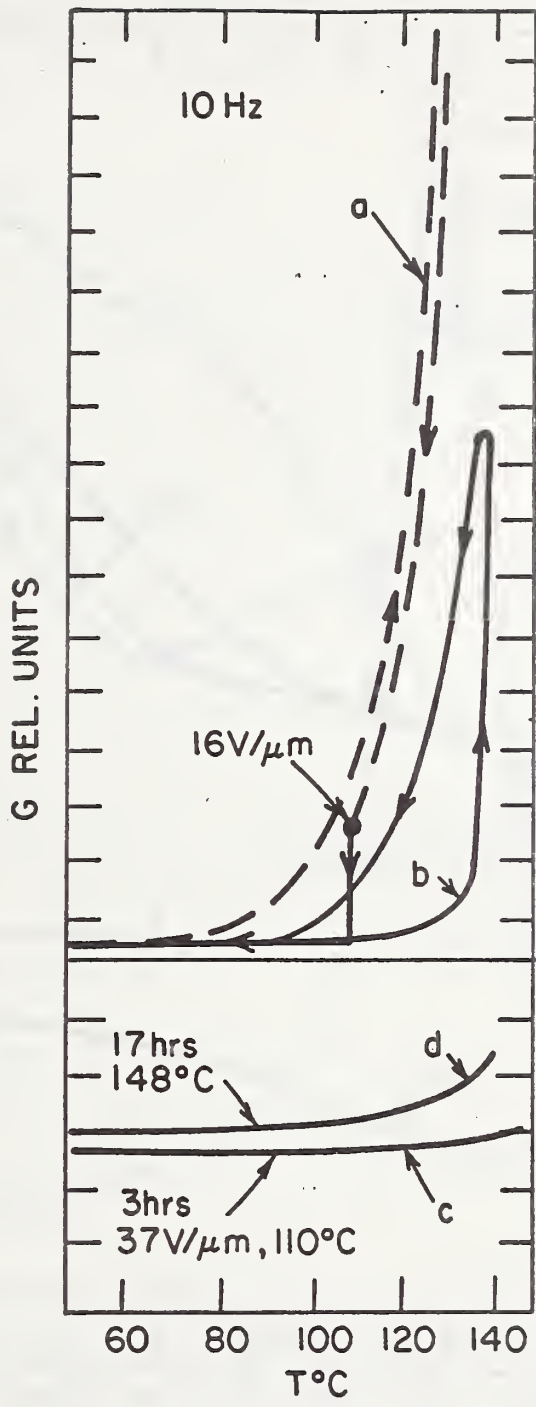


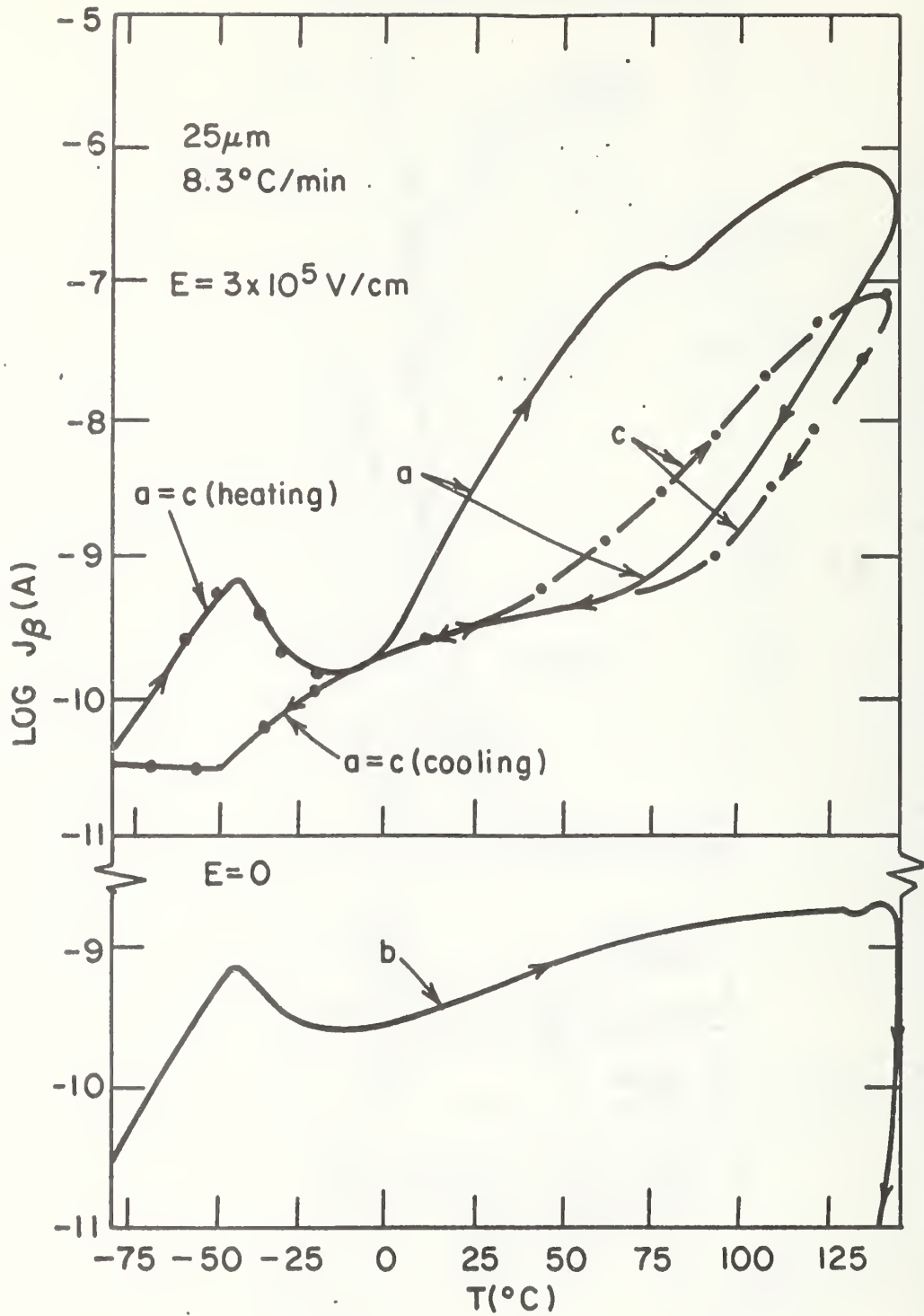


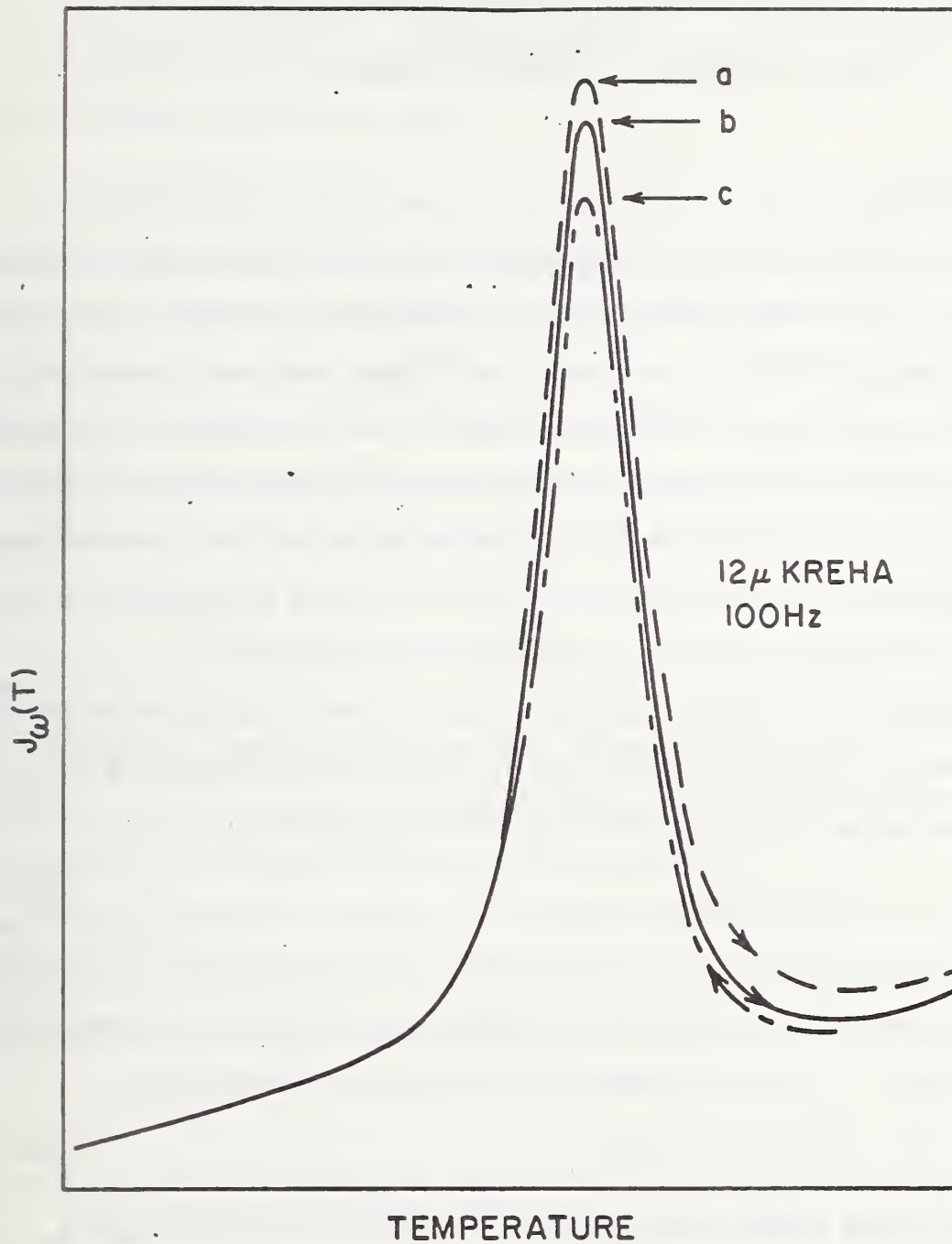












Piezoelectricity and Pyroelectricity in a  
Poly(vinylidene fluoride-tetrafluoroethylene) Copolymer

G. Thomas Davis

National Bureau of Standards, Washington, D. C.

This paper ascribes the piezoelectric and pyroelectric activity of polymers to frozen-in dipole alignment achieved during the poling procedure. In such a model, electrical response to temperature or pressure change results from a change in polarization arising from volume change and a change in fluctuation amplitude of oscillating dipoles. The development of the theory will be reviewed briefly and then compared with results obtained for polyvinylchloride and a copolymer of vinylidene fluoride and tetrafluoroethylene.

The theory to be outlined here has been developed and presented in more detail by Broadhurst et al<sup>(1)</sup> and by Mopsik and Broadhurst<sup>(2)</sup>.

Consider a thin film of polymer between two metal electrodes subjected to an electric field of intensity  $E_p$ . The dielectric displacement  $D$  in a direction normal to the surface of the film is given by:

$$D = \epsilon_0 E_p + P \quad (1)$$

where  $\epsilon_0$  is the permittivity of vacuum and  $P$  is the polarization. Since  $D$  at any point within the dielectric is defined as the product of  $E$  and the permittivity  $\epsilon' \epsilon_0$  one can express the resultant polarization as:

$$P = (\epsilon' - 1) \epsilon_0 E_p \quad (2)$$

where  $\epsilon'$  is the relative permittivity. The relative permittivity of a polar polymer which undergoes a glass transition varies with temperature as shown schematically in Figure 1 where an increase in  $\epsilon'$  occurs in the

vicinity of the glass transition temperature. If an electric field is applied at a temperature in the liquid range above  $T_g$ , where  $\epsilon' = \epsilon'_l$  the polarization induced is expected to be:

$$P_l = (\epsilon'_l - 1) \epsilon_0 E_p. \quad (3)$$

If the film is then cooled below  $T_g$  before removing the electric field, only that portion of the polarization that could have been induced at temperatures in the glassy region will disappear. That polarization is equal to  $(\epsilon'_g - 1) \epsilon_0 E_p$  where  $\epsilon'_g$  is the relative permittivity at the temperature in the glassy region where the field is removed. The polarization remaining after the removal of the field is expected to be:

$$P_r = \Delta\epsilon' \epsilon_0 E_p \quad (4)$$

where  $\Delta\epsilon' = \epsilon'_l - \epsilon'_g$ .

In the case of an amorphous polymer this phenomenological approach leads to the result that the numerical value of  $P_r$  is expected to increase linearly with  $E_p$ . In order to predict how  $P$  is expected to change with temperature or pressure, it is more helpful to consider  $P$  on a molecular level.

In molecular terms, polarization is the net dipole moment per unit volume, i.e.

$$P = \frac{N\langle m \rangle}{V} \quad (5)$$

where  $\langle m \rangle$  is the averaged moment considering both the vacuum dipole moment and the induced moment due to the electric field in which the dipole finds itself and which is caused by the preferred orientation imposed on the system during the poling process.  $N/V$  is the number of dipoles per unit volume. The problem of

calculating  $\langle m \rangle$  for frozen dipole alignment is similar to that solved by Onsager for uniform liquids and has been worked out for this case by Mopsik and Broadhurst<sup>(2)</sup> leading to the result that:

$$P = \frac{(\epsilon_{\infty} + 2)}{3} \frac{N\mu_0}{V} \langle \cos \theta \rangle. \quad (6)$$

where  $\epsilon_{\infty}$  is the dielectric constant for immobilized dipoles,  $\mu_0$  is the vacuum dipole moment of the molecule and  $\langle \cos \theta \rangle$  is the averaged cosine of the angle between the individual dipole moments and the total sample moment.

The polarization results in a compensating surface charge within the electrodes on the surface of the polymer film. Real charges trapped within the dielectric will also be compensated for by charges within the surface electrodes but in this treatment we assume that trapped real charges remain trapped and sample strains are uniform so that the trapped charges do not contribute to any current flow between electrodes when the sample is strained. The influence of any trapped charges on the induced dipole moment has also been neglected in this model. A change in temperature or pressure causes a change in volume polarization which results in a re-distribution of charge between the surfaces under short-circuit conditions or generates a voltage between the surfaces under open-circuit conditions. Since we treat the case where electrodes are evaporated onto the surface of the polymer and consequently maintain the same area (A) as the polymer, we can substitute the thickness (L) for V/A. An outline of the change to be expected in P for a change in temperature (T) or pressure (P) is presented in Figure 2 and may be found in more detail in Reference 2.

The piezoelectric coefficient  $d_p$  for a change in hydrostatic pressure as outlined in Figure 2 is

$$d_p = \frac{1}{A} \frac{dQ}{dp} = - P \epsilon_\infty \beta_L. \quad (7)$$

and the pyroelectric coefficient  $p$  is

$$p = \frac{1}{A} \frac{dQ}{dT} = - P \alpha_L \epsilon_\infty \left[ 1 + \frac{\Delta\phi^2}{\epsilon_\infty 2T\alpha_L} \right]. \quad (8)$$

Note that these coefficients are defined as the change in charge  $Q$ , the usual measured quantity, as opposed to the classical definition which considers the change in polarization  $P$  with strain. In the case of polyvinylchloride where  $P$  is linear with the poling field,  $E_p$ ,

$$P = \Delta\epsilon' \epsilon_0 E_p \quad (9)$$

so that:

$$d_p = \Delta\epsilon' \epsilon_0 \epsilon_\infty \beta_L E_p \quad (10)$$

and

$$p = \Delta\epsilon' \epsilon_0 \epsilon_\infty \alpha_L E_p \left[ 1 + \frac{\Delta\phi^2}{2T\alpha_L \epsilon_\infty} \right] \quad (11)$$

which upon rearrangement yields:

$$\frac{d_p}{E_p \beta_L \epsilon_0} = \Delta\epsilon' \epsilon_\infty \quad (12)$$

$$\frac{p}{E_p \alpha_L \epsilon_0} = \Delta\epsilon' \epsilon_\infty + \frac{\Delta\epsilon' \Delta\phi^2}{2T\alpha_L} \quad (13)$$

The measurement of  $p$  and  $d_p$  have been described elsewhere<sup>(1)</sup>, but briefly, one measures the amplified short-circuit current that flows from one electrode of the polymer film to the other for a measured rate of temperature change or a measured rate of pressure change supplied by a pressure fluid such as helium gas. The thermal expansion coefficient and compressibility of the polymer films have been measured by using three small pieces of the film to separate the plates of a parallel plate capacitor. The fractional change in thickness as one changes temperature or pressure is equal to the measured fractional change in capacitance (corrected for  $\epsilon'$  of the helium in the chamber).

A summary of results obtained with polyvinylchloride by Broadhurst et. al<sup>(1,2)</sup> is presented in Table I. Since the measured values of  $\Delta\epsilon'$  and  $\epsilon_{\infty}$  for this polymer were 10 and 3 respectively, the product of 30 is in very good agreement with the average value of 26.7 for the quantity  $d_p/E_p\beta_L\epsilon_0$ . At present, we have no direct measure of  $\Delta\phi_{RMS}$  which is required for comparison of the pyroelectric coefficients but a value of  $16^\circ$  at room temperature would be required to account for the measurements reported in the last column of Table I. Such a value seems very reasonable.

Polyvinylidene fluoride (PVF<sub>2</sub>) and some of its copolymers [as well as polyvinyl fluoride (PVF)] can be made to exhibit piezoelectric and pyroelectric responses much larger than those of PVC. These polymers differ from PVC in that they are partially crystalline at room temperature and the glass transition of the non-crystalline portion is far below room temperature, in the vicinity of  $-40^\circ\text{C}$ . Furthermore, the polarization (as implied by the piezoelectric response) induced during the poling procedure is not linear with applied field but appears to approach a saturation level<sup>(3,4)</sup>.

For our initial investigations we have chosen a copolymer of vinylidene fluoride containing 27% tetrafluoroethylene. The advantage of using the copolymer is that it crystallizes directly from the melt into a crystal form analogous to that of form I (or  $\beta$ ) of PVF<sub>2</sub> homopolymer. This obviates the need to determine crystal orientation (assumed random from the melt) and the relative amounts of  $\alpha$  and  $\beta$  crystal form in the sample. Furthermore, the copolymer is available commercially from the Pennwalt Corporation as Kynar 7200. The copolymer is soluble in a variety of polar solvents and also crystallizes from solution into the potentially active  $\beta$ -form crystal. Unfortunately the incorporation of so

much TFE reduces the maximum polarization to be expected and also lowers the melting point to the vicinity of 130°C which may affect the stability of the electret at room temperature.

Since  $T_g$  is so far below room temperature, we assume that no dipole orientation remains in the non-crystalline regions of the polymer at room temperature after removal of the poling field. When dipoles within the crystalline region of the polymer become aligned, it is unlikely that entire crystallites can be moved under the influence of the poling field because of the intercrystalline links which maintain the integrity of the polymer film. However, it is not unreasonable to assume that individual chain segments within a crystallite can rotate about the chain axis--a mechanism advanced for the so-called  $\alpha$  relaxation in polyethylene<sup>(5)</sup>. A model depicting such a rotation is sketched in Figure 3. The lefthand side of the figure depicts portions of two different crystallites in the unpoled film. The upper crystallite represents a chain orientation parallel to the plane of the film and normal to the cross-section shown. The lower one depicts a crystallite in which the molecular chains lie in a plane parallel to that of the paper but inclined to the plane of the film; furthermore, the b axis of the unit cell is inclined  $\theta$  degrees away from the plane of the paper. In the poling process, we envision rotation of the dipoles about the chain axis so as to align as much as possible in the direction of the field, coupled with slight translation relative to each other so that it "recrystallizes" with a re-orientation of unit cells within the crystallites. On the right, the upper

crystallite exhibits maximum dipole alignment after poling. Chains within the lower crystallite have been rotated so that the maximum dipole alignment consistent with not changing the chain axis orientation is achieved. That is, the b-axis of the unit cells (and therefore, the net dipole) now lies in a plane normal to that of the film. However, only that component of the chain lying in a plane parallel to the surface can contribute to the net polarization upon poling since we have assumed that the chain axis orientation remains fixed.

Since the polarization in the  $\text{PVF}_2$ -TFE copolymer is not linear with applied field, one cannot infer the polarization from the expression used previously for PVC. However, by using Equation 6 we can predict the maximum value of P to be expected for a single crystal of the homopolymer and then modify it to apply to the copolymer. When the dipole moment of vinylidene fluoride is taken as an average of those reported for difluoroethane (2.27 D) and difluoromethane (1.97 D)<sup>(6)</sup>, and the unit cell volume is  $53.9 \text{ \AA}^3$  as reported by Hasegawa et al<sup>(7)</sup> the polarization of a single crystal of  $\text{PVF}_2$  would be  $13.2 \text{ \mu C/cm}^2$  which becomes  $22 \text{ \mu C/cm}^2$  when corrected for the interaction of the polarizable dipoles with the surroundings according to  $(\epsilon_\infty + 2)/3$  where  $\epsilon_\infty = 3$ . The corrections to this maximum value when applied to the copolymer are outlined in Figure 4.

In the ratio of volumes in Figure 4,  $\bar{V}_{\text{copolymer}}$  is the volume occupied by an average copolymer unit calculated from the macroscopic density of the sample and then expressed in  $\text{\AA}^3$  per average repeat unit. In the model employed here, only the crystalline portions of the polymer contribute to the polarization so that the maximum polarization is reduced by the degree of crystallinity.

We have assumed a uniform distribution of TFE units between the crystalline and non-crystalline regions of the copolymer and since only the vinylidene fluoride portion contributes to the polarization, the maximum must be reduced by the fraction of  $\text{VF}_2$  in the copolymer. Even within the vinylidene fluoride portion of the copolymer, only the usual head to tail additions of monomer contribute to the net dipole. This has been assumed to be 95%. Finally, as mentioned in reference to Figure 3, only that component of the chain axis which lies in the plane of the film is considered to contribute to the realizable polarization. Since there is no "directionality" required in the chain axis, we take the average of  $\cos^2 \delta$  where  $\delta$  is the angle between the chain axis and the plane of the film. Assuming random orientation, this average is 2/3.

Measurements have been made on two types of films; one cast from solution and supplied to us by Pennwalt, the other pressed from molten polymer and quenched into ice water. The density of  $1.843 \text{ g/cm}^3$  and a diffuse low angle x-ray diffraction ring corresponding to spacings ranging from 120 to  $155^\circ \text{A}$  were nearly identical in the two types of films. Film thickness ranged from 25 to 50  $\mu\text{m}$ . Metal electrodes were evaporated on the films and the poling was done inside a can immersed in an oil bath at constant temperature. After the prescribed length of time at the poling temperature, the sample was cooled by quenching the can into room temperature water with the electric field still applied. At the time the experiments were started, it was assumed that all of the "poling" took place at the elevated temperature and the time that the field was applied at room temperature subsequent to that was not important. More recently we have found that appreciable poling can be achieved at room temperature. Poling at room temperature has also been reported for the  $\text{PVF}_2$  homopolymer<sup>(3,4)</sup>.

The results obtained using the cast film are summarized in Table II and those for the melt-crystallized films are summarized in Table III. The poling time was 35 minutes in all cases. Multiple entries indicate results for replicated experiments and are entered in the same order in the tables for both coefficients. (Note that the field strengths and the poling temperatures are not exactly the same in Tables II and III.) Results for the two types of sample preparation are essentially the same. At the higher temperatures and higher field strengths, the resulting electrical response to strain reaches a nearly constant value--especially when the pyroelectric coefficient is considered. There is appreciably more scatter in the data for response to pressure perhaps due to the inherent temperature changes which accompany the expansion or compression of the pressurizing fluid. In the case of the melt-crystallized film where data was obtained over a wider range of poling temperatures, the response is nearly independent of poling temperature at the highest field strength employed. There are frequent break-downs at 500 kV/cm and elevated temperatures so higher field strengths have not yet been tried.

To enable comparison of the results in Tables II and III with the expressions for  $d_p$  and  $p$ , (Equations 7 and 8) we have also measured  $\alpha_L$  and  $\beta_L$  for the two films indicated by the asterisk in the tables. For the cast film,  $\beta_L = 2.05 \times 10^{-10} \text{ m}^2/\text{N}$  and  $\alpha_L = 2.2 \times 10^{-4} \text{ K}^{-1}$  while for the melt-crystallized film we obtained  $\beta_L = 2.15 \times 10^{-10} \text{ m}^2/\text{N}$  and  $\alpha_L = 1.76 \times 10^{-4} \text{ K}^{-1}$ . (From volume dilatometry on a sample of the copolymer which is about 44% crystalline, we find  $\alpha_L = 1.72 \times 10^{-4} \text{ K}^{-1}$ ).

From the literature, the dielectric constant for immobilized dipoles has been taken to be about 3. Unfortunately, we do not as yet have a direct measure of P but we can now estimate what its value would have to be according to this model to account for the maximum measured value of  $d_p$ .

$$P = d_p / \beta_L \epsilon_\infty = 1.92 \times 10^{-6} \text{ C/cm}^2$$

This value of P is well within the maximum value of  $3 \mu\text{C/cm}^2$  which one might expect to achieve with this randomly oriented copolymer.

From the ratio of  $d_p$  to p and the measured values of  $\alpha$  and  $\beta$ , one can obtain an estimate of  $\Delta\phi$ , the RMS amplitude of oscillation of the dipoles in the copolymer. At 300 K,  $\Delta\phi$  would have to be  $44^\circ$  ( $\phi_0 = 62^\circ$ ) (calculated from tabulations of Bessel functions rather than the small angle approximation). As opposed to the  $14^\circ$  found for PVC which seemed very reasonable, a value of  $44^\circ$  seems unusually large. Because of the seemingly large estimate of  $\Delta\phi$ , the details of this model as applied to semicrystalline polymers may require refinements.

#### Acknowledgement

Partial support of this work by the Office of Naval Research is gratefully acknowledged.

## References

1. M. G. Broadhurst, C. G. Malmberg, F. I. Mopsik and W. P. Harris, Electrets, Charge Storage and Transport in Dielectrics, M. M. Perlman Ed., Proceedings of an International Conference on Electrets sponsored by the Electrochemical Society, October 1972, Miami Beach, Florida, p.492.
2. F. I. Mopsik and M. G. Broadhurst, NBS Report No.2 on ONR Task No. 74-622 ("Molecular Dipole Electrets") and also submitted for publication in J. Appl. Phys.
3. M. Tamura, K. Ogasawara, N. Ono and S. Hagiwara, J. Appl. Phys. 45, 3768 (1974).
4. M. Oshiki and E. Fukada, J. Materials Sci. 10, 1 (1975).
5. J. D. Hoffman, G. Williams, and E. Passaglia, J. Polymer Sci. C14, 173 (1966).
6. R. D. Nelson, Jr., D. R. Lide, Jr., and A. A. Maryott, "Selected Values of Electric Dipole Moments for Molecules in the Gas Phase" NSRDS-NB10; U. S. Government Printing Office, Washington, D. C. (1967).
7. R. Hasegawa, Y. Takahashi, Y. Chatani, and H. Tadokoro, Polymer J. 3, 600 (1972).
8. H. Kakutani, J. Polymer Sci. A-2 8, 1177 (1970).

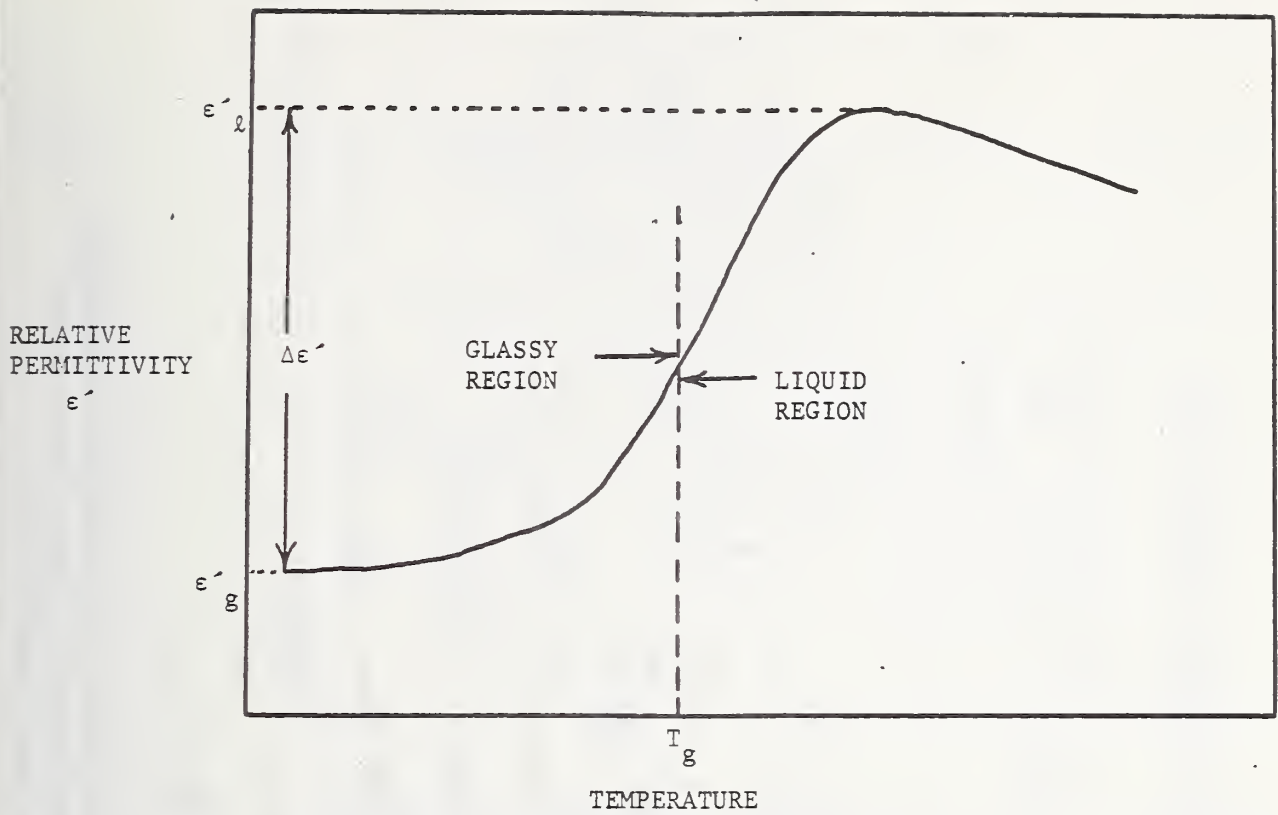


Figure 1. Schematic representation of relative permittivity of an amorphous polymer as a function of temperature at constant frequency.

$$P = \frac{(\epsilon_\infty + 2)}{3} \frac{N\mu_0}{V} \langle \cos \theta \rangle$$

$$Q_{\text{Total}} = Q_{\text{Real}} + PA = Q_{\text{Real}} + \frac{N\mu_0}{L} \langle \cos \theta \rangle \quad (\text{Note: } V = AL)$$

$$\frac{1}{A} \frac{dQ}{dT} = - \frac{(\epsilon_\infty + 2)}{3} \frac{N\mu_0}{A} \langle \cos \theta \rangle + \frac{1}{L^2} \frac{dL}{dT} + \frac{1}{3} \frac{N\mu_0}{AL} \langle \cos \theta \rangle + \frac{d\epsilon_\infty}{dT} + \frac{(\epsilon_\infty + 2)}{3} \frac{N\mu_0}{AL} \frac{d \langle \cos \theta \rangle}{dT}$$

$$(a) \quad + \quad (b) \quad + \quad (c)$$

$$(a) \quad \frac{1}{L} \frac{dL}{dT} = \frac{\alpha_V}{3} = \alpha_L$$

$$(b) \quad \frac{(\epsilon_\infty - 1)}{(\epsilon_\infty + 2)} = \frac{\text{constant}}{V} \quad \text{leads to} \quad \frac{d\epsilon_\infty}{dT} = \frac{-(\epsilon_\infty - 1)(\epsilon_\infty + 2)}{3} \alpha_V$$

(c) Harmonic oscillator with angular amplitude  $\phi = \phi_0 \cos \omega t$   
 $\frac{d \langle \cos \theta \rangle}{dT} = - \langle \cos \theta \rangle \frac{d\phi_0}{J_0(\phi_0)} \frac{d\phi_0}{dT} ; \langle \phi_0 \rangle = \frac{2kT}{I\omega^2} ; \frac{d\phi_0}{dT} = \frac{\phi_0}{2T}$

$J_1(\phi_0) =$  Bessel function of first kind, first order  $\approx \frac{\phi_0}{2}$  for small  $\phi_0$

$J_0(\phi_0) =$  " " " " , zero order  $\approx 1$  for small  $\phi_0$

$$\frac{d \langle \cos \theta \rangle}{dT} \approx - \langle \cos \theta \rangle \frac{\phi_0/2}{1} \frac{\phi_0}{2T} = - \langle \cos \theta \rangle \frac{\Delta\phi_{\text{RMS}}^2}{2T} \quad (\text{Note: } \Delta\phi_{\text{RMS}} = \Delta\phi/\sqrt{2})$$

$$p = \frac{1}{A} \frac{dQ}{dT} = - P[\alpha_L + (\epsilon_\infty - 1) \alpha_L + \frac{\Delta\phi_{\text{RMS}}^2}{2T}] = -P \left[ \epsilon_\infty \alpha_L + \frac{\Delta\phi_{\text{RMS}}^2}{2T} \right]$$

For change in pressure,  $\frac{d \langle \cos \theta \rangle}{dp} = 0$  and  $d_p = \frac{1}{A} \frac{dQ}{dP} = -P \epsilon_\infty \beta_L$

Figure 2. An outline of the derivation of piezoelectric and pyroelectric coefficients for a system of aligned dipoles. The quantity  $\alpha_L$  is the linear thermal expansion coefficient and  $\beta_L$  is the linear compressibility.

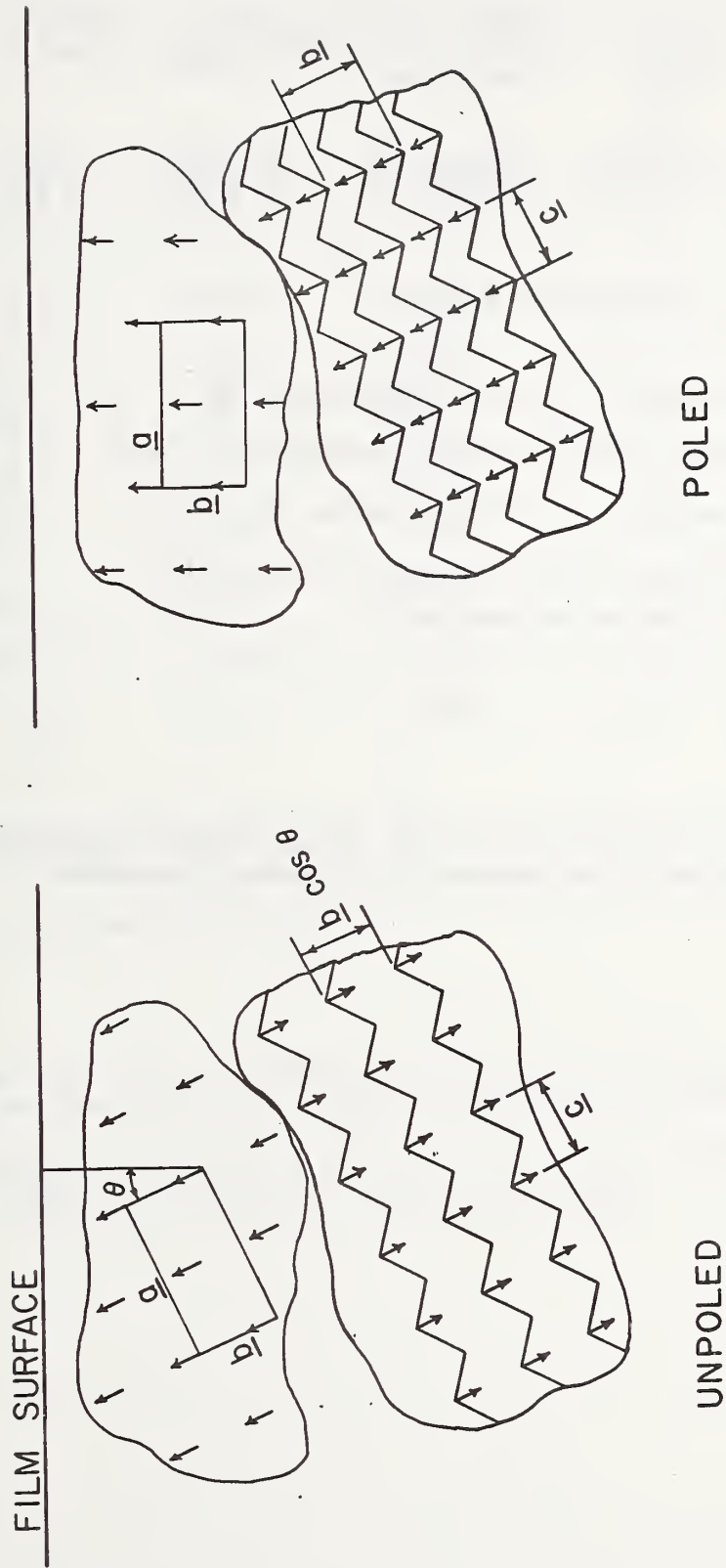


Figure 3. Schematic representation showing a proposed change in dipole orientation within polymer crystallinities as a result of poling.

$$P_{\max} = \frac{(\epsilon_{\infty} + 2)}{3} \frac{\mu}{V_{\text{PVF}_2}} \cdot \frac{V_{\text{PVF}_2}}{\bar{V}_{\text{copolymer}}} \cdot \chi \cdot X \cdot f_{\text{H-T}} \cdot \langle \cos^2 \delta \rangle$$

$$\frac{(\epsilon_{\infty} + 2)}{3} \frac{\mu}{V_{\text{PVF}_2}} = \frac{(3 + 2)}{3} \frac{2.12 \text{ D}}{53.9 \text{ \AA}^3} = \frac{5}{3} \cdot 13.1 \frac{\mu\text{C}}{\text{cm}^2} = 22 \frac{\mu\text{C}}{\text{cm}^2}$$

$$V_{\text{PVF}_2} / \bar{V}_{\text{copolymer}} = 53.9 / 66.4 = 0.81$$

$\chi$  = Fraction of sample which is crystalline = 0.36

$X$  = Fraction of sample which is vinylidene fluoride = 0.73

$f_{\text{H-T}}$  = Fraction of head to tail addition within  $\text{VF}_2$  = 0.95

$\langle \cos^2 \delta \rangle$  = Projection of chain axes into plane of film  
= 2/3 for random orientation

$$P_{\max} = 3.0 \frac{\mu\text{C}}{\text{cm}^2}$$

Figure 4. Maximum polarization of  $\text{PVF}_2$  single crystal corrected for semicrystalline copolymer with random orientation.

Table I. Summary of piezoelectric and pyroelectric data obtained with polyvinylchloride.

Sample	$E_p$ , kV/cm	$d_p^*$ , pC/N	$p^{*+}$ , nc/cm <sup>2</sup> K	$\frac{d_p}{E_p \beta_L \epsilon_0}$			$\frac{p}{E_p \alpha_L \epsilon_0}$		
				$E_p$	$\beta_L$	$\epsilon_0$	$E_p$	$\alpha_L$	$\epsilon_0$
A4	40	0.079	0.0127	25.9			46.1		
A3	80	0.173	0.025	28.4			44.7		
A2	160	0.363	0.056	29.8			45.8		
A1	320	0.619	0.095	25.4			43.1		
PA	344	0.777	0.114	29.7			48.1		
PB	350	0.735	0.105	27.6			43.3		
PC	349	0.649	0.104	24.4			43.2		
PD	351	0.604	0.102	22.6			42.0		
			Avg.	26.7			44.5		

$$\alpha_L = 0.78 \times 10^{-4} \text{ K}^{-1}$$

$$\beta_L = 0.86 \times 10^{-10} \text{ m}^2/\text{N}$$

\* The values reported in reference 1 incorrectly measured a contribution to the current from the region outside the area of the evaporated electrodes.

+ In addition to the area correction, the values in reference 1 were reported as  $p = \left(\frac{dP}{dT}\right)$  whereas here  $p$  is defined as  $\frac{1}{A} \left(\frac{dQ}{dT}\right)$ .

Table II. Pyroelectric and piezoelectric coefficients for PVF<sub>2</sub>-TFE copolymer film cast from solution.

p, nC/cm <sup>2</sup> K				
	T, °C			
<u>E, kV/cm</u>	<u>50</u>	<u>60</u>	<u>70</u>	<u>80</u>
200		1.4		
300	1.0	2.6	2.7	2.5*
500	1.9	2.4		

d <sub>p</sub> , pC/N				
	T, °C			
<u>E, kV/cm</u>	<u>50</u>	<u>60</u>	<u>70</u>	<u>80</u>
200		5.1		
300	3.9	10.4	11.2	8.5*
500	7.1	10.1		

\* Thermal expansion and compressibility measured on this specimen.

Table III. Pyroelectric and piezoelectric coefficients for PVF<sub>2</sub>-TFE copolymer film crystallized from the melt.

<u>E, kV/cm</u>	<u>p, nC/cm<sup>2</sup>K</u>			
	<u>T, °C</u>			
	<u>0</u>	<u>30</u>	<u>60</u>	<u>80</u>
100	0.04	1.1	1.4	1.2
300	1.5	1.9	2.6*, 2.7	2.0, 2.2
500	2.4, 2.2, 2.0	2.3	2.2	

<u>E, kV/cm</u>	<u>d<sub>p</sub>, pC/N</u>			
	<u>T, °C</u>			
	<u>0</u>	<u>30</u>	<u>60</u>	<u>80</u>
100	0.5	2.3	5.4	5.7
300	5.4	7.2	9.8*, 12.1	6.1, 8.1
500	11.7, 7.7, 9.0	7.5	8.2	

\*Thermal expansion and compressibility measured on this specimen.

POLYVINYLIDENE FLUORIDE AS AN ACTIVE DEVICE ELEMENT

by

J. G. Bergman  
Bell Laboratories  
Holmdel, New Jersey 07733

ABSTRACT

A general summary of some of the device applications which have recently been found for polyvinylidene fluoride, such as infrared detector elements, nonlinear optical mediums, as well as an active element in a copying process is given. These applications represent some of the first instances where the non-passive characteristics of polymers are successfully employed.

by

J. G. Bergman.  
Bell Laboratories  
Holmdel, New Jersey 07733

Over the last few decades polymer usage has shown enormous growth, in most all of these applications however one of the major rationales for usage has been the "passive" character or chemical inertness of polymers. Now however, the advent of polymers as "active" elements in state of the art electronic and optical devices is upon us. It is our purpose here to review some of the recent pyroelectric and nonlinear optical applications of one polymer in particular, polyvinylidene fluoride ( $\text{PVF}_2$ ). We will first review some of the structural and optical properties, then discuss some pyroelectric applications and lastly a particular device application namely using  $\text{PVF}_2$  as the active element in a copying process will be discussed.

$\text{PVF}_2$  is a highly crystalline polymer  $(\text{CH}_2\text{CF}_2)_n$  belonging to the acentric polar group  $\text{mm}2$ .<sup>1,2</sup> In Fig. 1 we see a model of  $\text{PVF}_2$  which shows that the C-F and C-H bond dipoles have a resultant dipole moment which is perpendicular to the polymer chain axis, i.e. parallel to Z in Fig. 1. (For later reference, a coordinate system is defined with Z parallel to the polar axis of the chain and Y parallel to the

chain as shown in Fig. 1). If we assume reasonable values<sup>3</sup> for the bond dipoles i.e. [ $\mu(\text{C-C}) \sim 0$ ,  $\mu(\text{C-F}) = 1.4\text{D}$  and  $\mu(\text{C-H}) = 0.4\text{D}$ ] we find that the calculated spontaneous polarization is between 8 and 16  $\mu\text{C}/\text{cm}^2$ , depending on the polarity of the C-H bond. The experimental value, obtained by Buchman<sup>4</sup> is 8  $\mu\text{C}/\text{cm}^2$ . It would be nice to be able to conclude here that this now determines the sense of the C-H bond polarity but this is not the case, since even in well defined cases where good structural data and measured molecular dipole moments exist (such as in the case of Thiourea<sup>5</sup>) the calculated  $P_s$  is only half the size of the observed value.

The mechanical treatment which produces the texture in the  $\text{PVF}_2$  film does not, of course, affect the sense of the microscopic polarization (as many dipoles point out one side of the film as out the other side). Electrical poling viz ( $10^6$  V/cm at  $\sim 120^\circ\text{C}$ ) is required<sup>6</sup> in order to make the films have uniform polarity. A possible poling mechanism is shown in Fig. 2. The model illustrates a  $180^\circ$  rotation of the molecular dipoles about the polymer chain axis.

The degree of ordering due to mechanical treatment is shown in Fig. 3 where we compare the two birefringes as a function of the thickness of the film. One also sees that the magnitude of the pyroelectric coefficient is also, as

expected, related to the degree of order, induced in the film by stretching. We see that the thinner biaxially oriented films have the largest pyroelectric coefficient ( $\sim 2.4 \text{ nC/cm}^2\text{ }^\circ\text{C}$ ). In the case of the biaxial films, there are three different values of the principal indices  $n_x$ ,  $n_y$  and  $n_z$ . Here  $n_z$  is the film normal or polar axis and  $n_y$  correspond to the preferred direction of the polymer chains. A confirmation of the biaxial nature of the film is shown in Fig. 4 which shows a conoscopic interference figure. (A stack of films was used in order to get a sufficiently long light path in the material).

Once the films are poled they become activated for second harmonic generation (SHG). A schematic representation of the experimental set up is shown in Fig. 5. A detail of the sample configuration is shown in Fig. 6. A Nd:YAG laser ( $\lambda=1.06\mu\text{m}$ ) with a peak power of  $\sim 100$  watts was used to generate harmonics at  $\lambda = 0.53\mu\text{m}$ . Samples were cut from the  $19\mu\text{m}$  thick biaxially-oriented film in the form of small wedges whose shape and orientation are shown in Fig. 6. The laser beam propagates in the plane of the film ( $||k$ ) and is focused so that its waist is contained in the film. To prevent burning, only  $\sim 15\%$  of the full laser power was employed. The second harmonic signal, separated from the fundamental by suitable

filter (Fig. 5), was then detected with a photomultiplier. According to the X-ray measurements, the polar phase of  $\text{PVF}_2$  has point symmetry  $\text{mm}2$  (Z is the polar axis). The components of the second harmonic polarization for  $\text{mm}2$  symmetry are given in terms of the fundamental electric field components by

$$P_x = 2d_{31}E_xE_z$$

$$P_y = 2d_{32}E_yE_z$$

$$P_z = d_{31}E_x^2 + d_{32}E_y^2 + d_{33}E_z^2.$$

Thus there are three independent second order nonlinear coefficients,  $d_{31}$ ,  $d_{32}$  and  $d_{33}$ . These equations predict that when the laser is polarized normal to the film ( $||z$ ), the second harmonic will also be polarized in the z direction ( $P_x = P_y = 0$ ,  $P_z = d_{33}E_z^2$ ). This result is observed experimentally i.e. ( $d_{33}$  coupling). The above equations also predict that when the laser is polarized in the plane of the film ( $||x$ ), the second harmonic signal should be polarized normal to the film i.e. orthogonal to the fundamental ( $P_x = P_y = 0$ ,  $P_z = d_{31}E_x^2$ ). This result ( $d_{31}$  coupling) is also observed experimentally. Finally, if a wedge is cut having its length parallel to y and the laser beam is polarized in y direction no SHG is observed. This result implies that

$d_{32}$  is very small compared to  $d_{31}$  and  $d_{33}$ . The magnitudes of the coefficients, relative  $d_{11}$  (Quartz) were found to be

$$d_{33}(\text{PVF}_2) \sim 2d_{31}(\text{PVF}_2) \sim d_{11}(\text{SiO}_2) \gg d_{32}(\text{PVF}_2)$$

We should note that the very small size of  $d_{32}$  is to be expected since from Fig. 1 we see that for  $E \parallel y$  we cannot couple to either the C-F or C-H bonds. Hence we must get our signal from only the carbon bonds, which because of their centrosymmetric nature should give a very weak (if any) signal.

It is easy to use the poled  $\text{PVF}_2$  films as pyroelectric detectors of electromagnetic radiation. The essentials of such a detector are shown in Fig. 7. The poled film is cemented with conductive epoxy to a metal heat sink. The conductive front-face electrode is made to be either highly absorbing (gold-black) or partially transmitting (very thin gold film) for the incident radiation. If the load resistor,  $R$ , is small compared to the resistance of the film and is also small enough that the RC time constant of the load circuit is negligible, the voltage response,  $V_o$ , of the detector to a modulated beam is given by

$$V_o = AR \frac{dP}{dt} = AR \left( \frac{dP}{dT} \right) \frac{dT}{dt}$$

where  $A$  is the electroded area of the film and  $P$  is the polarization of the film. Since  $dP/dt$  is the pyroelectric coefficient we see then that  $V_0$  is proportional to  $dT/dt$ , the heating or cooling rate of the film. The response of two detectors to a 90 Hz chopped beam is given in Fig. 8. Detector A is constructed as in Fig. 7 with its entire back surface in contact with the heat sink. In this case the thermal response time is only a few milliseconds and thermal equilibrium, as evidenced by the decreasing response, can take place during the beam-on or beam-off periods. Detector B has the  $PVF_2$  film mounted in a drum head fashion with only its periphery in contact with the heat sink. In this case the thermal response time is approximately one second with the result that the heating and cooling rates are constant during the on- and off-periods, and a square-wave response is obtained from detector B. The behavior exhibited in Fig. 8 identifies the effect observed as true pyroelectricity i.e. (a reversible dependence of the polarization on temperature) and not simply depolarization i.e. (an irreversible decay of the polarization with time when the sample is heated) as is often studied in electrets. In Fig. 9 we show the response of a  $PVF_2$  detector to a Q-switched  $CO_2$  laser pulse of submicrosecond risetime. Also shown is the same pulse as

detected by a Cu doped Ge photoconductive detector operating at 4.2°K. In Fig. 10 we see the set up for pyroelectric scanning experiment the results are shown in Fig. 11. We see from Fig. 11 that the pseudo 3-dimensional shows basically no response outside the poled area and considerable non-uniformity in the poled region. One can thus conclude that if domains exist in these samples they must be smaller than  $\sim 10 \mu\text{m}$ .

Common materials have pyroelectric coefficients  $dP/dt \sim 10^{-8} \text{ C/cm}^2\text{ }^\circ\text{C}$ . One can see that a localized 1°C temperature rise can generate a localized electrostatic charge on the order of  $10^{-8} \text{ C/cm}^2$ . Since conventional electrostatic copiers based on the photoconductive effect also involve local charges of this order, we have attempted to employ the pyroelectric effect as a basis for a copier. In Fig. 12 we see the simplified demonstration of the effect in  $\text{LiTaO}_3$ . The bottom surface of the  $\text{LiTaO}_3$  crystal ( $\sim 10 \text{ mil} \times 1 \text{ cm}^2$ ), coated with a conducting layer of aluminum, is at ground potential. Initially, both blocks of copper are at the same temperature, and the top surface of the crystal is wiped free of stray charges with a Tesla coil or salt solution. Then heat is applied to the left-hand copper block until a temperature rise of about 6°C is obtained on the left-hand side of the crystal, as shown in Fig. 13(a).

Since the pyroelectric coefficient of  $\text{LiTaO}_3$  is  $\sim 2 \times 10^{-8} \text{ C/cm}^2\text{ }^\circ\text{C}$ , one generates a charge density of  $\sim 120 \text{ nC/cm}^2$ . The approximate charge distribution is shown in Fig. 13(b). A developer consisting of negatively charged toner loosely bound to positively charged steel shot is poured over a baffle and then over the crystal surface. One then observes that the toner (negative charge) is attracted preferentially to the region where the electric field [Fig. 13(c)] is directed outward from the surface. This effect is enhanced if the baffle is at a negative potential (-1.2kV) in order to increase the negative charge on the ink and is degraded if the baffle is at a positive potential. The same effect was observed for a 0.020-in.-thick 1-in.-diam ceramic disk of lanthanum-modified lead zirconate-titanate (PLZT). In the material used, 6% of the lead was replaced by lanthanum and the Zr:Ti atom ratio was 65:35. A more dramatic demonstration of the localized heating and its concomitant charge distribution is shown in Fig. 14. A 650-W lamp passes light through the object slide, projecting the image on the pyroelectric element,  $\text{PVF}_2$  ( $dP/dt \sim 2 \times 10^{-9} \text{ C/cm}^2\text{ }^\circ\text{C}$ ). The  $\text{PVF}_2$  is oriented so that the heated region develops a negative charge and the cool region has a (relative) positive charge. Hence, the toner (negative) is attracted to the cool region. A photograph of the developed image is shown in Fig. 15(b). Negative images were readily

obtained by neutralizing the pyroelectric element after the image had been projected and then allowing the pyroelectric element to cool down, thus reversing the charge distribution in sign only. Images have been transferred from the  $\text{PVF}_2$  film to paper by standard techniques.<sup>7</sup> A representative printed copy is shown in Fig. 15(c).

If a crystalline (i.e., ordered dipolar) homogeneous medium is assumed, the expected resolution limit should be of the order of the film thickness, since any projected line whose width is thinner than the film thickness may be substantially broadened by thermal diffusion. The (0.8-mil)  $\text{PVF}_2$  samples used in these experiments were ~50% crystalline, the crystalline phases being divided between the useful orthorhombic phase and a second monoclinic phase. The distribution of the orthorhombic phase (i.e., homogeneity) in the film is not known at this time. We are therefore hopeful that improving  $\text{PVF}_2$  or finding other materials (hence, with even larger pyroelectric coefficients) will result in substantial improvements.

We have demonstrated that an electrostatic copying process based on the pyroelectric effect is indeed feasible. Furthermore, since the process is inherently wavelength independent (unlike a photoconductive process), it is more

readily adaptable to color copying or to studying thermal distributions in the infrared. Further experiments on other pyroelectric materials as well as other developing processes are in progress.

The author gratefully acknowledges the collaboration of J. H. McFee, G. R. Crane and A. M. Glass without whom these results would doubtless never be obtained.

## REFERENCES

1. J. B. Lando, H. G. Olf, and A. Peterlin, J. Polymer Sci. 4, 941 (1966).
2. H. Kawai, Japan J. Appl. Phys. 8, 975 (1969).
3. C. P. Smyth, "Dielectric Behavior and Structure", McGraw Hill, N. Y. (1955) p. 244.
4. P. Buchman, Ferroelectrics 5, 39 (1973).
5. G. J. Goldsmith and J. G. White, J. Chem. Phys. 31, 1175 (1959); the Handbook of Chem. and Phys. gives  $\mu(\text{Thiourea}) = 4.9\text{D}$ .
6. More detailed descriptions of these processes can be found in: J. G. Bergman, J. H. McFee and G. R. Crane, Appl. Phys. Lett. 18, 203 (1971); J. H. McFee, J. G. Bergman and G. R. Crane, Ferroelectrics 3, 305 (1972); A. M. Glass, J. H. McFee and J. G. Bergman, J. Appl. Phys. 42, 5219 (1971); J. G. Bergman, G. R. Crane, A. A. Ballman and H. O'Bryan, Appl. Phys. Lett. 21, 497 (1972); and references therein.

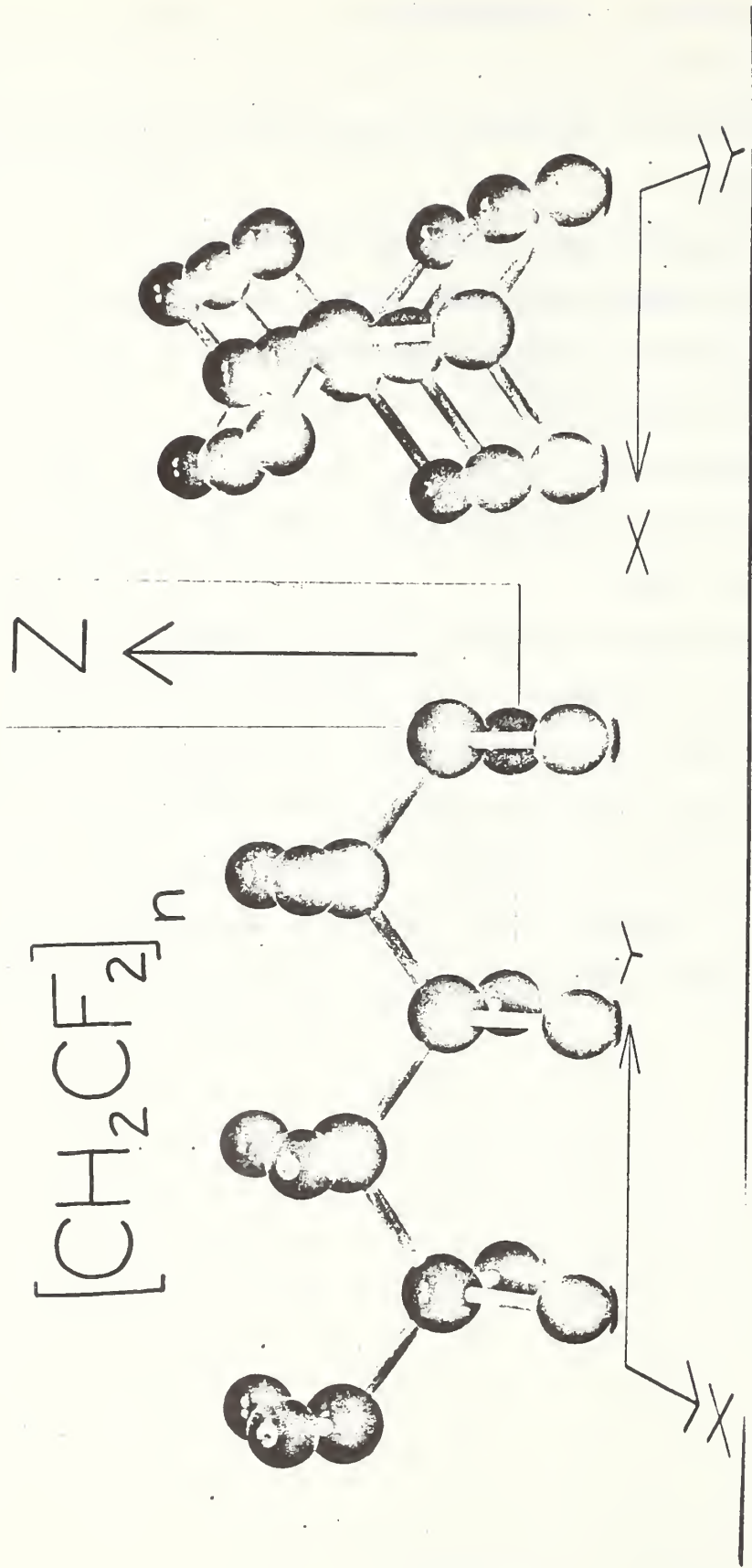


FIG. 1

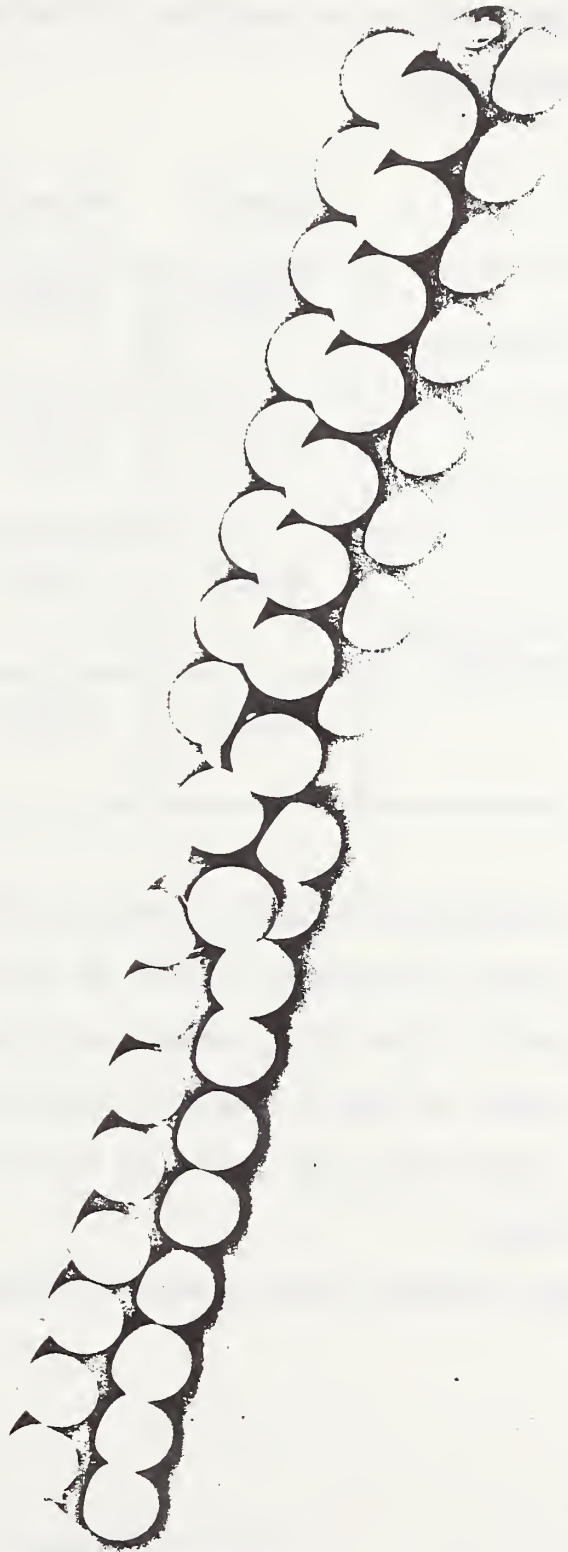


Fig. 2

Fig. 3

Birefringence<sup>a</sup> and pyroelectric coefficient of poled PVF<sub>2</sub> as a function of the method of film preparation.

Description <sup>b</sup>	( $n_y - n_z$ )	( $n_x - n_z$ )	Pyroelectric Coefficient (nC/cm <sup>2</sup> °C)
0.4 mil (biaxially stretched)	0.018	0.011	2.4 ± .7
0.8 mil (biaxially stretched)	0.019	0.011	2.4 ± .7
2.0 mil (uniaxially stretched in the x direction)	0.000	0.013	0.7 ± .2
5.0 mil	0.000	0.000	.03 ± .1

<sup>a</sup> Indices measured at 6328Å using an Abbé refractometer;  $n_{ave} = 1.425$ ; estimated errors in  $\Delta n$  are  $\pm 0.002$ ;  $n_z$  corresponds to the film normal or polar axis while  $n_x$  and  $n_y$  refer to the orthogonal directions in the plane of the film having the smallest and largest indices, respectively.

<sup>b</sup> All films obtained from Kureha Chemical Co., Tokyo, Japan.

Fig. 4

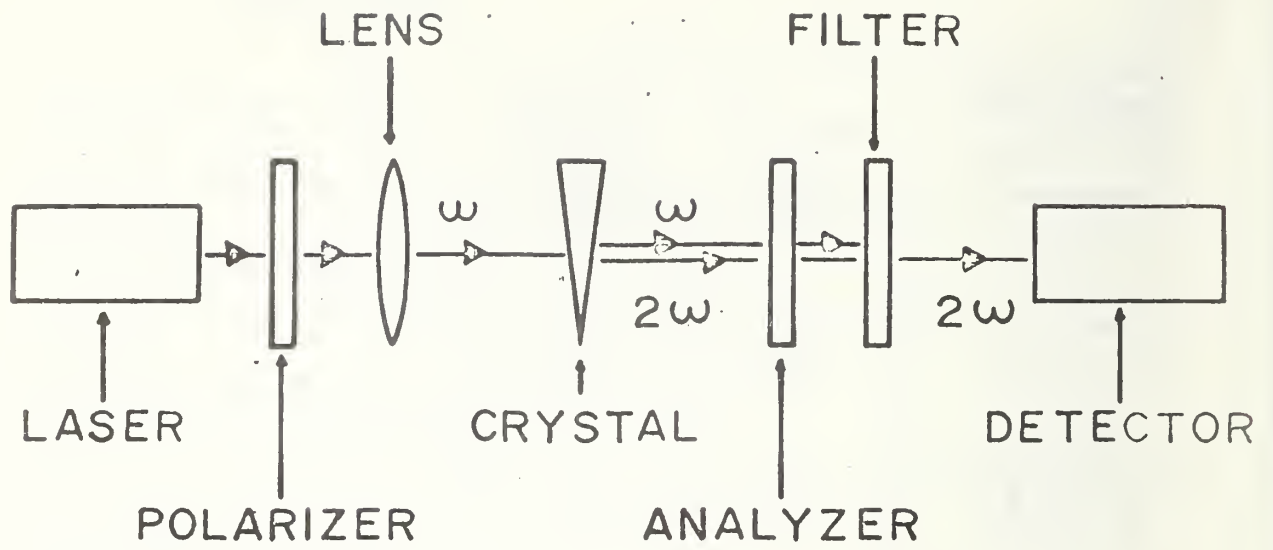
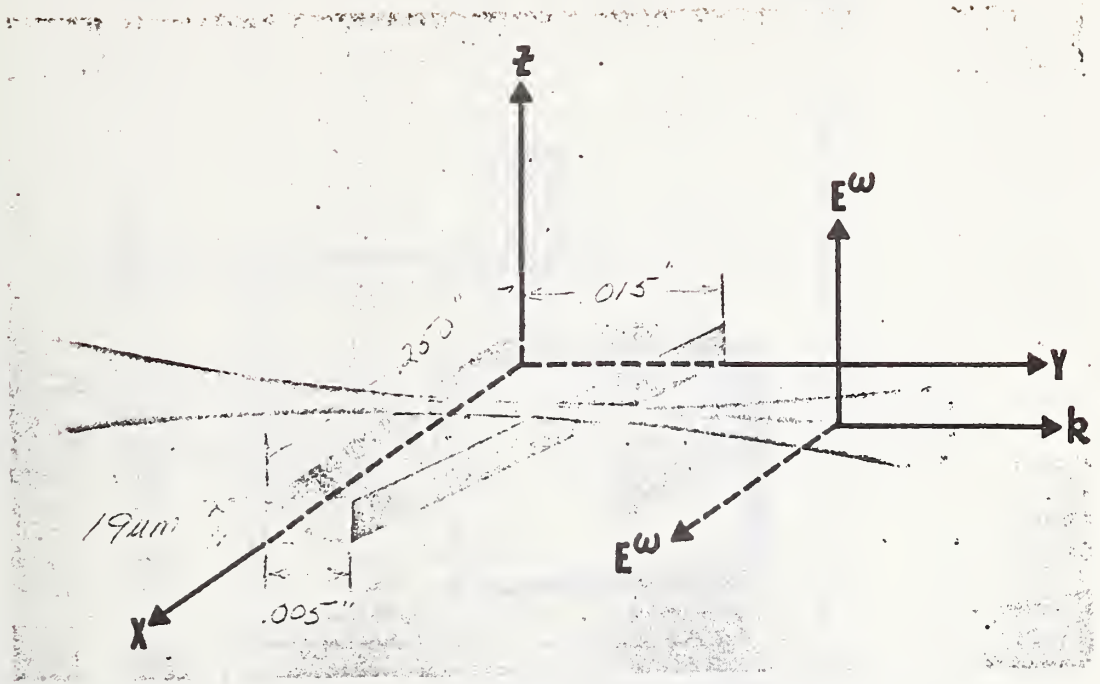


Fig. 5



mmz :

$$P_x = 2d_{31} E_x E_z$$

$$P_y = 2d_{32} E_y E_z$$

$$P_z = d_{31} E_x^2 + d_{32} E_y^2 + d_{33} E_z^2$$

Fig. 6

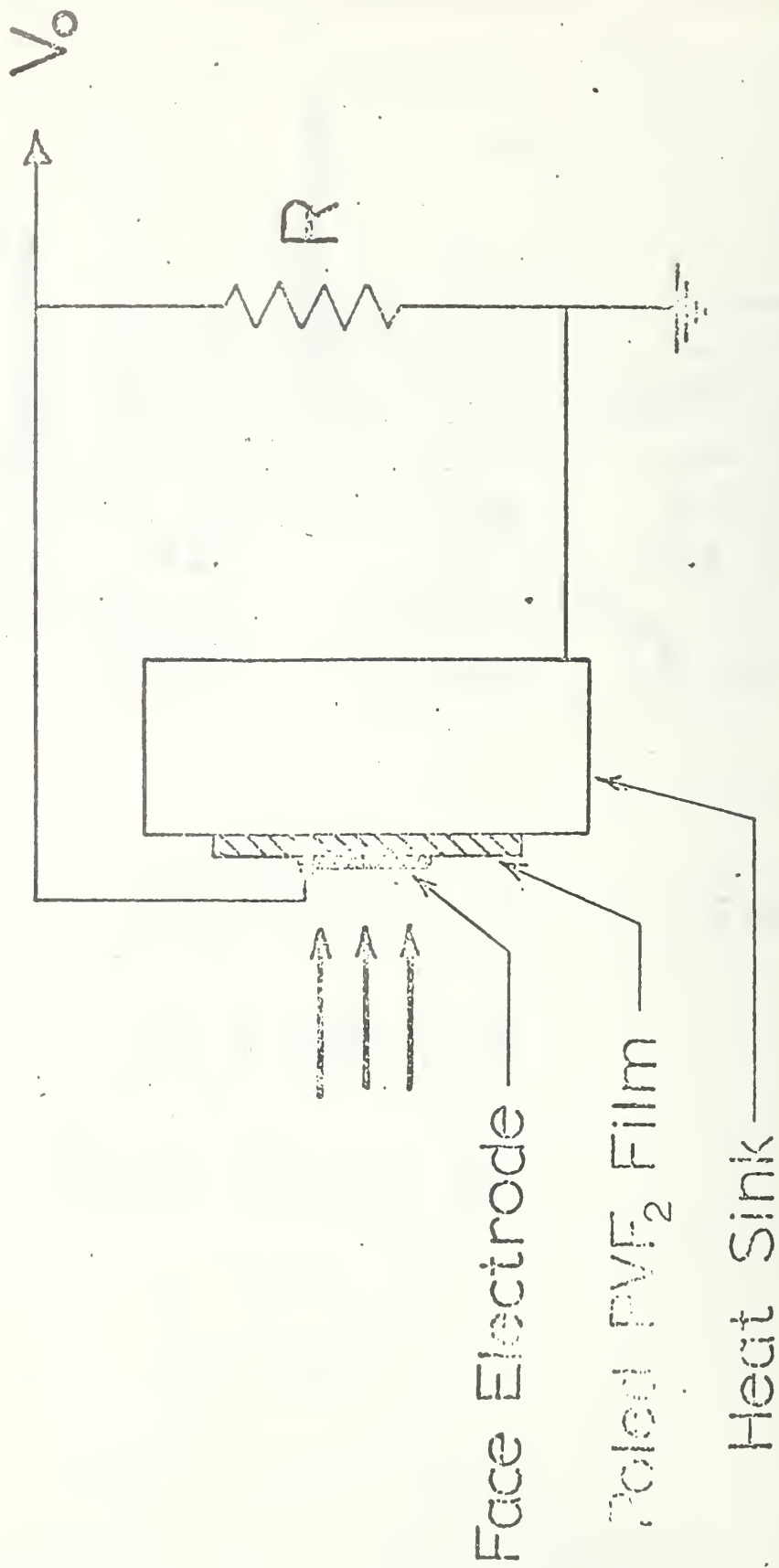


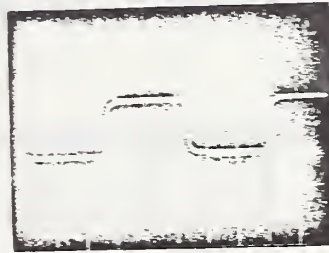
Fig. 7

Det. A  
 $\tau_i = 2 \times 10^{-3}$  sec



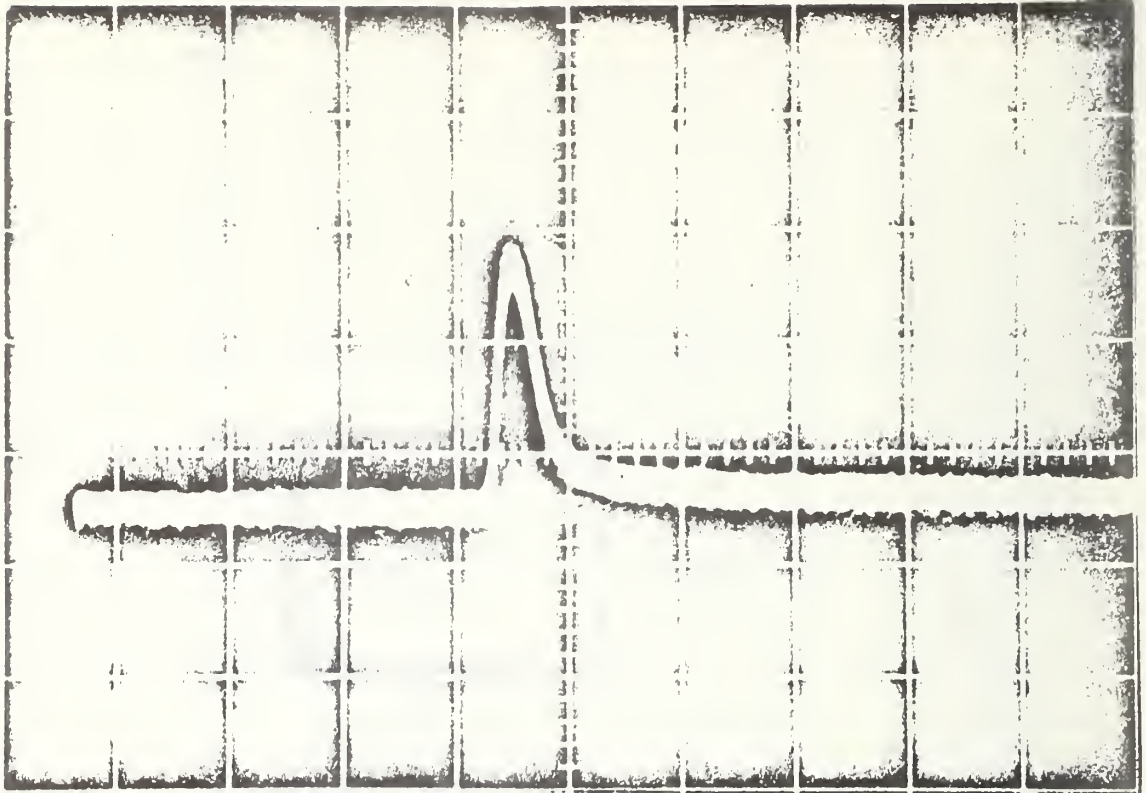
$2 \times 10^{-3}$  sec

Det. B  
 $\tau_i = 1$  sec



Response of  $PV F_2$  pyroelectric detectors to 90 Hz chopped beam from  $CO_2$  laser. Detector A: Thermal response time  $\tau_i \approx 2 \times 10^{-3}$  sec. Detector B:  $\tau_i \approx 1$  sec. In both cases the load resistance  $R$  is small enough that Eq. (1) is valid.

A.



B.

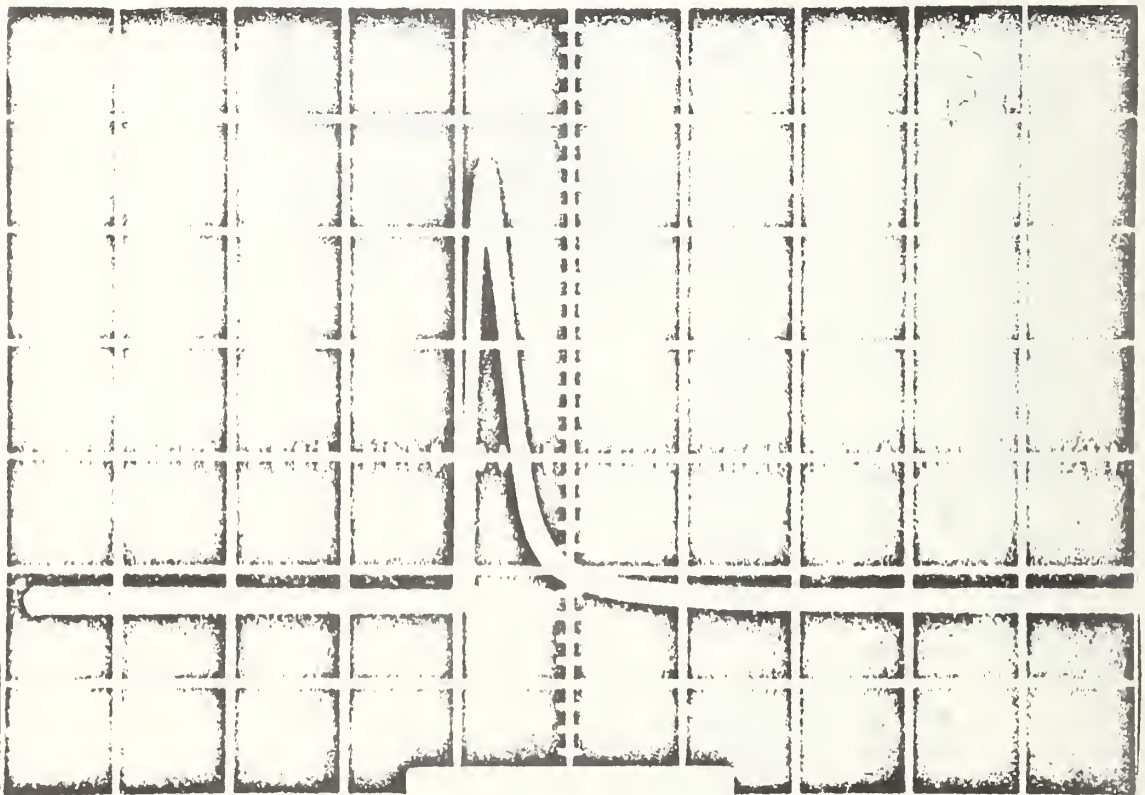
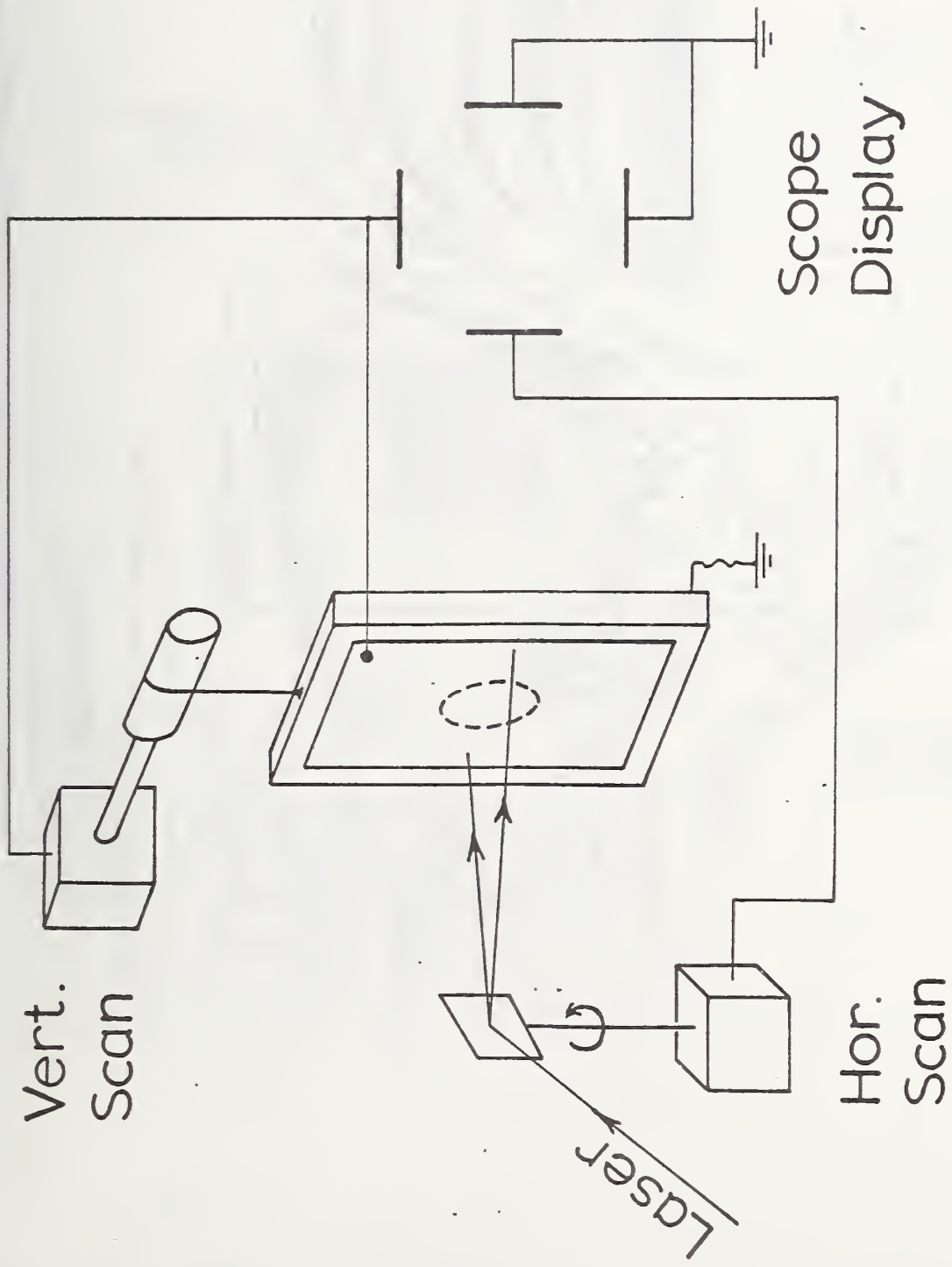
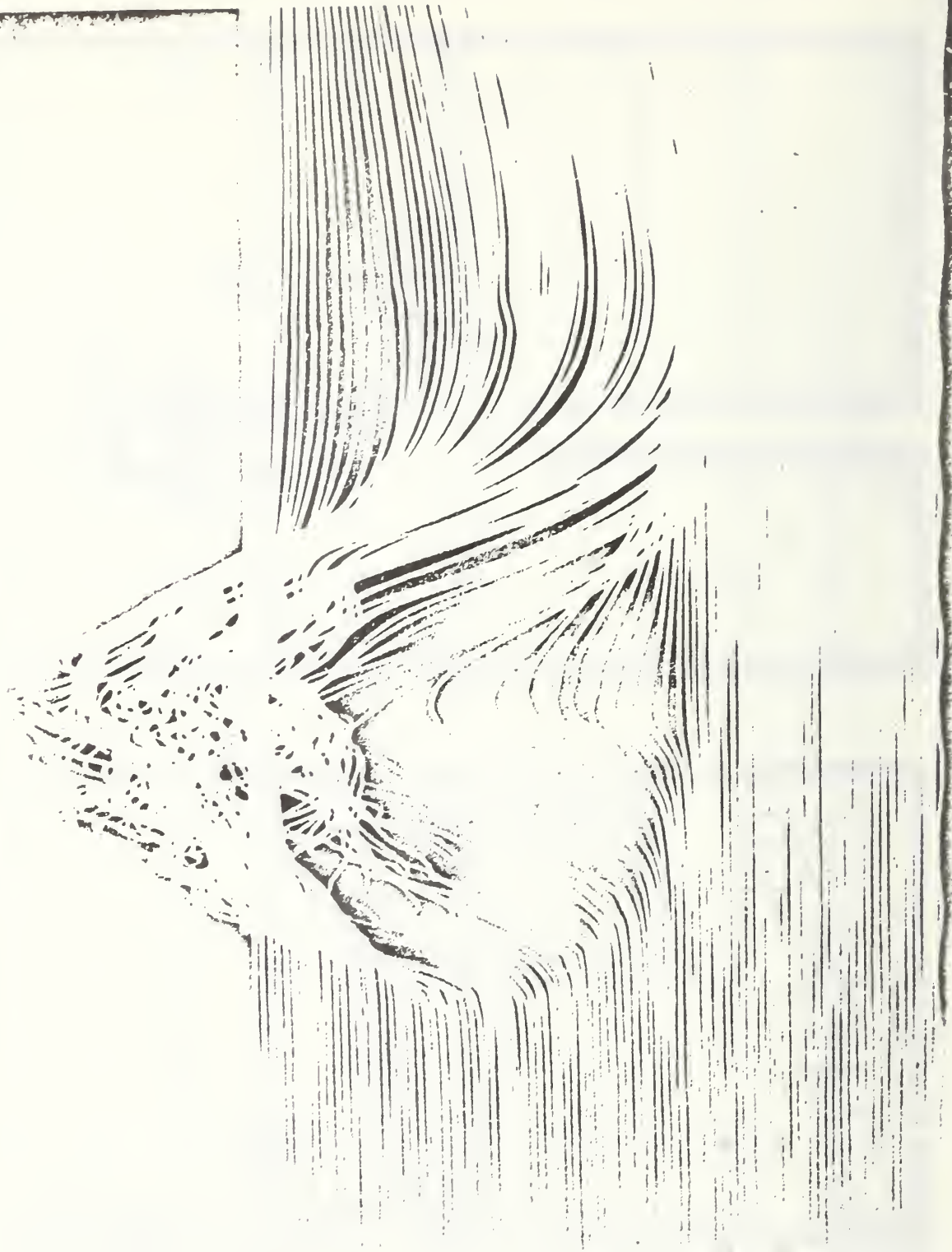


Fig. 9



Pyroelectric Scanning

Fig. 11



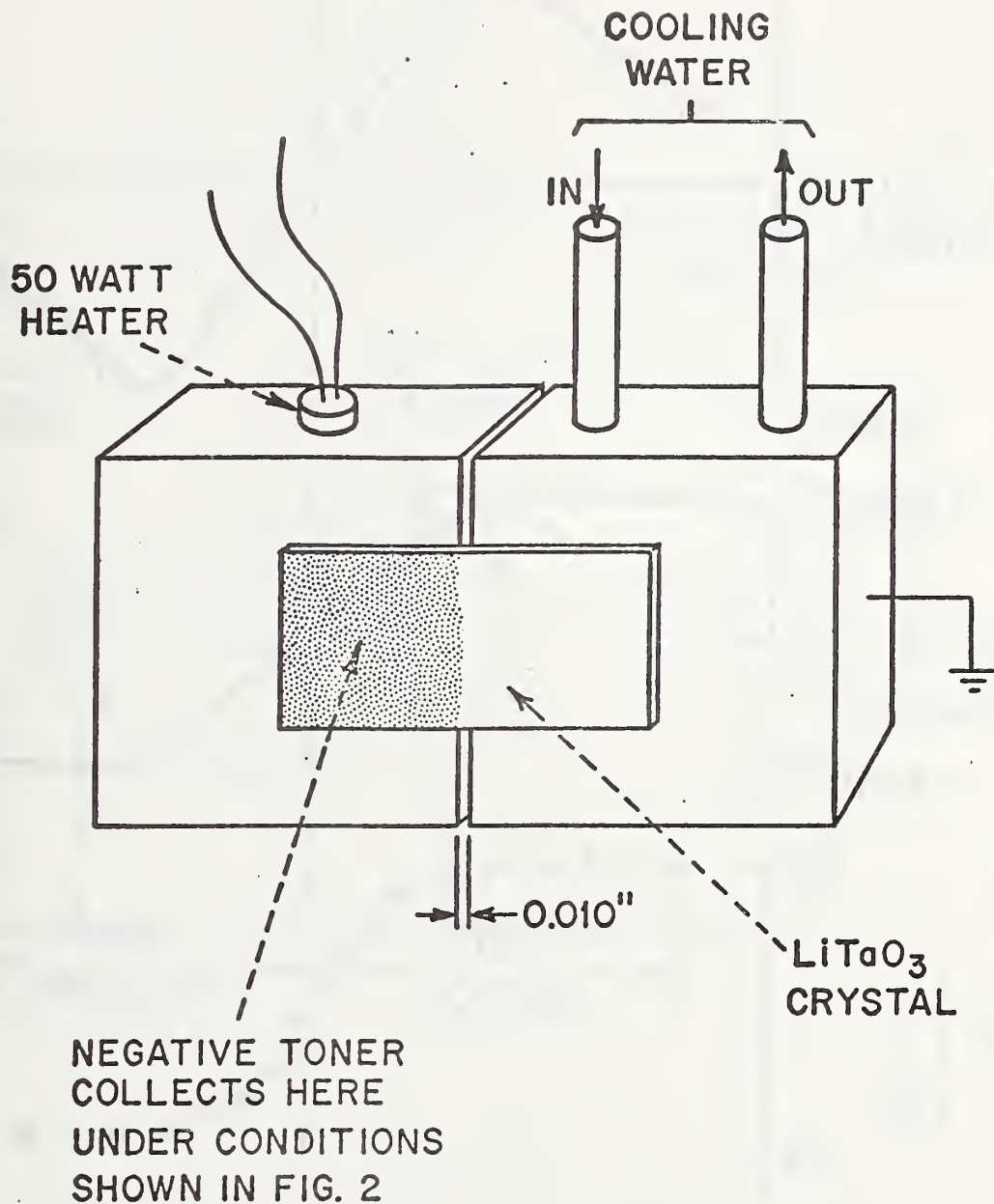


Fig. 12

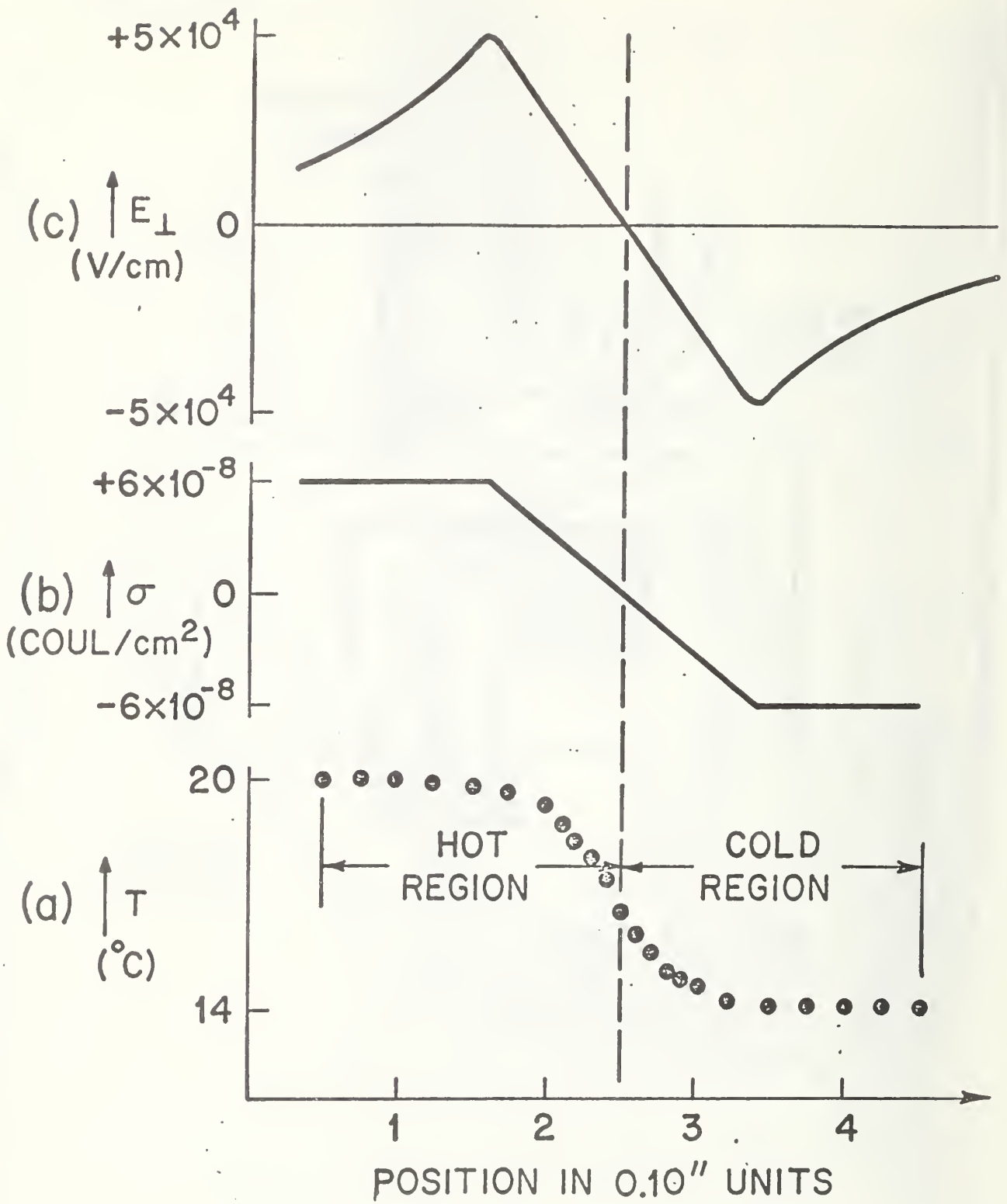


Fig. 13

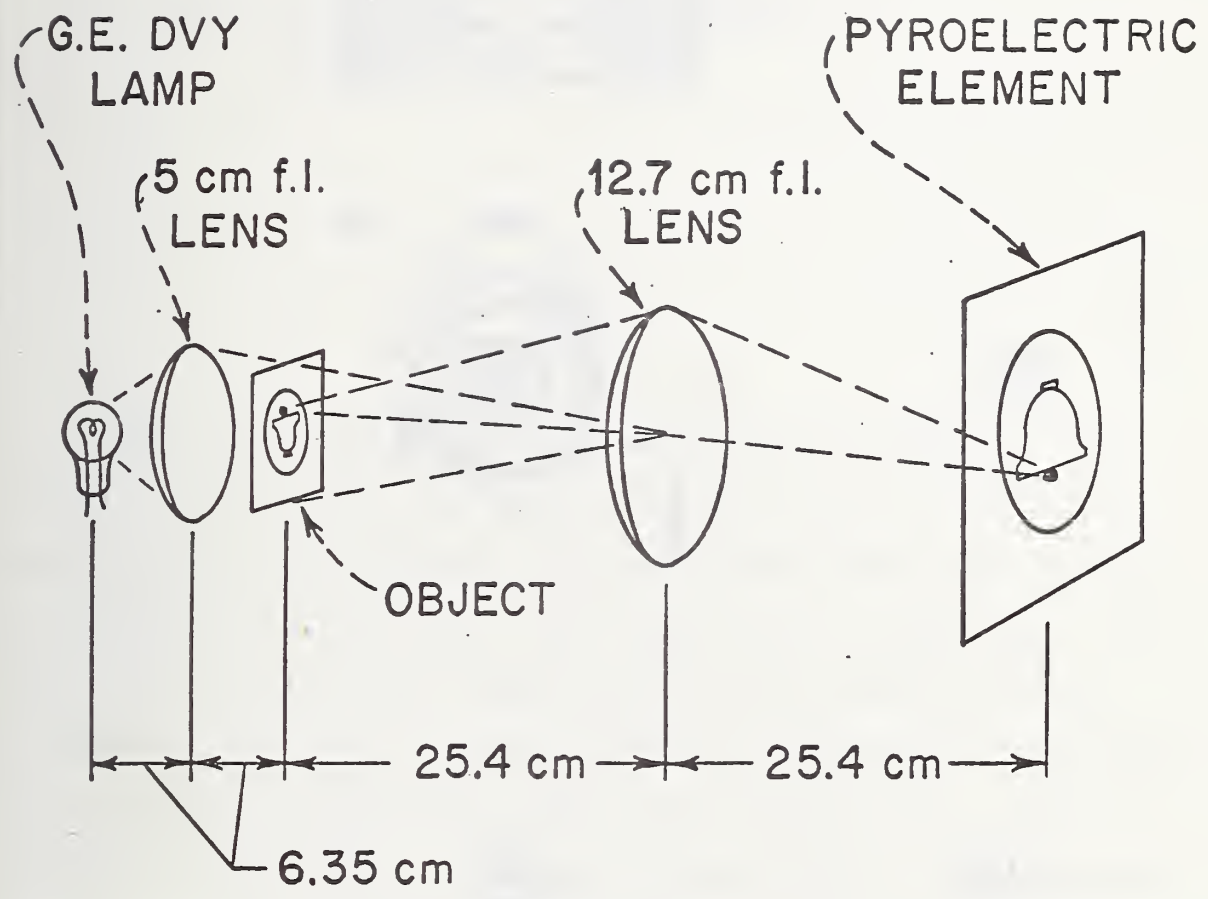
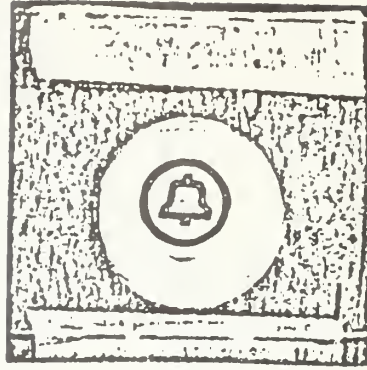


Fig. 14

(a)



(b)



(c)



Fig. 15

Scanning for Ferroelectricity in  
Polycrystalline Materials

by

M. Litt, Che-hsiung Hsu, P. Basu and S. M. Aharoni

Department of Macromolecular Science  
Case Western Reserve University  
Cleveland, Ohio 44106

ABSTRACT

The dielectric behavior of polycrystalline pellets of 2-alkyl benzimidazoles are reported in this paper. The experimental technique consists of measuring the dielectric constant of a polycrystalline pellet as a function of temperature. Dielectric anomalies were found for which the position of the dielectric and loss tangent peaks were independent of frequency, which showed a solid/solid first order transition. When the sample was held under a voltage gradient while the temperature was dropped through the transition temperature, reversible charge storage showed poling of the sample, and therefore, implies possible ferroelectric behavior.

The experimental procedure was validated on thiourea, a known ferroelectric. 2-Ethyl benzimidazole showed the same phenomena at a transition temperature of about  $-90^{\circ}\text{C}$  and is probably a new ferroelectric material.

# Scanning for Ferroelectricity in Polycrystalline Materials

by

M. Litt, Che-hsiung Hsu, P. Basu and S. M. Aharoni  
Department of Macromolecular Science  
Case Western Reserve University  
Cleveland, Ohio 44106

## INTRODUCTION

We have been interested in organic ferroelectric materials for several years and have been endeavoring to find some new classes in the group of materials which have infinite chains of H-bonds. It has been shown theoretically and experimentally that, when dipoles are associated to form a chain, the magnitude of the dielectric response increases with the number of dipoles in the chain<sup>1,2</sup>. In addition to chains of H-bonds, to be potentially ferroelectric, the bonding must be reversible. Thus the compound should have two isomers of identical stability, where the transformation from one isomer to the other is accomplished by proton switching. This also reverses the dipole involved. Benzimidazoles, were reasonable candidates to study for the following reasons. They are known to associate through H-bonding and have high dipole moments. NMR studies<sup>3</sup> indicate that the two nitrogen atoms in benzimidazole are electrostatically equivalent. This implies that the associated H-bonding dipoles could be capable of reversal from one position of equilibrium to another of equal energy. This is shown schematically in Fig. 1. Because of these factors, it was decided to investigate the dielectric properties of 2-substituted benzimidazoles<sup>4</sup>. Since

much time and strenuous effort is required to grow single crystals, and techniques for the study of dielectric constants and pyroelectric effects in polycrystalline materials have already been reported in the literature<sup>5,6</sup>, polycrystalline pellets of benzimidazoles were used in this study. However, since in ceramics the polarization directions are only 90° apart, there is a much larger resultant polarization on poling than in our case where the dipoles flip 180°. We feared initially that the effect would be too small to observe. This report describes the experimental method and its application to a control compound, thiourea, a known ferroelectric<sup>7,8</sup>, and to benzimidazoles with unusual dielectric properties. Furthermore, the pyroelectric effect and its voltage dependence will also be discussed.

### EXPERIMENTAL

#### A. Material Preparations

2-Ethylbenzimidazole (2-EBIA), obtained from Pfaltz & Bauer Co., was twice treated with activated charcoal in boiling distilled water and recrystallized from the filtered solution. Sample was dried thoroughly by a vacuum oven and then zone refined for 140 passes. The ground powder was pressed at 120°C while being maintained under vacuum. The resultant ½" diameter pellets were completely translucent but not optically clear. Gold film was deposited on both sides of pellets at a vacuum of 10<sup>-7</sup> torr.

2-Isopropylbenzimidazole (2-IBIA) was synthesized according to Philips' method<sup>9</sup>. Pellets were prepared from zone refined

powder at 200°C and were also gold shadowed.

Thiourea, obtained from Baker Co., was recrystallized twice from ethanol and was dried thoroughly. The well ground powder was pressed under vacuum at R.T. and gold shadowed.

## B. Apparatus

The dielectric constants were determined by calculating the ratio,  $\epsilon' = C/C_0$ , where  $C$  is the capacitance of the cell containing the material, exclusive of lead and insulator capacitance, and  $C_0$  is the corresponding vacuum capacitance. Capacitance was measured with a General Radio model 1620A bridge with a grounded shield using a three terminal configuration, shown in Figure 2.

The pellet was sandwiched between two brass electrodes of  $\frac{1}{2}$ " diameter. The sample chamber was placed in a grounded copper can which could be cooled or heated between -150° and 150°C. An electrically insulated thermocouple was mounted into the low-voltage electrode so that the temperature of the sample could be measured accurately. A Heath/Schlumberger Series EU 200 assembly consisting of a strip-chart recorder, a potentiometric amplifier, an offset module, and a four-channel signal multiplexer was used. The chart recorder was interfaced with a Keithley 610C electrometer, thus enabling us to record temperature and current or charge on the same strip chart. The electrometer leakage was about  $10^{-14}$  amps, and did not interfere with the measurements. A Eurotherm series consisting of a temperature controller and a programmer was employed to program

the sample temperature. Thus the pyroelectric effect could be examined.

## RESULTS AND DISCUSSION

a) Dielectric Measurements: Figure 3 shows the dielectric constant of the thiourea pellet as a function of temperature at the frequency of 1 KHz. (Thiourea is a known ferroelectric). The two transitions are in fairly good agreement with the positions of the two conspicuous peaks reported by other workers<sup>7,8</sup>. A narrow transition reported for the single crystal at  $-96^{\circ}\text{C}$ <sup>7</sup> was not seen even though the experiment was carried out continually recording the temperature and capacitance. This might be attributed to the clamping of constituent microcrystals. The magnitude of the dielectric constant peak at the lower temperature was reduced 100 times when compared with that of the single crystal, which is understandable because the sample is randomly oriented. The field thus encounters regions of both high and low permittivity, which is equivalent to incorporating a large amount of low dielectric constant material in the pellet. Therefore, the dielectric constant will be reduced<sup>4,10,11</sup>. The magnitudes of the dielectric constant peaks observed in the polycrystalline material were roughly proportional to the logarithm of the magnitudes of the corresponding peaks in the single crystal. Thus, dielectric constant studies on polycrystalline materials can reveal the presence of a transition at a specific temperature, but cannot determine the absolute magnitude of the peak.

Figure 4a shows the dielectric constant of the pelletized 2-EBIA as a function of temperature and frequency. A distinct maximum in the dielectric constant was observed at about  $-90^{\circ}\text{C}$ . An additional peak also occurred at about  $-60^{\circ}\text{C}$ , above which the dielectric constant decreased till the ice temperature. Above  $0^{\circ}$ , the dielectric constants first increased slowly and then rapidly. The variations seemed to be the same for three different frequencies. The loss tangent curve is shown in Figure 4b. It clearly indicates that a sharp transition occurred at about  $-90^{\circ}\text{C}$  for all three frequencies. At this transition point, the loss tangent at a given temperature was higher for the higher frequency. This means that the maximum dielectric absorption frequency is greater than 10 KHz. The loss tangent did not show a clear transition at  $-60^{\circ}\text{C}$  and it started to rise very rapidly above room temperature. The rapid increase of loss tangent and dielectric constant at higher temperature was attributed primarily to the onset of conductivity.

Temperature dependence of loss tangent and dielectric constant of 2-isopropyl benzimidazole is shown in Figure 5. There is a slight rise in dielectric constant and a very broad "peak" centering at  $-100^{\circ}\text{C}$ . There is also a transition at about  $105^{\circ}\text{C}$ . However, this maximum is small and cannot be reproduced when lowering the temperature. The loss tangent rose slightly below room temperature and reached a plateau. Above room temperature, it rose very steeply and showed a peak for 10 KHz at the temperature corresponding to the peak of the dielectric constant

curve. This indicates that there probably is a transition at 105°C.

b) Polarization: In order to understand the nature of dielectric transition of 2-EBIA at -90°C, pyroelectric measurements were performed on a 16.6 mil thick pellet. The experiment was carried out in the following way. D.C. voltage of 300 volts was applied to the pellet from R.T. to a temperature far below the transition point (about -140°C). The current flow in the electric field as a function of temperature is shown in Figure 6. It can be seen that at -90°C, while the sample was being cooled, a large peak of current (current maximum  $\approx 10^{-10}$  amps) was observed. The current flow was negligible ( $\approx 10^{-12}$  amps) below the transition temperature. On removing the electric field, the sample displayed a pyroelectric current and, on heating through the transition temperature, current discharge was observed, indicating that charge was stored in the sample. The sample was re-poled from -60 to -140°C at 100 volts and 200 volts and the flow of charge was measured by heating the sample. A steady increase of charge in coulombs continued until the sample discharged at the transition point, Figure 7. This curve indicated that the charge flow rose as the temperature approached the transition point. For comparison, the pellet was cooled down without being subjected to a D.C. electric field. The flow of charge when heating the sample was negligible.

Thiourea (33.0 mils thick) was tested in the same way for

pyroelectric effects at temperatures below its ferroelectric transition. The result is shown in Figure 8. It shows a close similarity with 2-EBIA except that the total charge stored for a given gradient was one quarter that of 2-EBIA.

The voltage dependence of total charge stored for a 16.6 mil thick pellet of 2-EBIA is shown in Figure 9. It clearly indicates that charge stored reached saturation at about 50 volts (1,200 V/cm) but started increasing linearly with voltage after 100 volts. This might indicate that properly aligned crystals in the sample were poled at 50V, but higher voltages either injected charge, poled crystallites which were not oriented in the direction of the field, or poled clamped crystallites.

Figure 10 shows discharge loops measured at a heating/cooling rate of 4°C/min. for a 16.6 mil thick 2-EBIA pellet poled at 200 volts. Cycle 1 represents the first thermal cycle between -144°C and -108°C after the pellet was poled. The charge flow rose when the pellet was heated. Upon cooling, the current reversed sign but only a fraction of charge was recovered. The recovered charge kept decreasing after each cycle. This was probably because stored charge was partly lost when the temperature approached the transition point. The loss is probably not due to migration of injected charge as Fig. 6 shows the charge flow is minimal at -70 and -110°C. The maximum in charge flow at -90° should be due to polarization as  $\tan \delta$  is largest at 10 KHz. Overall, the curve shows quali-

tatively that the transition at  $-90^{\circ}\text{C}$  is pyroelectric in nature.

The nature of the two transitions in 2-IBIA was also investigated by the foregoing techniques. No charge storage was observed when the pellet (20.2 mils thick) was poled through  $-100^{\circ}\text{C}$  at 100 volts. The same pellet was poled at 100V through  $105^{\circ}\text{C}$ ; it showed a change of slope in the current/temperature plot at the transition temperature. The transition might be swamped due to the high protonic conductivity of the sample at the high temperature.

The poled pellet was cooled to room temperature before removing the field. When it was heated from room temperature to  $78^{\circ}\text{C}$  the charge flow rose to  $8 \times 10^{-10}$  coulombs. Upon cooling, the charge was not recovered at all. In order to definitely establish the nature of high temperature transition, single crystal studies are required.

#### CONCLUSIONS

Dielectric measurements on polycrystalline pellets were demonstrated to be a useful method for screening organic compounds for anomalous transitions. As a consequence of this screening, 2-EBIA has been found to be an interesting material.

Polycrystalline 2-EBIA behaves pyroelectrically when poled above  $-90^{\circ}\text{C}$  in a D.C. electric field and cooled below the transition point before removing the field. It was shown by Aharoni that, upon substitution of deuterium for hydrogen participating in hydrogen bonding, the dielectric transition was shifted from  $-90^{\circ}\text{C}$  to  $-60^{\circ}\text{C}$ . From the above and the frequency independent

dielectric peak, it can be concluded that 2-EBIA shows a first order transition at about  $-90^{\circ}\text{C}$ , probably ferroelectric, which results from the dipoles coupled through hydrogen bonding.

The nature of the transition in 2-EBIA at about  $-60^{\circ}\text{C}$  has not yet been investigated. It will be undertaken in the near future. Single crystal growth of 2-EBIA is in process. Dielectric studies on single crystals will determine the accurate transition temperatures; these are not well defined in the pellet studies due to the clamping of constituent microcrystals and the random orientation of dipoles.

The combination of techniques, dielectric scanning at different frequencies and pyroelectric measurements, which had been used for ceramics is a powerful tool for establishing ferroelectric behavior in polycrystalline materials generally. The scanning establishes whether dielectric anomalies exist and whether they are probable first order transitions. The associated pyroelectric behavior, reversible energy storage at the transition, establishes probable ferroelectricity. We have demonstrated it for 2-ethyl benzimidazole after validating it on thiourea, a known ferroelectric.

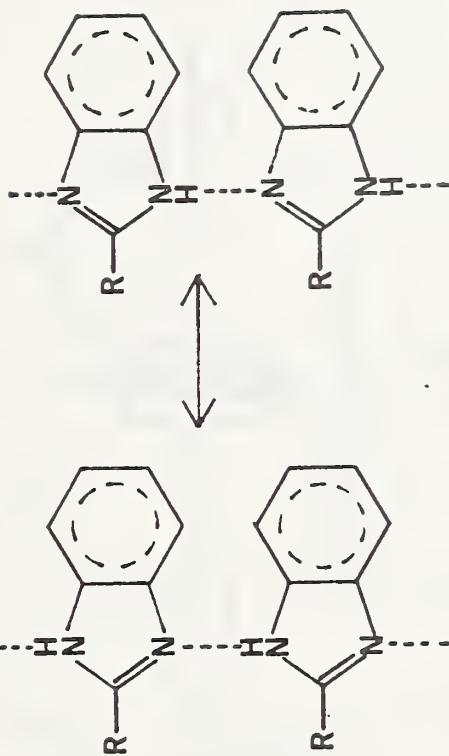
We thank the Office of Naval Research for partial support of this work. We also thank the Research Corporation for support.

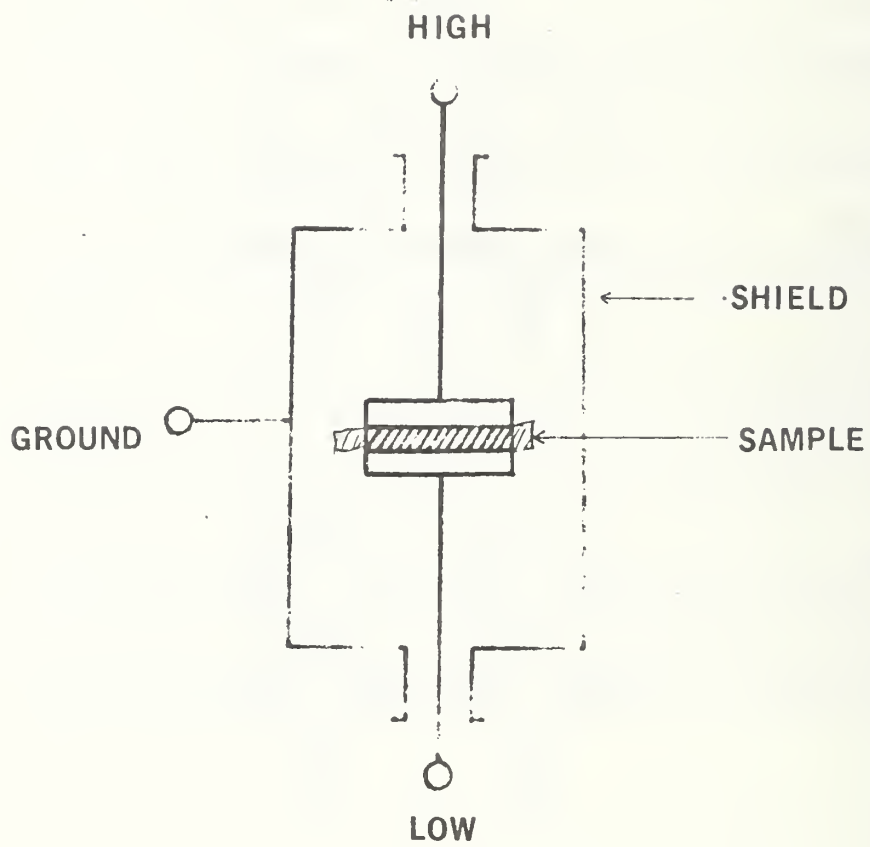
## REFERENCES

1. R. A. Sack, Austral. J. Sci. Res., A5, 135 (1952).
2. R. J. Meakins, Trans. Far. Soc., 58, 1955 (1962).
3. G. S. Reddy, R. T. Hobgood, Jr. and J. M. Goldstein, J. Am. Chem. Soc., 84, 336 (1962).
4. S. M. Aharoni, Ph.D. Thesis, Case Western Reserve University, (1972).
5. G. Shirane, R. Newnham and R. Pepinsky, Phys. Rev., 96, 581 (1954).
6. W. R. Cook, Jr., D. A. Berlincourt and F. J. Scholz, J. Appl. Phys., 34, 1392 (1963).
7. G. J. Goldsmith and J. G. White, J. Chem. Phys., 31, 1175 (1959).
8. K. Gesi, J. Phys. Soc. Japan, 26, 107 (1969).
9. M. A. Philips, J. Chem. Soc., 203, 2393 (1928).
10. R. C. Miller and C. P. Smyth, J. Am. Chem. Soc., 79, 20 (1957).
11. W. G. Cady, "Piezoelectricity", McGraw-Hill, N. Y. (1946). pp. 167-168.

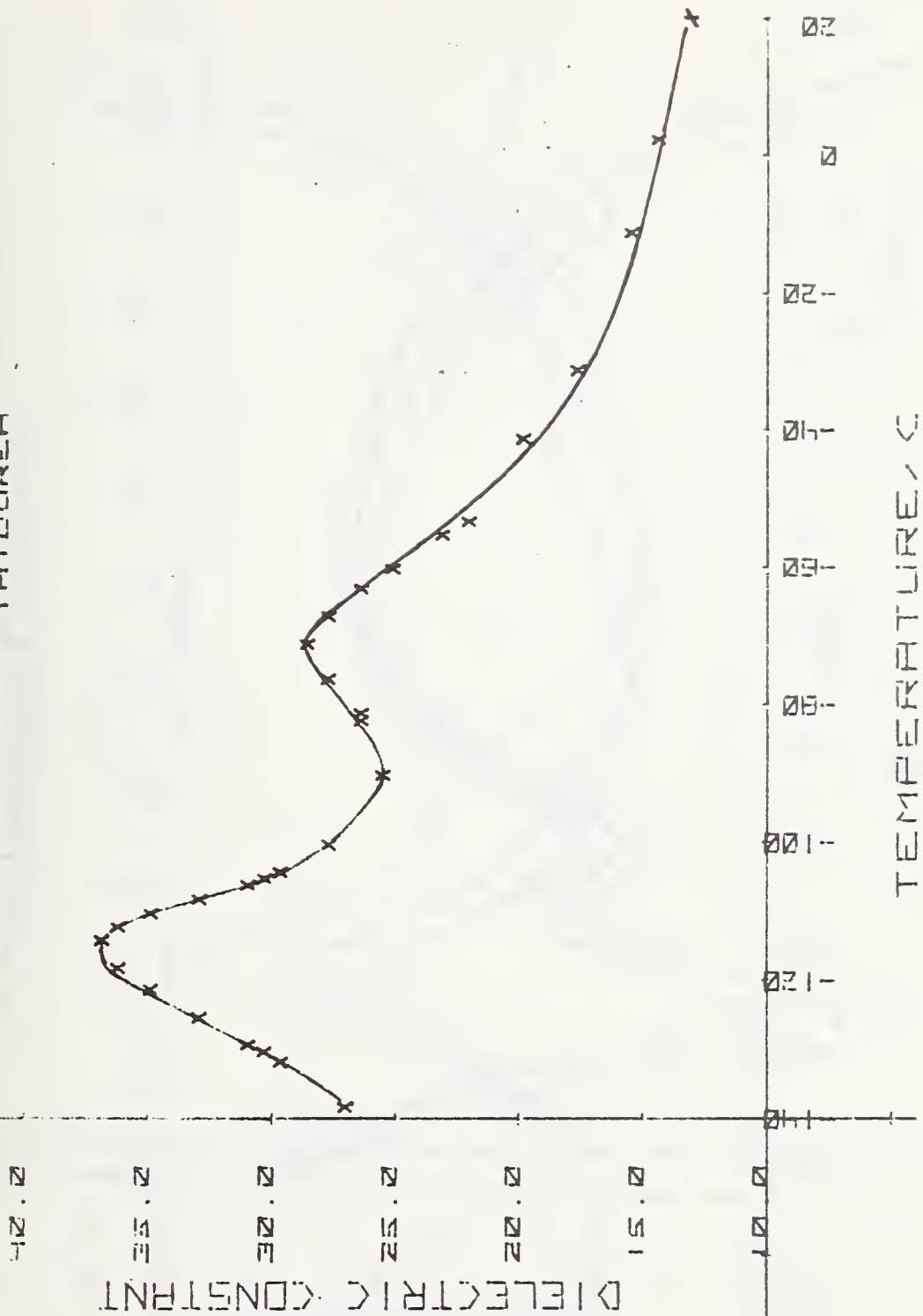
## FIGURE CAPTIONS

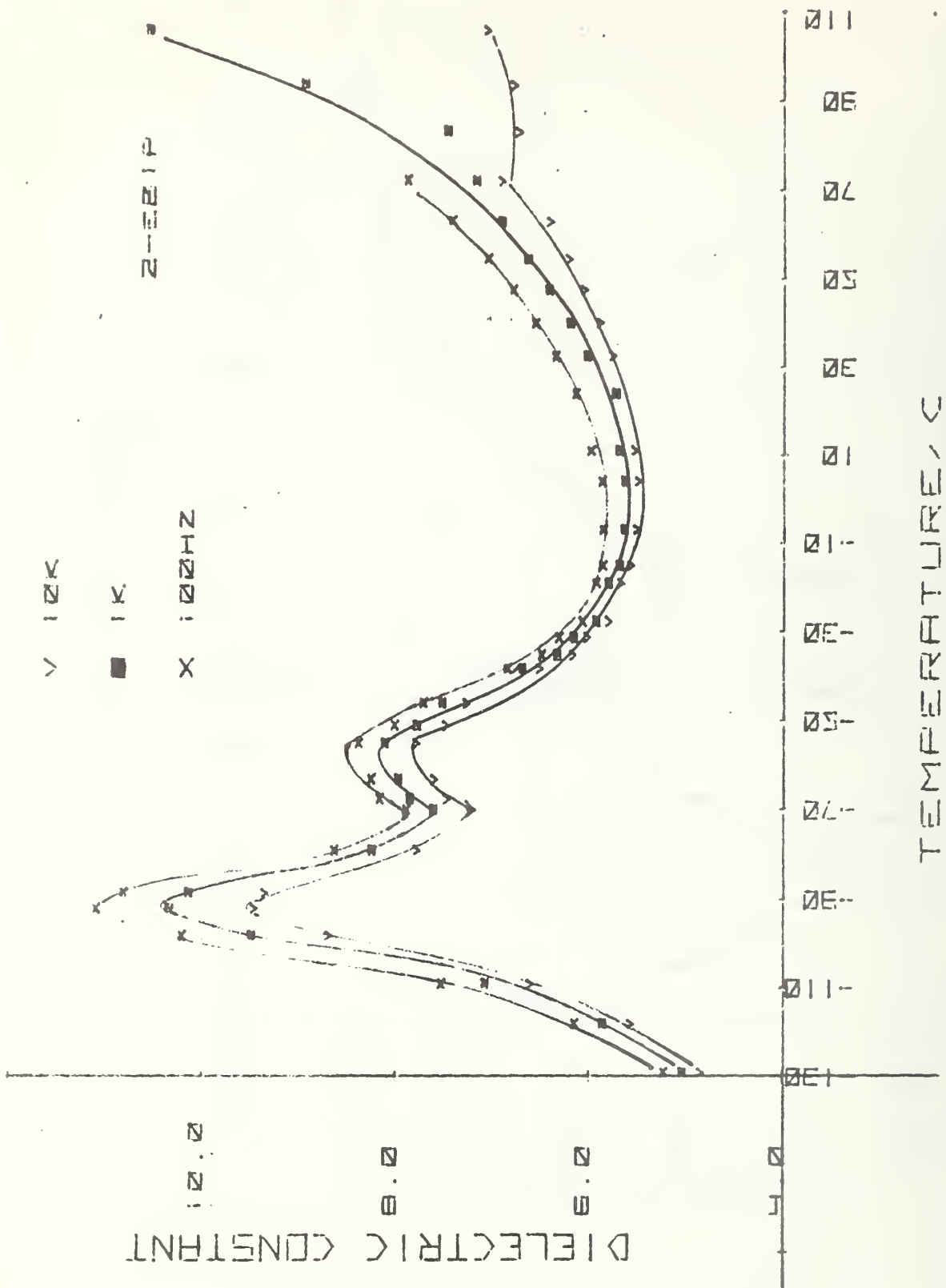
- Fig. 1. Structure of 2-alkyl benzimidazoles and the nature of the H-bonding reversal of dipoles.
- Fig. 2. Three terminal configuration for capacitance measurements.
- Fig. 3. Dielectric constant at 1 KHz of polycrystalline thiourea.
- Fig. 4a. Dielectric constant of polycrystalline 2-ethyl benzimidazole at 100 Hz, 1 KHz and 10 KHz.
- Fig. 4b.  $\tan \delta$  for polycrystalline 2-ethyl benzimidazole at 100 Hz, 1 KHz and 10 KHz.
- Fig. 5a. Dielectric constant of polycrystalline 2-isopropyl benzimidazole at 100 Hz, 1 KHz and 10 KHz.
- Fig. 5b.  $\tan \delta$  of polycrystalline 2-isopropyl benzimidazole at 100 Hz, 1 KHz and 10 KHz.
- Fig. 6. Current flow as a function of temperature (ramping rate of  $-4^{\circ}\text{C}/\text{min}$ ) for polycrystalline 2-ethyl benzimidazole. Poling voltage gradient was  $7.1 \times 10^3 \text{ V/cm}$ .
- Fig. 7. Current discharge of polycrystalline 2-ethyl benzimidazole after poling at indicated voltage gradient.
- Fig. 8. Current discharge of poled polycrystalline thiourea. Poling voltage gradient was  $3.6 \times 10^3 \text{ V/cm}$ .
- Fig. 9. Current discharge in poled polycrystalline 2-ethyl benzimidazole as a function of poling voltage.
- Fig. 10. Pyroelectric current flow in poled polycrystalline 2-ethyl benzimidazole as a function of temperature and cycle.

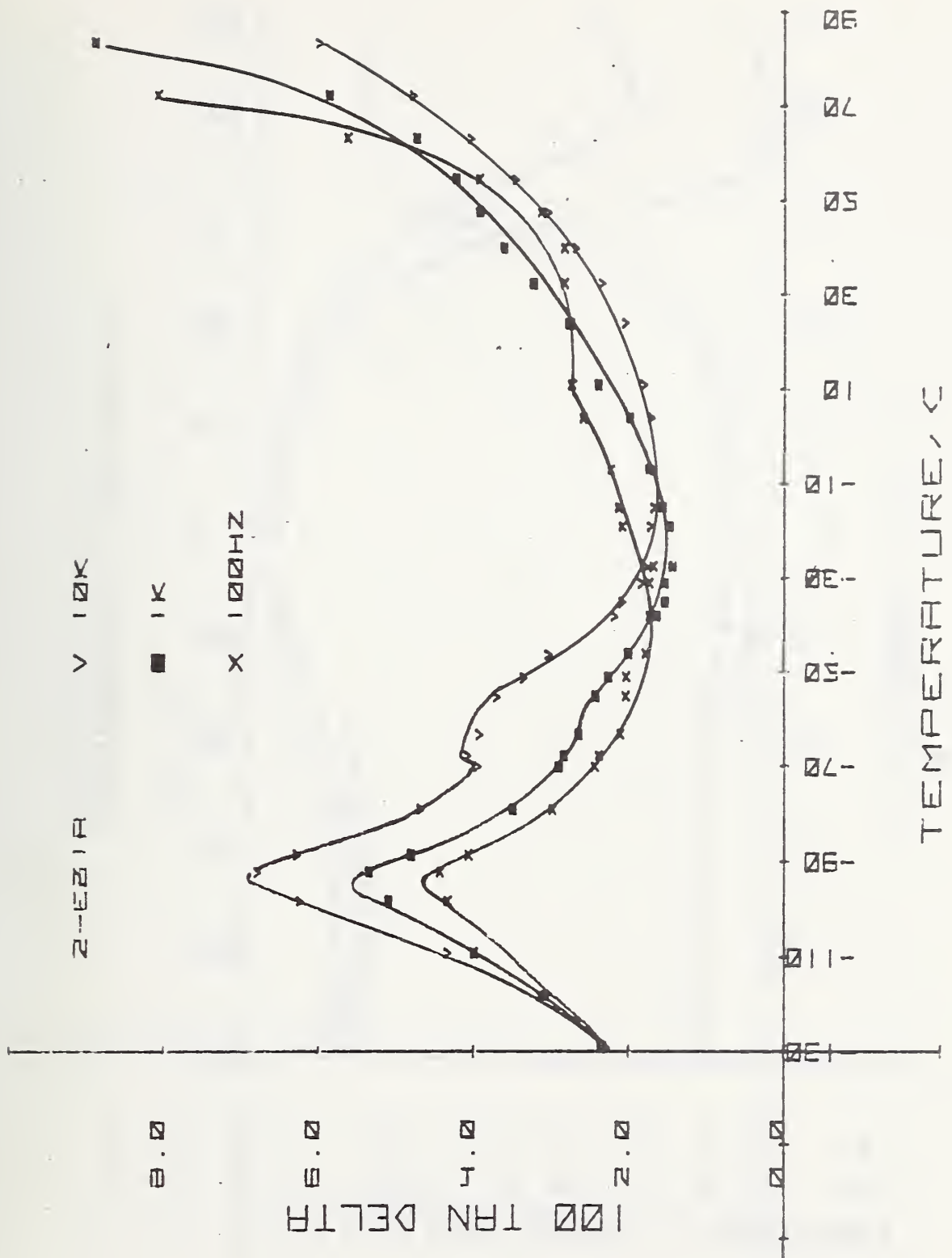


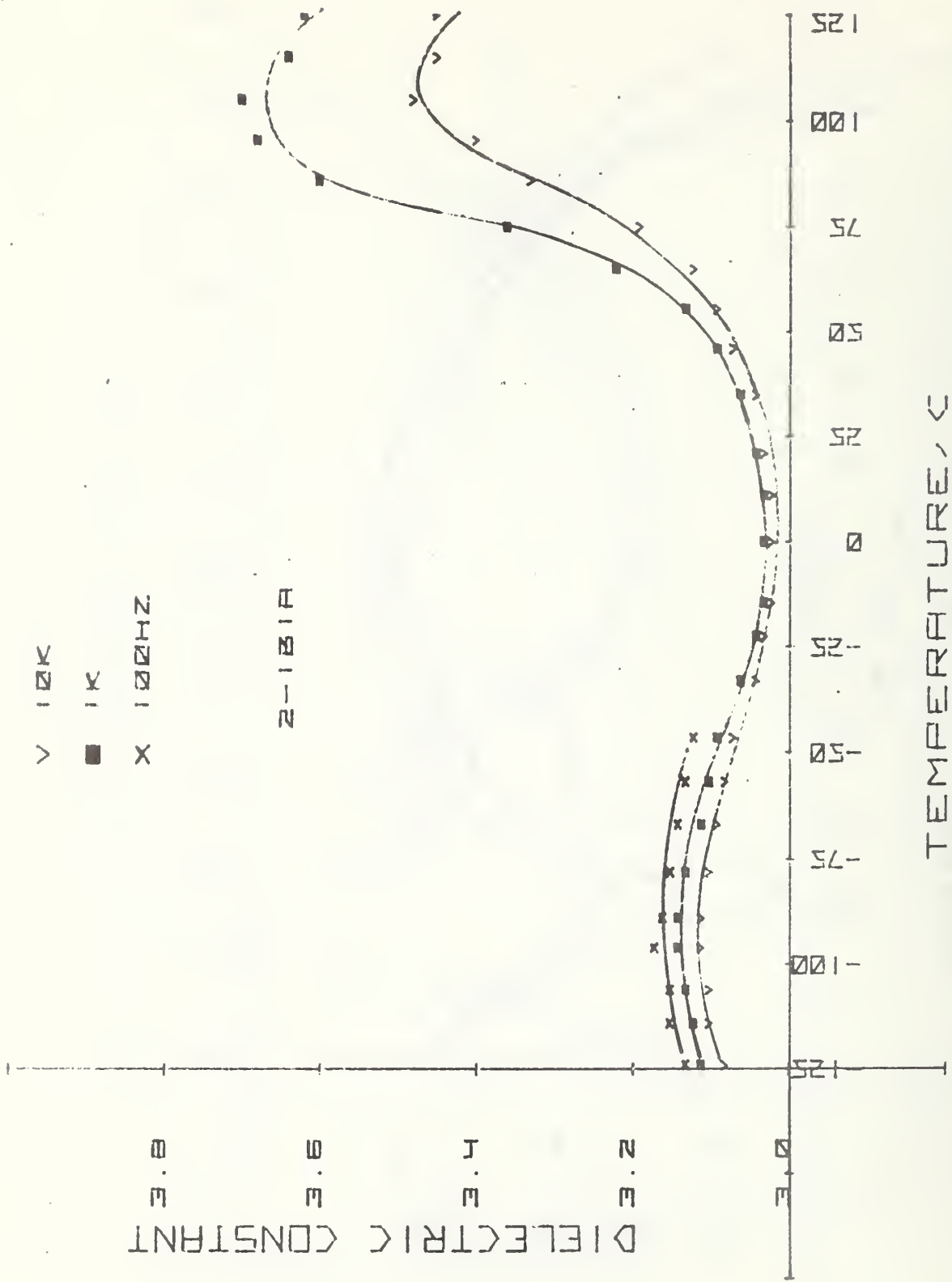


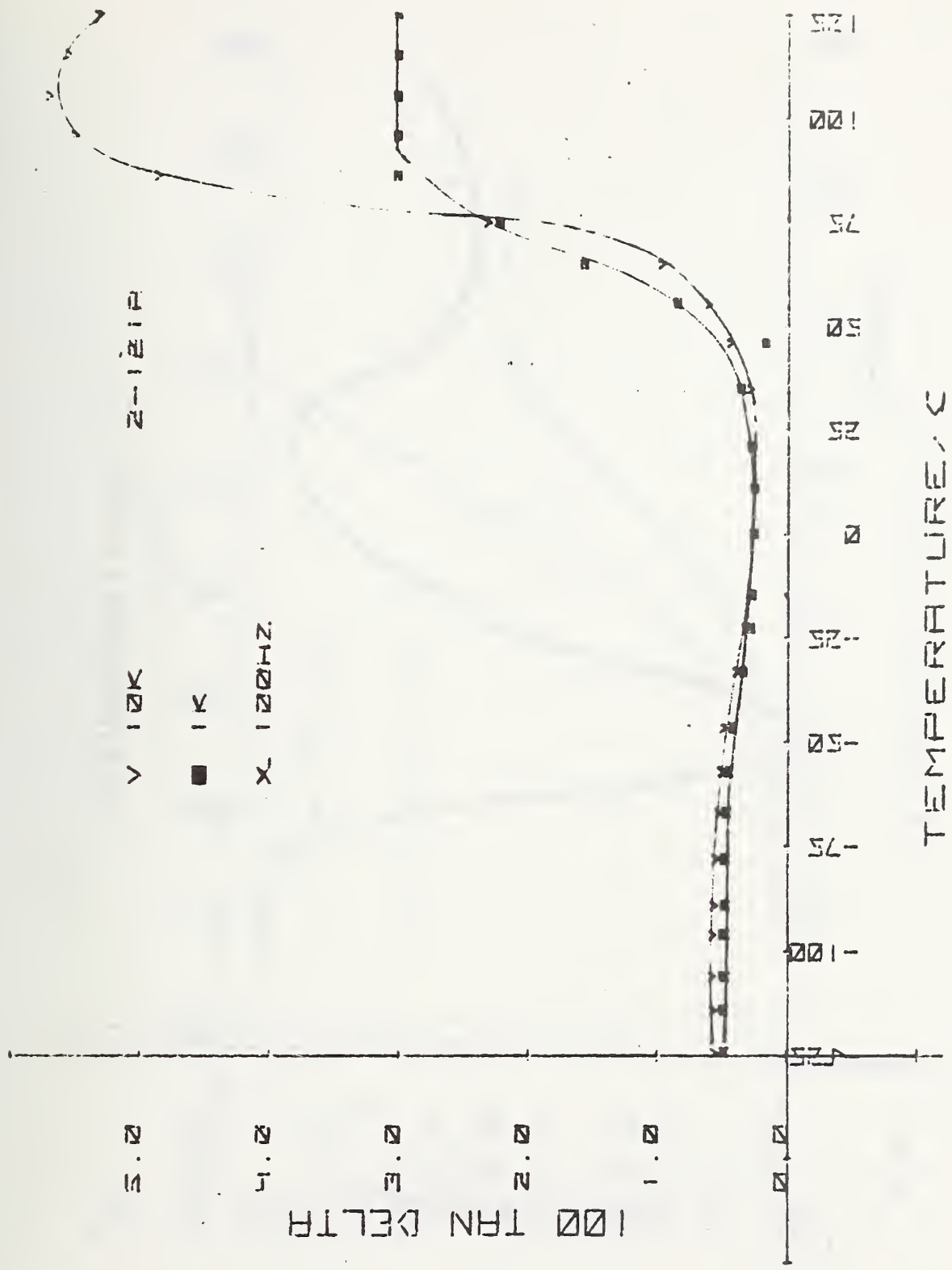
THIUREA



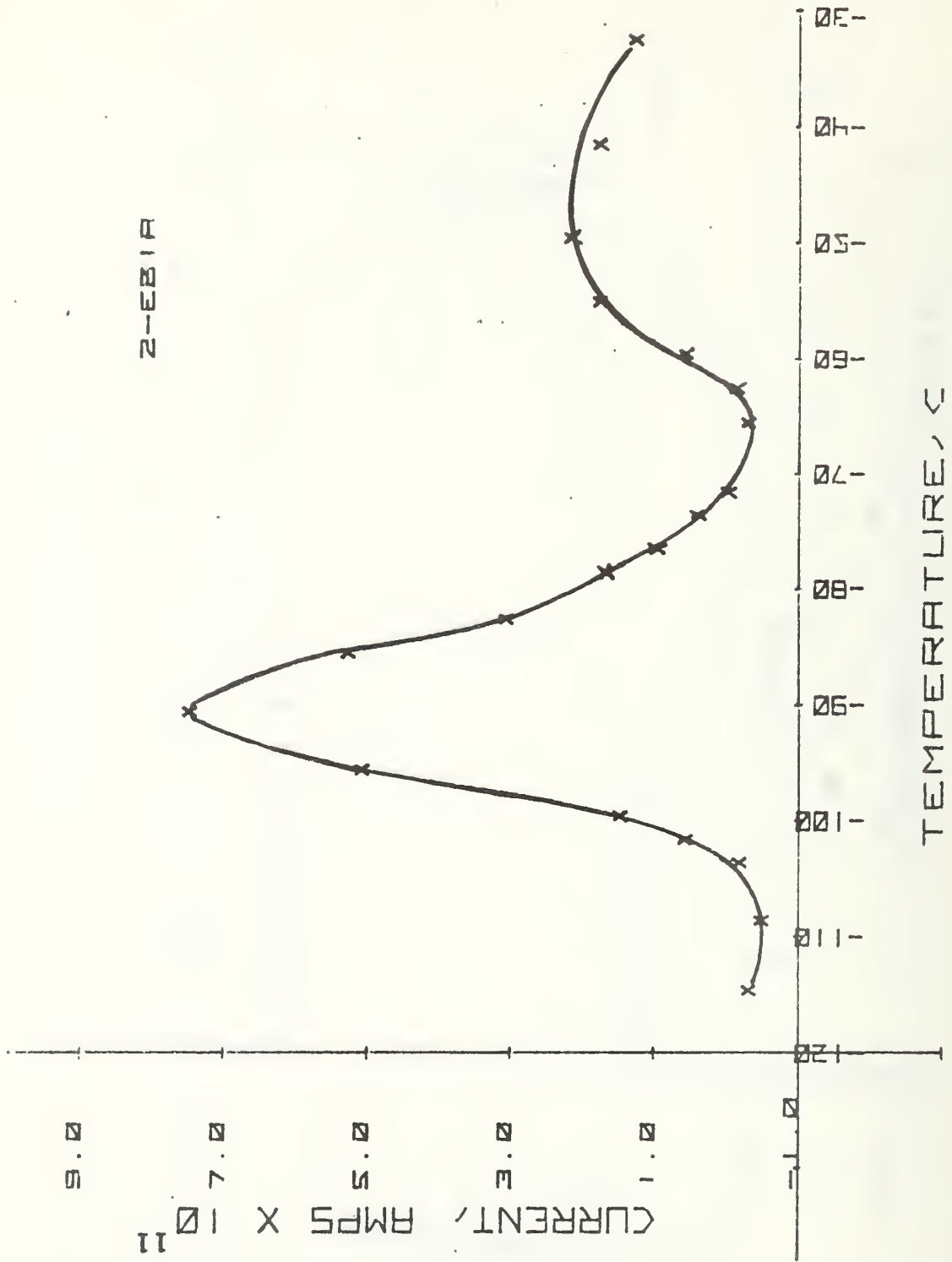


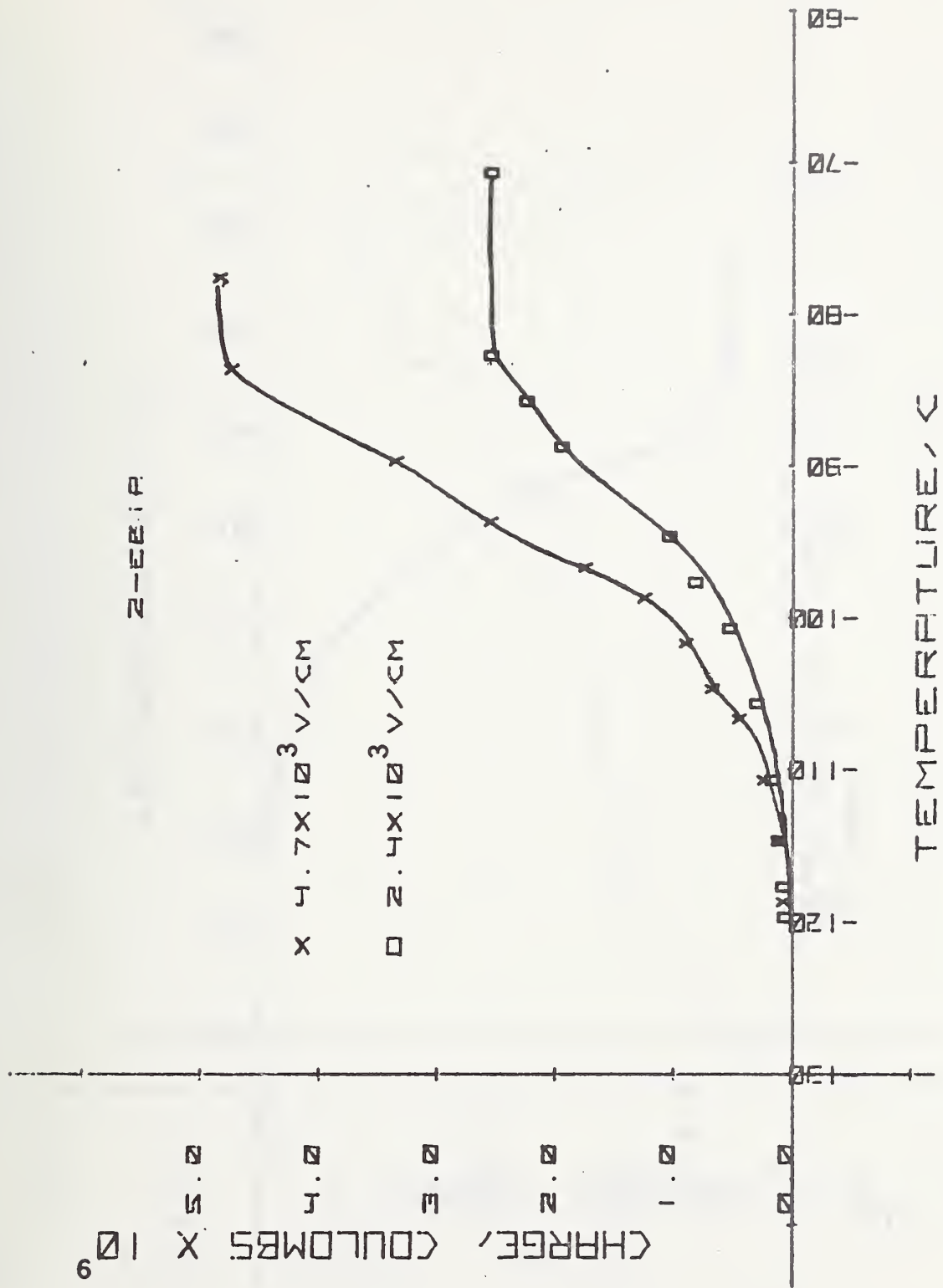


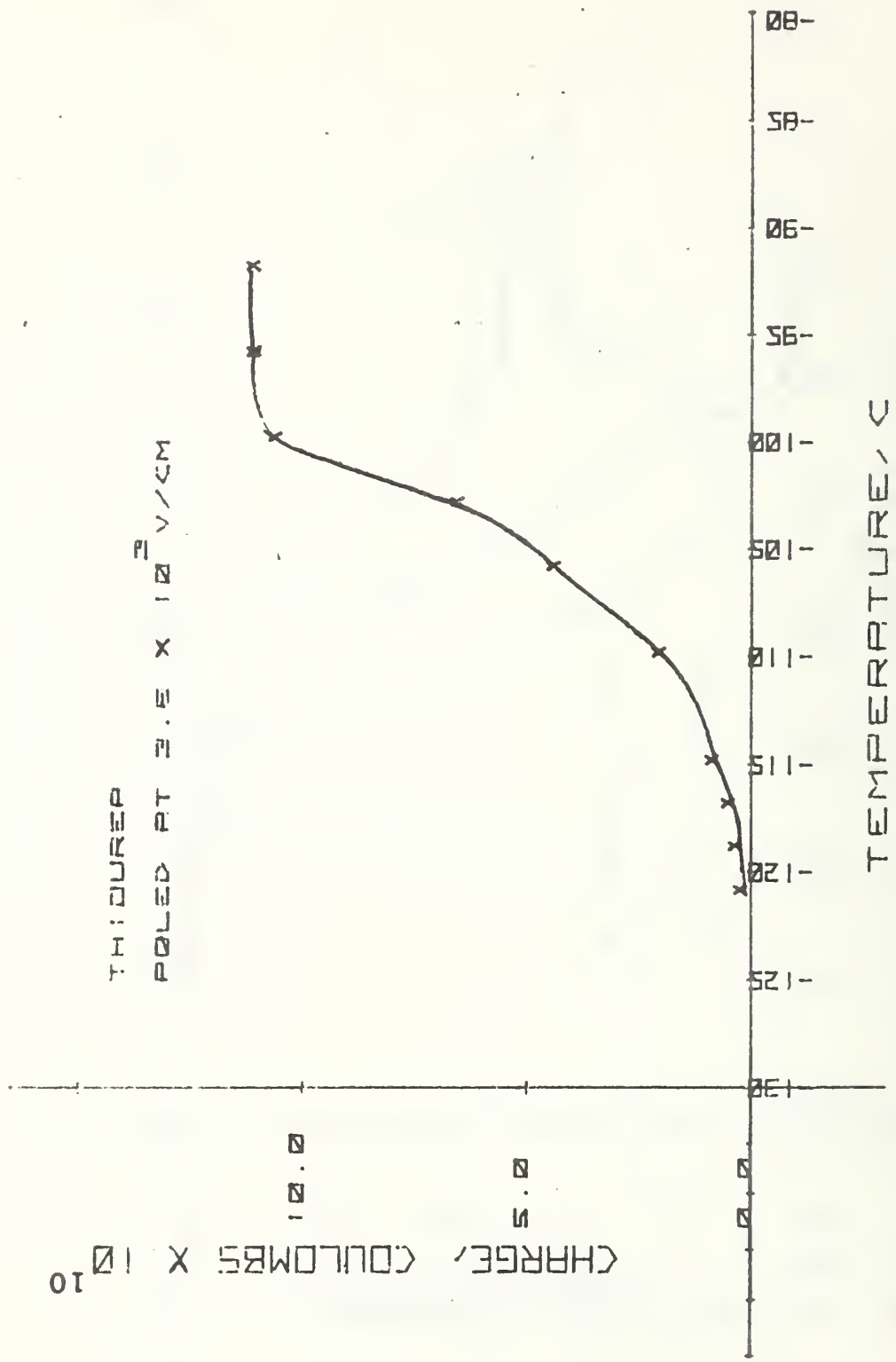


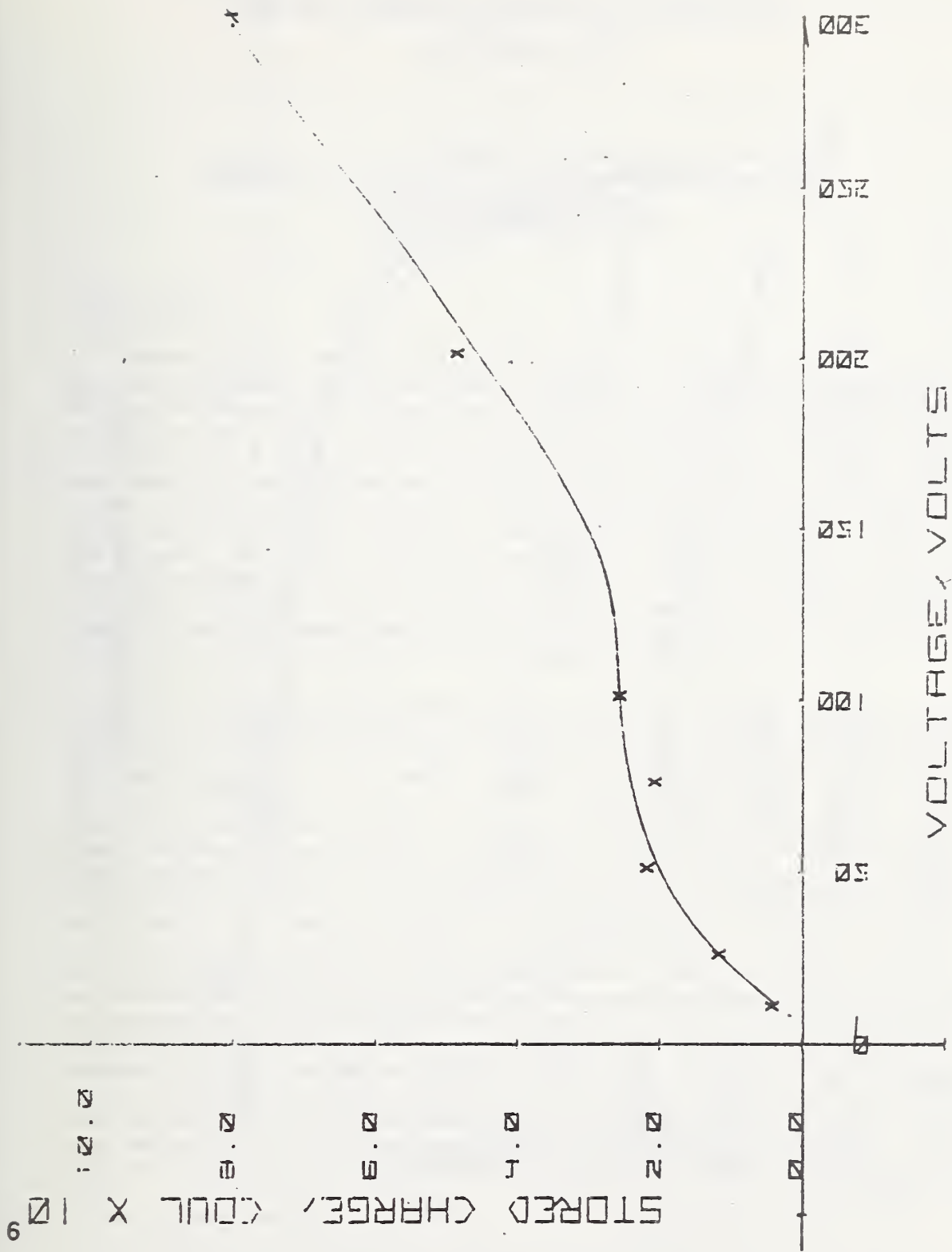


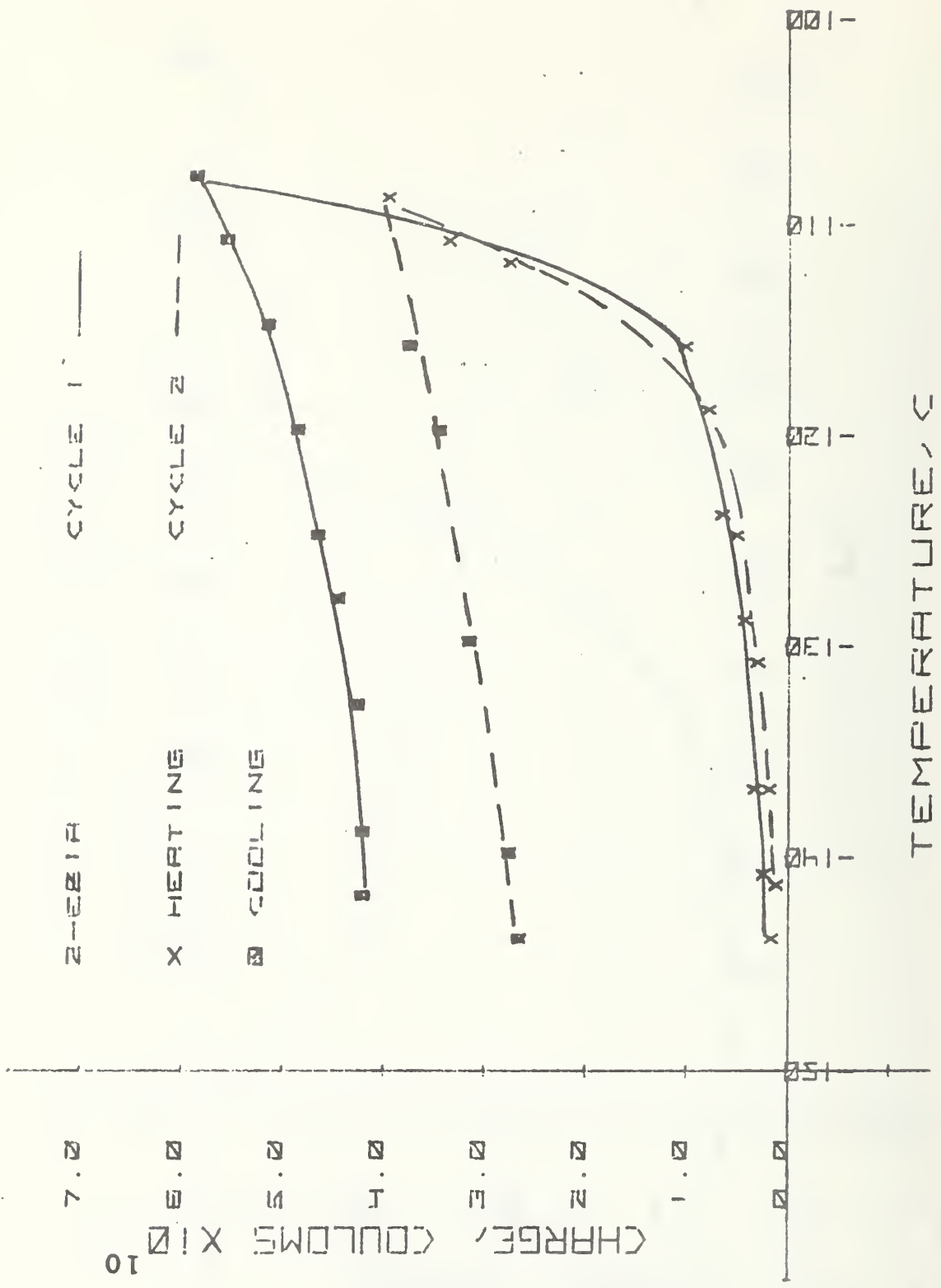
Z-EBIA











ORIGINS OF PERSISTENT ELECTRICAL POLARIZATION  
IN POLYMER SOLIDS

by

Stephen H. Carr  
Department of Materials Science and Engineering  
Northwestern University  
Evanston, Illinois 60201

Introduction:

Sensor-related properties of electrically polarized polymers, such as pyroelectricity and piezoelectricity, depend on a particular combination of physical properties and persistent electrical polarization,  $\underline{P}$ , that exists in these solids. Efforts to control pyroelectric and piezoelectric performance of such materials will necessarily involve a search for the best chemical compositions and physical microstructures that can be obtained with polymeric substances. Such explorations will produce materials having ranges of thermal expansion coefficients and compressibilities, but the property of these solids that can be varied by many factors of ten (and thus be the most effective parameter in controlling sensor-related activity) is magnitude of  $\underline{P}$ . Thus, the research results described on the following pages is concerned specifically with evaluation of the total magnitude of  $\underline{P}$  and with its relationship to physical microstructure.

Persistent electrical polarization can arise from a variety of sources (Slide 1). These individual contributions can have widely differing magnitudes, and they can be of opposing sign, such that the net polarization of the specimen could be very small. Examples of "electrets" created by each of these origins may be cited, but it is often regarded that poling with contacting electrodes simply results in permanent dipoles adopting a preferred orientation parallel to the applied poling field. Measurement of  $\underline{P}$  is somewhat difficult to do unambiguously, but (if one makes some simple assumptions) evaluation of thermally stimulated discharge (TSD) currents can be one of the best techniques for determining  $\underline{P}$ . An example of such currents is seen in Slide 2, where a family of curves represents depolarization of polyacrylonitrile (PAN) polarized at 130°C and  $5 \times 10^4$  Vcm<sup>-1</sup> for successively longer intervals of time. The peak maximum at 90°C corresponds to a mechanically active relaxation process, so it is suggested that the peak represents the loss of a part of  $\underline{P}$  which was due to preferentially oriented dipolar side groups in PAN. Additional information from TSD peaks can be obtained by plotting current vs. reciprocal temperature for the low-temperature limb of a TSD peak, as is shown in Slide 3. The slope of this plot indicates an activation energy for the depolarization process of 28 kcal/mole, which is a value somewhat consistent with the mechanism mentioned above. A more complete treatment of a TSD peak is represented by the analytical expression given in Slide 4. Here, the adjustable parameter is E, the activation energy, and successful fit of experimental data by this relationship can be regarded as evidence that 1) the polarization was uniformly distributed throughout the specimen thickness and 2) the distribution of relaxation times is fairly narrow. Slides 5 and 6 show the match of

Cowell and Woods plots to TSD data obtained on PAN poled as in Slide 2. The values of activation energy used to get successful fit were 28 kcal/mole for the 90°C peak and 45 kcal/mole for the 185°C peak.

Of special interest is the relative strengths of these two TSD peaks. As shown in Slide 7, the 185°C peak is two orders of magnitude larger than the 90°C peak. It is also one order of magnitude larger than the normalized polarization one would expect if saturation polarization ( $\sim 16 \mu\text{coul}/\text{cm}^2$ ) had resulted due to perfect alignment of nitrile side groups parallel to the polarizing field. Thus, one can infer that this peak is caused by relaxation of some source of polarization other than oriented nitrile groups. Interestingly, changing molecular organization by the simple process of uniaxial elongation prior to poling has a marked effect on the magnitude of both peaks, indicating that both contributions to  $\underline{P}$  are structure-sensitive (and therefore that changes in microstructure can be effective ways to control  $\underline{P}$  in PAN). Somewhat direct evidence for dipolar orientation in poled PAN is seen in birefringence data (Slide 8). It is observed that a higher value of birefringence exists in stretched films after they have been polarized. This is consistent with the concept that birefringence in oriented PAN is dominated by the nitrile groups and that they had undergone rotation into directions parallel with the polarizing field during poling. Also of interest is the information obtained by X-ray scattering (Slide 9). These data suggest that an initial "as-cast" film (a) is somewhat glasslike in its scattering properties but that it will become (b) fairly ordered (one-dimensional order that lacks crystallographic registry in directions normal to chain backbones) as a result of annealing. However, the X-ray diffractometer scan shown in (c), which is from a film that had been annealed and polarized, differs very little (if at all) from that shown in (b). Thus it might be either 1) that the extent to which there is a preferred orientation of nitrile groups in polarized PAN is insufficient to create a change in molecular organization or 2) that the same molecular organization exists in films before and after being polarized. A plausible way to reconcile both the birefringence data and the X-ray data is to postulate the existence of ferroelectric-like domains.

Other evidence for interactions between internal field and molecular organizations is seen in Slide 10. Here, the effects of poling at increasingly stronger electrical fields is seen not to lead simply to progressively higher amounts of polarization (as judged by area under TSD peaks). Specifically, it can be seen that unpolarized PAN actually possesses some degree of polarization. Also, fields above  $5 \times 10^4 \text{ Vcm}^{-1}$  produce a polarization which has a component that is of opposite polarity to the strong peaks whose maxima are in excess of 200°C. The exact explanation for these observations is not available at this point, but they suggest that poling may be affecting (independently or dependently) several contributions to the total value of  $\underline{P}$ . It is possible that particular organizations of nitrile groups, such as are listed in Slide 11, are playing an important role in causing these effects and the final result may be nonuniformities of polarization in thickness and in lateral directions of these "electret" solids.

Slide 1.

Possible Origins of Persistent Electrical Polarization

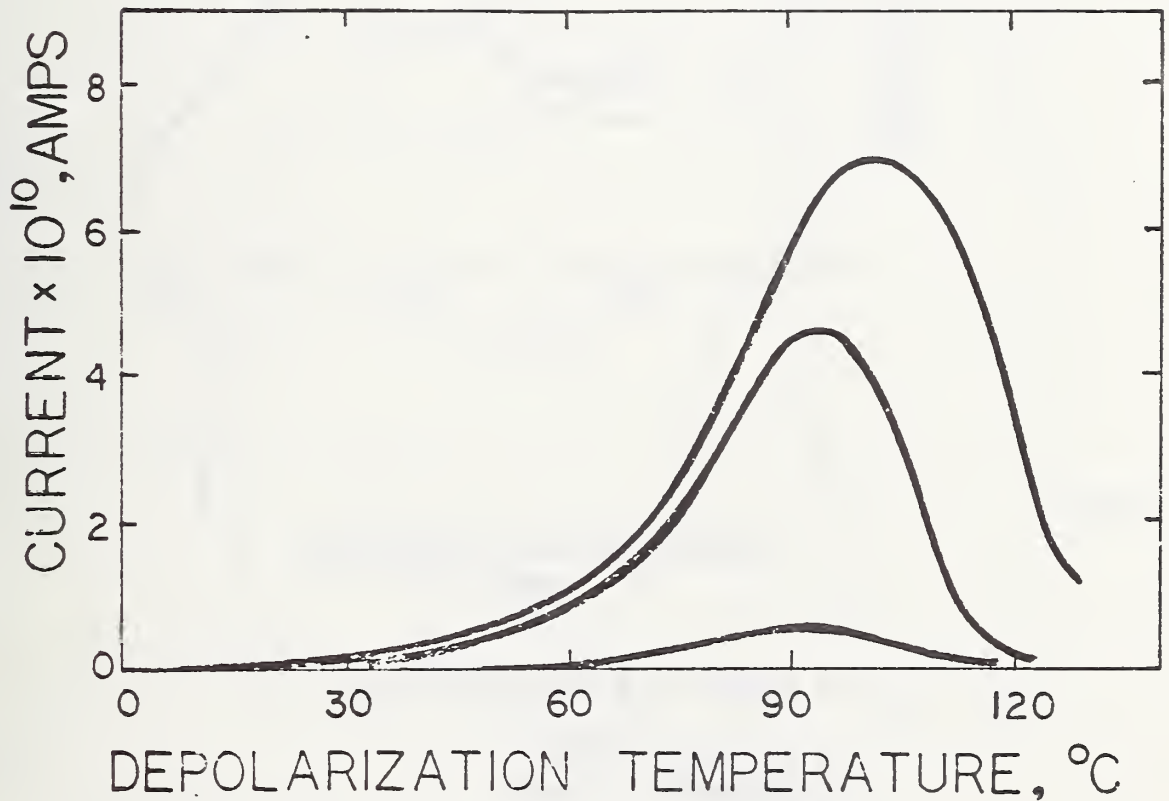
Homocharge:

Injected species from surroundings  
Chemical moieties created from mobile ions.

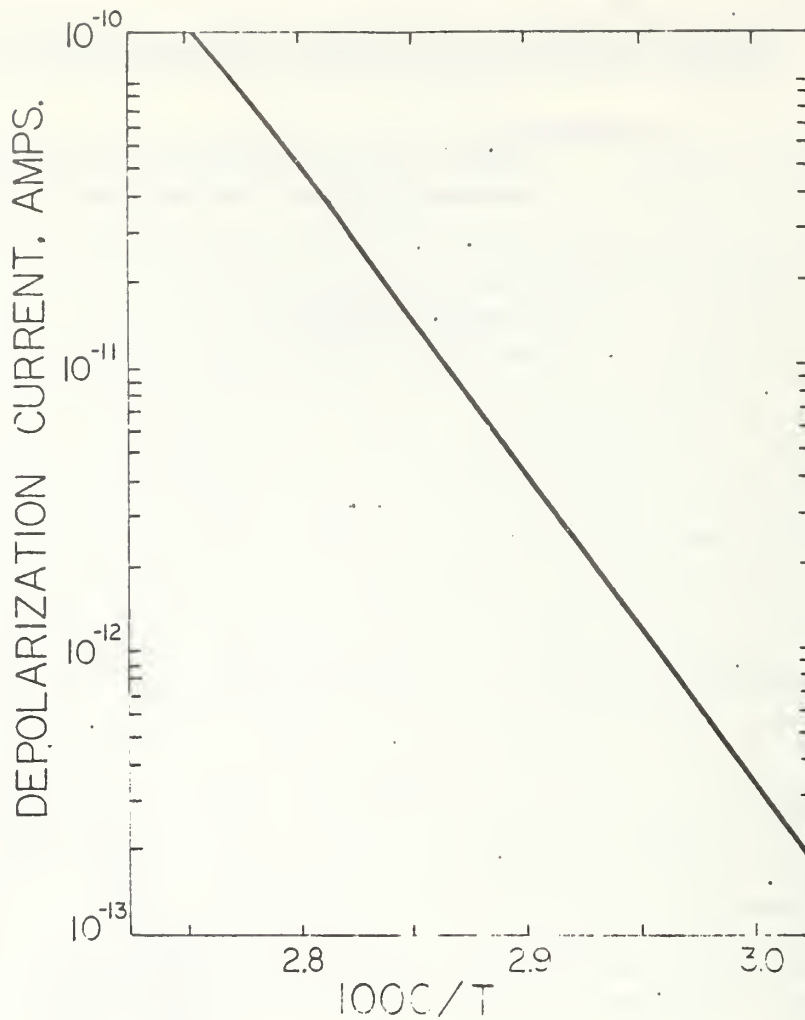
Heterocharge:

Oriented Dipoles  
Composition gradient of ions

Slide 2.



Slide 3.



Slide 4.

THERMALLY STIMULATED DISCHARGE

(TSD)

$$i = A \exp\{-t - B \exp\{-t\} t^{-2}\}$$

$i$  = discharge current

$A, B$  = constants

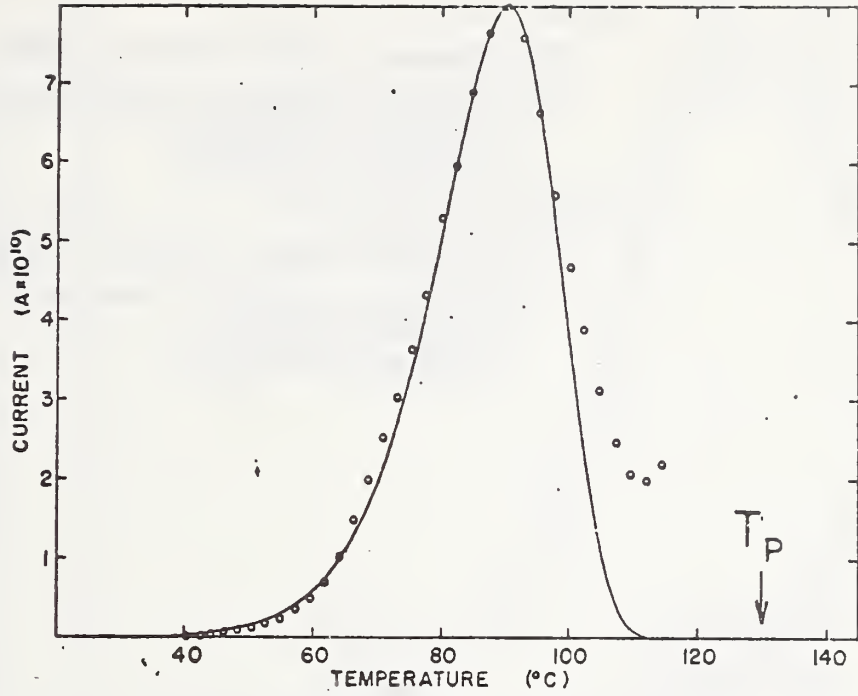
$t$  =  $E/kT$

$E$  = activation energy for depolarization process

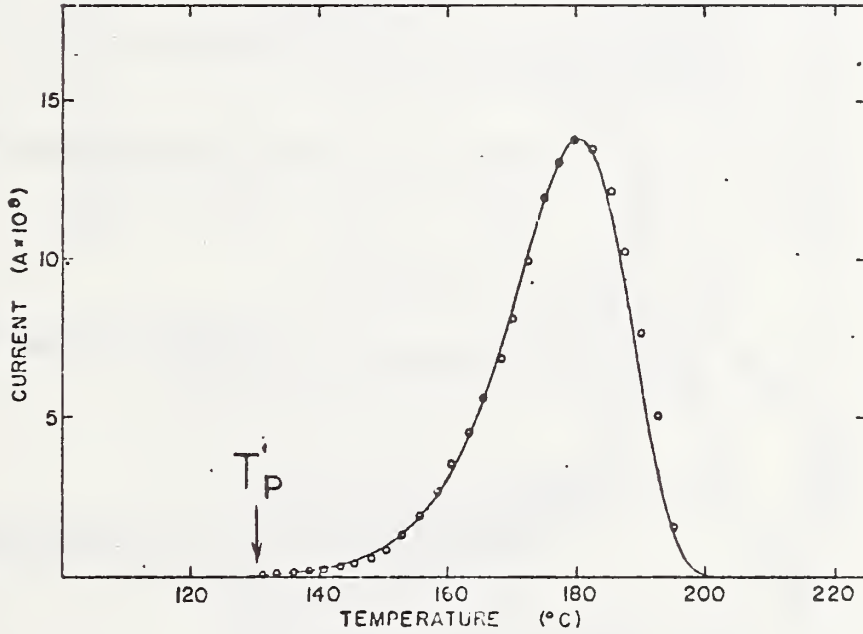
---

T.A.T. Cowell and J. Woods, Brit. J. Appl. Phys.  
18, 1045 (1967).

Slide 5.



Slide 6.



Slide 7.

NORMALIZED POLARIZATIONS  
OF POLYACRYLONITRILE FILMS

<u>TSD Peak</u>	<u>Sample</u>	$\frac{P}{\epsilon_0 E_p}$
90°C	Not stretched	120
	Stretched	210
185°C	Not stretched	13,000
	Stretched	51,000

BIREFRINGENCE ANALYSIS OF PAN

Stretched PAN:

Birefringence normal to draw: -0.005

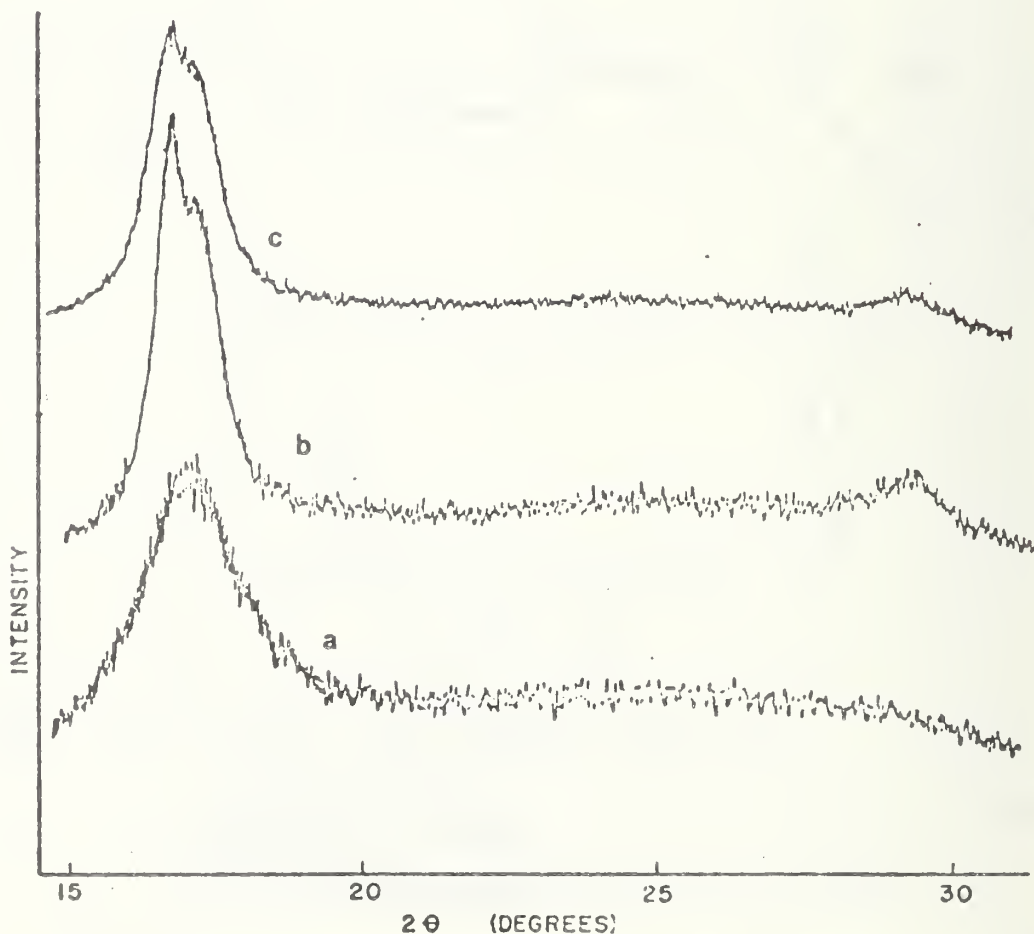
Birefringence parallel to draw: -0.002  
(Optic axis parallel to  
transverse direction)

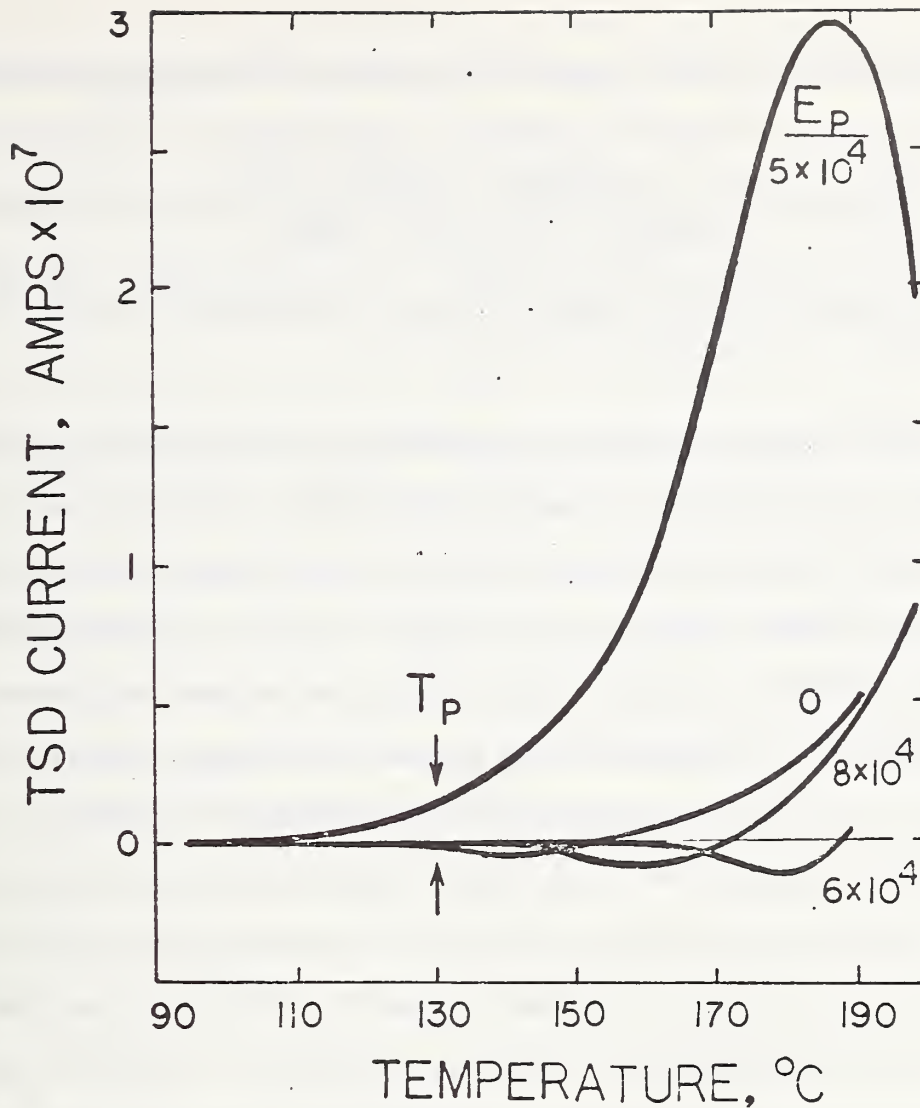
Stretched-polarized PAN:

Birefringence normal to draw: -0.009

Birefringence parallel to draw: -0.001  
(Optic axis 25° from  
transverse direction)

Slide 9.





Associations of Nitrile Side Groups

Intramolecular Structure:

Causes chains to adopt a compact (aperiodic) conformation

Intermolecular Structure:

Leads to fluctuations in local order.  
May organize into ferroelectric-like domains.

Nonuniformities of Polarization in Dielectric Foils

Local variations of physical microstructure.  
Local variations of chemical microstructure.  
Lateral nonuniformity of poling field.  
Variation of polarization structure in thickness direction.

# "Pyroelectric Polymers Applied to Optical Radiation Measurements"

Robert J. Phelan, Jr.  
Electromagnetics Division, National Bureau of Standards  
Boulder, Colorado 80302

Presented at the Symposium-Workshop on Piezoelectric Polymers, NBS, Washington, D. C., April 15-16, 1975.

We have demonstrated the potential of using pyroelectrics in optical radiation measurement instruments that can be electrically calibrated, fast, sensitive, accurate, and usable over an extremely wide spectral range. In the development of these instruments, we have made considerable use of polymer pyroelectrics. To optimize and prove the systems has required extensive characterizations of the pyroelectric polymers.

We have focused on structures compatible with optical measurements; properties and characteristics irrelevant to optimizing detectors have been of secondary concern. In the presentation we describe our measurements, indicate accuracies obtained, give the parameters we have considered significant, and give what we believe to be the state-of-the-art in applying pyroelectric polymers to optical radiation measurements. The presentation is a summary of a number of publications referenced at the end of this paper.

The principal points of the presentation are: (1) to compare the polymers PVF and PVF<sub>2</sub> with other pyroelectrics and show that they have favorable properties; (2) to describe and demonstrate the limits of spatial uniformities and their significances (extremely uniform response detectors can be made); (3) the responsivities of

the detectors depend both on material properties and device fabrication details; (4) modulation frequency responses can be predicted in detail - except at high frequencies where we have some loose ends; (5) the  $D^*$  can be made equal to the highest available from any pyroelectric; (6) studies of long term stabilities have shown that the drift in responsivity can be less than 5% per year, but by adding electrical calibration detector drift problems are eliminated; (7) the detectors are useful at temperatures down to  $77^{\circ}\text{K}$  and probably even lower; (8) spectral responses can be made flat to better than 2% over the wavelength range of 1 to  $12\ \mu\text{m}$ ; and (9) complete systems based on a polymer pyroelectric are being evaluated as a new standard for optical radiation measurements.

References to available published reports from the "Optical Electronics Program" at NBS, Boulder - relevant to the application of PVF and PVF<sub>2</sub> pyroelectrics.

1. "High D\* Pyroelectric Polyvinylfluoride Detectors", Robert J. Phelan, Jr., Robert J. Mahler, and Alan R. Cook, Applied Physics Letters 19, 337 (1971).
2. "Absolute, Pyroelectric Radiometers and Two Dimensional Arrays", R. J. Phelan, Jr., R. L. Peterson, G. P. Klein, C. A. Hamilton, and G. W. Day, Proceedings of the Technical Program, Electro-Optical Systems Design Conference, Sept. 18-20, 1973, New York, New York.
3. "Electrically Calibrated Pyroelectric Optical-Radiation Detector", Robert J. Phelan, Jr., and A. R. Cook, Applied Optics 12, 2494 (1973).
4. "The Polarization of PVF and PVF<sub>2</sub> Pyroelectrics", R. J. Phelan, Jr., R. L. Peterson, C. A. Hamilton, and G. W. Day, Ferroelectrics 7, 375 (1974).
5. "Effects of poling conditions on responsivity and uniformity of polarization of PVF<sub>2</sub> pyroelectric detectors", G. W. Day, C. A. Hamilton, R. L. Peterson, R. J. Phelan, Jr., and L. O. Mullen, Applied Physics Letters 24, 456 (1974).
6. "Analysis of response of pyroelectric optical detectors", R. L. Peterson, G. W. Day, P. M. Gruzensky, and R. J. Phelan, Jr., Journal of Applied Physics 45, 3296 (1974).
7. "A Pyroelectric Power Meter for the Measurement of Low Level Laser Radiation", C. A. Hamilton and G. W. Day, NBS Technical Note #665, Feb. (1975).
8. "Electrically Calibrated Detectors versus Black Body Sources", R. J. Phelan, Jr., Proceedings of the IRIS Specialty Group on Infrared Detectors, Mar. (1975).
9. "A Flat Spectral Response Detector for the Visible to 12  $\mu$ m Region", G. W. Day, C. A. Hamilton, and K. W. Pyatt, Proceedings of the IRIS Specialty Group on Infrared Detectors, Mar. (1975).
10. "An Absolute Pyroelectric Radiometer (A Reference for Detector Responsivities)", C. A. Hamilton and G. W. Day, Proceedings of the IRIS Specialty Group on Infrared Detectors, Mar. (1975).

## Pyroelectricity in PVF<sub>2</sub>

R. E. Salomon and M. M. Labes

Department of Chemistry, Temple University, Philadelphia, Penna. 19122

We have underway a combined experimental and theoretical program aimed at understanding the mechanism of pyroelectric phenomena in electrically poled PVF<sub>2</sub> in order to identify the key parameters which can be altered so as to enhance the pyroelectric coefficient of this material.

Our experimental work has already led to the observation that a copolymer of vinylidene fluoride (95%) and tetrafluoroethylene (5%) has a significantly higher pyroelectric coefficient than the poly(vinylidene fluoride) homopolymer.<sup>1</sup> We furthermore find that the temperature dependence of the pyroelectric coefficient of the copolymer is significantly greater than that of the homopolymer. The effect of poling time and the nature of the first cycle thermally stimulated currents are also compared. We find that in poling, saturation times are significantly greater in the copolymer.

The theoretical modelling, which is the main subject to be discussed here, has been primarily directed towards an understanding of the poling process. The experimental findings to date have not really helped to distinguish between the various poling mechanisms. It has seemed to us, from both the limited structural information available as well as a general consideration of semi-crystalline polymers, that the rotation of polar monomers has two serious restrictions which must be dealt with in any adequate theory. The first is concerned with interactions within a chain. Except for small torsions, the rotation of one monomer is strongly coupled to the next and so on. Hence, it would seem that appreciable polarization would require that entire chains or large segments of chains flip over. The second restriction concerns the inter-

actions between the chains, particularly within the polar crystalline phase.

It is clear that the chains can not reorient in a random manner.

Accordingly, we have developed four models which reflect these considerations. These models are referred to as the Rigid Rod Model, the Perimeter of Separation Model, the Molecular Rearrangement Model and the Space Charge Model. In the Rigid Rod Model, we envision polar cylinders whose axis correspond to the chain axis. The cylinders are caused to rotate in the poling field. The temperature is elevated so as to lower the viscosity sufficiently. Reversible pyroelectric phenomena can be described by this, and the next three models, by introducing a Lorentz type of internal electric field. The Perimeter of Separation Model is a domain type of theory. We have recently been able to calculate the domain shape and size for a simple assumed crystal morphology. The Molecular Rearrangement Model is based on a theory of field induced changes in polymer conformation, namely, going from helical to planar zig-zag in the electric field. This model, if correct, would predict some changes in the diffuse x-ray scattering which thus far have not been observed. The Space Charge Model is based, to some extent, on the reported effects of blocking electrodes on pyroelectricity. In this model, the poling process simply leads to a space charge, while the pyroelectric current is a result of the temperature dependence of the piezoelectric strain coefficient and the space charge distribution.

The first model has been used to predict the form of the kinetics of poling and depoling, while the others are essentially equilibrium models. The Space Charge Model treats the piezoelectric properties phenomenologically and thereby suffers as a basic model. These treatments are currently being refined so that they may be tested in a definitive manner against experimental results.

## Figure Captions

Figure 1. Measurements of pyroelectric current  $I_p$  from the decay of the total current after the heating cycle was stopped at  $t = 0$ .

Figure 2. Pyroelectric coefficients for  $PVF_2$  ( $\bullet$ ) and  $VF_2$ -TFE copolymer ( $\circ$ ) at poling fields of  $4 \times 10^5$  (---) and  $6 \times 10^5$  (—) V/cm.  
 $T_p = 80^\circ\text{C}$ ,  $t_p = 5$  h.

Figure 3. Rigid Rod Model. Space between rods considered as containing an amorphous, viscous, apolar material.

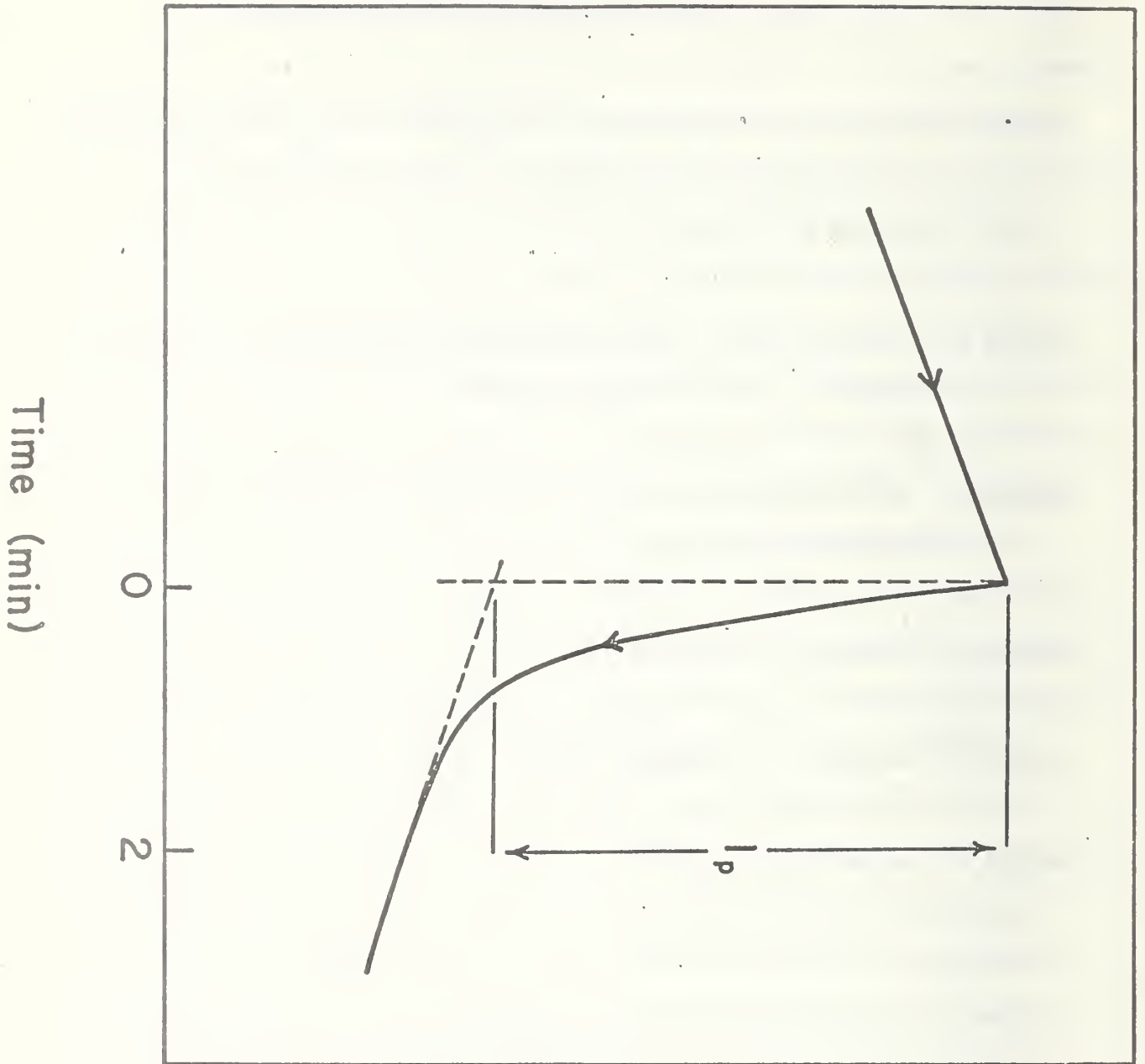
Figure 4. Calculated polarization rate for Rigid Rod Model during poling versus reduced time.

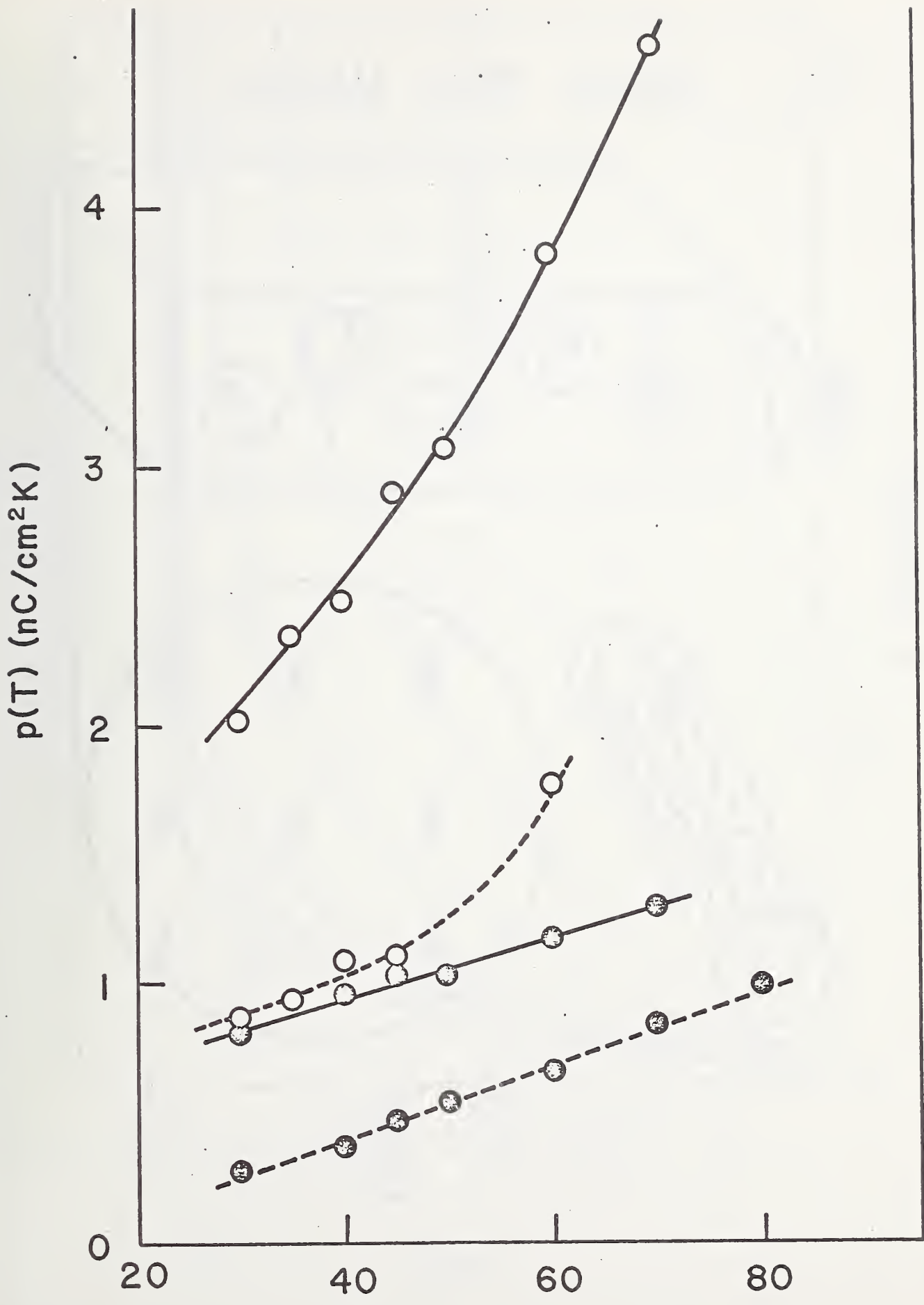
Figure 5. Perimeter of Separation Model.

Figure 6. Molecular Rearrangement Model.

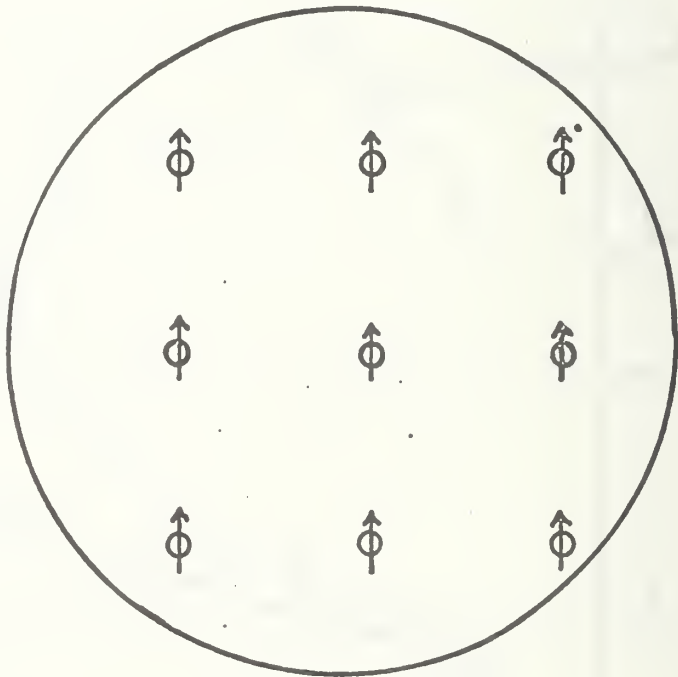
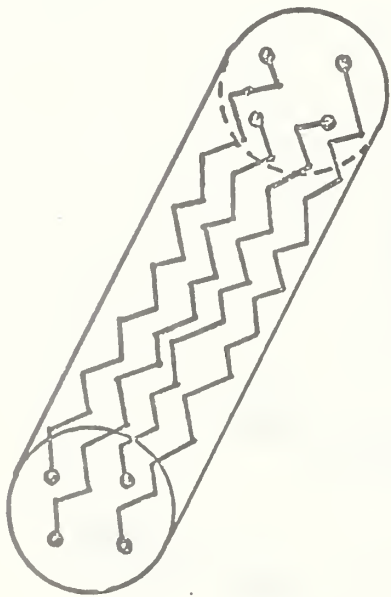
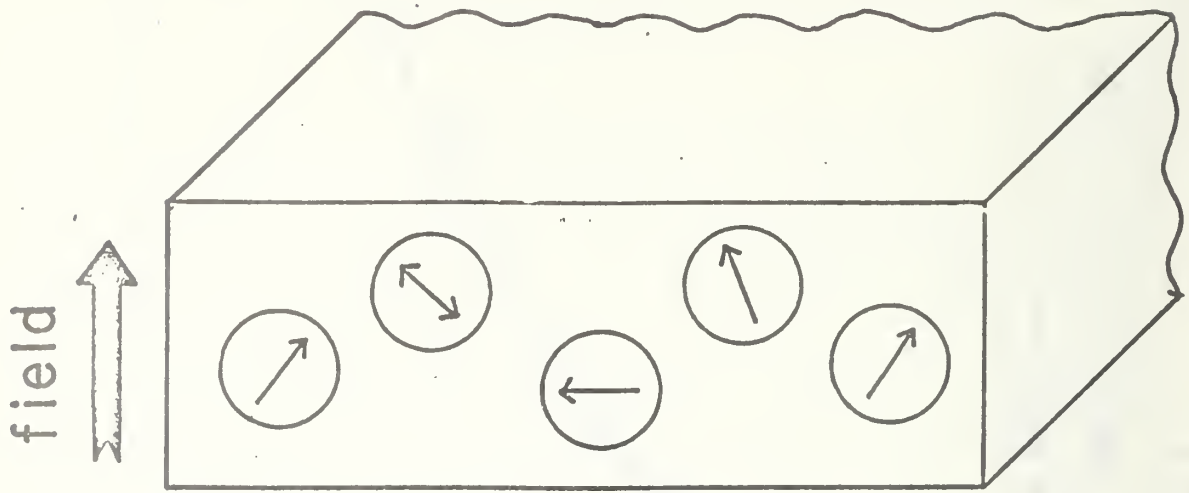
Figure 7. Space Charge Model.

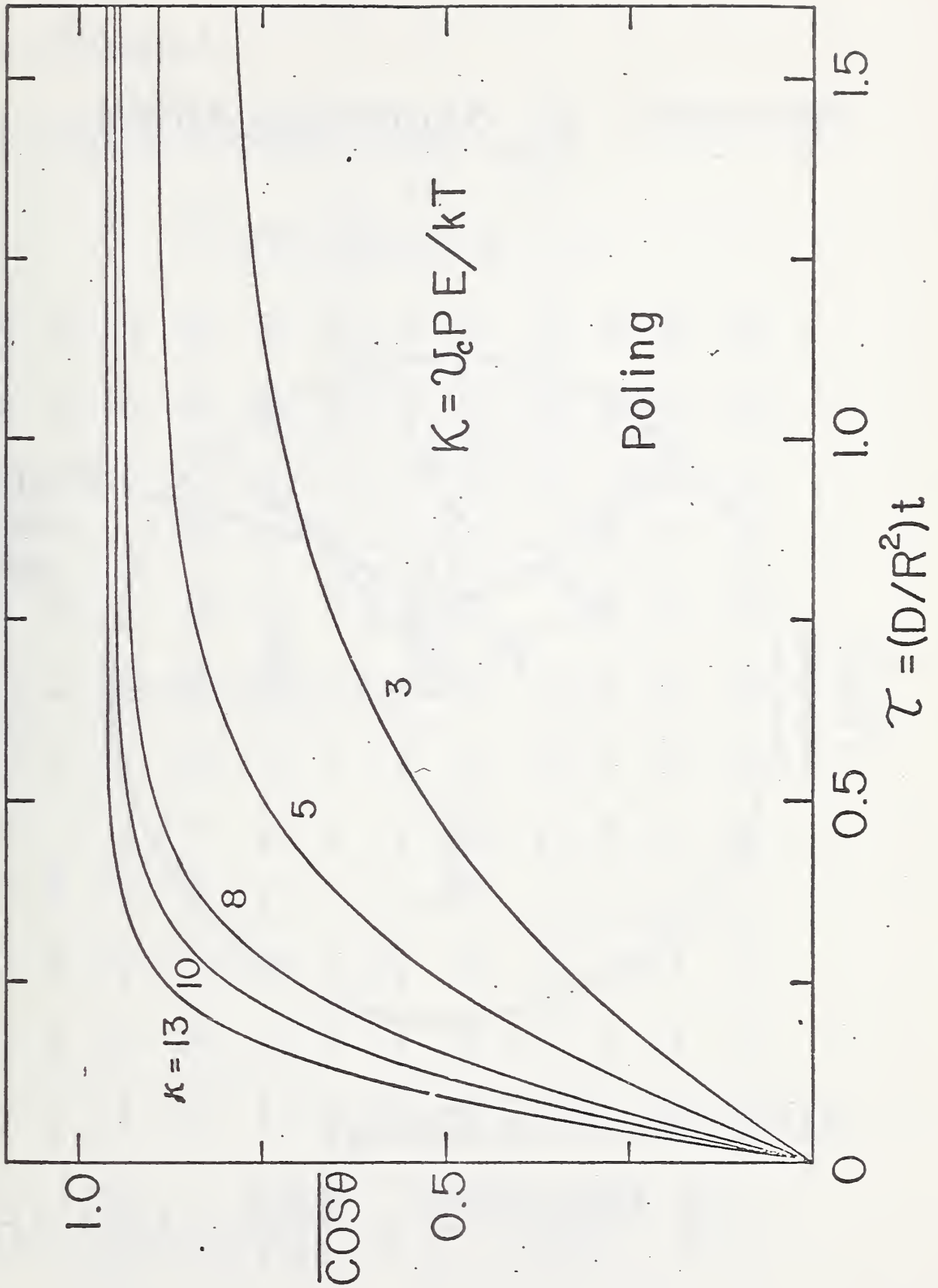
# Current



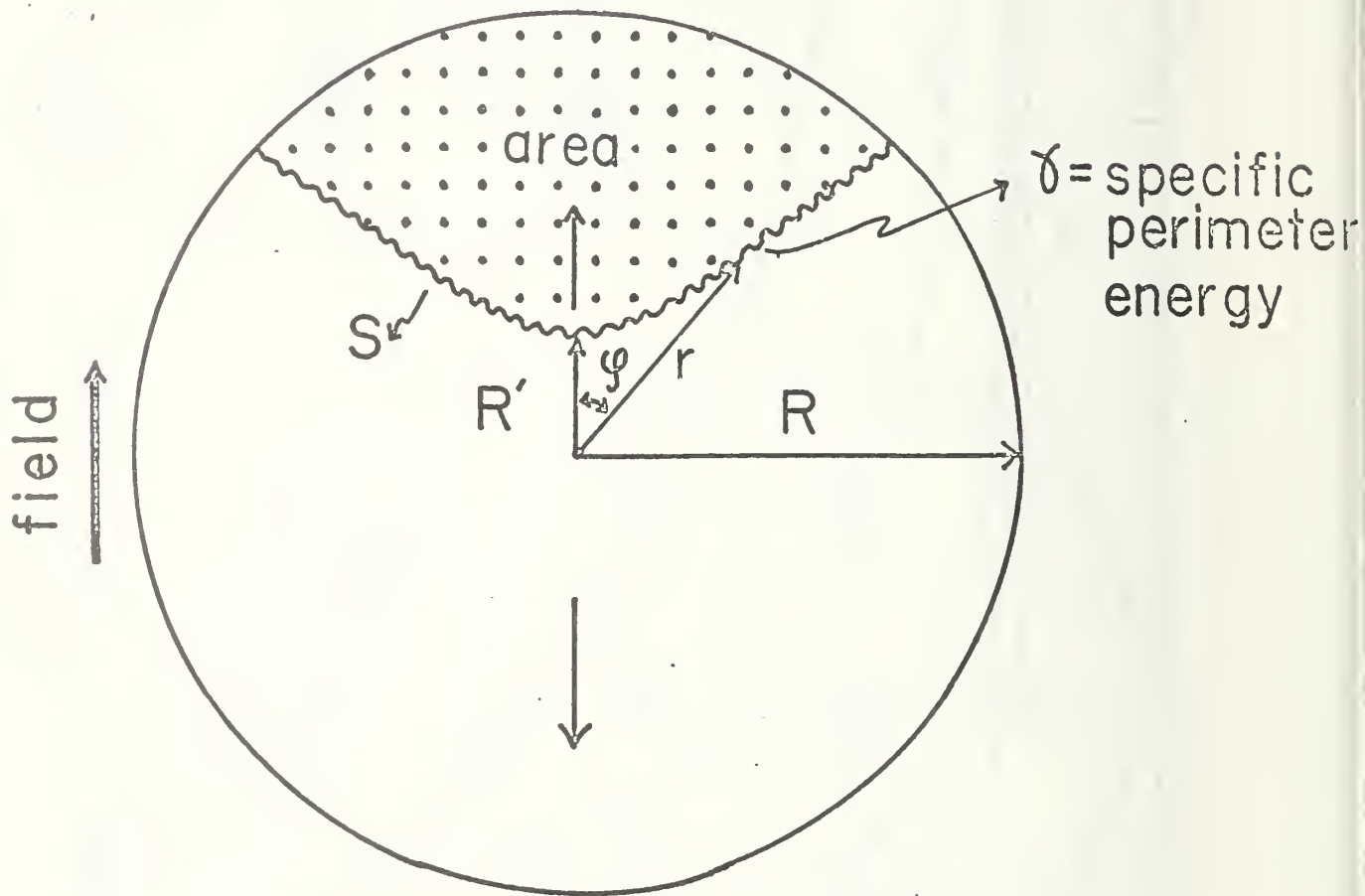


# RIGID ROD MODEL





# Perimeter of Separation Model



Helmholtz Free Energy

$$= -\frac{2}{\pi} \cdot \frac{E\mu N(\text{area})}{kT} + \frac{\gamma RS}{kT} - \ln \left[ 1 - (R'/R)^2 \right]$$

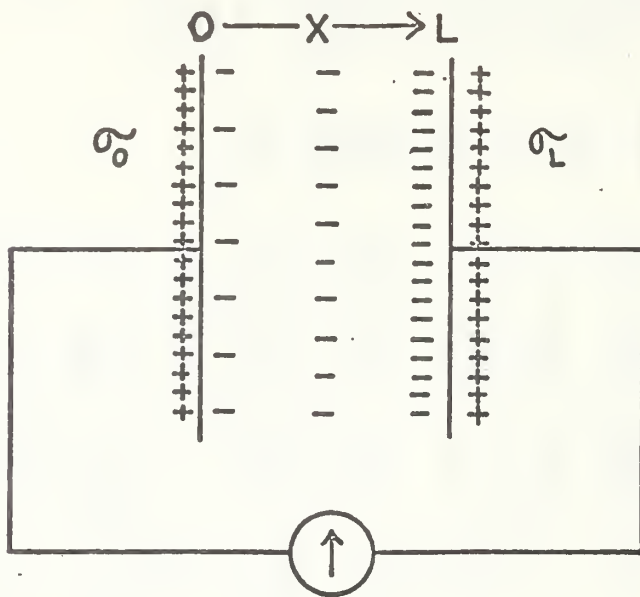
S = Helical

↑ and ↓ = Planar Zig-zag

↑ ⇌ S ⇌ ↓

S	S	S	S	S	S	S	S	S	S	S	S
S	S	S	S	S	S	S	S	↓	S	S	S
S	S	S	S	S	S	S	S	↓	S	S	S
S	S	↓	S	S	S	↑	S	↓	S	S	S
S	S	↓	S	S	S	↑	S	↓	↑	S	S
↑	S	↓	S	S	↓	↑	S	↓	↑	S	S
↑	↑	↓	S	↓	↓	↑	S	↓	↑	S	↓
↑	↑	↓	↑	↓	↓	↑	S	↓	↑	↑	↓
↑	↑	↓	↑	↓	↓	↑	S	↓	↑	↑	↓
↑	↑	↓	↑	↓	↓	↑	↑	↓	↑	↑	↓
↑	↑	↓	↑	↓	↓	↑	↑	↓	↑	↑	↓

# SPACE CHARGE MODEL



$$\frac{\partial^2 V}{\partial x^2} = -\frac{\rho(x)}{\epsilon_0}, \quad \sigma_0 = \epsilon_0 E_0, \quad \sigma_L = -\epsilon_0 E_L$$

$$\lambda_k = \lambda^0 (1 + \Omega E_k)$$

$\lambda_k$  = length of sample under field  $E_k$

$\lambda_0$  = length of sample under field  $E=0$

For  $\rho_n = -a_n x^n$  with  $\int_0^L \rho dx = q_{\text{tot}}$ .

$i$  = Pyroelec. Current

$$= -\frac{(n+1)^2}{(2n+3)(n+2)^2} \cdot \frac{q_{\text{tot}}^2}{\epsilon_0} \cdot \left(\frac{d\Omega}{dT}\right) \left(\frac{dT}{dt}\right)$$

PRELIMINARY INVESTIGATIONS OF PIEZOELECTRIC POLYMERS  
FOR SONAR APPLICATIONS

James M. Powers  
Naval Underwater Systems Center  
New London, Conn. 06320

ABSTRACT

Two Navy sonar applications in which piezoelectric polymer might be used as hydrophone elements are for small diameter towed arrays and large aperture hull mounted arrays. In these applications polymer hydrophones would offer the following advantages over piezoceramic; availability of large dimensions allowing noise reduction by spatial averaging, low density for increased buoyancy, ability to withstand high pressure, and low cost. To date we have prepared various polymer samples, set up measurement systems to evaluate piezoelectric  $g$  coefficients, and have measured samples supplied by Dr. Edelman of NBS which exhibit  $g_h$  an order of magnitude higher than ceramic.

## PIEZOELECTRIC POLYMER MEASURING INSTRUMENTS

S. Edelman  
Institute for Materials Research  
National Bureau of Standards  
Washington, D. C. 20234

### ABSTRACT

Piezoelectric polymer sensors have advantages over conventional instruments for measuring dynamic mechanical quantities in special cases because of their low density, flexibility, resistance to damage by mechanical shock, thinness, and low cost. A number of examples are given and a typical polymer sensor is described.

## Piezoelectric Polymer Measuring Instruments

The polymer transducers group uses favorable properties of polymers to advance the science of measurement. Considered as piezoelectric materials, polymers are less active than the ceramics which are used in conventional measuring instruments. However, polymers have other properties which make their use advantageous in particular kinds of measurements. There are some cases of considerable importance where polymer instruments are uniquely suited. Usually the advantages of polymer instruments show up in dynamic measurements. A typical case is measuring the level of vibration at a point on a thin metal sheet. Any point on the metal sheet to which an accelerometer is attached will have significantly greater surface density than the rest of the sheet. The vibration pattern of the sheet will rearrange itself so that the motion at that point is minimized and the measurement is unrepresentative. On the other hand, cementing a small piece of polymer film to the metal sheet need not change the surface density significantly and a meaningful measurement can be made. The amplitude of vibration and the variation of vibration level with frequency measured by the polymer are representative of what the level at the point would be with no instrument attached. Conversely, both the vibration amplitude and the spectrum of resonances measured by an accelerometer would be affected by the presence of the instrument. Thus, it is practicable to distribute a number of polymer vibration gages over the surface of a panel and to deduce from their reading the mode of vibration of the panel under various conditions. This kind of study can not be performed effectively with conventional vibration measuring instruments. Polymers have somewhat similar advantages for studying the noise signatures of bearings, gears and transmission

systems. The mass of a conventional instrument introduces a set of resonances which confuse the noise spectrum being studied and which may hide the changes of the spectrum which indicate the first signs of deterioration. Also, the size of conventional instruments and their need for a threaded mounting hole may dictate their location at some distance from the origin of the noise. A polymer gage, almost always, can be mounted directly to the noise source with a much better chance of picking up an uncluttered spectrum. Polymer gages are handy for acoustic emission studies because of the ease with which they can be bonded to metal and because their thinness and high internal damping make their response fairly flat with frequency up to several megahertz.

As strain gages, polymer gages have about two-thirds of the sensitivity of semi-conductor gages but they can be used without the need for bias voltage or bridge balancing. Also, they are not brittle and can be used where mechanical shock occurs and on curved surfaces.

With the addition of lead foil as a seismic mass, polymer gages can be used as flexible accelerometers with an unusually wide frequency range.

The fact that polymer gages can provide good coupling to soil can be used as the basis for another group of important applications. At present, seismometers are used to study stress waves in the ground. Seismometers are large, expensive instruments and usually they are made larger and more expensive by being enclosed in a body of grout to provide better coupling to the soil. A thin sheet of polymer can be installed much more easily and it provides good coupling without any special effort. A figure of merit used by those who work with stress waves in the ground is proportional to the ratio of the diameter of the gage to its thickness. A polymer gage can be so thin that even a relatively small gage can have a good figure of merit. In some cases polymer gages benefit from encapsulating to minimize unwanted signals due to bending or shear

effects but, even so, the polymer gage is cheap, easily installed, and well coupled compared with seismic instruments. We have been doing some work in developing such gages in cooperation with the Air Force Weapons laboratory and Bolt Beranek and Newman and also in connection with some work we are doing for the Federal Highway Administration. We have discussed the use of similar stress gages for earthquake studies and for monitoring the condition of earth dams. Another possible application is in underground geophysical exploration.

The thinness and flexibility of polymer gages make them feel and act mechanically very much like skin. This characteristic is used in automobile crash studies. A pattern of polymer stress gages are to be put on the head and chest of anthropomorphic dummies to detect the areas of contact and the time history of the impact. Since the gages behave very much like skin, they do not disturb the anthropomorphic behavior of the dummy and, since they are flexible, they are not likely to be damaged in the crash. Conventional pressure gages form concentrated masses whose behavior during a crash would be much different from the behavior of the rest of the skin of the dummy and they are likely to be damaged during a crash. Their impact is also likely to damage parts of the automobile in ways that are not characteristic of real crashes.

Polymer gages are being considered to initiate air bag inflation and to measure pressure and temperature pulses in tires.

The similarity of polymer gages to body tissues has other potential uses. We are developing gages to be inserted into monkey brains to determine how much of an impact to the outside of the head is felt as a pressure pulse in the brain. The polymer gage is to be used here because its density is close to that of the brain material. If a conventional pressure gage were used, inertial effects would produce more signal than the pressure change.

Polymer gages can be applied like bandaids to monitor heart sounds and pulse rates of patients during exercise. Conventional instruments can be used. Their size and mass make the patient conscious of their presence and his behavior is not entirely normal. He is much more likely to forget polymer gages.

A different kind of application depends on the fact that poling a polymer stores about one and a half times as much energy per unit volume as is stored in piezoelectric ceramic under similar conditions. One example we have worked on is development of detonators for ordnance where polymer sheet is preferable to ceramic because it is lighter for a given energy storage, can be connected to provide a desired electrical output impedance more readily, and can be used to line enough of a shell to provide detonation for any angle of incidence. An obstacle in the use of polymers for this kind of application is the fact that it is more difficult to release the energy stored in the polymer than that stored in the ceramic because the ceramic has a greater electromechanical coupling constant. The situation is analogous to comparing paper and wood as fuel. Paper is easier to light but wood gives more energy per unit volume. In the case of artillery there is plenty of energy available to release the stored energy. We have considered a number of other applications where this would be true; for example, powering some prosthetic devices.

We have not done any work on devices to generate and detect sound in air except for our own amusement. Dr. Fukada demonstrated a polymer microphone several years ago and the Plessey Company, in England, has demonstrated a polymer microphone. Recently, Pioneer Corp. has announced commercially available microphones, loudspeakers, and head sets.

We have worked on sound measurement under water. Polymer hydrophones have several obvious advantages over the conventional piezoelectric ceramics such as a good acoustic impedance match to sea water, flexibility which makes them capable of being unreeled behind a ship and rereeled after use, low cost, ease of fabrication and manipulation, and others. These advantages promise to make polymer hydrophones useful for fish finding, fathometry, geophysical exploration, and military applications. Single sheets of  $PVF_2$  are considerably less sensitive than conventional hydrophones. When we started working on hydrophones we were advised that a sensitivity of -208 dB relative to 1V/ $\mu$ Pa would be needed before polymer hydrophones could be considered seriously. Our attempts to reach this level make up a kind of year-long detective story whose hero is Aime de Reggi. When we started, it seemed clear that the way to increase sensitivity while preserving the advantages of polymer hydrophones was to form a stack of sheets connected in series electrically and in parallel mechanically. When we did this, the sensitivity of different stacks varied greatly. Some stacks were no more active than single sheets. After much investigation, Dr. de Reggi found that the output of the separate sheets in a stack differed in phase and that the output of a stack was the vectorial sum of the outputs of the separate sheets rather than the arithmetic sum. Considerable further investigation showed that the reason for the phase difference was the presence of microscopic bubbles at the interface between sheets. The presence of only a few bubbles was enough to change the output phase drastically, showing that the sensitivity of the small area of material in the walls of the bubbles had output comparable with the output of the much greater area where there were no bubbles. Dr. de Reggi deduced that the greater activity of the material in the walls of bubbles arose because that material was acting as a membrane and was being strained by the sound pressure against a resisting area consisting of the thickness of the polymer film multiplied by the diameter of the bubble while the portion of the surface which was

free of bubbles was subjected to a compressive stress which was resisted by the whole surface area. This development suggested two courses for further progress. One was to avoid bubbles in making stacks. That work is proceeding. The other was to take advantage of the greater sensitivity supplied by using the membrane mode of operation. A sensor was devised which was essentially a big bubble. It consists of a pad of compressed foam rubber between two sheets of piezoelectric polymer. In this way, the polymer is held under tension by the foam rubber and the sound pressure modulates the tension. The output of this type of gage is about 30 dB greater than the output of single sheets of polymer subjected to compressive stress so far as our preliminary measurements show, and the output is reasonably flat with frequency to about 500 Hz. The sensitivity is about 10 dB better than our goal of -208 dB re 1V/ $\mu$ Pa. Much more work needs to be done to allow us to understand the behavior of this gage completely and to optimize the various design parameters. However, in its present preliminary form it is within the range of conventional hydrophones in sensitivity while providing the advantages of low density, flexibility, good impedance match with water, ability to withstand shock, and low cost.

A typical sensor consists of a sandwich of two thin polymer sheets. Each sheet has evaporated metal electrodes on both faces and the sheets are fused together so that charges of the same polarity appear on the inner faces. The center conductor of a coaxial cable is connected to the electrodes on these inner faces and the shield of the cable is connected to the electrodes on the outer faces. In this way all exposed surfaces are at ground potential and the signal inside the sensor is well shielded. Usually, the active area of the gage is connected to the coaxial cable by a long thin strip of metal evaporated onto an inactive

portion of the same polymer sheet that contains the active part of the gage. In this way, the masses of the connectors and cables are kept from affecting the measurement. The active portion of the gage can be cut to any reasonable size and shape needed for the measurement.

U.S. DEPT. OF COMM. BIBLIOGRAPHIC DATA SHEET	1. PUBLICATION OR REPORT NO.  NBSIR 75-760	2. Gov't Accession No.	3. Recipient's Accession No.
4. TITLE AND SUBTITLE  Proceedings of Piezoelectric and Pyroelectric Symposium-Workshop		5. Publication Date  September 1975	6. Performing Organization Code
7. AUTHOR(S)  M. Broadhurst	8. Performing Organ. Report No.		
9. PERFORMING ORGANIZATION NAME AND ADDRESS  NATIONAL BUREAU OF STANDARDS DEPARTMENT OF COMMERCE WASHINGTON, D.C. 20234		10. Project/Task/Work Unit No.	11. Contract/Grant No.
12. Sponsoring Organization Name and Complete Address (Street, City, State, ZIP) Office of Naval Research                      Army Research Office Arlington, Va. 22044                              Durham, North Carolina 27706		13. Type of Report & Period Covered Final	14. Sponsoring Agency Code
15. SUPPLEMENTARY NOTES			
<p>16. ABSTRACT (A 200-word or less factual summary of most significant information. If document includes a significant bibliography or literature survey, mention it here.)</p> <p>The purpose of this Symposium-Workshop was to bring together scientists and program managers from federal (primarily DoD), industrial, university, and foreign laboratories who are involved in the research on and manufacture of piezoelectric and pyroelectric polymer materials and devices, in order to exchange information about and stimulate further work on the new and rapidly developing measurement technology involving polymer transducers. This meeting is particularly important at this time because highly active polymer films are not yet available to device manufacturers in the U.S. or to potential users such as DoD.</p>			
<p>17. KEY WORDS (six to twelve entries; alphabetical order; capitalize only the first letter of the first key word unless a proper name; separated by semicolons) Electrets; hydrophone; piezoelectric; polymers; polyvinylidene fluoride; pyroelectric; radiometer; transducers</p>			
<p>18. AVAILABILITY                      <input checked="" type="checkbox"/> Unlimited</p> <p><input type="checkbox"/> For Official Distribution. Do Not Release to NTIS</p> <p><input type="checkbox"/> Order From Sup. of Doc., U.S. Government Printing Office Washington, D.C. 20402, SD Cat. No. C13</p> <p><input checked="" type="checkbox"/> Order From National Technical Information Service (NTIS) Springfield, Virginia 22151</p>		<p>19. SECURITY CLASS (THIS REPORT)</p> <p>UNCLASSIFIED</p>	<p>21. NO. OF PAGES</p> <p>223</p>
<p>20. SECURITY CLASS (THIS PAGE)</p> <p>UNCLASSIFIED</p>		<p>22. Price</p> <p>\$7.25</p>	